### **VOLUME 55 | 2023**

## **GEUS Bulletin**



The Upper Jurassic – Lower Cretaceous of East and North-East Greenland: Rødryggen-1 and Brorson Halvø-1 boreholes, Wollaston Forland Basin

Edited by Jon R. Ineson, Jørgen A. Bojesen-Koefoed and Karen Dybkjær



#### **GEUS Bulletin 55**

### Keywords

Geochemistry, sedimentology, stratigraphy, Upper Jurassic, Wollaston Forland

#### Cover

The view of Wollaston Forland towards the north from the Rødryggen ridge illustrates the key stratigraphic units encountered in this bulletin: in the immediate foreground, the grey mudstones of the Stratumbjerg Formation passing down-section through the brick-red Rødryggen Member, the yellow-weathering Albrechts Bugt Member (both Palnatokes Bjerg Formation) to the grey weathering shales of the Storsletten Member (Lindemans Bugt Formation) in the middle distance (Photo: J.A. Bojesen-Koefoed 2008).

### Frontispiece: facing page

The drilling team at the Rødryggen-1 drillsite, all soiled in mud during the extremely wet field-season of 2009. From above: Peter Turner, driller; Henrik J. Vosgerau, well-site geologist; John Boserup, drilling technician; Annette Ryge, cook and camp manager; Andreas Hjorth Frandsen (presently Rasmussen), drilling hand and assistant; Hjørdis (dog), polar bear guard (Photo: J.A. Bojesen-Koefoed 2009).

Editor in chief of this series: Catherine N. Jex (GEUS, Denmark)

Editors of this volume: Jon R. Ineson, Jørgen A. Bojesen-Koefoed and Karen Dybkjær (GEUS, Denmark)

External editorial board for this series: Hoori Ajami, University of California Riverside, USA; Karen Hanghøj, British Geological Survey, UK; Nicolaj Krogh Larsen, GLOBE Institute, Section for Geogenetics, University of Copenhagen, Denmark; Espen Torgersen, Norwegian University of Science

& Technology and Geological Survey of Norway, Norway Copy editing: Caroline Dea Rutter (GEUS, Denmark)

Illustrations: Authors and GEUS drawing office

Layout and graphic production: DataPage & Stine Øckenholt (GEUS, Denmark)

Printers: Prinfo Denmark A/S
Printed: December 2023

eISSN: 2597-2154 ISSN print: 2597-2162

### How to cite this volume

See each article for the recommended citation. The special issue can be cited as:

Ineson, J.R., Bojesen-Koefoed, J.A. & Dybkjær, K. (eds) 2023: The Upper Jurassic – Lower Cretaceous of East and North-East Greenland: Rødryggen-1 and Brorson Halvø-1 boreholes, Wollaston Forland Basin. GEUS Bulletin **55**. 118 pp. https://doi.org/10.34194/geusb.V55i

### Available from

Geological Survey of Denmark and Greenland (GEUS) Øster Voldgade 10, DK-1350 Copenhagen K, Denmark Read online (open access): geusbulletin.org Purchase a printed copy: geusbulletin.org/shop Phone: +45 38 14 20 00, e-mail: enquiries@geusbulletin.org / geus@geus.dk

### © 2023 The author(s)



This article is distributed under a CC-BY 4.0 licence, permitting free redistribution, and reproduction for any purpose, even commercial, provided proper citation of the original work. Author(s) retain copyright.

Read the full open access policy:

https://geusbulletin.org/index.php/geusb/oapolicy



### **Contents**

| The Rødryggen-1 and Brorson Halvø-1 fully cored boreholes (Upper Jurassic - Lower Cretaceous), Wollaston Forland, North-East Greenland - an introduction Bojesen-Koefoed, J.A., Alsen, P., Bjerager, M., Hovikoski, J., Ineson, J.R., Johannessen, P.N., |      |
|--|------|
| Olivarius, M., Piasecki, S. & Vosgerau, H  | 5    |
| Stratigraphy of the Upper Jurassic to lowermost Cretaceous in the Rødryggen-1 and Brorson Halvø-1 boreholes, Wollaston Forland, North-East Greenland   |      |
| Alsen, P., Piasecki, S., Nøhr-Hansen, H., Pauly, S., Sheldon, E. & Hovikoski, J  | . 13 |
| Upper Jurassic - Lower Cretaceous of eastern Wollaston Forland, North-East Greenland:  |      |
| Hovikoski, J., Ineson, J.R., Olivarius, M., Bojesen-Koefoed, J.A., Piasecki, S. & Alsen, P   | . 53 |
| Mudstone diagenesis and sandstone provenance in an Upper Jurassic – Lower Cretaceous   |      |
| evolving half-graben system, Wollaston Forland, North-East Greenland   |      |
| Olivarius, M., Kazerouni, A.M., Weibel, R., Kokfelt, T.F. & Hovikoski, J   | . 73 |
| Organic geochemistry of an Upper Jurassic – Lower Cretaceous mudstone succession   |      |
| n a narrow graben setting, Wollaston Forland Basin, North-East Greenland   |      |
| Bojesen-Koefoed, J.A., Alsen, P., Bjerager, M., Hovikoski, J., Johannessen, P.N., Nøhr-Hansen, H.,<br>Petersen, H.I., Piasecki, S. & Vosgerau, H   | 95   |
| Ctc1 3c11, 1111, 1 103CcN1, 3. & V03gc1 au, 11.  | . 53 |

## **GEUS Bulletin**



# The Rødryggen-1 and Brorson Halvø-1 fully cored boreholes (Upper Jurassic – Lower Cretaceous), Wollaston Forland, North-East Greenland – an introduction

Jørgen A. Bojesen-Koefoed<sup>1</sup>\*<sup>10</sup>, Peter Alsen<sup>2</sup><sup>10</sup>, Morten Bjerager<sup>3</sup><sup>10</sup>, Jussi Hovikoski<sup>3,4</sup><sup>10</sup>, Jon R. Ineson<sup>3</sup><sup>10</sup>, Peter N. Johannessen<sup>5</sup>, Mette Olivarius<sup>2</sup><sup>10</sup>, Stefan Piasecki<sup>3,6,7</sup><sup>10</sup>, Henrik Vosgerau<sup>3</sup><sup>10</sup>

<sup>1</sup>Department for Mapping and Mineral Resources, Geological Survey of Denmark and Greenland (GEUS), Copenhagen, Denmark; <sup>2</sup>Department for Geo-energy and Storage, Geological Survey of Denmark and Greenland (GEUS), Copenhagen, Denmark; <sup>3</sup>Department for Geophysics and Sedimentary Basins, Geological Survey of Denmark and Greenland (GEUS), Copenhagen, Denmark; <sup>4</sup>Geological Survey of Finland (GTK), Espoo, Finland; <sup>5</sup>Geological Survey of Denmark and Greenland (GEUS), now retired; <sup>6</sup>Globe Institute, University of Copenhagen, Copenhagen, Denmark; <sup>7</sup>Retired

### **Abstract**

Two fully cored boreholes, the Rødryggen-1 and the Brorson Halvø-1, were drilled in Wollaston Forland, North-East Greenland, in 2009 and 2010, respectively. The objective was to test the stratigraphic development of the Upper Jurassic – Lower Cretaceous mud-dominated succession in two different settings within the same fault block of a developing half-graben: centrally (Rødryggen-1 borehole) and near the uplifted crest of the rotating fault block (Brorson Halvø-1 borehole). The drilled deposits are equivalent to the principal petroleum source-rock sequence of the petroliferous basins of North-West Europe, Siberia, and basins off eastern Canada and provide a new record of an important phase of marine deoxygenation in the proto-North Atlantic region.

### 1. Introduction

In 2007-2008, the Geological Survey of Denmark and Greenland (GEUS) initiated a major collaborative project with a consortium of companies of the international petroleum industry with the aim of addressing aspects of the geology of North-East and North Greenland, which were generally recognised as being insufficiently studied. One such aspect was the elucidation of the imperfectly known stratigraphy, sedimentary and lithologic development, and petroleum generation potential of the Upper Jurassic - Lower Cretaceous succession, equivalent to the well-known petroleum source-rock succession of the North Sea graben system, that is, the Kimmeridge Clay sensu lato. In North-East Greenland, the equivalent succession is widely distributed, and a considerable number of outcrop samples as well as some samples from cored shallow boreholes had been analysed previously, generally showing surprisingly poor petroleum generation potential. This was suspected to be the result of a combination of poor representation in the sample set of the more prolific intervals and adverse effects of weathering of outcrop samples. Hence, a drilling program was designed to obtain full core representation of the entire stratigraphic succession ranging from the Oxfordian to the Ryazanian. Three fully cored boreholes were planned, the first of which, the Blokelv-1 borehole, was drilled in Jameson Land in 2008. Blokelv-1 penetrated 233.8 m of Oxfordian-Volgian deposits,

\*Correspondence: jbk@geus.dk Received: 26 May 2023 Revised: 27 Jun 2023 Accepted: 27 Jun 2023 Published: 21 Dec 2023

**Keywords:** stratigraphic boreholes, technical data, sedimentology, biostratigraphy, geochemistry

### **Abbreviations:**

GEUS: Geological Survey of Denmark and Greenland TD: total depth GR: gamma ray

b.rfl.: below reference level

GEUS Bulletin (eISSN: 2597-2154) is an open access, peer-reviewed journal published by the Geological Survey of Denmark and Greenland (GEUS). This article is distributed under a *CC-BY 4.0* licence, permitting free redistribution, and reproduction for any purpose, even commercial, provided proper citation of the original work. Author(s) retain copyright.

**Edited by:** Karen Dybkjær (GEUS, Denmark)

Reviewed by: Not peer-reviewed

Funding: See page 11

Competing interests: None

Additional files: None.

intruded by a few basaltic sills, as reported in a series of papers published in a volume edited by Ineson & Bojesen-Koefoed (2018). Two additional boreholes, both situated in Wollaston Forland, the Rødryggen-1 and Brorson Halvø-1 boreholes, were drilled in 2009 and 2010, respectively (Fig. 1). These boreholes aimed at testing that part of the succession not drilled by the Blokelv-1 borehole whilst attaining a reasonable stratigraphic overlap. The two boreholes were planned to be drilled centrally within, and near the uplifted crest of, a rather narrow half-graben, which evolved during the time of deposition, thus allowing the assessment of the

effects of synsedimentary tectonic movements on the nature of the deposits. The main results of the drilling are reported in a series of papers dealing with stratigraphy (Alsen *et al.* 2023, this volume): sedimentology and basin evolution (Hovikoski *et al.* 2023a, this volume), mineralogy and diagenesis (Olivarius *et al.* 2023, this volume) and organic geochemistry and petroleum potential (Bojesen-Koefoed *et al.* 2023, this volume). The aim of this paper is to introduce the location, drilled successions, drilling procedure and technical specifications of the Rødryggen-1 and Brorson Halvø-1 boreholes.

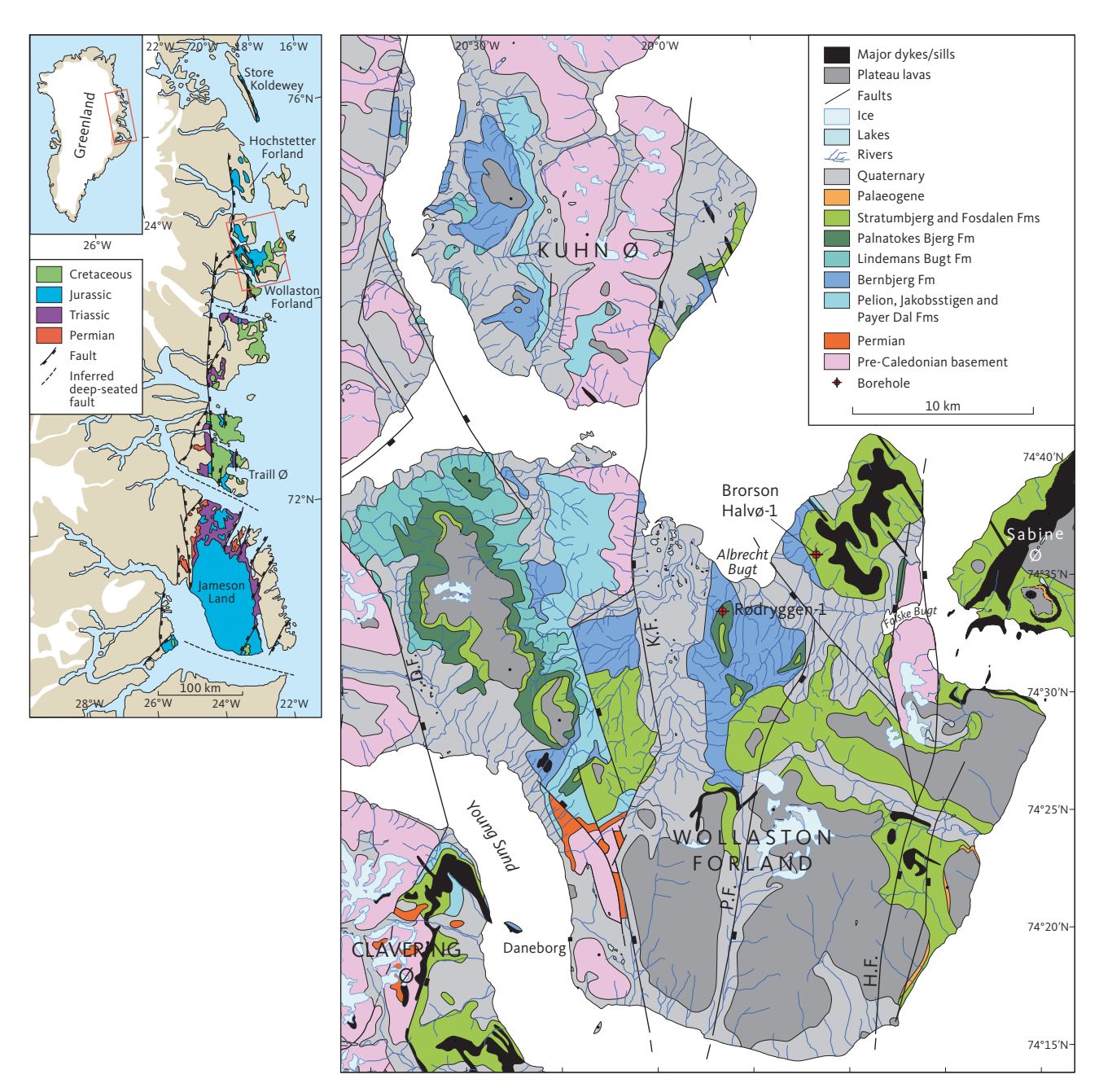


**Fig. 1** Location maps. Overview map (**left**; Modified from Surlyk *et al.* 2023). Positions of the Rødryggen-1 and Brorson Halvø-1 boreholes in Wollaston Forland are shown on a simplified geological map (**right**; Modified from Surlyk *et al.* 2021). **K.F.**: Kuhn fault; **P.F.**: Permpas Fault; **H.F.**: Hühnerbjerg Fault; **D.F.**: Dombjerg Fault. The Dombjerg Fault was the main fault to control the position of the coastline during the Late Jurassic. The Permpas–Hühnerbjerg block(s) was bounded by the Kuppel and Hühnerbjerg Faults during the Late Jurassic.

### 2. Drilling and samples

### 2.1 Rødryggen-1 borehole

Drilling and technical specifications of the Rødryggen-1 fully cored borehole are summarised in Table 1. The Rødryggen-1 borehole was drilled from 27 July to 16 August 2009 at the Rødryggen locality, central Wollaston Forland. The drilling rig and the drill camp were mobilised by helicopter (sling and cabin load) from the military station at Daneborg approximately 30 km to the SSW of the drill site (Fig. 1). Rødryggen ("Red Ridge") is a prominent NS-oriented, elongated hill, separating two broad depressions: Storsletten to the west and Sumpdalen to the east. The drill-site was selected during the 2008 field season by Henrik Nøhr-Hansen and Jørgen A. Bojesen-Koefoed. The well location was chosen with the aim of testing the Upper Jurassic - Lower Cretaceous succession centrally in the westward-tilted Permpas-Hühnerbjerg fault block. The rig was placed on outcrops of the bright yellow-weathering mudstones of the Albrechts Bugt Member of the Palnatokes Bjerg Formation (Figs 2 and 3). Debris from the overlying Rødryggen Member of the Palnatokes Bjerg Formation unit imparts a conspicuous red colour to the Rødryggen hill and thus forms the basis for its name. The rig and the drilling team spent 22 days on the location, with only 11 effective days of drilling. The marked discrepancy between time on location and time spent on active drilling was caused by prolonged periods of very bad weather with strong winds and large volumes of snow and rain, which tended to liquefy the upper decimeters of the very muddy ground, thus creating massive problems for camping and for the stability of the rig.

The drilled succession is summarised in Table 2. The borehole penetrated 24.4 m of the Albrechts Bugt Member of the Palnatokes Bjerg Formation (light grey, yellow-weathering mudstones), followed by 72.6 m of the Lindemans Bugt Formation (dark grey/black laminated mudstones), a succession that was later defined as a new member, the Storsletten Member (Alsen et al. 2023, this volume). Beneath the Lindemans Bugt Formation, the borehole encountered 137.5 m of the Bernbjerg Formation (dark grey mudstones with occasional thin sandstone stringers and carbonate-filled thin fractures) before reaching total depth (TD) at 234.5 m below reference level (b.rfl.; top of casing). For details of the sedimentology, the mineralogy and diagenesis, and the organic geochemistry and petroleum potential see Hovikoski et al. (2023a, this volume) Olivarius et al. (2023, this volume) and Bojesen-Koefoed et al. (2023, this volume), respectively.

A total gamma-ray (GR) wireline log was collected in the borehole over the interval 0–209 m b.rfl., later supplemented by spectral-GR and bulk-density scanning of the cores over the interval 192.56 m to 234.54 m.

Table 1 Drilling and technical data on the Rødryggen-1 and Brorson Halvø-1 boreholes.

| Specifications                   | Rødryggen-1   | Brorson Halvø-1                         |
|----------------------------------|---|---|
| Borehole number                  | GGU 517001  | GGU 517003                              |
| Borehole name                    | Rødryggen-1   | Brorson Halvø-1                         |
| Area                             | Wollaston Forland, North-East Greenland                     | Wollaston Forland, North-East Greenland |
| Operator                         | GEUS  | GEUS                                    |
| Drilling operator                | GEUS  | GEUS                                    |
| Altitude                         | 110 m above mean sea level                                  | 101 m above mean sea level              |
| Coordinates (WGS 84)             | 74°32.561′N; 19°50.924′W                                    | 74°35.227′N; 19°34.327′W                |
| UTM Zone                         | 27W   | 27W                                     |
| Easting                          | E465752   | E457646                                 |
| Northing                         | N8272914  | N8278142                                |
| Drill rig                        | Sandvik DE 130  | Sandvik DE 130                          |
| Casing diameter (O/I)            | 64/57 mm  | 64/57 mm                                |
| Casing depth                     | 15.8 m  | 35.0 m                                  |
| Borehole diameter                | 56 mm   | 56 mm                                   |
| Core diameter                    | 42 mm   | 42 mm                                   |
| Reference level                  | Top of casing   | Top of casing                           |
| Total depth                      | 234.5 m   | 225.6 m                                 |
| Core recovery                    | 99%   | 99%                                     |
| Status                           | Abandoned open hole, top of casing closed with a steel cap. | Abandoned open hole. Hole collapsed.    |
| Drilling crew arrival (Daneborg) | 24 July 2009  | n.a.                                    |
| Mobilisation to drill site       | 27 July – 29 July 2009                                      | 30 July – 1 August 2010                 |
| Preparation of camp              | 27 July – 2 August 2009                                     | 2–3 August2010                          |
| Spud                             | 3 August 2009   | 3 August 2010                           |
| Drilling completed               | 14 August 2009  | 12 August 2010                          |
| Demobilisation                   | 16 August 2009  | 14 August 2010                          |
| Effective drilling               | 11 days   | 10 days                                 |
| Total days at drill location     | 22 days   | 14 days                                 |



Fig. 2 The Rødryggen-1 drill-site and camp, viewed approximately towards the west with the broad plain of Storsletten as backdrop (Photo: Annette Ryge). The rig was placed on the brightly coloured, yellow-weathering mudstones of the Albrechts Bugt Member (Palnatokes Bjerg Formation). The overlying Rødryggen Member (Palnatokes Bjerg Formation) in the foreground consists of purple to brick-red mudstones. Debris from this unit imparts the slopes of the landscape with a reddish colour that can be seen from afar, and from which is derived the location's name Rødryggen, meaning "the red ridge."

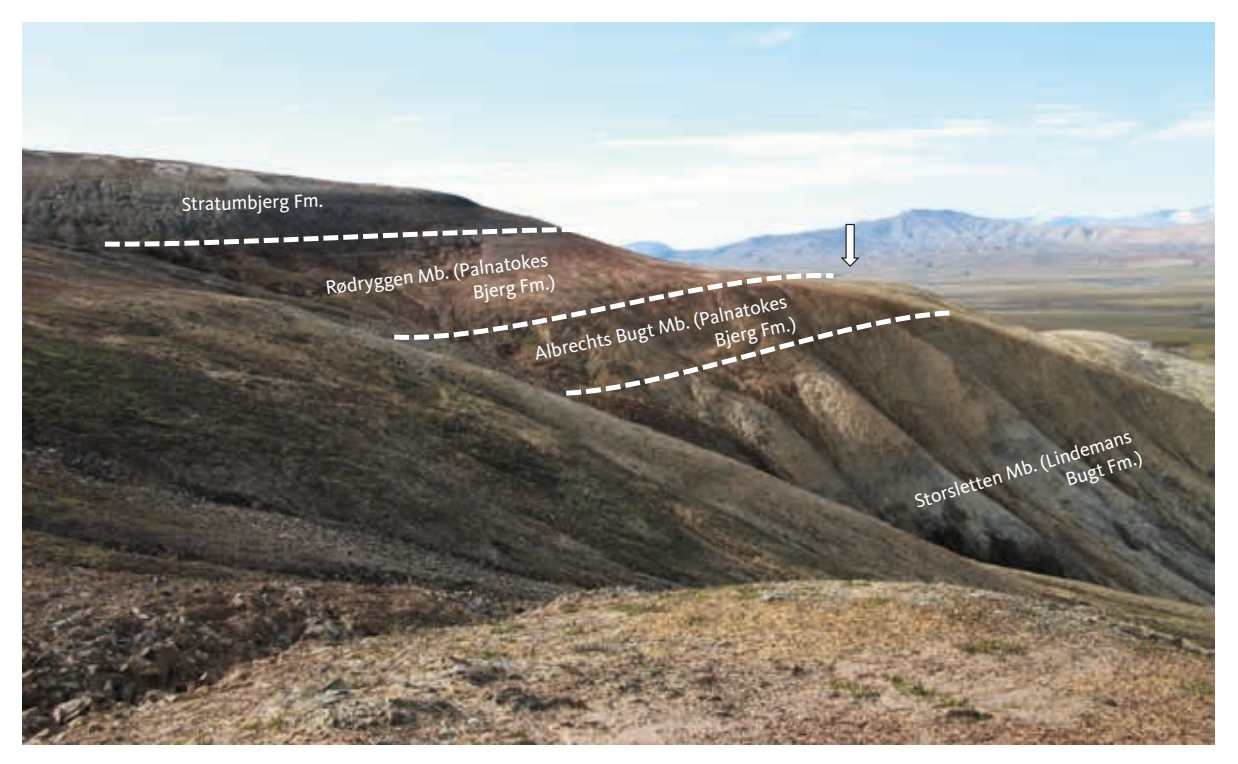


Fig. 3 Section at Rødryggen viewed approximately from the north in 2008 when the drill-site was selected. Arrow indicates the approximate position of the borehole (Photo: Jørgen A. Bojesen-Koefoed).

 Table 2 Stratigraphic units encountered by the Rødryggen-1 and Brorson Halvø-1 boreholes.

| Lithostratigraphy                                | Rødryggen-1          | Brorson Halvø-1        |
|--|----------------------|------------------------|
| Stratumbjerg Formation                           | n.d.                 | 8.7 m (0-8.7 m)        |
| Palnatokes Bjerg Formation, Rødryggen Member     | n.d.                 | 21.3 m (8.7-30 m)      |
| Palnatokes Bjerg Formation, Albrects Bugt Member | 24.4 m (0-24.4 m)    | 7.5 m (30-37.5 m)      |
| Lindemans Bugt Formation, Storsletten Member     | 72.6 m (24.4-97 m)   | 8.0 m (37.5-45.5 m)    |
| Bernbjerg Formation                              | 137.5 m (97-234.5 m) | 180.1 m (45.5-225.6 m) |

Thickness in m (intervals in m b.rfl.). n.d.: not drilled.

The wireline log and the scanned GR core logs were then merged into one single total GR log.

The core recovery was 99%, with losses of core primarily occurring in the uppermost part of the succession, which was affected by surface weathering. The core quality was mostly excellent, with significant fracturing only found in intervals scattered throughout the succession, whilst coherent core in general predominated (Fig. 4). A total of 70 whole core samples for gas analysis, each c. 10 cm in length, were collected on site at approximately 3 m intervals and stored in airtight containers immediately after the cores were extruded from the core barrel. A large number of samples for different types of analyses were subsequently collected from the core. Most of these analyses are reported in papers by Alsen et al. (2023, this volume), Hovikoski et al. (2023a, this volume), Olivarius et al. (2023, this volume) and Bojesen-Koefoed et al. (2023, this volume). Additional data are reported by Hovikoski et al. (2023b), whereas a minor volume of miscellaneous data that have not found a place in the publications listed above are reported in internal GEUS reports.

### 2.2 Brorson Halvø-1 borehole

Drilling and technical specifications of the Brorson Halvø-1 fully cored borehole are summarised in Table 1. The Brorson Halvø-1 borehole was drilled from 30 July

to 14 August 2010 at Brorson Halvø (Brorson Peninsula), northeastern Wollaston Forland. The Brorson Halvø-1 borehole was the second to be drilled during the 2010 field season, and the drilling rig and camp were mobilised from the first drill site on the island of Store Koldewey, approximately 200 km north of the Brorson Halvø drill-site (Fig. 1). The rig frame was transported by helicopter in one piece as sling load directly from the Store Koldewey drill site to the Brorson Halvø drill site. The drilling team, the drill camp and other equipment were moved either directly by helicopter or via Danmarkshavn by Twin Otter plane to Daneborg and from there by helicopter to the Brorson Halvø-1 drill-site. The original drill site was selected during the 2008 field season by Henrik Nøhr-Hansen and Jørgen A. Bojesen-Koefoed, later redefined by Morten Bjerager and Michael B.W. Fyhn in 2009, and eventually, for practical reasons, moved another few 100 m by Stefan Piasecki and Jørgen A. Bojesen-Koefoed in 2010 to secure a stable substratum for the rig. A consequence of this last relocation of the drill site was the drilling of part of the Stratumbjerg Formation and the entire Rødryggen Member of the Palnatokes Bjerg Formation, which was initially not planned.

The well location was selected with the aim of testing the Upper Jurassic – Lower Cretaceous succession near the uplifted crest of the westward-tilted Permpas-Hühnerbjerg fault block. The rig was placed on outcrops of



Fig. 4 Example of core quality and recovery, Rødryggen-1 borehole, 59.81 – 66.16 m, Lindemans Bugt Formation (Photo: John Boserup).



Fig. 5 The Brorson Halvø-1 drill site viewed approximately towards the ENE. The drill-rig stands on the dark grey mudstones of the Stratumbjerg Formation with the well-defined contact to the bright red Rødryggen Member clearly visible below. Downhill, the contact between the Rødryggen Member and the underlying Albrechts Bugt Member (yellow) stands out. The contact to the Storsletten Member (grey), in turn, underlying the Albrechts Bugt Member appears somewhat gradational, but in a clean section, it is very well defined (see Fig. 6; Photo: Annette Ryge).



**Fig. 6** Example of core quality and recovery, Brorson Halvø-1 borehole, 34.44–41.24 m, Albrechts Bugt Member of the Palnatokes Bjerg Formation (light grey) and the sharp boundary with the underlying Storsletten Member of the Lindemans Bugt Formation (dark grey; Photo: John Boserup).

the dark-grey mudstones of the Stratumbjerg Formation (Fig. 5). The rig and the drilling team spent 14 days on the location, with 10 effective days of drilling.

The drilled succession is summarised in Table 2. The borehole penetrated 8.7 m of the Stratumbjerg Formation (dark-grey mudstones), followed by 21.3 m of the Rødryggen Member (purple to brick-red mudstones) and 7.5 m of the Albrechts Bugt Member (light grey, yellow-weathering

mudstones) of the Palnatokes Bjerg Formation. Beneath the Palnatokes Bjerg Formation, the borehole encountered 8.0 m of the Lindemans Bugt Formation (dark grey/black laminated mudstones), later referred to the new Storsletten Member (Alsen *et al.* 2023, this volume), and eventually, 180.1 m of the Bernbjerg Formation (dark grey mudstones with occasional thin sandstone stringers and carbonate-filled, thin fractures). TD was reached

at 225.6m b.rfl. (top of casing). Drilling was terminated due to notable water production from the borehole at TD. For details of the sedimentology, the mineralogy and diagenesis, and the organic geochemistry and petroleum potential, see Hovikoski *et al.* (2023a, this volume), Olivarius *et al.* (2023, this volume) and Bojesen-Koefoed *et al.* (2023, this volume), respectively.

A total GR wireline log was collected in the borehole over the interval 0–210 m b.rfl., later supplemented by spectral-GR and bulk-density scanning of the cores over the interval 193 m – 225.6 m. The wireline log and the scanned GR core logs were then merged into one single total GR log.

The core recovery was 99%, with significant losses of recovery mainly in the uppermost part of the succession, which was affected by surface weathering. The core quality was mostly excellent, with significant fracturing only found in intervals scattered throughout the succession, whilst coherent core predominated (Fig. 6). A total of 34 whole-core samples for gas analysis, each c. 10 cm in length, were collected on site and stored in airtight containers immediately after the cores were extruded from the core barrel. A large number of samples for different types of analyses were subsequently collected from the core. Most of these analyses are reported in papers by Alsen et al. (2023, this volume), Hovikoski et al. (2023a, this volume), Olivarius et al. (2023, this volume) and Bojesen-Koefoed et al. (2023, this volume). Additional data are reported by Hovikoski et al. (2023b), whereas a minor volume of miscellaneous data that have not found a place in the publications listed above are reported in internal GEUS reports.

### 2.3 Perspectives

The primary data from the three fully cored, complementary boreholes Blokelv-1, Rødryggen-1 and Brorson Halvø-1 are presented in Ineson & Bojesen-Koefoed (2018) and this volume. Together these cored sections represent a unique geological archive from a high latitude setting, recording a key period when super-regional deoxygenation prevailed in the marine waters of the proto-North Atlantic region. Though the significance of this archive may have waned commercially, given the imperative to adopt carbon-free energy sources, its continued importance lies in understanding the climatic, tectonic and oceanographic factors involved in watermass stratification, deoxygenation and carbon burial, as examined recently by Hovikoski et al. (2023b). It is predicted that this integrated core record will be the source of much multidisciplinary research in future years.

### **Acknowledgements**

The drilling teams including John Boserup, Anders Clausen, Annette Ryge, Peter Turner, Lars (Lasse) Thomsson, Andreas Hjort Frandsen and Anders Pilgaard are thanked for their hard work and stamina, and for maintaining good spirits, particularly during the very challenging 2009 field season. The pilots Finn Rusanes and Göran Lindmark (both Air Greenland) are thanked for diligent sling-work under very difficult conditions. Twin Otter plane support by Nordlandair (Akureyri, Iceland) is gratefully acknowledged. Jesper Weiss Andersen and Thea Weiss Andersen (in 2009 only) did an excellent job running the logistics of the 2009 and 2010 expeditions.

### **Additional information**

### **Funding statement**

The drilling campaign was funded by GEUS in collaboration with a large number of companies of the international petroleum industry, which for contractual reasons cannot be named.

### **Author contributions**

JABK: Conceptualisation; Writing – Original Draft; Funding Acquisition; Project Administration; Investigation; Writing – Review & Editing. PAL: Conceptualisation; Funding Acquisition; Investigation; Writing – Review & Editing. MBJ: Investigation; Writing – Review & Editing. JHOV: Investigation; Writing – Review & Editing. JI: Conceptualisation; Writing – Original Draft: Investigation; Writing – Review & Editing. PJ: Investigation. MOL: Investigation; Writing – Review & Editing. SP: Conceptualisation; Investigation; Writing – Review & Editing. HV: Investigation; Writing – Review & Editing. HV: Investigation; Writing – Review & Editing.

#### **Competing interests**

None declared

### **Additional files**

None provided

### References

Alsen, P., Piasecki, S., Nøhr-Hansen, H., Pauly, S., Sheldon, E. & Hovikoski, J. 2023: Stratigraphy of the Upper Jurassic to lowermost Cretaceous in the Rødryggen-1 and Brorson Halvø-1 boreholes, Wollaston Forland, North-East Greenland. GEUS Bulletin 55, 8342 (this volume). https://doi.org/https://doi.org/10.34194/geusb.v55.8342

Bojesen-Koefoed, J.A., Alsen, P., Bjerager, M., Hovikoski, J., Johannessen, P., Nøhr-Hansen, H., Petersen, H.I., Piasecki, S. & Vosgerau, H. 2023: Organic geochemistry of an Upper Jurassic – Lower Cretaceous mudstone succession in a narrow graben setting, Wollaston Forland Basin, North-East Greenland. GEUS Bulletin 55, 8320 (this volume). https://doi.org/https://doi.org/10.34194/geusb.v55.8320

Hovikoski, J., Ineson, J.R, Olivarius, M., Bojesen-Koefoed, J.A, Piasecki, S. & Alsen, P. 2023: Upper Jurassic – Lower Cretaceous of eastern Wollaston Forland, North-East Greenland: a distal marine record of an evolving rift. GEUS Bulletin 55, 8349 (this volume). https://doi.org/https://doi.org/10.34194/geusb.v55.8349

Hovikoski, J. et al. 2023b: Late Jurassic – Early Cretaceous marine deoxygenation in NE Greenland. Journal of the Geological Society 180 (3), jgs2022–058. https://doi.org/10.1144/jgs2022-058

Ineson, J.R. & Bojesen-Koefoed, J.A. (eds). 2018: Petroleum geology of the Upper Jurassic – Lower Cretaceous of East and North-East Greenland: Blokelv-1 borehole, Jameson Land Basin. Geological Survey of Denmark and Greenland Bulletin **42**, 168pp. https://doi.org/10.34194/geusb.v42

Olivarius, M., Kazerouni, A.M., Weibel, R., Kokfelt, T.F. & Hovikoski, J. 2023: Mudstone diagenesis and sandstone provenance in an Upper Jurassic – Lower Cretaceous evolving half-graben system, Wollaston Forland, North-East Greenland. GEUS Bulletin **55**, 8309 (this volume). https://doi.org/https://doi.org/10.34194/geusb.v55.8309

Surlyk, F. 1978: Submarine fan sedimentation along fault scarps on tilted fault blocks (Jurassic–Cretaceous boundary, East Green-land). Bulletin Grønlands Geologiske Undersøgelse 128, 117 pp. https://doi.org/10.34194/bullggu.v128.6670

Surlyk, F. 2003: The Jurassic of East Greenland: a sedimentary record of thermal subsidence, onset and culmination of rifting. In: Ineson, J.R.

- & Surlyk, F. (eds): The Jurassic of Denmark and Greenland. Geological Survey of Denmark and Greenland Bulletin **1**, 659–722. https://doi.org/10.34194/geusb.v1.4674
- Surlyk, F. et al. 2021: Jurassic stratigraphy of East Greenland. GEUS Bulletin **46**, 6521. https://doi.org/10.34194/geusb.v46.6521
- Surlyk, F., Alsen, P., Hovikovski, J. & Piasecki, S. 2023: Uplift, deflation and marine onlap of a Jurassic rift dome, illustrated by a backstepping Middle Upper Jurassic shelf-to-slope succession, Geographical Society Ø, East Greenland. Terra Nova **00**, 1–8. https://doi.org/10.1111/ter.12673

## **GEUS Bulletin**



# Stratigraphy of the Upper Jurassic to lowermost Cretaceous in the Rødryggen-1 and Brorson Halvø-1 boreholes, Wollaston Forland, North-East Greenland

Peter Alsen\*¹ , Stefan Piasecki²,³,⁴ , Henrik Nøhr-Hansen¹, Sebastian Pauly⁵,⁶, Emma Sheldon¹ , Jussi Hovikoski²,७ ,

<sup>1</sup>Department for Geo-energy and Storage, Geological Survey of Denmark and Greenland (GEUS), Copenhagen, Denmark; <sup>2</sup>Department for Geophysics and Sedimentary Basins, Geological Survey of Denmark and Greenland (GEUS), Copenhagen, Denmark; <sup>3</sup>Globe Institute, University of Copenhagen, Copenhagen, Denmark; <sup>4</sup>Retired; <sup>5</sup>Ruhr Universität Bochum, Bochum, Germany; <sup>6</sup>INGENUM GmbH, Bottrop, Germany; <sup>7</sup>Geological Survey of Finland (GTK), Espoo, Finland

### **Abstract**

Two shallow cores drilled in northern Wollaston Forland, North-East Greenland, provide a combined section covering the upper Kimmeridgian (Upper Jurassic) – Barremian (Lower Cretaceous) and comprising the Bernbjerg, Lindemans Bugt, Palnatokes Bjerg and Stratumbjerg Formations. A new lithostratigraphic unit, the Storsletten Member, is defined within the Lindemans Bugt Formation. The black mudstone-dominated intervals are dated primarily by dinoflagellate cysts and ammonites, whereas the calcareous mudstones of the Palnatokes Bjerg Formation – sandwiched between the black mudstones – are dated by calcareous nannofossils. The stratigraphy demonstrates an almost complete succession in the Rødryggen-1 core, representing a deeper position in the basin, where the hiatus at the latest Jurassic rift climax predicted in previous models for the eastern Wollaston Forland Basin is absent. In contrast, the Brorson Halvø-1 core represents a position closer to a block crest where unconformities developed. In combination, the cores provide a key biostratigraphic reference section for the Jurassic–Cretaceous boundary interval in the Arctic.

### 1. Introduction

The Rødryggen-1 and Brorson Halvø-1 cores were drilled in northern Wollaston Forland, North-East Greenland (Figs 1, 2). They are the second and third cores in an onshore drilling programme designed to characterise the Upper Jurassic source-rock succession in North-East Greenland (Bojesen-Koefoed *et al.* 2014). The programme started with the drilling of the Blokelv-1 core in central Jameson Land (Fig. 1; Ineson & Bojesen-Koefoed 2018).

The Rødryggen-1 borehole is located on the western side of Rødryggen (meaning 'red ridge') at the eastern margin of Storsletten, Wollaston Forland. Previous studies in the area have suggested that the Rødryggen ridge consists of Upper Jurassic dark mudstones, separated with a major hiatus from overlying Ryazanian–Hauterivian (Lower Cretaceous) light grey or yellowish and red mudstones and is capped by dark, mid-Cretaceous mudstones (Surlyk 1978; Alsen 2006; Pauly *et al.* 2013; Bjerager *et al.* 2020; Surlyk *et al.* 2021). Coring was initiated in the Valanginian and terminated in upper Kimmeridgian strata at 234 m depth.

The Brorson Halvø-1 drill site at the south-western flank of Bern Plateau is situated approximately 10 km to the NE from the Rødryggen-1 drill site, across the Sumpdalen lowland that separates the Rødryggen ridge from the Brorson Halvø peninsula (Fig. 2). Coring was initiated stratigraphically somewhat higher, in Barremian dark mudstones, and reached 225 m depth, also in Kimmeridgian strata.

\*Correspondence: pal@geus.dk

Received: 10 Feb 2023 Revised: 04 Sep 2023 Accepted: 05 Sep 2023 Published: 21 Dec 2023

**Keywords:** ammonite stratigraphy, calcareous nannofossil stratigraphy, Jurassic–Cretaceous boundary, palynostratigraphy, Storsletten Member

#### Abbreviations:

sp. juv.: species juvenile

undiff.: undifferentiated

AOM: amorphous organic matter
API: American Petroleum Institute
FO: first occurrence
GEUS: Geological Survey of Denmark and
Greenland
GR: gamma ray
GSSP: global boundary stratotype section
and point
TD: total depth
aff.: affinis
spp.: species plural

GEUS Bulletin (eISSN: 2597-2154) is an open access, peer-reviewed journal published by the Geological Survey of Denmark and Greenland (GEUS). This article is distributed under a *CC-BY 4.0* licence, permitting free redistribution, and reproduction for any purpose, even commercial, provided proper citation of the original work. Author(s) retain copyright.

**Edited by:** Jon R. Ineson & Jørgen A. Bojesen-Koefoed (GEUS, Denmark)

**Reviewed by:** Simon Schneider (CASP, UK) and Claudia Schröder-Adams (Carleton University, Canada)

Funding: See page 49

Competing interests: See page 49

Additional files: See page 49

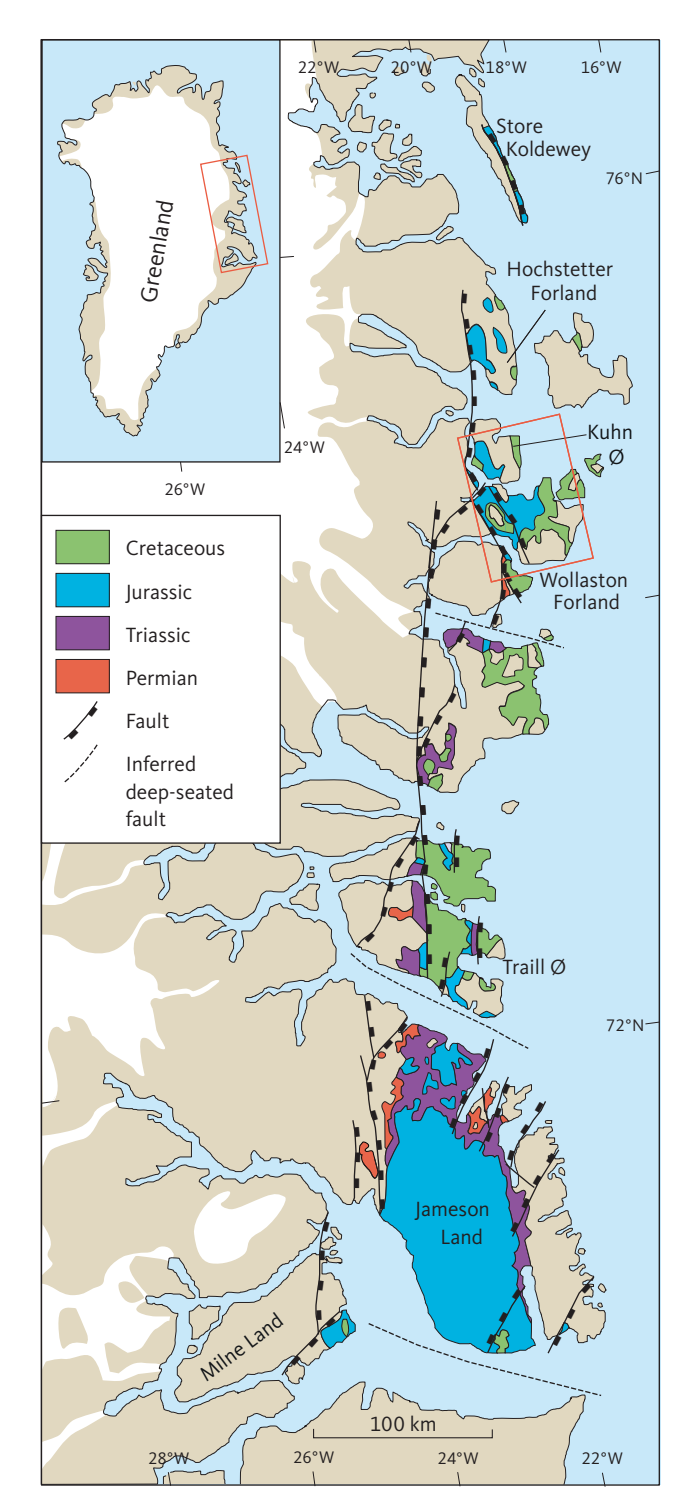


**Fig. 1** Simplified geological map showing the distribution of Permian-Cretaceous sedimentary rocks in North-East Greenland. Position of study area in Fig. 2 indicated with a **red box**. Reproduced from Bojesen-Koefoed *et al.* (2023a, this volume, fig. 1).

The Blokelv-1 core in Jameson Land documents black mudstone deposition during the Oxfordian–Kimmeridgian (Alsen & Piasecki 2018; Bjerager *et al.* 2018). The two cores in Wollaston Forland document the longevity and termination of the Late Jurassic black mudstone deposition in North-East Greenland. The Blokelv-1 core reflects a sag basin setting, whereas the Wollaston Forland

area is characterised by block faulting and rotation and half-graben formation (Surlyk 1978, 2003). The two cores drilled in Wollaston Forland document different depositional histories at different structural positions within the half-graben complex. Hence, the Brorson Halvø-1 well is located near the elevated hanging wall crest of the Permpas Block (Fig. 2; Surlyk 1978), whereas the Rødryggen-1 well is located near the basin centre of the same block.

The aim of this study is to document in detail the lithostratigraphy and biostratigraphy of the composite cores section. This study not only adds significantly to the knowledge on the complexity of the Upper Jurassic stratigraphy in the area, but also presents new data of regional significance on the biostratigraphy of the Jurassic–Cretaceous boundary interval in the Arctic. The targeted core interval, the Upper Jurassic dark mudstone succession, consists of two lithostratigraphic units: (1) the Kimmeridgian – lower Volgian Bernbjerg Formation and (2) a middle Volgian – lower Ryazanian new unit, which is here established as a new member – the Storsletten Member – within the Lindemans Bugt Formation.

## 2. Previous stratigraphic studies of the Upper Jurassic and Lower Cretaceous in Wollaston Forland

Upper Jurassic – Lower Cretaceous strata in Wollaston Forland were mapped during the Lauge Koch-led mapping campaigns in the 1940s (Vischer 1943; Maync 1947). The Jurassic-Cretaceous boundary interval was further investigated by Donovan (1964) in the northern Wollaston Forland, eastern Kuhn Ø and Lindeman Fjord areas (Fig. 2). The Jurassic – lowermost Cretaceous lithostratigraphy was formally established by Surlyk (1977, 1978) and recently revised and updated (Surlyk et al. 2021), whereas a Cretaceous lithostratigraphy was established by Bjerager et al. (2020). The Late Jurassic ammonite faunal succession in western Wollaston Forland was described by Sykes & Surlyk (1976), whereas the ammonite and Buchia bivalve zonation in the thick rift-climax succession at the Jurassic-Cretaceous boundary was established by Surlyk (1978) and Surlyk & Zakharov (1982). Nøhr-Hansen (1993) presented a dinoflagellate cyst biostratigraphic subdivision of the Barremian-Albian in North-East Greenland, partly based on sampled sections in Wollaston Forland. The zonation was recently extended and revised by Nøhr-Hansen et al. (2020). Macrofossils and the biostratigraphy of the Palnatokes Bjerg Formation from localities in central Wollaston Forland were described by Alsen & Rawson (2005), Harper et al. (2005), Alsen (2006) and Alsen & Mutterlose (2009), followed by calcareous nannofossil and isotope stratigraphic studies by Pauly et al. (2012a) and Möller et al. (2015).

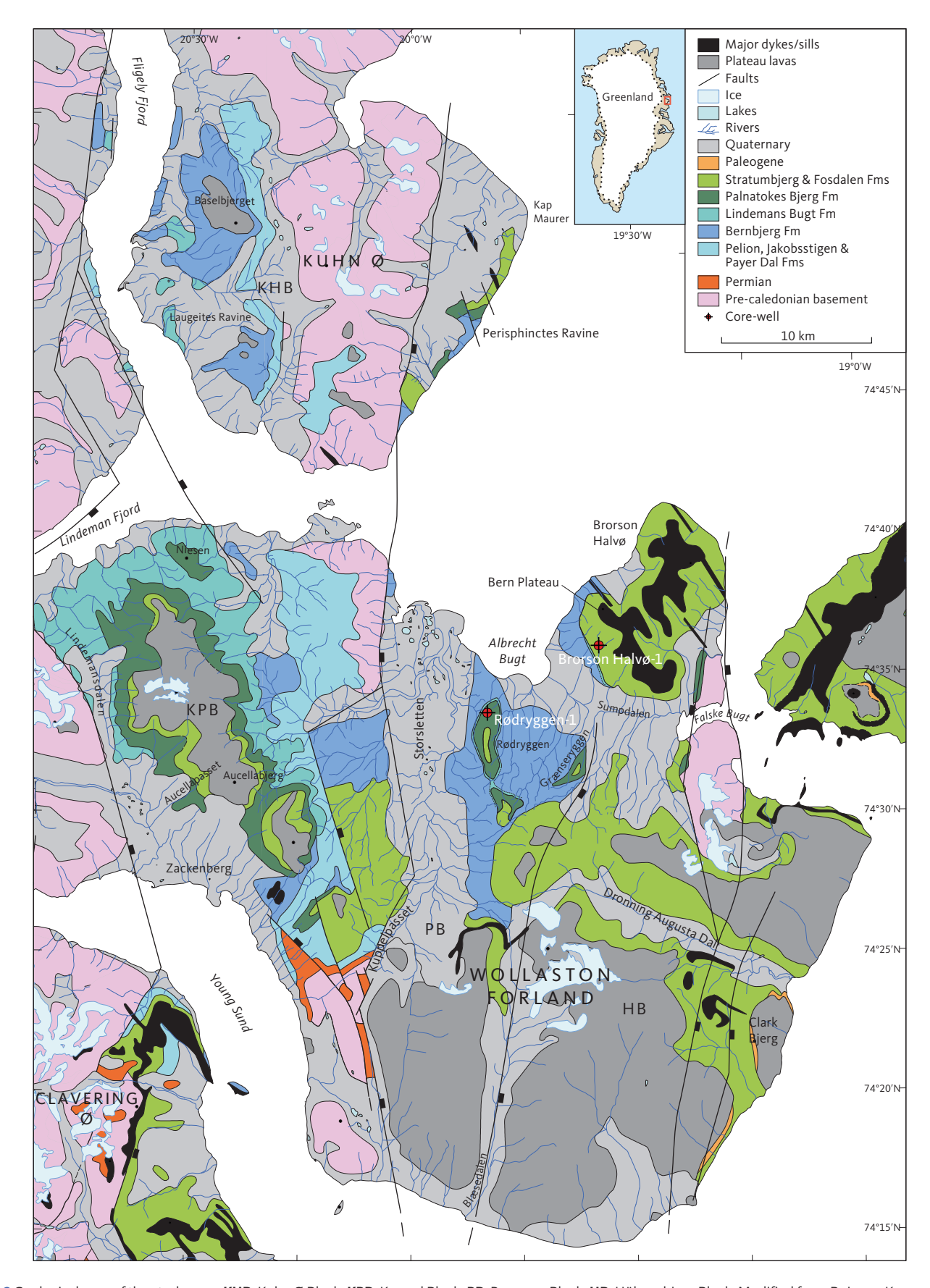


Fig. 2 Geological map of the study area. KHB: Kuhn Ø Block. KPB: Kuppel Block. PB: Permpas Block. HB: Hühnerbjerg Block. Modified from Bojesen-Koefoed et al. (2023a, this volume, fig. 1).

## 3. Geological framework and lithostratigraphy

The Upper Jurassic - lowermost Cretaceous in the East Greenland Rift Basin was deposited in a series of sub-basins between Jameson Land in the south at c. 70.5°N to Store Koldewey at c. 76.5°N in the north (Fig. 1; Surlyk 2003). The southernmost sub-basin in the Jameson Land area acted as an extensive, gently tilted platform subsiding asymmetrically with greatest subsidence to the west. North of Jameson Land, especially in the Wollaston Forland - Kuhn Ø area, basins are characterised by block faulting and tilting, initiated in the Middle Jurassic and culminating in the latest Jurassic (Volgian), with segmentation into narrower, strongly tilted fault blocks (Surlyk 1978). Middle-Late Jurassic deposition records an overall transgression and backstepping of the depositional system (Surlyk 1977, 1978). The Middle Jurassic sandstone-dominated succession is thus overlain by Upper Jurassic offshore mudstones with a diachronous boundary, younging towards the north. The upper Oxfordian - lower Volgian comprises a 500-600 m thick black mudstone succession in the study area. Highest sea level and maximum transgression was in the Kimmeridgian, but greatest water depths were likely reached during the Volgian rift climax, in the deepest parts of westerly tilted half-grabens (Surlyk 2003). Thick successions of very coarse, deep marine, clastic material were deposited in half-graben basins along the western, major fault scarp but rapidly passed into finer clastic deposition towards the east away from the scarp (Surlyk 1978). The more easterly situated half-graben segments are almost all covered by younger successions. The Late Jurassic stratigraphy and deposition of those segments are thus poorly understood but are addressed by Hovikoski et al. (2023a, this volume) and in the present study based on the new core data obtained from the Rødryggen-1 and Brorson Halvø-1 cores. Rifting waned in the earliest Cretaceous (Ryazanian-Hauterivian) when half-graben sediment prisms were draped by relatively finer-grained sediments (Surlyk 2003). The following early to mid-Cretaceous (Barremian – early Albian) period was characterised by tectonic quiescence, thermal subsidence and deposition of a relatively thick succession of dark, marine siltstones and mudstones.

Both boreholes were initiated in the Lower Cretaceous and reach down into the Upper Jurassic. Together they penetrate three major lithostratigraphic units, the Vardekløft, Wollaston Forland and Brorson Halvø Groups (Figs 3, 4). Both cores exhibit the Bernbjerg, Lindemans Bugt and Palnatokes Bjerg Formations. The Bernbjerg Formation represents the upper part of the Upper Jurassic (Oxfordian – lower Volgian) tectonostratigraphic unit, reflecting increased rifting and marine flooding (J2.4 in Surlyk 2003). The Lindemans Bugt and Palnatokes Bjerg Formations of the Wollaston Forland Group represent the

culmination of rifting and tilting of fault blocks (J2.5) and the end of rifting and regional drowning (J2.6), respectively. In Rødryggen-1, coring began within the Albrechts Bugt Member, the lower member of the Palnatokes Bjerg Formation. The Brorson Halvø-1 core was initiated stratigraphically higher and contains the Rødryggen Member, the upper member of the Palnatokes Bjerg Formation and the overlying Stratumbjerg Formation. The Stratumbjerg Formation is the lower part of an upper Hauterivian – mid-Albian (Cretaceous) tectonostratigraphic unit defined by Bjerager *et al.* (2020).

### 3.1 Bernbjerg Formation (Vardekløft Group)

The upper Oxfordian - lower Volgian Bernbjerg Formation is a widespread depositional unit in North-East Greenland cropping out on Store Koldewey in the north to Traill Ø in the south (Surlyk et al. 2021 and references therein). Its type and reference sections are located in Wollaston Forland and south-western Kuhn Ø (Surlyk 1977), where the formation reaches a maximum thickness of 500-600 m (Surlyk 1977; Surlyk & Clemmensen 1983; Alsgaard et al. 2003). The Bernbjerg Formation sharply overlies either the Payer Dal Formation or the Jakobsstigen Formation (Surlyk et al. 2021). Neither the Rødryggen nor the Brorson Halvø cores reached the lower boundary of the Bernbjerg Formation. The nature of the upper contact to the Wollaston Forland Group depends on location within a tilted fault block; in the downfaulted part of a fault block, the boundary is conformable, whereas the contact is an angular unconformity on the elevated fault block crests (Surlyk 1977, 1978, 1991). Lithologically, the formation is characterised mainly by dark grey to black mudstone and interlaminated sandstone and mudstone. Sandstone beds, 5–50 cm thick, may locally show current and wave-ripple cross-stratification (Surlyk 1977). Surlyk (2003) referred the lowermost heterolithic unit to the Ugpik Ravine Member. The cores described here from the Rødryggen-1 and Brorson Halvø-1 boreholes reveal only the mud-dominated upper part of the Bernbjerg Formation.

## 3.2 Lindemans Bugt Formation (Wollaston Forland Group)

Prior to this study, middle Volgian – lower Ryazanian deposits were not known to crop out in the tilted Permpas Block, and the Palnatokes Bjerg Formation was considered to rest directly on the Bernbjerg Formation. The outcropping Bernbjerg Formation forms a badland area east of the Rødryggen ridge (Figs 2, 5) towards the Grænseryggen ridge. To the north, the Bernbjerg Formation is poorly exposed in the foot of the south-western slopes of the Bern Plateau (Fig. 6) separated from the badland exposures in the Rødryggen–Grænseryggen

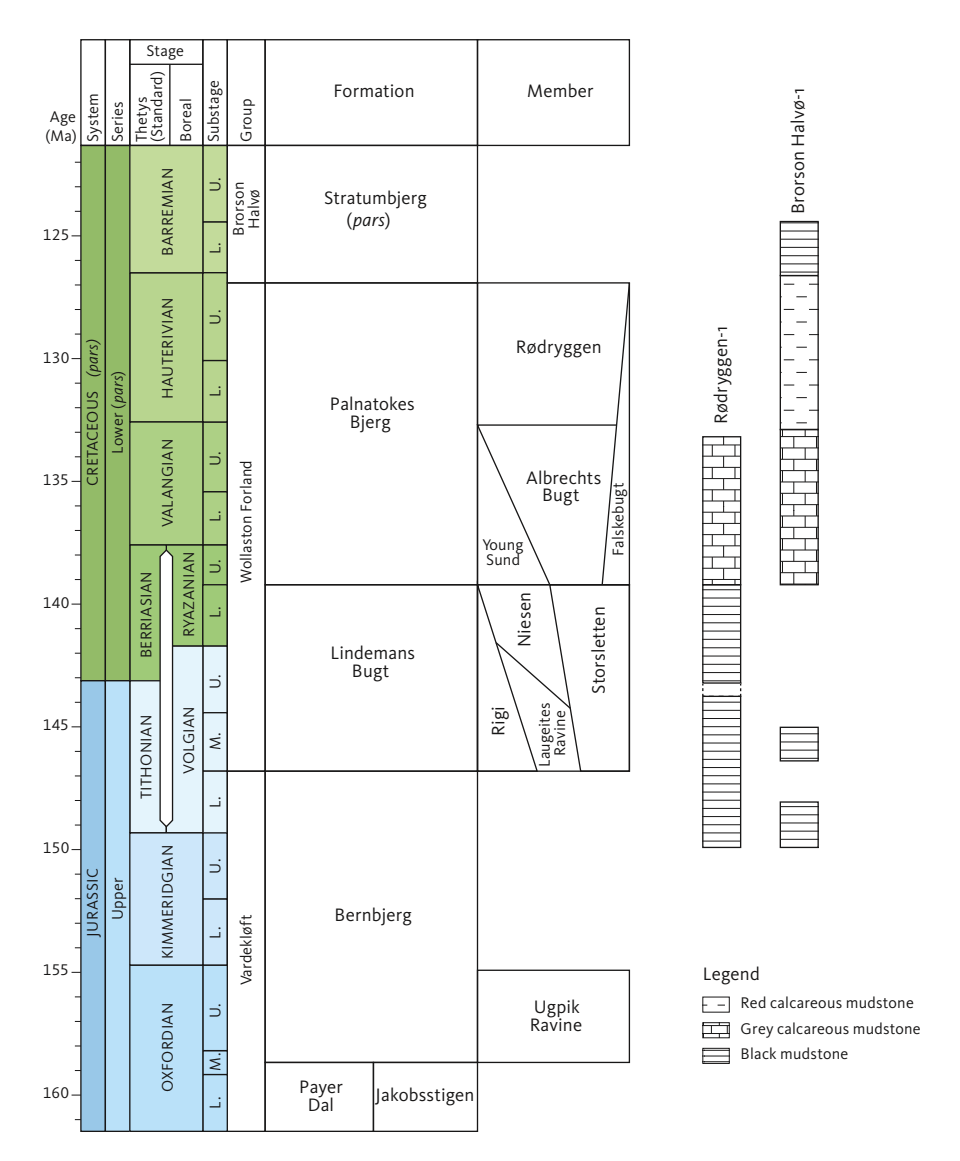


Fig. 3 Oxfordian-Barremian lithostratigraphy for Wollaston Forland. L.: lower. M.: middle. U.: upper.

area by the Sumpdalen valley (Fig. 2). Vischer (1943) and Maync (1947) reported Kimmeridgian black shales with ammonites, some referred to Amoeboceras, others unidentified, from south of Albrechts Bugt and south and north of Sumpdalen. The upper part of the Bernbjerg Formation was thus considered removed by 'pre-Valanginian' erosion, i.e. pre-Palnatokes Bjerg Formation, during the rift culmination at the Jurassic-Cretaceous transition (Surlyk 1977, 1978). Maync (1947) reported the Kimmeridgian to be directly overlain by 'Aptian' strata in places, i.e. the Stratumbjerg Formation. The poorly exposed mudstones below the Albrechts Bugt Member at the foot of the Rødryggen ridge (and at Brorson Halvø) were thus also considered Upper Jurassic Bernbjerg Formation, in older terminology the so-called Black Series (e.g. Maync 1947; Koch & Haller 1971; Surlyk 1978). However, the palynostratigraphic ages obtained in the present work from these exposed strata demonstrate the presence of middle Volgian - lower Ryazanian mudstones in this area, as confirmed by the borehole data. The equivalent and comparable deposits in terms of age and lithology to the west are the fine-grained Laugeites Ravine and, particularly, Niesen Members of the Lindemans Bugt Formation. Those units are, however, confined to the westernmost tilted Kuppel and Kuhn Ø Blocks (Surlyk 1978) and are related to distal parts of fan deltas. We therefore consider the middle Volgian - lower Ryazanian mudstones in the cored sections on the Permpas Block as separate, detached from those other members, and thus group them into a new member, the Storsletten Member (Fig. 3), as defined formally here (Section 3.1.2.1). The unit is probably distributed throughout the Permpas Block, which was blocked from receiving the coarse-grained sediments that dominated deposition along the main fault to the west, since it was separated by the elevated block crest of the Kuppel Block and the Kuhn Block. Other tilted block basins separated from the westernmost blocks are also likely to have been dominated by mud deposition during the middle Volgian - early Ryazanian.

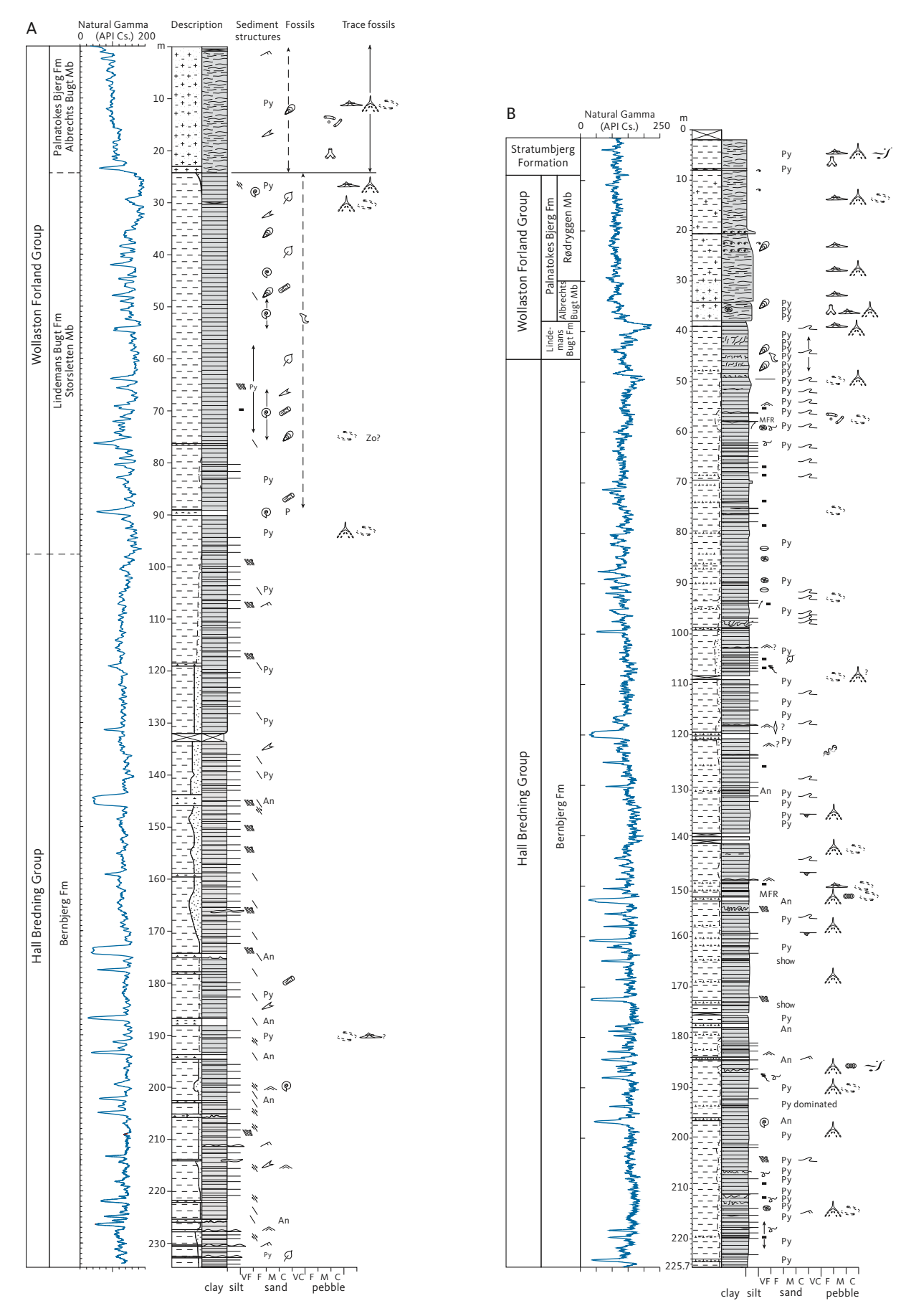


Fig. 4 Sedimentological logs of (A) the Rødryggen-1 core, (B) the Brorson Halvø-1 core and (C) legend to both logs. API Cs.: American Petroleum Institute units. VF: very fine. F: fine. M: medium. C: coarse. VC: very coarse.

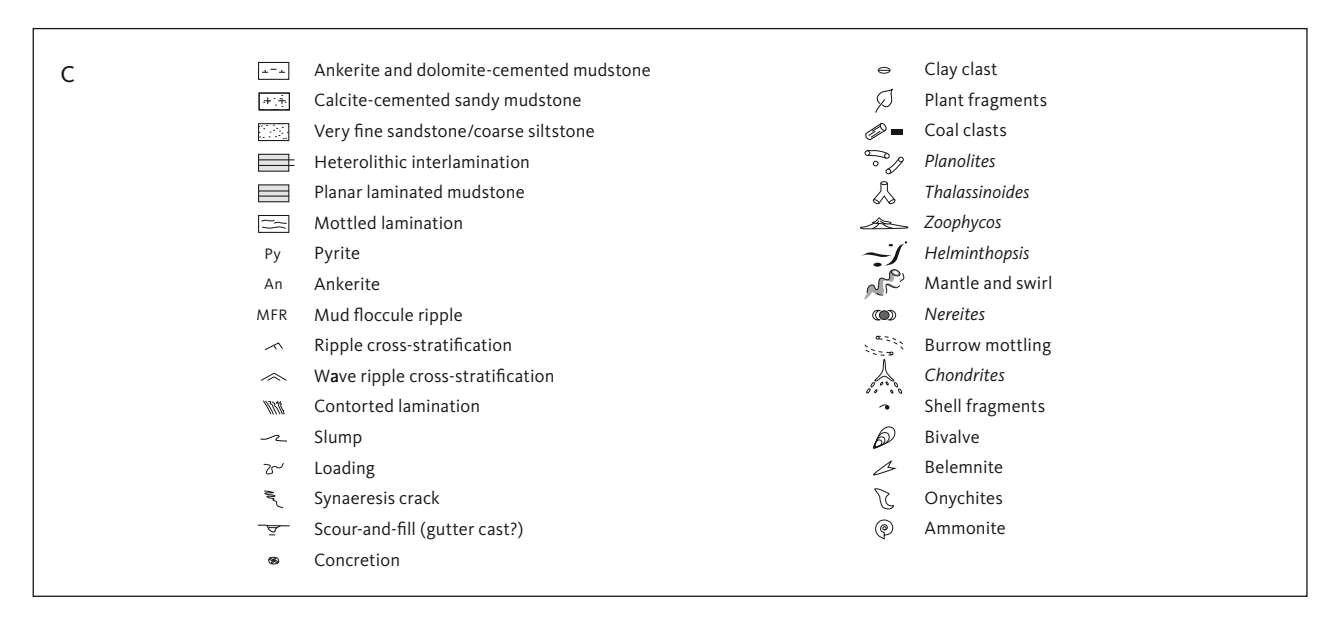


Fig. 4 (Continued) Sedimentological logs of (A) the Rødryggen-1 core, (B) the Brorson Halvø-1 core and (C) legend to both logs. API Cs.: American Petroleum Institute units. VF: very fine. F: fine. M: medium. C: coarse. VC: very coarse.

### 3.2.1 Storsletten Member

new member

History. The member was not known when the Lindemans Bugt Formation was erected (Surlyk 1978). The formation encompasses mudstones deposited on the Permpas Block during the tectonostratigraphic phase J2.5 in Surlyk (2003).

Type section. The Rødryggen-1 core between 97 and 24.4 m depth (Fig. 4A). Position: N 74°32.561′, W 19°50.924′ (Figs 2, 5).

Reference section. The Brorson Halvø-1 core between 45.5 and 37.5 m depth (Fig. 4B). Position: N 74°35.227′, W 19°34.327′ (Figs 2, 6).

Thickness. The thickness of the member varies depending on the position on the tilted fault block. The unit is thickest where it is most complete, in the deeper, western part of the half-graben basin. It is 72.5 m thick in the Rødryggen-1 core (Fig. 4A). Due to major hiatuses, it is only 8 m thick in the Brorson Halvø-1 core (Fig. 4B).

Lithology. Dark grey to black, laminated to structureless mudstone, commonly rich in pyrite and marine fossils. Slump folding is common locally (Brorson Halvø-1 core); for lithological and diagenesis data, see Hovikoski et al. (2023a, this volume) and Olivarius et al. (2023, this volume), respectively. The member differs from the other coeval members by its higher content of organic carbon and the oxygen-restricted nature of its deposits (Bojesen-Koefoed et al. 2023b, this volume). *Fossils*. Ammonites, buchiid bivalves, common fragments of inoceramids and palynomorphs.

Depositional environment. Deep oxygen-restricted basin and slope, below storm wave base. The oxygen-restricted character is demonstrated by inorganic and organic geochemistry as well as the scarcity of bioturbation (Bojesen-Koefoed *et al.* 2023b, this volume; Olivarius *et al.* 2023, this volume; Hovikoski *et al.* 2023b).

Boundaries. The boundary between the Bernbjerg Formation and the Lindemans Bugt Formation is lithologically transitional in the type section and occurs between 125 and 76 m (Fig. 4A). The formation boundary in the type section is placed at 97 m, where the gamma-ray values increase to c. 200 API (American Petroleum Institute units) for the first time (Bojesen-Koefoed et al. 2023b, this volume). The formation change is also recognisable as gradational facies change from mudstone showing silt-clay interlamination to laminated clayey mudstone, increasing pyrite and fossil content and locally increasing slump-folding. Moreover, the formation change is well-expressed in a variety of source-rock characteristics such as increasing Hydrogen Index, S2 and C<sub>30</sub> desmethyl sterane values, reflecting increasing marine organic matter content (Bojesen-Koefoed et al. 2023b, this volume). The upper boundary towards the Albrechts Bugt Member of the Palnatokes Bjerg Formation is gradational in the Rødryggen-1 core, whereas in the Brorson Halvø-1 core, the boundary is erosional and represents a hiatus (Fig. 4). The gradation occurs within 1 m in the type section,

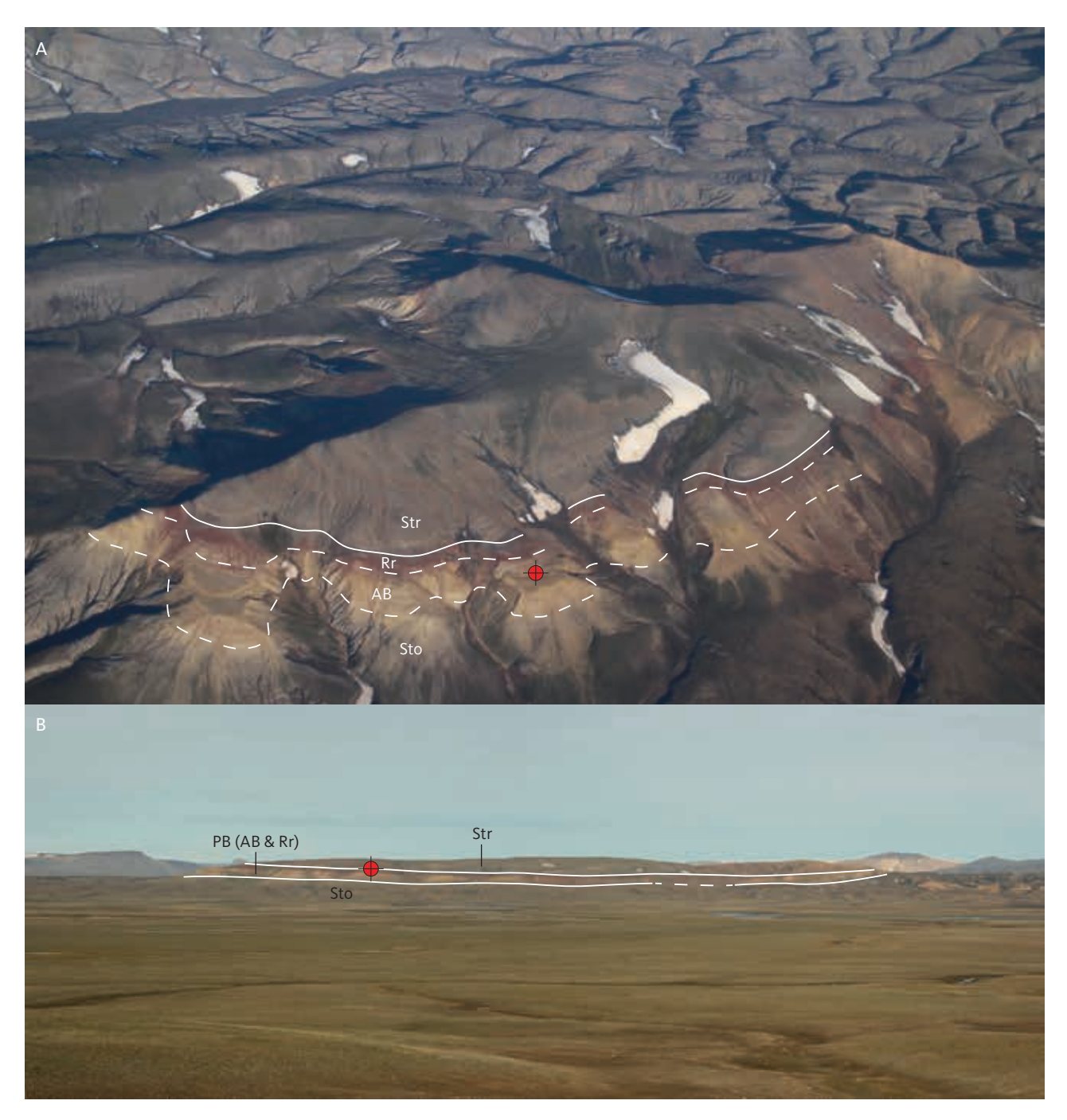


**Fig. 5** Views of the Rødryggen-1 drill site. **(A)** Oblique aerial view, towards the south-east of the Rødryggen ridge showing the outcropping units and the position of the Rødryggen-1 drill site (**red dot**) situated on a plateau within the yellowish weathering Albrechts Bugt Member. The badlands area in the background is the Upper Jurassic Bernbjerg Formation. **(B)** View across the Storsletten plain towards the east and the Rødryggen ridge. **AB**: Albrechts Bugt Member. **PB**: Palnatokes Bjerg Formation. **Rr**: Rødryggen Member. **Sto**: Storsletten Member. **Str**: Stratumbjerg Formation.

25.5–24.4 m (Fig. 4A). The boundary is readily recognisable by an abrupt decrease in gamma-ray values, increasing matrix carbonate content, a change in matrix colour from black to light grey, increasing bioturbation intensity and a change in fossil content with nannofossils, foraminifera and *Buchia* shells becoming abundant.

*Distribution*. Recorded only in the Rødryggen-1 and Brorson Halv-1 core wells and in restricted exposures close to the well sites.

Chronostratigraphy. Middle Volgian Dorsoplanites primus ammonite chronozone – lower Ryazanian upper Gochteodinia villosa villosa dinoflagellate cyst zone.

## 3.3 Palnatokes Bjerg Formation (Wollaston Forland Group)

The upper syn-rift to early post-rift succession is represented by the Palnatokes Bjerg Formation. It contains the Albrechts Bugt Member, overlain by the

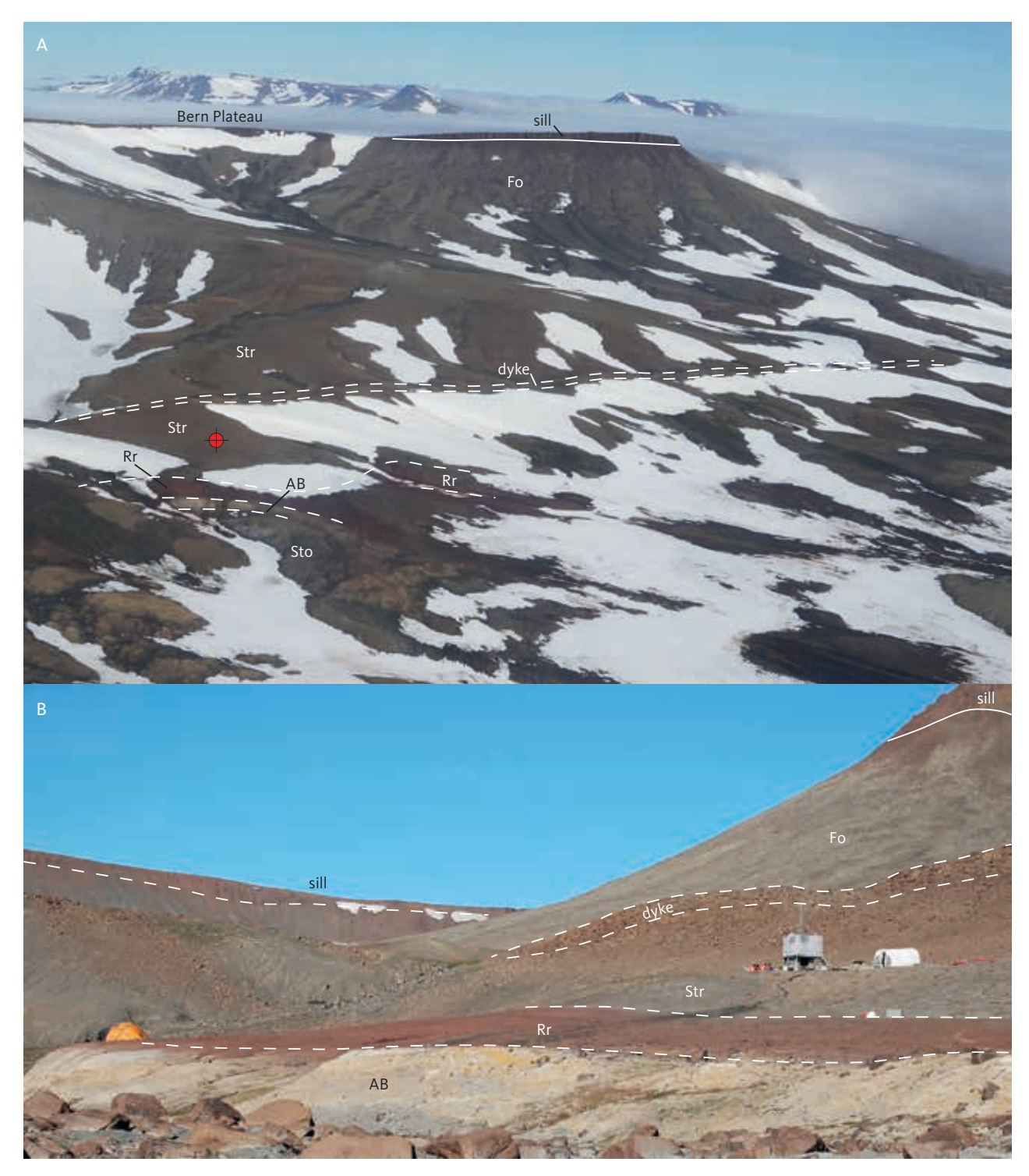


**Fig. 6** Views of the Brorson Halvø-1 drill site. **(A)** Oblique aerial view of the Brorson Halvø-1 drill site (**red dot**) at the foot of the southern slope of Bern Plateau, SW Brorson Halvø. **(B)** Geology around the drill site. Pale, yellowish weathering of the Albrechts Bugt Member is seen sharply overlain by the Rødryggen Member (both Palnatokes Bjerg Formation), overlain by the Stratumbjerg Formation. A roughly SE–NW-oriented doleritic dyke intersects the Stratumbjerg Formation and a doleritic sill caps the Bern Plateau (sill; upper right). The drill site was situated on a small plateau in the lower part of the Stratumbjerg Formation (grey tent on platform). Photo: A. Ryge. **AB**: Albrechts Bugt Member. **Fo**: Fosdalen Formation. **Rr**: Rødryggen Member. **Sto**: Storsletten Member. **Str**: Stratumbjerg Formation.

Rødryggen Member. The Young Sund and Falske Bugt Members are coarse-grained units that developed in western and eastern parts of the basin, respectively, and were not encountered in the wells drilled in the Permpas Block.

### 3.3.1 Albrechts Bugt Member

The Albrechts Bugt Member consists of calcareous sandy, light grey to yellowish mudstone with abundant calcareous concretions (Surlyk 1978; Surlyk *et al.* 2021). At outcrop, the member weathers in conspicuous

bright, yellow colours that contrast strongly with the essentially grey colour of the fresh and unweathered rock. The deposits are typically highly bioturbated and rich in *Buchia* bivalves, belemnites and ammonites (see also Alsen 2006).

The lithological contact between the Lindemans Bugt Formation and Albrechts Bugt Member of the Palnatokes Bjerg Formation is gradational in the Rødryggen-1 core and sharp in the Brorson Halvø-1 core. The boundary is readily recognisable by an abrupt decrease in gamma-ray (GR) values, increasing matrix carbonate and sand content, decreasing clay content, a change in matrix colour from black to light grey, increasing bioturbation intensity and a change in fossil content, with nannofossils, foraminifera and Buchia shells becoming abundant. The boundary is placed at 24.4 m in the Rødryggen-1 core and at 37.5 m in the Brorson Halvø-1 core (Fig. 4). The thickness of the unit is laterally variable; it reaches a maximum thickness of c. 300 m at Mt. Niesen (Wollaston Forland), where it interfingers with the fine-grained facies of the Young Sund Member. Towards the east, on the Permpas Block, the member rapidly pinches out to c. 30 m (Surlyk 1978). The upper boundary is transitional when overlain by the red mudstones of the Rødryggen Member.

## 3.3.2 Rødryggen Member (only in the Brorson Halvø-1 core)

The Rødryggen Member consists of red, massive or laminated hematitic mudstones with intercalated fine sandy yellow mudstones (Surlyk 1978; Surlyk *et al.* 2021). The contact between the Albrechts Bugt and Rødryggen Members is transitional and interlayered within a 70 cm interval in the Brorson Halvø-1 core. The change is visible as a gradational change in colour from light grey to red; the boundary is placed at 30.0 m where the matrix turns permanently red (Fig. 4B). Moreover, the Rødryggen Member differs from the Albrechts Bugt Member in microfossil and macrofossil content with foraminifers and inoceramid shell becoming more common.

## 3.4 Stratumbjerg Formation (Brorson Halvø Group; only in Brorson Halvø-1 core)

The Stratumbjerg Formation marks a return to deposition of dark, fine-grained sediments in an oxygen-restricted environment below storm wave base during the tectonically quiescent phase after the Volgian rift climax and Ryazanian–Valanginian late rift phases. The unit is widely distributed throughout North-East Greenland, from Traill Ø in the south to Store Koldewey in the north (Bjerager *et al.* 2020). The boundary to the underlying Rødryggen Member is gradational within an 80 cm interval in the Brorson Halvø-1 core. The boundary is placed at 8.7 m (top of transition), where the bioturbated grey

mudstones no longer interfinger with reddish mudstones (Fig. 4B).

## 4. Biostratigraphic methods and approach

The Rødryggen-1 borehole is 234.5 m deep, and the Brorson Halvø-1 borehole is 225.7 m deep. Both boreholes were fully cored, with recoveries of 99%. The core diameter in both cores is 42 mm. Each core is essentially treated as one sample and assigned codes with the prefix 'GEUS'. The Rødryggen-1 well is designated as GEUS 517001, and the Brorson Halvø-1 is designated as GEUS 517003. Sub-numbers were assigned to the extracted material, which was sampled for a suite of core analysis, including biostratigraphy, geochemistry, rock properties and provenance (see also Bojesen-Koefoed et al. 2023b, this volume; Olivarius et al. 2023, this volume). For simplicity, in this study, we only refer to the levels or borehole depths (below surface) for the respective subsamples, for example in range charts, tables and figure captions.

### 4.1 Macrofossils

Before the cores were subject to slabbing and sampling for the standard analytical programme, they were examined for macrofossils. Examination for macrofossils was particularly directed to where the core had naturally split along bedding planes, commonly along planes with fossils, so that all ends of the individual core pieces were inspected. Most of the fossils are fragmented. Identification also suffers from the relatively small diameter of the core such that only small portions of a fossil were usually available for study, and thus fewer diagnostic characters are available in these cases.

## 4.2 Palynomorphs and calcareous nannofossils

Mudstones for palynostratigraphic analysis were initially sampled at an even spacing throughout the core. Upon initial biostratigraphic screening, additional material was subsequently sampled in selected intervals, for example, across lithostratigraphic or chronostratigraphic boundaries such as the Jurassic–Cretaceous boundary interval, to obtain higher biostratigraphic subdivision and precision. The calcareous mudstone intervals of the Palnatokes Bjerg Formation were sampled specifically for calcareous nannofossil stratigraphy. Each sample for palynomorphs and nannofossil analysis comprised a split/slabbed, 4 to 6 cm thick core interval. The well depth of a mudstone sample is the medium point of the thickness of the sample.

The palynological preparation methods of the crushed sample material include processing with HCl,

HF, oxidation with HNO $_3$  and heavy-liquid separation. Samples from the Bernbjerg and Lindemans Bugt Formations contain abundant marine and terrestrial organic matter, which required repeated oxidation and ultrasonic treatment to release identifiable dinoflagellate cysts, with slides produced after each repeated preparation step. When a state of sufficient oxidation was reached, the organic residue was sieved with a 21  $\mu m$  filter. The coarser fraction was swirled and eventually mounted on glass slides using a glycerine jelly medium.

The dinoflagellate cyst content was analysed using a normal light microscope. All dinoflagellate cysts in one slide from each sample were counted to perform a semiquantitative analysis. This approach applies to dark mudstone intervals, whereas the diversity and abundance in the very low organic, calcareous mudstones of the Palnatokes Bjerg Formation do not allow for comparison with data from the dark mudstone units. In addition to dinoflagellate cysts, acritarchs and phrasinophycean and freshwater algae were also counted. The palynological taxonomy follows the Lentin and Williams Index of Fossil Dinoflagellates, 2004 Edition (Fensome & Williams 2004), unless otherwise indicated by author references.

Nannofossil slides were prepared using the simple smear slide technique of Bown & Young (1998). Where samples appeared to be barren with respect to calcareous nannofossils, three length traverses of the smear slide were examined. Where a particular species of nannofossil dominated the slide, one length traverse was counted, and then two further lengths were checked for rare forms. Biostratigraphic ranges of nannofossils are adapted from Burnett (1998), Bown et al. (1998) and Pauly et al. (2012a).

## 4.3 Stratigraphic nomenclature and methodology

The Tithonian and Berriasian are the standard stages for the uppermost Jurassic and lowermost Cretaceous, respectively, as defined in the Tethyan Realm. Due to pronounced faunal provincialism around the system boundary and the recognition of faunally clearly separated Tethyan and Boreal Realms, a parallel stage nomenclature has evolved for the Boreal area. Until improved correlation between Boreal and Tethyan areas is obtained, a Boreal subdivision and stage nomenclature are commonly adopted in Greenland, including in this study. This study also follows the stratigraphic concept commonly applied for Middle-Upper Jurassic stratigraphic studies in East Greenland, which considers ammonite zones as chronozones, representing rock units that are also identifiable by means of fossil groups other than ammonites. The East Greenland Upper Jurassic ammonite zonation is thus closely integrated with the dinoflagellate cyst record (see also discussion in Alsen & Piasecki 2018 and references therein).

### 4.4 Rødryggen-1 core

The Rødryggen-1 core was initially sampled at 37 levels for palynostratigraphy and nannofossil stratigraphy with a standard c. 10 m spacing, but with somewhat denser sampling in the lowermost and uppermost parts of the core. Subsequent sampling at critical levels resulted in a total of 63 sampled levels being analysed for palynostratigraphy. The dark mudstones of the Bernbjerg, Lindemans Bugt and Stratumbjerg Formations were primarily dated with palynostratigraphy aided by ammonite stratigraphy. The pale, calcareous mudstones of the Albrechts Bugt Member (Palnatokes Bjerg Formation) were dated by a combination of palynostratigraphy and calcareous nannofossil stratigraphy.

Ammonites occur only in two intervals, between 225 and 197 m, and in a c. 65 m thick interval between 90 and 26 m (Fig. 4A). The few ammonites in the lower interval are of little biostratigraphic value (Table 1), so age-significant ammonites are essentially restricted to the Storsletten Member of the Lindemans Bugt Formation. No ammonites were found in the interval between 90 and roughly 200 m. The latter interval is characterised by finely laminated dark mudstones, which theoretically have a good preservation potential for fossils. Ammonites are thus probably present. However, the interval is intensely fractured hampering both the preservation and detection of fossils.

Ten samples from the Rødryggen-1 core were examined for nannofossil content. Seven mudstone samples from the Bernbjerg and Lindemans Bugt Formations were almost barren with respect to calcareous nannofossils. Thus, only the three samples from the calcareous mudstones of the Albrechts Bugt Member (Palnatokes Bjerg Formation) yielded relatively good nannofossil recovery.

### 4.5 Brorson Halvø-1 core

The Brorson Halvø-1 core was sampled for palynostratigraphy and nannofossil stratigraphy with default sample spacing of *c*. 10–15 m, a slightly less dense sampling strategy than used for the Rødryggen-1 core. Subsequent closer sampling was undertaken in lithostratigraphic and chronostratigraphic boundary intervals to obtain higher precision, for example, to ascertain the stratigraphic significance of hiatuses.

Well-preserved ammonites are absent in the core and the integration of ammonite and palynostratigraphy, which was of great benefit in the analysis of the Rødryggen-1 core, could not be undertaken. The biostratigraphy of the core receives only minor support from the

 Table 1 Summary of macrofossils recorded in the Rødryggen-1 core.

| Depth    | GEUS 517001 and sub-sample number | MGUH no.ª | Figure no. (this study) | Description / taxononomy                            | Faunal horizon<br>sensu Callomon &<br>Birkelund (1982) | Ammonite stratigraphy      |
|----------|-----------------------------------|-----------|-------------------------|---|--|----------------------------|
| 27.73 m  | -401                              | 34200     | 10.S                    | Hectoroceras Sp.                                    |  | H. kochi Zone              |
| 35.80 m  | -402                              |           |                         | bivalve   |  | P. maynci Zone             |
| 37.49 m  | -438                              | 34199     | 10.R                    | cf. Praetollia maynci Spath                         |  | P. maynci Zone             |
| 40.22 m  | -437                              |           |                         | Buchia bivalve                                      |  | S. (Sw.) primitivus Zone   |
| 43.18 m  | not sampled                       |           |                         | Ammonite indet.                                     |  | S. (Sw.) primitivus Zone   |
| 43.21 m  | -403                              | 34198     | 10.Q                    | Subcraspedites (Swinnertonia)<br>sp. juv.           |  | S. (Sw.) primitivus Zone   |
| 45.37 m  | -404                              | 34197     | 10.P                    | S. (Swinnertonia) cf. subundulatus<br>Swinnerton    |  | S. (Sw.) primitivus Zone   |
| 45.73 m  | -405                              |           |                         | bivalve   |  | (P. exoticus Zone)         |
| 47.20 m  | -406                              | 34196     | 10.0                    | aptychus  |  | (P. exoticus Zone)         |
| 47.52 m  | -407                              |           |                         | bivalve   |  | (P. exoticus Zone)         |
| 47.94 m  | -436                              |           |                         | ?Praechetaites Sp.                                  |  | (P. exoticus Zone)         |
| 48.09 m  | -435                              |           |                         | Buchia bivalve                                      |  | (P. exoticus Zone)         |
| 48.37 m  | -408                              | 34195     | 10.N                    | Ammonite indet.                                     |  | (P. exoticus Zone)         |
|          |                                   |           |                         | cf. Praechetaites exoticus                          |  |                            |
| 48.54 m  | -427                              | 34194     | 10.M                    | (Shulgina) cf. Praechetaites exoticus               |  | ( <i>P. exoticus</i> Zone) |
| 48.82 m  | -434                              | 34193     | 10.L                    | (Shulgina)  |  | (P. exoticus Zone)         |
| 49.94 m  | -433                              |           |                         | ammonite; indeterminate<br>juvenile                 |  | (P. exoticus Zone)         |
| 50.14 m  | -432                              |           |                         | cf. Praechetaites exoticus<br>(Shulgina)            |  | (P. exoticus Zone)         |
| 51.55 m  | -409                              | 34192     | 10.K                    | Laugeites cf. planus<br>Mesezhnikov                 | M 47   | L. groenlandicus Zone      |
| 52.30 m  | -431                              |           |                         | ammonite fragment; indeterminate                    |  | L. groenlandicus Zone      |
| 52.50 m  | -430                              |           |                         | L. cf. biplicatus                                   | M 47   | L. groenlandicus Zone      |
| 52.82 m  | -410                              | 34191     | 10.J                    | Laugeites cf. intermedium<br>Donovan                |  | L. groenlandicus Zone      |
| 53.27 m  | -429                              |           |                         | ammonite aptychi                                    |  | L. groenlandicus Zone      |
| 53.67 m  | -411                              | 34190     | 10.1                    | Laugeites cf. biplicatus<br>Mesezhnikov             | M 47   | L. groenlandicus Zone      |
| 54.53 m  | -412                              |           |                         | ?Laugeites Sp.                                      |  | L. groenlandicus Zone      |
| 55.25 m  | -413                              |           |                         | Ammonite indet.                                     |  | E. pseudapertum Zone       |
| 55.98 m  | -414                              | 34189     | 10.H                    | Epipalliceras cf. pseudapertum<br>Spath             | M 42   | E. pseudapertum Zone       |
| 62.43 m  | -415                              | 34188     | 15.B                    | micro-onychites                                     |  | D. gracilis Zone           |
| 66.54 m  | -416                              |           |                         | belemnite   |  | D. gracilis Zone           |
| 66.84 m  | -417                              |           |                         | Ammonite indet.                                     |  | D. gracilis Zone           |
| 70.06 m  | -418                              | 34187     | 10.G                    | Dorsoplanites jamesoni Spath                        | M 40?  | D. gracilis Zone           |
| 74.03 m  | -419                              | 34186     | 10.F                    | Pavlovia cf. corona Callomon & Birkelund            | M 37   | D. liostracus Zone         |
| 74.20 m  | -420                              | 34185     | 10.E                    | Dorsoplanites aff. liostracus                       | M 37   | D. liostracus Zone         |
| 75.43 m  | -421                              | 34184     | 10.D                    | Pavlovia cf. variocostata Callo-<br>mon & Birkelund | M 35   | P. communis Zone           |
| 89.26 m  | -422                              | 34183     | 15.A                    | mega-onychites                                      |  | D. primus Zone             |
| 89.30 m  | -423                              | 34182     | 10.C                    | Dorsoplanites primus Callomon<br>& Birkelund        | M 31   | D. primus Zone             |
| 90.85 m  | -424                              | 34181     | 10.B                    | Dorsoplanites sp.                                   |  | D. primus Zone             |
| 199.42 m | -425                              |           |                         | Ammonite indet.                                     |  | ?                          |
| 227.72 m | -426                              | 34180     | 10.A                    | Amoeboceras? sp.                                    |  | ?                          |

<sup>&</sup>lt;sup>a</sup>The specimens are stored in the Palaeontology Type Collection at the Natural History Museum of Denmark and each labelled with an MGUH number – Museum Geologica Universitas Hafniensis.

macrofossils collected in exposures near the drill site, where Alsen (2006) recorded the ammonite fauna in the Albrechts Bugt and Rødryggen Members.

A total of 41 samples were analysed for palynomorphs: 19 in the Bernbjerg Formation, 7 in the Lindemans Bugt Formation (Storsletten Member), 12 in the Palnatokes Bjerg Formation and 3 in the Stratumbjerg Formation. From the upper part of the Brorson Halvø-1 core (40.27 to 6.16 m), analysis of calcareous nannoplankton was applied in 19 samples. The lowest sample represents dark mudstone of the Lindemans Bugt Formation and is barren, as are equivalent black mudstone samples from the Rødryggen-1 core. In the remaining samples, the preservation of the calcareous nannoplankton varies from good to moderate. Most samples of the Albrechts Bugt Member yield well-preserved calcareous nannoplankton. The calcareous nannoplankton in the Rødryggen Member shows good to moderate preservation and overgrowth by iron oxide minerals. Surprisingly, the organic-rich grey mudstones of the Stratumbjerg Formation also yielded well-preserved calcareous nannoplankton assemblages.

## 5. Biostratigraphy of the Rødryggen-1 core

The biostratigraphic subdivision of the Rødryggen-1 core is described from total depth (TD) at 234.40 m upwards. The location of bulk-rock samples for palynostratigraphy is seen in the charts illustrating the distribution and ranges of dinoflagellate cyst taxa, palyno events and calcareous nannofossil taxa (Figs 7, 8). The recorded ammonite levels are listed in Table 1 and illustrated in a stratigraphic distribution chart (Fig. 9). Selected ammonites and dinoflagellate cysts are illustrated in Figs 10–13.

## 5.1 *Aulacostephanus eudoxus* Chronozone (234.40 m (TD) – 220.51 m)

Fossils. The recognition of the zone is based on its dinoflagellate cyst record. One poorly preserved ammonite is a possible Amoeboceras (227.72 m; Fig. 10A; Table 1). The base of the zone is arbitrarily placed at the base of the core (at TD). The dinoflagellate cyst assemblage is relatively diverse, and cysts are abundant. The zone is dominated by Perisseiasphaeridium pannosum, Paragonyaulacysta capillosa and Cribroperidinium spp., whereas Epiplosphaera reticulospinosa and Paragonyaulacysta borealis are common taxa at discrete levels within the zone.

Biostratigraphy. Abundant *P. pannosum* is reported to range from ammonite faunal horizon M 20, at the base of the *Aulacostephanus eudoxus* Zone, to a level between faunal horizons M 22 and M 23 near the top of the *A.* 

eudoxus Zone in Milne Land (Fig. 14; Piasecki 1996). P. pannosum was used as a key taxon of the A. eudoxus Zone in the Blokelv-1 core in Jameson Land (Alsen & Piasecki 2018) and the Brorson Halvø-1 core (herein). Rhycodiniopsis cladophora has its uppermost occurrence at M 21 in Milne Land (Piasecki 1996). P. borealis is common in these assemblages and is present from 234.41 m, but it is known to range much deeper, to the P. baylei Zone level in Milne Land (Piasecki 1996). Dingodinium minutum, Gonyaulacysta jurassica, Taeniophora iunctispina and possibly Nannoceratopsis pellucida occur scattered and are rare in this chronozone, either as last occurrences or reworked from strata below.

Age. Kimmeridgian, Late Jurassic.

Organic matter. Amorphous kerogen (often termed AOM) together with a large proportion of terrestrial organic material from higher land plants, especially degraded black grains of woody material, dominate the interval. The presence of dinoflagellate cysts indicates a marine environment, and the dominance of AOM is suggestive of oxygen-deficient bottom conditions.

### 5.2 Aulacostephanus autissiodorensis Chronozone (220.51–150.25 m)

Fossils. The recognition of this chronozone is based on its dinoflagellate cyst record. It contains only one indeterminable ammonite (199.42 m; Table 1). The base of the zone is recognised as the level with the lowest occurrence of abundant Oligosphaeridium patulum (220.51 m). The composition of the dinoflagellate cyst assemblage changes from 220.51 m to be characterised by abundant Oligosphaeridium patulum, Cribroperidinium spp. and Cyclonephelium distinctum. Paragonyaulacysta capillosa is common but less frequent upwards. The assemblage is characterised by low diversity and low abundance, probably due to the high content of organic material.

Biostratigraphy. Abundant *O. patulum* appears in the basal *A. autissiodorensis* Chronozone between ammonite faunal horizons M 22 and M 23 in Milne Land (Fig. 14; Piasecki 1996; Alsen & Piasecki 2018). *Cribroperidinium complexum* has its highest occurrence at the boundary of the *A. autissiodorensis* and *P. elegans* Chronozones (BioStrat 2018).

Age. Kimmeridgian, Late Jurassic.

Organic matter. The interval is characterised by abundant amorphous kerogen together with a large proportion of terrestrial organic material from higher land plants, especially brown to black woody material. The

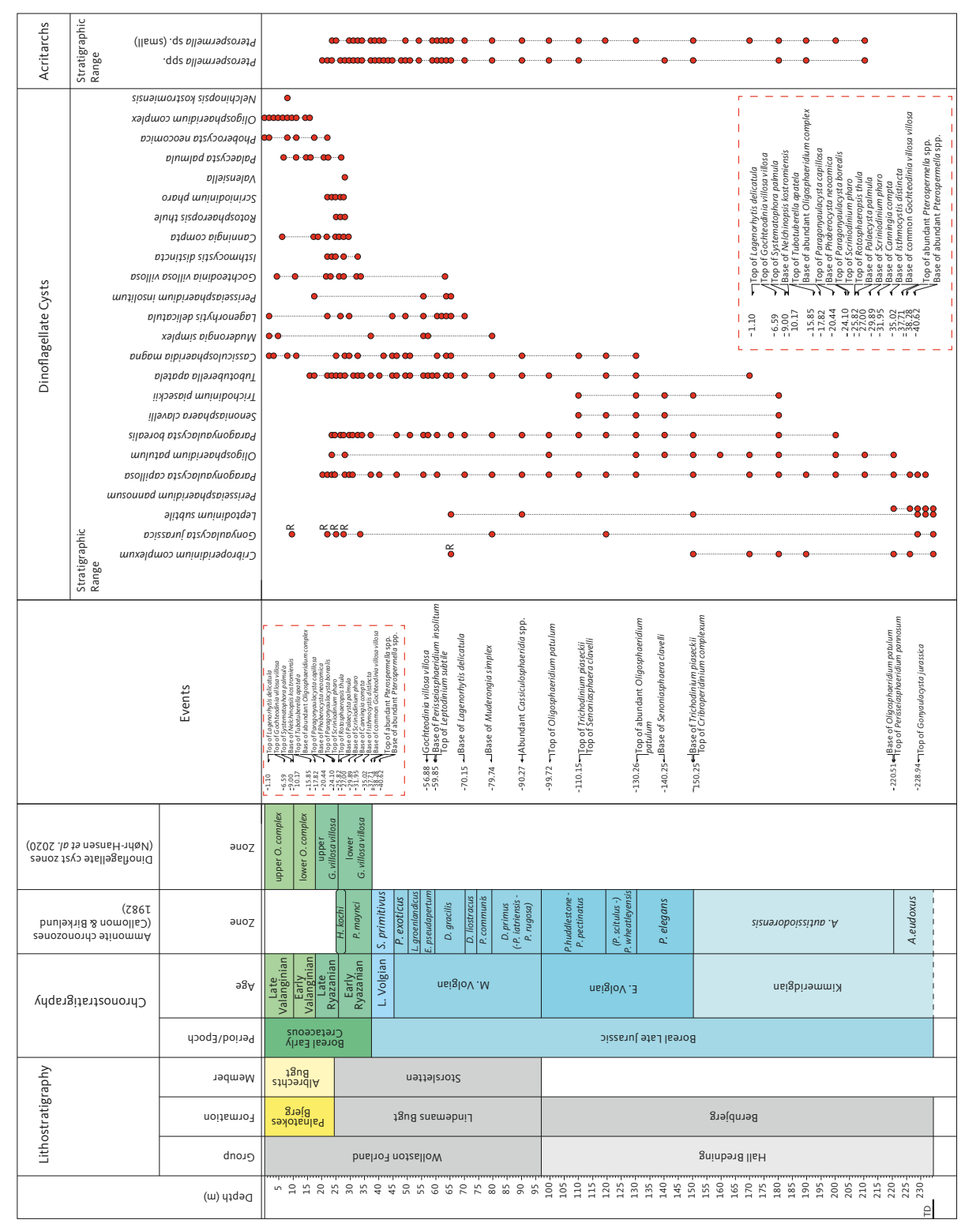


Fig. 7 The ranges of key dinoflagellate cyst taxa in the Rødryggen-1 core. The dinoflagellate cyst species are stratigraphically arranged according to the succession of their lowest occurrences. A range chart showing all taxa recorded in the core is available in Supplementary Data File 1.

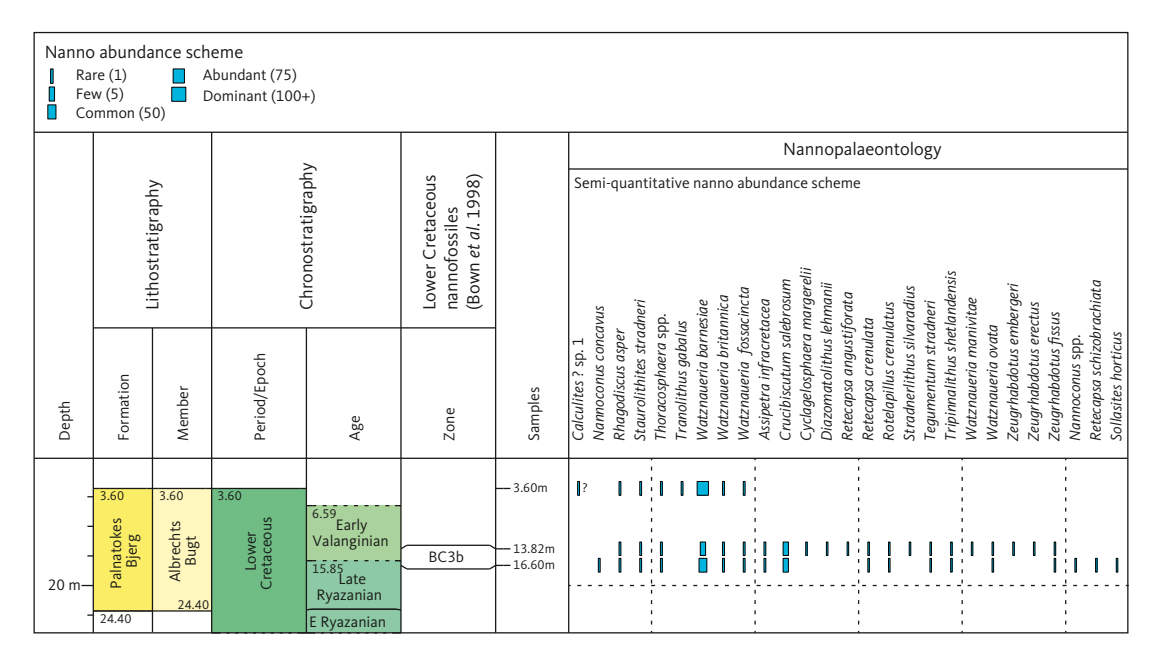


Fig. 8 The distribution of calcareous nannofossils in the Rødryggen-1 core.

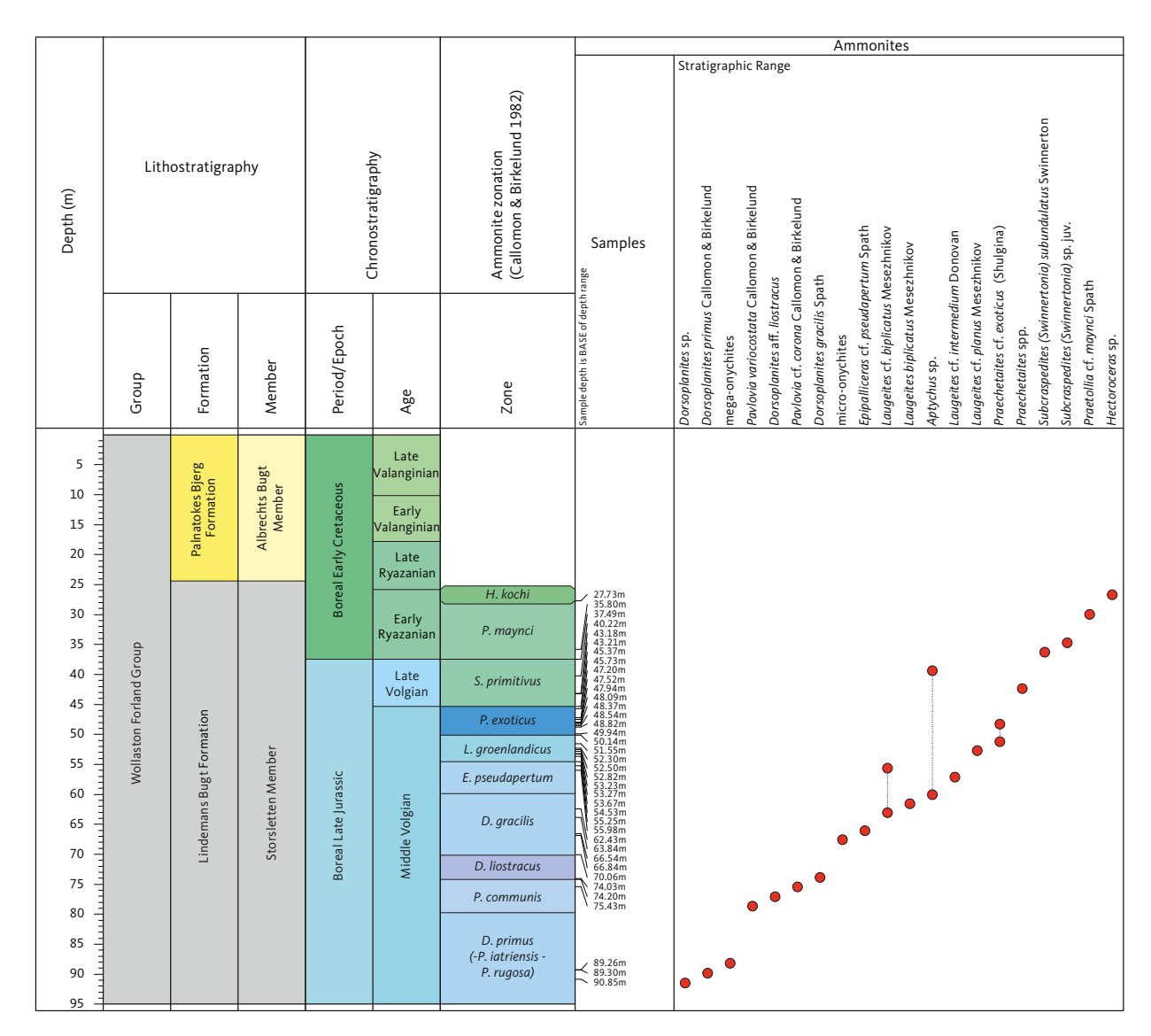


Fig. 9 The ranges of ammonite taxa recorded in the Rødryggen-1 core.

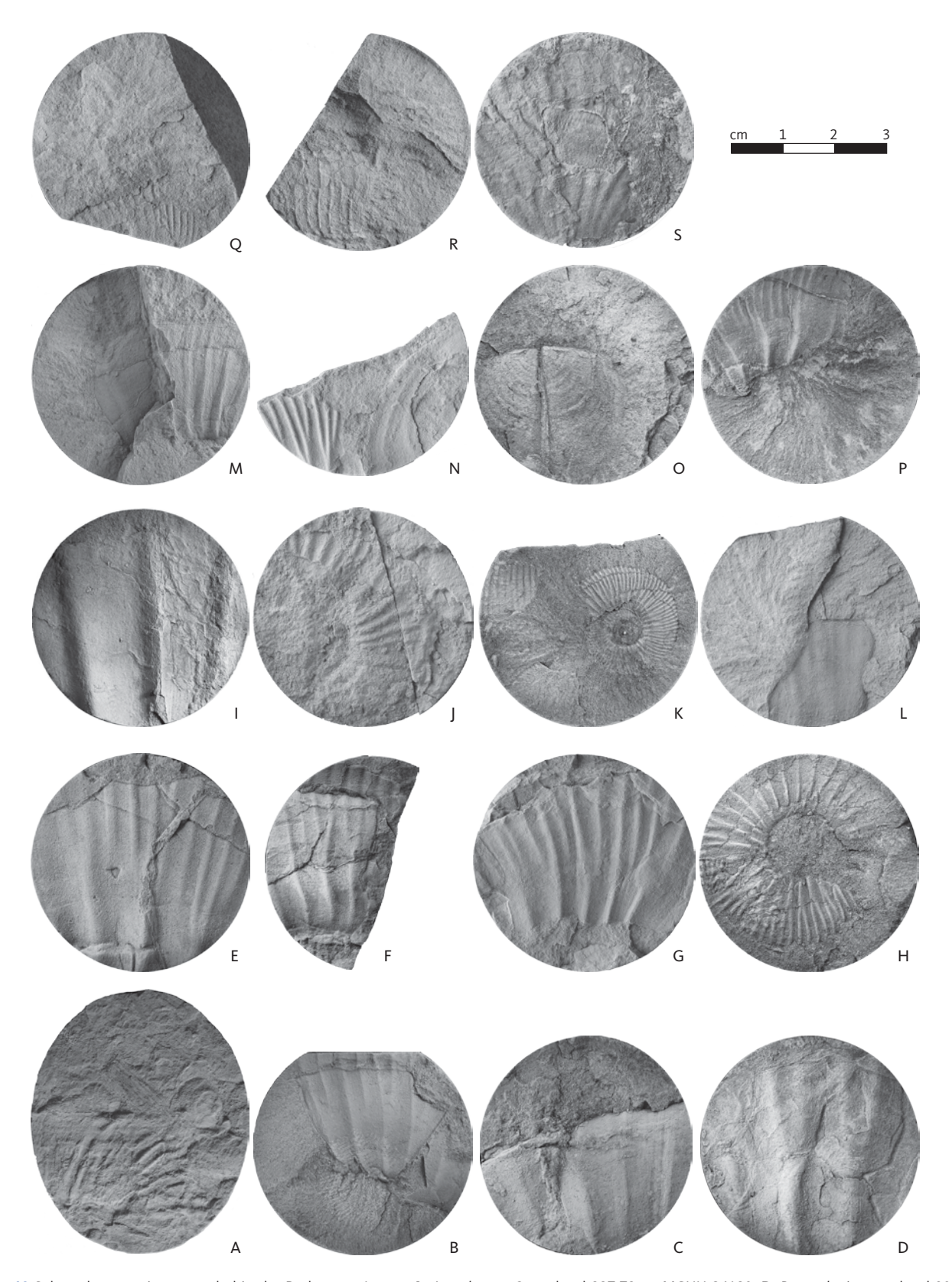


Fig. 10 Selected ammonites recorded in the Rødryggen-1 core. A: Amoeboceras? sp., level 227.72 m, MGUH 34180. B: Dorsoplanites sp., level 90.85 m, MGUH 34181. C: Dorsoplanites primus, level 89.30 m, MGUH 34182. D: Pavlovia cf. variocostata, level 75.43 m, MGUH 34184. E: Dorsoplanites aff. liostracus, level 74.20 m, MGUH 34185. F: Pavlovia cf. corona, level 74.03 m, MGUH 34186. G: Dorsoplanites jamesoni, level 70.06 m, MGUH 34187. H: Epipallasiceras cf. pseudapertum, level 55.98 m, MGUH 34189. I: Laugeites cf. biplicatus, level 53.67 m, MGUH 34190. J: Laugeites cf. intermedium, level 52.82 m, MGUH 34191. K: Laugeites cf. planus, level 51.55 m, MGUH 34192. L: cf. Praechetaites exoticus, level 48.82 m, MGUH 34193. M: cf. Praechetaites exoticus, level 48.54 m, MGUH 34194. N: Ammonoidea indet., level 48.37 m, MGUH 34195. O: aptychus, level 47.20 m, MGUH 34196. P: S. (Swinnertonia) cf. subundulatus, level 45.37 m, MGUH 34197. Q: Subcraspedites (Swinnertonia) sp. Juv., level. 43.21 m, MGUH 34198. R: cf. Praetollia maynci Spath, level 37.49 m, MGUH 34199. S: Hectoroceras sp., level 27.73 m, MGUH 34200. The specimens are stored in the Palaeontology Type Collection at the Natural History Museum of Denmark and each labelled with an MGUH number – Museum Geologica Universitas Hafniensis.

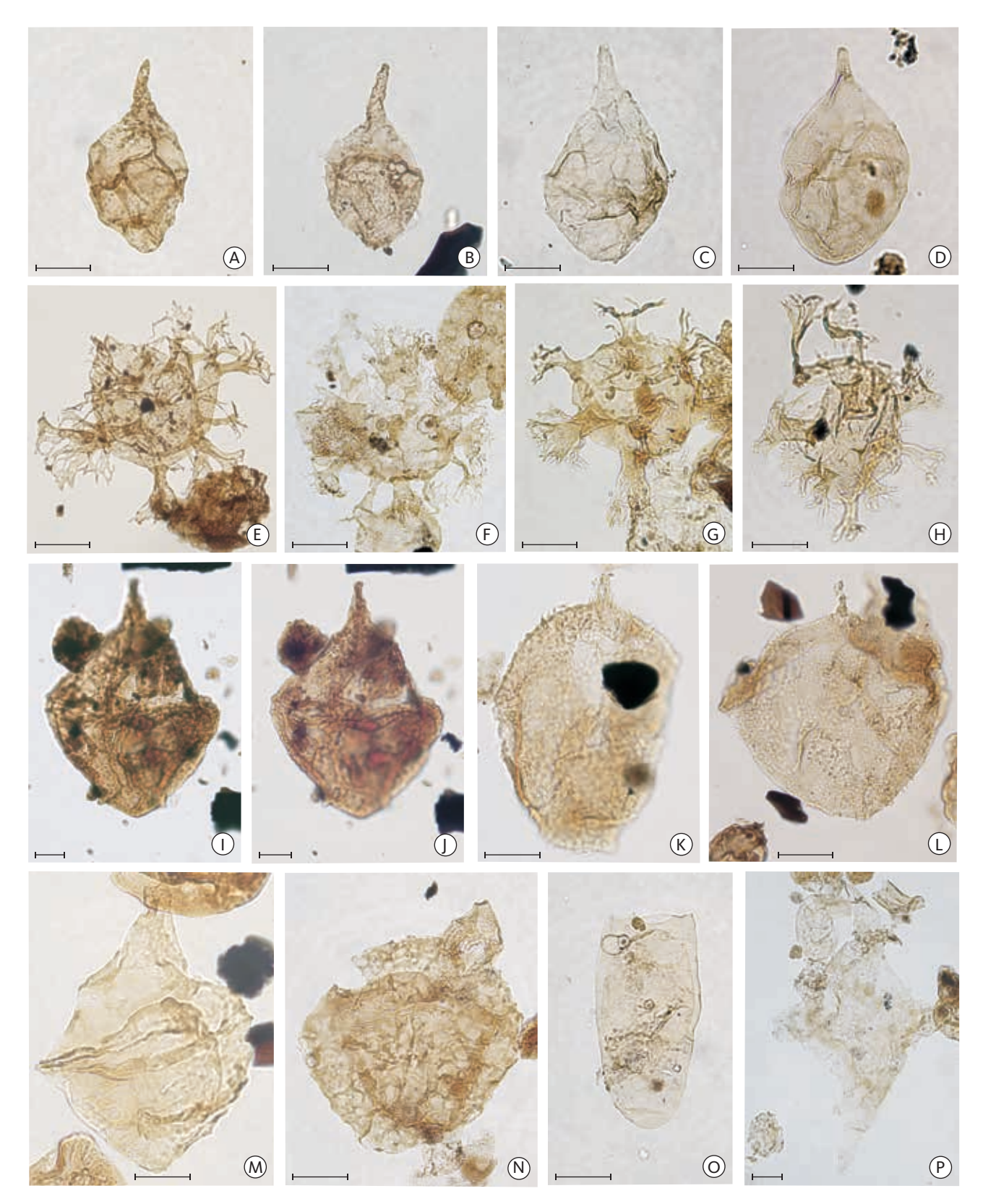


Fig. 11 Selected biostratigraphically significant dinoflagellate cysts and acritarchs from the Rødryggen-1 core. Scale bars: 25 µm. A and B: Paragonyaulacysta capillosa, sample 234.4 m, slide 2. C and D: Paragonyaulacysta borealis, sample 140.25 m, slide 6, and 136.26 m, slide 5. E and F: Perisseiasphaeridium pannosum, sample 226.22 m, slide 4. G and H: Oligosphaeridium patulum, sample 130.26 m, slide 6. I and J: Cribroperidinium complexum, low and high focus on the same specimen, sample 234.5 m, slide 5. K and L: Trichodinium piaseckii, sample 136.26 m, slide 6. M: Senoniasphaera clavellii, sample 90.27 m, slide 5. N: Cassiculosphaeridium magna, sample 90.27 m, slide 5. O: Wallodinium krutzschii, sample 110.15 m, slide 4. P: Muderongia simplex, sample 76.74 m, slide 4.

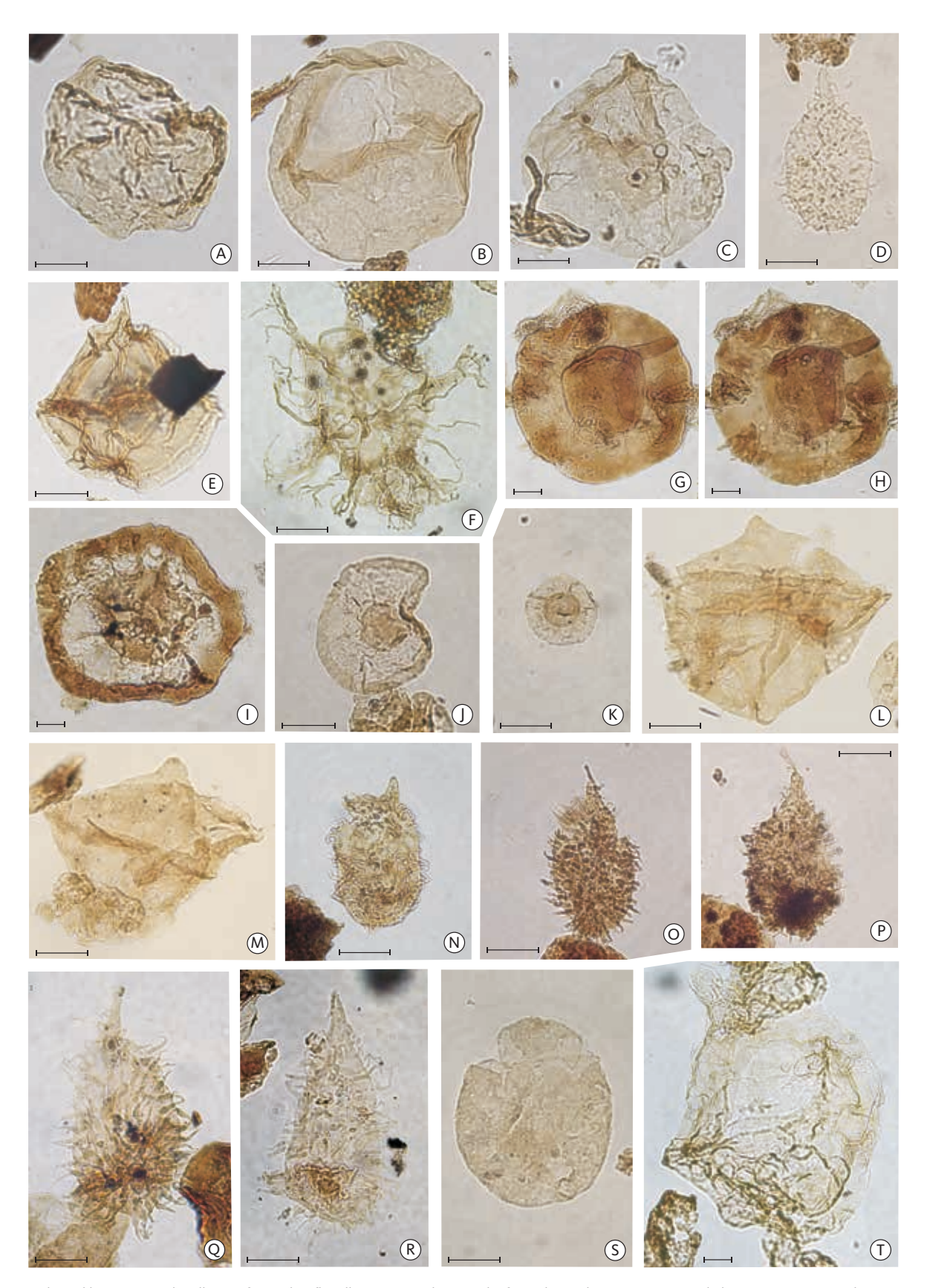


Fig. 12 Selected biostratigraphically significant dinoflagellate cysts and acritarchs from the Rødryggen-1 core. Scale bars: 25 µm. A, B and C: Lagenorhytis delicatula, showing variable morphology, sample 54.31 m, slide 7. D: Gochteodinia villosa subsp. villosa, sample 56.88 m, slide 4 and 5. E: Leptodinium subtile, sample 90.27 m, slide 5. F: Perisseiasphaeridium insolitum, sample 59.85 m, slide 4. G, H and I: large Pterospermella spp., sample 40.62 m, slide 5, and sample 35.2 m, slide 7. J and K: small Pterospermella spp., sample 43.43 m, slide 5 and sample 35.2, slide 7. L and M: Isthmocystis distincta, sample 35.02 m, slide 3. N, O, P, Q and R: morphological variations of Gochteodinia villosa subsp. villosa, (N-Q) sample 37.71 m, slide 7, and (R) sample 35.02 m, slide 4. S: Circulodinium compta, sample 31.95 m, slide 4. T: Scriniodinium pharo, sample 24.1 m, slide 3.

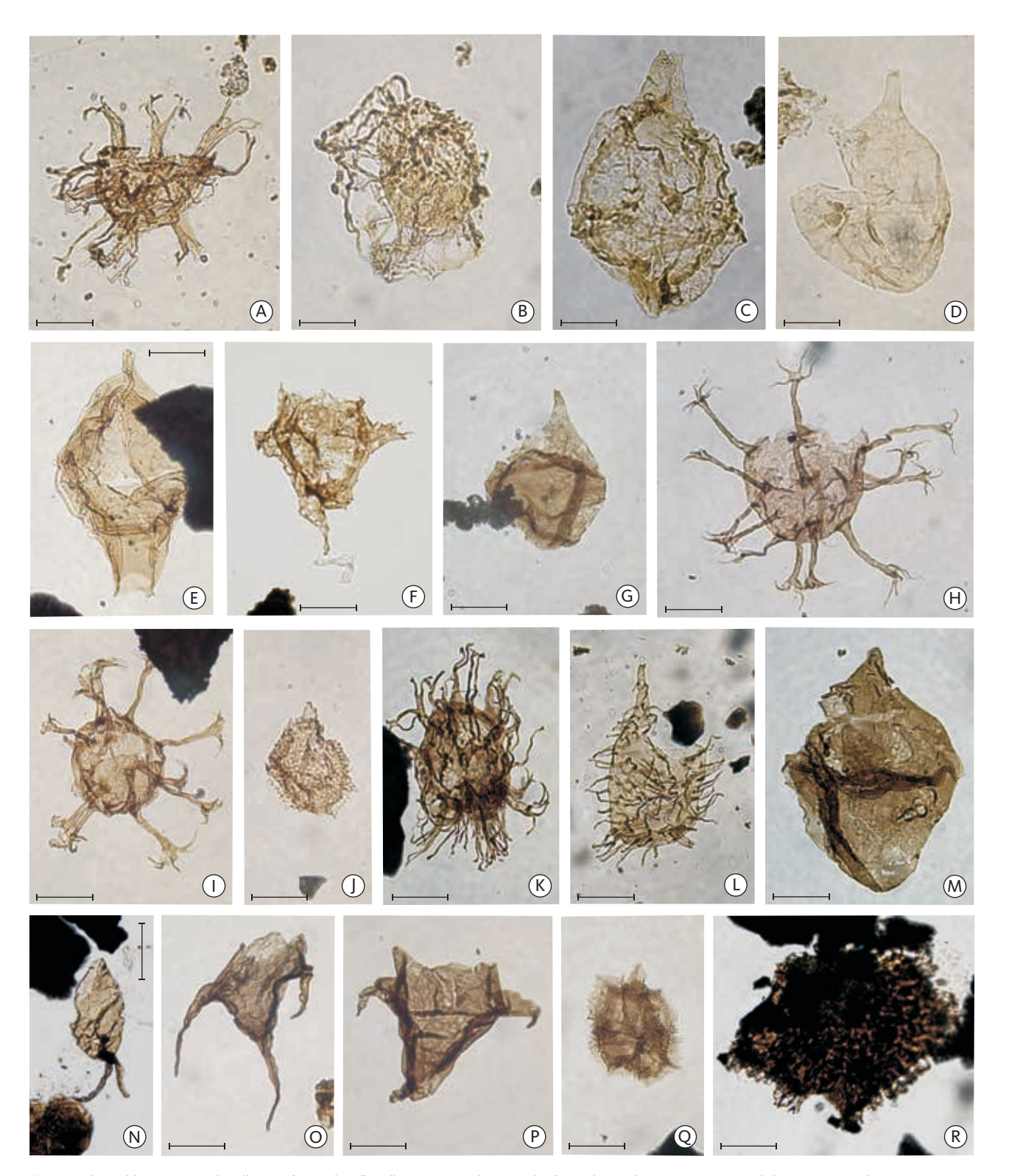


Fig. 13 Selected biostratigraphically significant dinoflagellate cysts and acritarchs from the Rødryggen-1 (A–M) and the Brorson Halvø-1 (N–R) cores. Scale bars: 25 µm. A: Palaecysta palmula, sample 24.1 m, slide 2. B: Rotosphaeropsis thule, sample 27.0 m, slide 7. C: Scriniodinium pharo, sample 27.1 m, slide 3. D: Paragonyaulacysta borealis, sample 35.2 m, slide 4. E: Tubotuberella apatela, sample 25.0 m, slide 9. F: Phoberocysta neocomica, sample 13.2 m, slide 2. G: Paragonyaulacysta capillosa, sample 21.38 m, slide 2. H: Oligosphaeridium complex, sample 10.17 m, slide 2. I: Oligosphaeridium complex, sample 17.82 m, slide 2. J: Nelchinopsis kostromiensis, sample 10.17 m, slide 2. K: Palaecysta palmula, sample 9.00 m, slide 2. L: Gochteodinia villosa subsp. villosa, sample 24.1 m, slide 3. M: Lagenorhytis delicatula, sample 2.78 m, slide 4. N: Batioladinium longicornutum, sample 3.37 m, slide 3. R: Muderongia tetracantha, sample 9.18 m, slide 3. P: Muderongia staurota, sample 9.18 m, slide 3. Q: Nelchinopsis kostromiensis, sample 6.16 m, slide 3. R: Pseudoceratium anaphrissum, sample 3.37 m, slide 3.

|  | ostra | atigrap      | ony         | Zone/su   | ibzorie  |                                       |  |  |  |  |  |  |  |  |
|--|-------|--------------|-------------|---|--|---------------------------------------|--|--|--|--|--|--|--|--|
|  |       |              |             | Parancyloceras bid  | lentatum Zone  |                                       |  |  |  |  |  |  |  |  |
|  | ı     | BARREMIAN    | U.          | biostratigra  | phic hiatus  |                                       |  |  |  |  |  |  |  |  |
|  |       | SARRE        |             | Paracrioceras deno  |  | 1                                     |  |  |  |  |  |  |  |  |
|  |       | ω            |             | Paracrioceras el  | *  | -                                     |  |  |  |  |  |  |  |  |
|  |       |              | نـ          | Fissicostaciceras fissi<br>biostratigra   |  |                                       |  |  |  |  |  |  |  |  |
|  | H     |              |             | Diostratigra  | pine matus   | 1                                     |  |  |  |  |  |  |  |  |
|  |       | z            | j.          | Simbirskites de   | cheni Zone   |                                       |  |  |  |  |  |  |  |  |
| (5)  |       | Ν            |             | Simbirskites (Speetonicer   | as) inversum Zone  |                                       |  |  |  |  |  |  |  |  |
| CRETACEOUS (pars)  Lower (pars)  HAUTERIVIAN | l.    | biostratigra | phic hiatus |   |  |                                       |  |  |  |  |  |  |  |  |
| Ă.   | ۱۲    |              |             | Dichotomites bidicho  | otomoides Zone   | 1                                     |  |  |  |  |  |  |  |  |
| C.R.E  |       | 7            | ⊃           | biostratigra  |  | 4                                     |  |  |  |  |  |  |  |  |
|  |       | VALANGIAN    |             | Dichotomites cr<br>biostratigra   |  | ł                                     |  |  |  |  |  |  |  |  |
|  |       | Ä            |             | Dichotomites hollv  |  | 1                                     |  |  |  |  |  |  |  |  |
|  |       | VAL          |             | Polyptychites mid   | chalskii Zone  |                                       |  |  |  |  |  |  |  |  |
|  |       |              | Γ.          | Nikitinoceras hop   |  | 1                                     |  |  |  |  |  |  |  |  |
|  |       |              |             | Delphinites undulat   |  | 1                                     |  |  |  |  |  |  |  |  |
|  |       | z            | Ü.          | Peregrinus alb<br>Surites tzikwin   |  | 1                                     |  |  |  |  |  |  |  |  |
|  |       | ANIA         | ا ر         | Surites analo   |  | 1                                     |  |  |  |  |  |  |  |  |
|  |       | RYAZANIAN    |             | Hectoroceras k  | -  | 1                                     |  |  |  |  |  |  |  |  |
|  |       | ά            | Ε.          | Praetollia ma   | ynci Zone  | ]                                     |  |  |  |  |  |  |  |  |
|  |       |              | U.          | Subcraspedites pr   | imitivus Zone  | 1                                     |  |  |  |  |  |  |  |  |
|  |       |              |             | Praechetaites tenuicostatus Zone<br>Epilaugeites surlyki Zone<br>(vogulicus Zone sensu Surlyk 1978)   | Praechetaites exoticus Zone  |                                       |  |  |  |  |  |  |  |  |
|  |       |              |             | Laugeites groenla   | ndicus Zone  | N                                     |  |  |  |  |  |  |  |  |
|  |       |              |             | biostratigra  | phic hiatus  | 1 5                                   |  |  |  |  |  |  |  |  |
|  |       |              |             | Crendonites and   |  | Δ                                     |  |  |  |  |  |  |  |  |
|  |       |              |             | biostratigra  |  |                                       |  |  |  |  |  |  |  |  |
|  |       |              |             |   |  |                                       |  |  |  |  |  |  |  |  |
|  |       |              |             |   |  | N                                     |  |  |  |  |  |  |  |  |
|  |       |              | Σ̈́         | Epipallasiceras pseud   | lapertum Zone  | 1 H                                   |  |  |  |  |  |  |  |  |
|  |       |              | 2           |   |  | 1 1/0                                 |  |  |  |  |  |  |  |  |
|  |       |              | 2           |   |  |                                       |  |  |  |  |  |  |  |  |
|  |       | AN           | Ν           |   |  | N                                     |  |  |  |  |  |  |  |  |
|  |       | OLGIAN       | N           | Dorsoplanites g   | racilis Zone   | ^<br>^                                |  |  |  |  |  |  |  |  |
|  |       | VOLGIAN      | N           | Dorsoplanites g   | racilis Zone   | N<br>N                                |  |  |  |  |  |  |  |  |
|  |       | VOLGIAN      | N           | Dorsoplanites g<br>Dorsoplanites lio:   |  | \ \ \ \ \ \ \ \ \ \ \ \ \ \ \ \ \ \ \ |  |  |  |  |  |  |  |  |
| O  |       | VOLGIAN      | N           | Dorsoplanites lio   | stracus Zone   | \ \ \ \ \ \ \ \ \ \ \ \ \ \ \ \ \ \ \ |  |  |  |  |  |  |  |  |
| ASSIC  | pper  | VOLGIAN      | N           |   | stracus Zone   | \ \ \ \ \ \ \ \ \ \ \ \ \ \ \ \ \ \ \ |  |  |  |  |  |  |  |  |
| URASSIC                                      | Upper | VOLGIAN      | N           | Dorsoplanites lio:<br>Pavlovia comn<br>Pavlovia rug:  | stracus Zone<br>nunis Zone<br>osa Zone   | \ \ \ \ \ \ \ \ \ \ \ \ \ \ \ \ \ \ \ |  |  |  |  |  |  |  |  |
| JURASSIC                                     | Upper | VOLGIAN      | N           | Dorsoplanites lio:<br>Pavlovia comn<br>Pavlovia rug<br>Pavlovia iatrie  | stracus Zone<br>nunis Zone<br>osa Zone<br>ensis Zone   | N                                     |  |  |  |  |  |  |  |  |
| JURASSIC                                     | Upper | VOLGIAN      | N           | Dorsoplanites lio:<br>Pavlovia comn<br>Pavlovia rug:  | stracus Zone<br>nunis Zone<br>osa Zone<br>ensis Zone   | \ \ \ \ \ \ \ \ \ \ \ \ \ \ \ \ \ \ \ |  |  |  |  |  |  |  |  |
| JURASSIC                                     | Upper | VOLGIAN      | N           | Dorsoplanites lio:<br>Pavlovia comn<br>Pavlovia rug<br>Pavlovia iatrie  | stracus Zone<br>nunis Zone<br>osa Zone<br>ensis Zone   | \ \ \ \ \ \ \ \ \ \ \ \ \ \ \ \ \ \ \ |  |  |  |  |  |  |  |  |
| JURASSIC                                     | Upper | VOLGIAN      | N           | Dorsoplanites lio:<br>Pavlovia comn<br>Pavlovia rug<br>Pavlovia iatrie  | ostracus Zone nunis Zone osa Zone ensis Zone rimus Zone P. paravirgatus Subzone  | \ \ \ \ \ \ \ \ \ \ \ \ \ \ \ \ \ \ \ |  |  |  |  |  |  |  |  |
| JURASSIC                                     | Upper | VOLGIAN      |             | Dorsoplanites lio:<br>Pavlovia comn<br>Pavlovia rug<br>Pavlovia iatrie<br>Dorsoplanites p   | stracus Zone nunis Zone osa Zone ensis Zone rrimus Zone  | A A A A A A A A A A A A A A A A A A A |  |  |  |  |  |  |  |  |
| JURASSIC                                     | Upper | VOLGIAN      | L.          | Dorsoplanites lio:<br>Pavlovia comn<br>Pavlovia rug<br>Pavlovia iatrie<br>Dorsoplanites p   | ostracus Zone nunis Zone osa Zone rimus Zone rimus Zone P. paravirgatus Subzone P. eastlecottensis Subzone   | N                                     |  |  |  |  |  |  |  |  |
| JURASSIC                                     | Upper | VOLGIAN      |             | Dorsoplanites lio:  Pavlovia comn  Pavlovia rug  Pavlovia iatrie  Dorsoplanites p  Pectinatites pectinatus Zone  Pectinatites hud  Pectinatites wheat   | stracus Zone nunis Zone osa Zone ensis Zone rimus Zone P. paravirgatus Subzone P. eastlecottensis Subzone lestoni Zone   | A A A A A A A A A A A A A A A A A A A |  |  |  |  |  |  |  |  |
| JURASSIC                                     | Upper | VOLGIAN      |             | Dorsoplanites lio:  Pavlovia comn  Pavlovia rugi Pavlovia iatrie  Dorsoplanites p  Pectinatites pectinatus Zone  Pectinatites hud  Pectinatites (Virgatosphin  Pectinatites (Virgatosphin   | stracus Zone  nunis Zone  osa Zone ensis Zone rimus Zone  P. paravirgatus Subzone  P. eastlecottensis Subzone  lestoni Zone leyensis Zone nctes) scitulus Zone   |                                       |  |  |  |  |  |  |  |  |
| JURASSIC                                     | Upper | VOLGIAN      |             | Dorsoplanites lio:  Pavlovia comn Pavlovia iatrie Dorsoplanites p  Pectinatites pectinatus Zone  Pectinatites hud Pectinatites (Virgatosphin Pectinatites (Virgatosphin   | stracus Zone nunis Zone posa Zone posa Zone primus Zone p. paravirgatus Subzone p. eastlecottensis Subzone lestoni Zone leyensis Zone pleyensis Zone |                                       |  |  |  |  |  |  |  |  |
| JURASSIC                                     | Upper | VOLGIAN      |             | Dorsoplanites lio:  Pavlovia comn  Pavlovia rugi Pavlovia iatrie  Dorsoplanites p  Pectinatites pectinatus Zone  Pectinatites hud  Pectinatites (Virgatosphin  Pectinatites (Virgatosphin   | stracus Zone nunis Zone posa Zone posa Zone primus Zone p. paravirgatus Subzone p. eastlecottensis Subzone lestoni Zone leyensis Zone pleyensis Zone |                                       |  |  |  |  |  |  |  |  |
| JURASSIC                                     | Upper | VOLGIAN      | L. L.       | Dorsoplanites lio:  Pavlovia comm  Pavlovia rug  Pavlovia iatrie  Dorsoplanites p  Pectinatites pectinatus Zone  Pectinatites hud  Pectinatites (Virgatosphin  Pectinatites (Virgatosphin  Aulacostephanus autis:   | stracus Zone  osa Zone ensis Zone ensis Zone  P. paravirgatus Subzone  P. eastlecottensis Subzone  lestoni Zone leyensis Zone octes) scitulus Zone ctes) elegans Zone ctes) elegans Zone   |                                       |  |  |  |  |  |  |  |  |
| JURASSIC                                     | Upper |              |             | Dorsoplanites lio:  Pavlovia comn Pavlovia iatrie Dorsoplanites p  Pectinatites pectinatus Zone  Pectinatites hud Pectinatites (Virgatosphin Pectinatites (Virgatosphin   | stracus Zone  osa Zone ensis Zone ensis Zone  P. paravirgatus Subzone  P. eastlecottensis Subzone  lestoni Zone leyensis Zone octes) scitulus Zone ctes) elegans Zone ctes) elegans Zone   |                                       |  |  |  |  |  |  |  |  |
| JURASSIC                                     | Upper |              | L. L.       | Dorsoplanites lio:  Pavlovia comm  Pavlovia rug  Pavlovia iatrie  Dorsoplanites p  Pectinatites pectinatus Zone  Pectinatites hud  Pectinatites (Virgatosphin  Pectinatites (Virgatosphin  Aulacostephanus autis:   | stracus Zone  nunis Zone  osa Zone ensis Zone  P. paravirgatus Subzone  P. eastlecottensis Subzone  lestoni Zone leyensis Zone ctes) scitulus Zone ctes) elegans Zone siodorensis Zone  udoxus Zone  |                                       |  |  |  |  |  |  |  |  |
| JURASSIC                                     | Upper |              | L. L.       | Dorsoplanites lio:  Pavlovia comn  Pavlovia rug  Pavlovia iatrie  Dorsoplanites p  Pectinatites pectinatus Zone  Pectinatites hud  Pectinatites (Virgatosphin  Pectinatites (Virgatosphin  Aulacostephanus autis:   | stracus Zone  nunis Zone  osa Zone ensis Zone  P. paravirgatus Subzone  P. eastlecottensis Subzone  lestoni Zone leyensis Zone ctes) scitulus Zone ctes) elegans Zone siodorensis Zone  udoxus Zone  |                                       |  |  |  |  |  |  |  |  |
| JURASSIC                                     | Upper |              | U. L.       | Dorsoplanites lio:  Pavlovia comn  Pavlovia rug  Pavlovia iatrie  Dorsoplanites p  Pectinatites pectinatus Zone  Pectinatites hud  Pectinatites wheat  Pectinatites (Virgatosphin  Petinatites (Virgatosphin  Aulacostephanus autis:  Aulacostephanus nus n | stracus Zone  nunis Zone  osa Zone ensis Zone  P. paravirgatus Subzone  P. eastlecottensis Subzone  lestoni Zone leyensis Zone ctes) citulus Zone ctes) elegans Zone siodorensis Zone uudoxus Zone nutabilis Zone  |                                       |  |  |  |  |  |  |  |  |
| JURASSIC                                     | Upper | KIMMERIDGIAN | L. L.       | Dorsoplanites lio:  Pavlovia comn  Pavlovia rug  Pavlovia iatrie  Dorsoplanites p  Pectinatites pectinatus Zone  Pectinatites hud  Pectinatites (Virgatosphin  Pectinatites (Virgatosphin  Aulacostephanus autis:   | stracus Zone  nunis Zone  osa Zone ensis Zone  P. paravirgatus Subzone  P. eastlecottensis Subzone  lestoni Zone leyensis Zone ctes) citulus Zone ctes) elegans Zone siodorensis Zone uudoxus Zone nutabilis Zone  |                                       |  |  |  |  |  |  |  |  |

Fig. 14 Kimmeridgian – Barremian ammonite zonation for North-East Greenland. M 14 to M 47 are faunal horizons recorded in Milne Land by Callomon & Birkelund (1982). L.: lower. M.: middle. U.: upper.

presence of dinoflagellate cysts indicates a marine environment, and the dominance of AOM is suggestive of oxygen-deficient bottom conditions.

## 5.3 *Pectinatites elegans* Chronozone (150.25–130.26 m)

Fossils. The recognition of this chronozone is based on its dinoflagellate cyst record. The dinoflagellate cyst assemblage is characterised by abundant Oligosphaeridium patulum, Cribroperidinium spp., Sirmiodinium grossii and C. distinctum. Paragonyaulacysta capillosa is common but less frequent upwards. The assemblage is mostly of low diversity and low abundance, probably due to the abundance of organic material.

Biostratigraphy. The base of the zone is recognised as the level with the last occurrence of *Cribroperidinium complexum* and the first occurrence of *Trichodinium piaseckii*.

Age. Early Volgian, Late Jurassic

Organic matter. The interval is characterised by abundant amorphous kerogen together with a large proportion of terrestrial organic material from higher land plants, especially brown to black woody material. The presence of dinoflagellate cysts indicates a marine environment, and the dominance of AOM is suggestive of oxygen-deficient bottom conditions.

## 5.4 (*Pectinatites scitulus* –) *Pectinatites wheatleyensis* Chronozones undiff. (130.26–119.70 m)

Fossils. The recognition of the interval is based on its dinoflagellate cyst record. The base is placed above the last occurrence of abundant Oligosphaeridium patulum. The dinoflagellate cyst assemblage is characterised by Cribroperidinium spp. and Sirmiodinium grossii. Apteodinium spp., Cassiculosphaeridium magna, Paragonyaulacysta capillosa and P. borealis are locally common. The assemblage is recorded as moderately diverse and abundant.

Biostratigraphy. The *P. scitulus* ammonite Zone has never been proven by ammonites in Greenland but is included in the zonal scheme due to the general resemblance of the ammonite successions in Greenland and England (Fig. 14; Birkelund *et al.* 1984). Hence, we refer to it with caution, as indicated by the brackets. The top of abundant *O. patulum* occurs in ammonite faunal horizon M 25 (Piasecki 1996). This succession therefore correlates with the (*P. scitulus* –) *P. wheatleyensis* Chronozones.

Age. Early Volgian, Late Jurassic.

Organic matter. The interval is characterised by abundant amorphous kerogen together with a large proportion of terrestrial organic material from higher land plants, especially brown to black woody material. The presence of dinoflagellate cysts indicates a marine environment, and the dominance of AOM is suggestive of oxygen-deficient bottom conditions.

## 5.5 Pectinatites huddlestoni – Pectinatites pectinatus Chronozones undiff. (119.70–97.00 m)

Fossils. The recognition of the interval is based on its dinoflagellate cyst record. Trichodinium piaseckii and Senoniasphaera clavellii have the highest occurrence in 110.15 m, and the last occurrence of O. patulum is at 99.72 m near the top of the interval. The assemblage is characterised by Oligosphaeridium patulum, Paragonyaulacysta capillosa, P. borealis and Sirmiodinium grossii. The assemblage is considered moderately diverse and abundant. Within this interval, Pterospermella spp. acritarchs have their first appearance and become common and abundant from this interval and upwards until their highest occurrence at 21.38 m.

Biostratigraphy. The last occurrences of *Trichodinium piaseckii* and *Senoniasphaera clavellii* are recorded between ammonite fauna horizons M 25 and M 29, *P. wheatleyensis* and *P. pectinatus* Chronozones in Milne Land (Fig. 14; Piasecki 1996). This is in accordance with the type occurrences of the zonal index species in the North Sea region, UK (Bailey *et al.* 1997). The last consistent occurrence of *O. patulum* in Milne Land is a few metres above fauna M 25, *P. wheatleyensis* Zone.

Age. Early Volgian, Late Jurassic.

Organic matter. Abundant amorphous kerogen together with terrestrial organic material from higher land plants, especially sporomorphs and brown to black woody material, characterises the interval. The black woody material becomes more lath-shaped upwards in the succession. The presence of dinoflagellate cysts indicates a marine environment, and the dominance of AOM is suggestive of oxygen-deficient bottom conditions.

## 5.6 *Dorsoplanites primus* Chronozone (and *Pavlovia iatriensis* and *Pavlovia rugosa* Chronozones; 97.00–79.74 m)

Fossils. The recognition of this zone(s) is based on its content of dinoflagellate cysts and ammonites. The base is placed below the lowest occurrence of *Dorsoplanites* ammonites (Table 1) at the lithostratigraphic boundary between the Bernbjerg and Lindemans Bugt Formations (97 m). The interval marks the first appearance of ammonites after

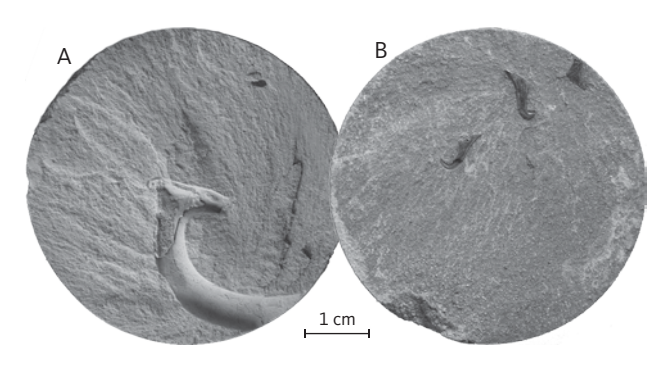


Fig. 15 Onychites in Rødryggen-1 core. A: mega-onychites, level 89.26 m, MGUH 34183. B: micro-onychites, level 62.43 m, MGUH 34188.

an interval barren of ammonites between 199.42 m and 90.85 m. A crushed, medium-sized ammonite fragment at 90.85 m, showing subdued ribbing with straight primaries and intercalated secondaries beginning on mid-flank and a gently sloping umbilical wall, is assigned to *Dorsoplanites* sp. (Fig. 10B; Table 1). A small fragment of a large specimen found at 89.30 m has straight, blunt distant ribs that bifurcate very high. The specimen is crushed but identified as the zonal index species *D. primus* by Callomon & Birkelund (1982; Fig. 10C; Table 1). In addition, megaonychites – arm hooks of belemnites – are encountered (Fig. 15A; Table 1).

The palynomorph assemblage from one sample contains abundant dinoflagellate cysts: *Cassiculosphaeridium magna* and *Leptodinium subtile* and common *Cribroperidinium* spp., *Paragonyaulacysta borealis*, *Sirmiodinium grossii*, *Tubotuberella apatela*, as well as the acritarch *Pterospermella* spp. The dinoflagellate cyst assemblage is relatively diverse and abundant, but chorate dinoflagellate cysts are essentially absent.

Biostratigraphy. Dorsoplanites primus indicates the faunal horizon M 31 in Milne Land. The general appearance of the genus *Dorsoplanites* in the East Greenland ammonite succession is recorded in the *D. primus* Zone and ranges up to M 42 in the upper middle Volgian Crendonites anguinus Zone (Fig. 14; Callomon & Birkelund 1982). The first occurrence of *Dorsoplanites* encountered here agrees well with the presence of the *D. primus* Zone. Mega-onychites are generally considered indicative of Upper Jurassic deposits, Kimmeridgian-Volgian strata, in the Arctic part of the Boreal Realm (Hammer et al. 2013). The lack of age-diagnostic fossils in the upper part of this interval leaves room for the presence of the P. iatriensis and P. rugosa Zones, which are thus indicated with caution. The dinoflagellate cysts Cassiculasphaeridium spp. have their maximum abundance in this interval. BioStrat (2018) reports a maximum occurrence of Cassiculasphaeridium spp. in the middle of the Subboreal P. pallasioides ammonite Chronozone, which probably corresponds to the Boreal D. primus - P. iatriensis ammonite Chronozones (Callomon & Birkelund 1982).

Age. Earliest middle Volgian, Late Jurassic.

Organic matter. Abundant amorphous kerogen together with terrestrial organic material from higher land plants, especially sporomorphs and brown to black woody material, characterises the interval. Lath-shaped, black woody material is common. The presence of dinoflagellate cysts indicates a marine environment, and the dominance of AOM is suggestive of oxygen-deficient bottom conditions.

## 5.7 *Pavlovia communis* Chronozone (79.74–74.20 m)

Fossils. The recognition of the zone is based on its content of dinoflagellate cysts and ammonites. The base is placed at the lowest appearance of *Muderongia simplex*. One ammonite is recorded in the interval (75.43 m; Table 1). The visible section of the ammonite shows coarse, biplicate rursiradiate ribbing from a large form, resembling various species within the genus *Pavlovia*. It appears closest to *P. variocostata* Callomon & Birkelund, characterised by a modification to subdued, irregular widely spaced and extremely coarse biplicate ribs in adult stage. Considering the restricted visible part, the present specimen is cautiously referred to as *P. cf. variocostata* (Fig. 10D).

The dinoflagellate cyst assemblage, based on one sample (79.74 m), contains *Apteodinium* spp., *Cribroperidinium* spp., *Muderongia simplex*, *Sirmiodinium grossii*, *Paragonyaulacysta borealis* and *P. capillosa*. The diversity of the assemblage is relatively high, whereas the abundance is low. Chorate cysts are almost absent.

Biostratigraphy. In North-West Europe, the lowest appearance of common Muderongia simplex spp. is well established in the P. rotunda (ammonite) Zone (e.g. Riding & Thomas 1992; Riding et al. 2000). The P. rotunda Zone is correlated with the P. communis Zone (M 34 to M 35) in East Greenland (Fig. 14; Birkelund et al. 1984). The first appearance of Muderongia simplex is thus here considered to indicate the *P. communis* Zone. This agrees well with the presence of the ammonite P. cf. variocostata, recorded c. 4 m higher in the core. The ammonite indicates the M 35 faunal horizon, which lies in the upper part of the P. communis Zone (Fig. 14; Callomon & Birkelund 1982). The appearance of Muderongia simplex in Milne Land occurs somewhat higher, in the faunal horizon M 46, in the C. anguinus ammonite zone (Piasecki 1996) corresponding to its highest common occurrence in North-West Europe (Riding et al. 2000).

Age. Middle Volgian, Late Jurassic.

*Organic matter*. Abundant amorphous kerogen together with terrestrial organic material from higher land plants,

mainly spores and pollen and brown to black woody material, characterises the interval. Lath-shaped, black woody material is common. The presence of dinoflagel-late cysts indicates a marine environment, and the dominance of AOM is suggestive of oxygen-deficient bottom conditions.

## 5.8 *Dorsoplanites liostracus* Chronozone (74.20–70.15 m)

Fossils. The base of this zone is placed at the occurrence of an ammonite specimen. No samples were analysed for dinoflagellate cysts within this interval. Two ammonite specimens were found at closely spaced levels (Table 1). The lower ammonite, a large form, shows dense, subdued ribbing, with blunt primaries that divide almost in a fasciculate manner into 3-4 secondaries and intercalatories. The subdued ribbing somewhat resembles, but does not exactly match, that of Dorsoplanites *liostracus* Callomon & Birkelund. The present specimen is thus tentatively referred to *Dorsoplanites* aff. *liostracus* (Fig. 10E). The higher specimen is a crushed fragment with slightly flexuous, relatively strong, blunt primary ribs and weak intercalating secondaries (Fig. 10F). This ribbing style resembles that of the much larger Pavlovia corona Callomon & Birkelund (1982, pl. 3, fig. 1). The present specimen is thus referred to P. cf. corona.

Biostratigraphy. Both *P.* aff. *liostracus* and *P.* cf. corona indicate the faunal horizon M37 in the upper part of the *D. liostracus* Zone (Fig. 14; Callomon & Birkelund 1982). *Age.* Middle middle Volgian, Late Jurassic. *Organic matter.* No palynological samples.

## 5.9 *Dorsoplanites gracilis* Chronozone (70.15–59.85 m)

Fossils. The base of this interval is placed at the lowest occurrence of the dinoflagellate cyst Lagenorhytis delicatula. The interval contains both ammonites and dinoflagellate cysts. A few centimetres above the base of the zone, an ammonite fragment from an apparently evolute form shows ornamentation with relatively distant ribs (Fig. 10G). Primaries are blunt, gently prorsiradiate and forward concave. Secondaries mostly intercalate and develop at mid-flank. Considering the presence of P. cf. corona in the underlying zone and E. cf. pseudapertum in the overlying zone, the closest resembling ammonite forms are likely to be found in the Dorsoplanites gracilis group in the faunal horizons M 37 to M 42 and are assigned to the D. liostracus - E. pseudapertum Zones, middle Volgian East Greenland (Spath 1936; Callomon & Birkelund 1982). The ribbing pattern of the present specimen resembles the 'indistinct' pattern of *Dorsoplanites jamesoni* Spath (1936, pl. 29, fig. 3). Additional fossils include a crushed indeterminate ammonite, a poorly preserved recrystallised belemnite rostrum and small onychites (Fig. 15B; Table 1). The dinoflagellate cyst assemblage is relatively diverse and moderately abundant. It is dominated by *Lagenorhytis delicatula*, the acritarch *Pterospermella* spp. and *Cribroperidinium* spp. Chorate cysts are absent.

*Biostratigraphy*. The exact assignment of the species *Dorsoplanites jamesoni* to a faunal horizon remains, but it probably belongs to the upper part of the *D. gracilis* Zone and possibly the M 40 faunal horizon (Fig. 14; Birkelund *et al.* 1984).

The first appearance of Lagenorhytis delicatula is just below the occurrence of the ammonite Dorsoplanites jamesoni at 70.06 m. L. delicatula is generally assigned a Lower Cretaceous range (Costa & Davey 1992) and is also present here in Ryazanian strata higher in the core. Hence, its first appearance in the middle Volgian D. gracilis Zone and consistent presence into the overlying Ryazanian are surprising, and its first occurrence in the middle Volgian potentially represents an excellent local marker event.

Age. Middle middle Volgian, Late Jurassic.

Organic matter. The interval is characterised by abundant amorphous kerogen, together with limited terrestrial organic material, mainly as spores and pollen, black woody material and carbonised, rounded grains. The presence of dinoflagellate cysts indicates a marine environment, and the dominance of AOM is suggestive of oxygen-deficient bottom conditions.

### 5.10 *Epipallasiceras pseudapertum* Chronozone (59.85–54.53 m)

Fossils. The base of this zone is placed at the uppermost occurrence of *Leptodinium subtile*. The interval contains both ammonites and dinoflagellate cysts. A small ammonite with well-preserved, relatively distant ribbing has strong, straight, prorsiradiate primaries that divide rather high up on the flank into two secondaries (Fig. 10H). It resembles *Epipallasiceras pseudapertum* Spath (1936; pl. 9, fig. 4) and is cautiously referred to *E. cf. pseudapertum*. A level less than one metre higher contains another, but poorly preserved and indeterminate, ammonite (Table 1).

The dinoflagellate cyst assemblage, based on three samples, is abundant and diverse. It is dominated by *Cribroperidinium* spp. with common *Lagenorhytis delicatula* and *Apteodinium daveyi* in the lower part. Rare, small and poorly preserved *Gochteodinia villosa villosa* and *Gochteodinia* spp. occur at 56.88 m but are not

recorded in any samples above until 37.71 m, in the *Subcraspedites primitivus* Zone (upper Volgian). Chorate and cavate cysts are rare in the lower sample and slightly more common in the upper sample.

Biostratigraphy. The ammonite indicates the M-42 faunal horizon and is the index of the middle Volgian E. pseudapertum Zone (Fig. 14). This is in good biostratigraphic accordance with the record of the uppermost occurrence of the dinoflagellate cyst *L. subtile*, which is a well-known marker from North-West Europe, where it has its highest occurrence in the P. albani Zone (Riding & Thomas 1992). The upper P. albani Zone is correlated with the E. pseudapertum Zone in the East Greenland ammonite zonation (Birkelund et al. 1984). The first appearances of Perisseiasphaeridium insolitum and Apteodinium daveyi at 59.85 m are slightly earlier than the recorded first occurrence of both species in the Galbanites okusensis - G. kerberus ammonite zones in England (Davey 1982). The dinoflagellate cyst assemblage (59.85-55.88 m) is dominated by Cribroperidinium spp. but becomes poorer upwards.

Age. Middle middle Volgian, Late Jurassic.

Organic matter. This interval records a significant change to a low content of organic matter in general, especially of terrestrial woody material; this shift appears in the lower *E. pseudapertum* Chronozone and continues upwards to the *Subcraspedites primitivus* Chronozone in the upper Volgian. This is combined with low abundance and diversity of the dinoflagellate cysts assemblage. A fully marine environment is indicated by the fossil record.

### 5.11 *Laugeites groenlandicus* Chronozone (54.53–50.14 m)

Fossils. The zone is recognised by its ammonite assemblage, whereas the dinoflagellate cyst assemblage is impoverished and poorly preserved. Acritarchs are present but have little stratigraphic value. The base of the zone is placed at the lowest occurrence of a possible Laugeites ammonite (54.53 m), a few centimetres below a fragment of an apparently very large Laugeites (Table 1). The latter is characterised by straight, strong and distant primary ribs, which begin sharp but appear to become blunt and flatten on or towards the (mid?-)flank (Fig. 10I). It resembles Laugeites biplicatus Mesezhnikov figured by Repin et al. (2006), although that specimen is somewhat different from the holotype established by Mesezhnikov (in Zakharov & Mesezhnikov 1974). Considering its fragmented nature, the specimen from the core is cautiously referred to L. cf. biplicatus. Further levels with ammonites include L. cf. intermedius Donovan,

another L. cf. biplicatus and L. cf. planus Mesezhnikov (in Zakharov & Mesezhnikov 1974; Table 1). The former closely resembles the specimen figured by Donovan (1964, pl. 1, fig. 5) from Laugeites Ravine, Kuhn Ø (Fig. 10J). The second is a fragment with distant, low, blunt ribs, which resembles the ornamentation on the mid-flank in the outer whorls of Laugeites biplicatus as seen in, for example, Repin et al. (2006, pl. 47, fig. 2) and Rogov (2010, pl. 4, fig. 6). The latter is a complete, small juvenile (?) specimen with relatively high whorl sides and narrow umbilicus, very dense and delicate ribbing with more than 31 primaries per whorl that divide or bifurcate almost immediately or low on the flank into dense and fine secondaries (Fig. 10K). Ribbing is slightly concave. By comparison with material figured by Donovan (1964) and Surlyk et al. (1973), the specimen is referred to the genus Laugeites, which is characterised as being smaller, more compressed and more delicately ribbed than its predecessor Dorsoplanites (see discussion in description of Dorsoplanites intermissus in Callomon & Birkelund 1982, appendix, p. 368). L. parvus Donovan and other Greenland Laugeites closely resemble the specimen but have more forward-leaning ribs, whereas the ribbing on the present specimen is almost radiate. The closest resemblance of our specimen is with Laugeites planus Mesezhnikov (in Zakharov & Mesezhnikov 1974) from subarctic Urals, Russia. In addition, the interval contains indeterminate, crushed ammonite fragments and aptychi (Table 1).

The dinoflagellate cyst assemblage (samples from 54.31–50.53 m) is poor in the lower part of the zone with common *Apteodinium*, *Cribroperidinium* and *Lagenorhytis*. The acritarchs *Cymatiosphaera*, *Veryhachium*, *Pterospermella*, *Leiosphaeridia* and the prasinophyte algae *Tasmanites* occur scattered amongst the dinoflagellate cysts and become common in the upper part of the zone where dinoflagellate cysts disappear.

Biostratigraphy. In North-East Greenland, the genus Laugeites is restricted to the M 47 faunal horizon in the Laugeites groenlandicus Zone (Fig. 14; Spath 1936; Donovan 1964; Surlyk 1978; Callomon & Birkelund 1982). The present records of L. cf. planus and L. cf. biplicatus are new for Greenland, where L. groenlandicus (Spath 1936), L. parvus Donovan (1964) and L. intermedius Donovan (1964) had been recorded previously. L. biplicatus indicates the Epivirgatites nikitini Zone in Russia, which is correlative to the upper part of the Laugeites groenlandicus Zone and the overlying Epilaugeites vogulicus Zone sensu Surlyk (1978), i.e. M 47 and higher levels (Rogov 2010, 2020). In the Rødryggen-1 core, L. cf. biplicatus occurs below *L.* cf. *planus*, which indicates the *Laugeites* groenlandicus Zone and M 47 faunal horizon; this delimits the occurrence of L. cf. biplicatus in the core to the

L. groenlandicus Zone. Note that Kelly et al. (2015) and Rogov (2020), based on observations of the ammonite faunal succession in Perisphinctes Ravine, eastern Kuhn Ø (Fig. 2), added another faunal horizon, the L. lambecki horizon, above the M 47 Laugeites groenlandicus horizon, to the L. groenlandicus Zone. However, Callomon & Birkelund (1982) argued that the Laugeites fauna recorded in the northern Wollaston Forland and Kuhn Ø areas by Donovan (1964) and Surlyk (1978) represents the higher part of the L. groenlandicus Zone. It seems more justified to introduce a L. parvus horizon, based on Donovan's and Surlyk's documentation of the fauna, above the M 47 horizon, rather than an L. lambecki horizon and zone.

The absence of *Crendonites anguinus* Zone fossils is not necessarily attributed to a hiatus, given that there are no sedimentological or depositional signs of erosion. The zone is thus considered not proven in the core, either due to the low sample density or due to low sedimentation rates.

Age. Late middle Volgian.

*Organic matter*. The interval contains very little organic matter with few or no dinoflagellate cysts. Despite the dominance of acritarchs and terrestrial organic material, the presence of ammonites testifies to continued fully marine conditions.

### 5.12 *Praechetaites exoticus* Chronozone (50.14–45.37 m)

Fossils. The zone is recognised by its ammonite assemblage, whereas the dinoflagellate cyst assemblage is poor and poorly preserved. Acritarchs are present but have little stratigraphic value. The interval is relatively rich in macrofossils containing several ammonites, various bivalves, including Buchia, and ammonite aptychi. The base is placed at 50.14 m, at the occurrence of a crushed ammonite fragment with relatively distant, low, sharp, primary ribs that divide into three closely spaced low, sharp, secondary ribs (Table 1). The ornamentation is close to that in inner-middle whorls of Praechetaites exoticus (Shulgina) as illustrated in, for example, Shulgina (1967, pl. 1, fig. 1b). An ammonite occurring c. 1.5 m higher is a fragment, probably from mid-flank, with very faint ribbing of distant primaries that are very low, almost smooth, developing into faint secondaries and intercalatories (Fig. 10L) similar to ornamentation in the mid-flank of *Praechetaites exoticus* (Shulgina; e.g. Shulgina 1967, pl. 4, fig. 1; Rogov 2010, pl. 6, fig. 5). A few centimetres higher in the core, another ammonite fragment has low, wide, relatively sharp crested ribs that appear to develop into faint sheaves of very fine lirae-like secondaries (Fig. 10M), resembling the ornamentation observed in *Praechetaites*  exoticus (Shulgina; e.g. Shulgina 1967, pl. 4, fig. 1). Considering their preservation, the fragments are with some caution referred to *Praechetaites* cf. exoticus (Shulgina). Two additional ammonites are indeterminate fragments, one of them possibly also belonging to the genus *Praechetaites* (Fig. 10N; Table 1).

The dinoflagellate cyst assemblage varies from barren to poor. Reworked specimens become more common, with specimens of *Wanaea* and *Nannoceratopsis*. Acritarchs are present in all samples, for example, *Fromea*, *Pterospermella* and *Leiosphaeridia*.

Biostratigraphy. P. exoticus is the index species of the Northern Siberian P. exoticus Zone. Its presence in Greenland closely above the L. groenlandicus Zone does not leave much room for the Epilaugeites vogulicus Zone that supposedly overlies the Laugeites groenlandicus Zone (Fig. 14; Surlyk 1978). It could thus be that the P. exoticus and E. vogulicus Zones may be time-equivalent correlatives. However, since representatives of the two zones were so far not found together, it remains uncertain whether P. exoticus occurs in the E. vogulicus Zone in Greenland and thus would link the Russian and Greenland zones, or whether the P. exoticus Zone may represent a level in between the L. greenlandicus Zone and the E. vogulicus Zone. Rogov (2010, 2020) correlated the P. exoticus Zone to both the E. vogulicus Zone and the P. tenuicostatus Zone or beds in Greenland. Rogov & Zakharov (2011) noted that the specimens of E. vogulicus from Greenland (Surlyk et al. 1973; Surlyk 1978) differ from 'true' E. vogulicus in Siberia (Ilovaisky 1917; Mikhailov 1966; Zakharov & Mesezhnikov 1974). Accordingly, the Greenland records were referred to a new species, E. surlyki Rogov (2020), which thus also becomes index for the E. surlyki Zone in Greenland.

Age. Latest middle Volgian. It should be noted, however, that there is disagreement amongst Russian ammonite stratigraphers about whether the *P. exoticus* Zone should be attributed to the uppermost middle or the lowermost upper Volgian (Meledina *et al.* 2010; Rogov & Zakharov 2011). The unit was originally introduced as a subzone in the lowest part of the *Craspedites okensis* Zone (upper Volgian), whereas the ammonite succession in the Jurassic–Cretaceous boundary key section at Nordvik suggests that the *P. exoticus* Zone should be referred to the uppermost middle Volgian (e.g. Zakharov & Rogov 2006, 2008; Rogov & Zakharov 2009, 2011; Rogov 2020).

Organic matter. The interval has a very low organic content. Marine palynomorphs are rare or absent, although acritarchs are present. They contain a limited component of terrestrial organic material, mostly sporomorphs and unstructured organic material. Woody

material is mostly carbonised and degraded to small angular fragments. Although the palynomorphs provide a predominantly terrestrial signal, ammonites are present indicating a fully marine environment.

## 5.13 Subcraspedites primitivus Chronozone (45.37–37.49 m) and lowermost Gochteodinia villosa villosa Zone (NEG Cr 1; 37.71–37.49 m)

Fossils. The interval is recognised from its ammonite and dinoflagellate cyst content. The base of the S. primitivus Zone is located at the occurrence of an ammonite fragment showing strong, distant, bullate primaries that divide into somewhat weak secondaries (Fig. 10P; Table 1). These sets of secondaries are intercalated with weak ribs that start at a level equal to the furcation level of the primaries, resulting in an appearance of distant primaries and dense secondaries and intercalatories. The bullate primaries are forward-leaning, whereas the rear secondary in the rib sets is relatively rectiradiate on the mid-flank before leaning forward towards the ventral shoulder. This gives a sinuous appearance of the ornamentation. The closest resemblance is found outside Greenland in the taxon Subcraspedites (Swinnertonia) subundulatus, known from England (Casey 1973). It has similar distant primaries and dense secondaries with a sinuous appearance. The limited material only allows cautious reference to S. (S.) cf. subundulatus. Another fragment of a small ammonite, a couple of metres higher in the core, shows dense, fine, delicate parallel ribbing (Fig. 10Q; Table 1). Its reference to Subcraspedites (Swinnertonia) sp. juv. rests both on the other specimen described from the zone and on comparison with the similarly finely ribbed juvenile Subcraspedites (Swinnertonia) sp. juv. from England (Casey 1973, pl. 4). In addition, the interval contained another ammonite fragment, poorly preserved and not sampled, and a Buchia bivalve.

Dinoflagellate cysts are rare or absent. Relatively common taxa are Apteodinium daveyi, Cribroperidinium spp., Cassiculosphaeridium magnum and Sirmiodnium grossii. Other species are present but very rare in one or two samples, whereas acritarchs, especially Pterospermella spp., are common to abundant in a thin interval (40.62–38.28 m). Stratigraphically significant species are generally missing, but the appearance of Gochteodinia villosa villosa in the S. primitivus Chronozone indicates the lower boundary of the G. villosa villosa Zone (NEG Cr 1; Nøhr-Hansen et al. 2020) and is followed by consistent G. villosa villosa in higher strata. This event is stratigraphically slightly higher (one ammonite zone) than the reported first appearances in the Subboreal region (Paracraspedites oppressus Zone; e.g. Woollam & Riding 1983), but, in contrast, the odd occurrence of rare G. villosa villosa mentioned above in the E. pseudapertum Chronozone (59.85-54.53 m) is much lower. From the Russian Platform, Riding et al. (1999) report the first appearance of rare *G. villosa* in the *Kachpurites fulgens* ammonite Zone, which they correlate with the *Subcraspedites preplicomphalus* Ammonite Zone of North-West Europe (Rogov 2020).

Presumed reworked dinoflagellate cysts are present, for example, Ambonosphaera staffinensis, Gonyaulacysta jurassica, Endoscrinium galeritum, Nannoceratopsis sp., Pareodinia halosa and Taeniaesporites iunctispina, mostly derived from Oxfordian–Kimmeridgian strata.

Biostratigraphy. Subcraspedites (Swinnertonia) subundulatus occurs in the upper Volgian Subcraspedites (Swinnertonia) primitivus Zone in England (Casey 1973, pl. 4, fig. 1). That zone is now adopted in the East Greenland zonation (Fig. 14). The upper Volgian is poorly represented by ammonites in Greenland, and the Upper Jurassic key section in Milne Land has a hiatus between the middle Volgian Epilaugeites surlyki Zone and the lower Valanginian (Callomon & Birkelund 1982). A more complete Volgian succession appears to occur in the Wollaston Forland area. In addition to the S. primitivus Zone recorded here in the Rødryggen-1 core, Rogov (2010, 2020) recognised Supracraspedites sowerbyi in the faunal succession, presumably in the CASP collection from Perisphinctes Ravine, eastern Kuhn Ø (Fig. 2; Kelly et al. 2015). The specimens were assigned to 'Beds with S. sowerbyi'. The species as such indicates the S. preplicompalus Zone in England, where it overlies the S. primitivus Zone (Casey 1973). Rogov (2010, 2020) also identified beds with Chetaites chetae overlying Subcraspedites sowerbyi. The upper Volgian may thus possibly be subdivided into S. primitivus - S. preplicomphalus -C. chetae zones. The Gochteodinia villosa villosa Zone (Nøhr-Hansen et al. 2020) is revised. The lower boundary is now defined by the first occurrence of common presence G. villosa villosa. It was previously defined by the first occurrence of the taxon, but random records of G. villosa villosa stratigraphically lower than the G. villosa villosa Zone in the East Greenland successions makes the former definition inaccurate.

Age. Late Volgian.

*Organic matter*. The organic content is low, and terrestrial woody material is rare. The diversity and abundance of marine plankton is low in this zone and becomes significantly reduced up through the zone; the lowest content is recorded in the uppermost sample (38.28 m).

## 5.14 *Praetollia maynci* Chronozone and lower *Gochteodinia villosa villosa* Zone (NEG Cr 1; 37.49–27.73 m)

Fossils. The interval is recognised from its ammonite and dinoflagellate cyst content. The base of the zone is placed

at the occurrence of an ammonite fragment (37.49 m) with delicate, low, sharp, slightly sinuous ribs (Fig. 10R; Table 1). Its ornamentation resembles *Praetollia maynci* Spath as illustrated in, for example, Spath (1952) and Surlyk (1978, pl. 5, fig. 1). A *Buchia* bivalve was also recorded in this interval.

Four samples with abundant and diverse dinoflagellate cysts assemblages are placed in this ammonite chronozone. Sirmiodinium grossi and Cribroperidinium spp. dominate the assemblage together with common Cassiculosphaeridium magnum, Gochteodinia villosa villosa and Paragonyaulacysta borealis. The acritarch Pterospermella spp. is common. Istmocystis distincta appears for the first time at 35.02 m, and Canningia compta, Scriniodinium pharo and Palaecysta palmula have their first appearances higher in the zone.

Biostratigraphy. P. maynci is the index species of the P. maynci Zone (Fig. 14). The base of the Ryazanian is the base of the Cretaceous in a Boreal sense. However, a formally chosen base of the Cretaceous, in terms of the global boundary stratotype section and point (GSSP) of the Berriasian stage in the Tethyan Realm, is yet to be defined. It has recently been proposed to take the base of the Calpionella alpina calpionellid Zone as the boundary, which would most probably correlate to the Russian Taimyroceras taimyrensis and C. nodiger zones and the English S. lamplughi Zone in the Boreal upper Volgian stage (Gale et al. 2020; Wimbledon et al. 2020).

Age. Earliest Ryazanian, Early Cretaceous.

Organic matter. The organic content is low, and terrestrial woody material is rare. In contrast, the dinoflagellate cyst assemblage is rich and diverse, in contrast to the poor assemblages in the underlying *S. primitivus* Chronozone, and indicates fully marine conditions.

## 5.15 *Hectoroceras kochi* Chronozone and lower *Gochteodinia villosa villosa* Zone (NEG Cr 1; 27.73–25.82 m)

Fossils. The interval is recognised from its ammonite and dinoflagellate cyst content. An ammonite with ribs that radiate from a very narrow umbilicus indicates pronounced involuteness (Fig. 10S; Table 1). Primaries divide into two secondaries and bend forward from the level of furcation. This ornamentation and the narrow umbilicus characterise the genus *Hectoroceras*, and the specimen is referred to *Hectoroceras* sp.

Regarding the dinoflagellate cysts (one sample), *Palaecysta palmula* dominates the unit. The acritarch *Pterospermella* spp. is common. The assemblage is relatively diverse and abundant.

Biostratigraphy. Species of the ammonite genus Hectoroceras are only recorded in the Hectoroceras kochi Zone

(Fig. 14; Wright et al. 1996). The base of the zone is placed at the ammonite in the core at 27.73 m. The top of the zone is based at the last occurrence of *Rotosphaeropsis thule* (*G. villosa* Zone, top of DSK1 Subzone; Poulsen & Riding 2003). *Palaecysta palmula* appears in the top of the *H. kochi* Zone of the North-West European Subboreal ammonite zonation (Riding & Thomas 1992). In the Rødryggen-1 core, *P. palmula* appears just above the ammonite. The *P. maynci* and *H. kochi* ammonite zones correlate with the lower *G. villosa villosa* Zone (Nøhr-Hansen et al. 2020).

The *Hectoroceras kochi* Zone is the highest ammonite zone identified and is correlated with the dinoflagellate cyst stratigraphy in this core. Alsen (2006) identified ammonites and ammonite zones in the Albrechts Bugt Member in sections near the Rødryggen-1 core. Due to solifluction in the outcrop sections, precise correlation with the core is not possible. Correlation of the dinoflagellate cyst stratigraphy with local ammonite stratigraphy in the upper Ryazanian to Valanginian is therefore beyond the scope of this study. The Ryazanian fauna is strictly Boreal, whereas the Valanginian fauna comprises Tethyan, Subboreal and Boreal elements (Alsen 2006).

Age. Latest early Ryazanian, Early Cretaceous.

*Organic matter*. The organic content is low. Degraded organic material dominates, terrestrial material is represented by sporomorphs and woody material is very rare. The fossil record testifies to a fully marine environment.

### 5.16 Upper *Gochteodinia villosa villosa* Zone (NEG Cr 1; 25.82–17.82 m)

Fossils. The interval is recognised based on its content of dinoflagellate cysts from the last occurrence of *R. thule* at 25.82 m to the first appearance of *Oligosphaeridium complex* at 17.82 m. The last occurrences of *Paragonyaulacysta borealis* and *P. capillosa* are in this interval. *Epiplosphaera* spp., *Heterosphaeridium*? spp., *Sirmiodinium grossii*, *Palaecysta palmula* and *Systematophora daveyi* dominate this unit locally. The assemblage is relatively diverse and abundant in the lower part but becomes poorer in the upper part. This change is associated with a significant depositional shift from black shale to calcareous mudstone, probably reflecting a shift to more oxygen-rich bottom conditions.

Biostratigraphy. R. thule has its last occurrence in the H. kochi Zone of the Subboreal ammonite zonation in North-West Europe (Riding & Thomas 1992; BioStrat 2018). O. complex appears for the first time at the Ryazanian–Valanginian boundary in North-West Europe (Riding & Thomas 1992) and in the Peregrinoceras albidum Zone, uppermost Ryazanian, on Store Koldewey, North-East Greenland (Nøhr-Hansen et al. 2020).

Age. Late Ryazanian, Early Cretaceous.

Organic matter. The organic content is very low and totally dominated by black, rounded grains, probably reflecting strongly oxidising bottom conditions. The presence of marine plankton, however, is indicative of a fully marine environment.

### 5.17 Lower *Oligosphaeridium complex* Zone (NEG Cr 2; 17.82–10.17 m)

Fossils. The interval is recognised based on its content of dinoflagellate cysts in the succession from the first appearance of Oligosphaeridium complex (15.85 m) to the first occurrence of Nelchinopsis kostromiensis. Oligosphaeridium complex, Oligosphaeridium spp. and Epiplosphaera spp. dominate the assemblage. The assemblage is relatively diverse and abundant in the lower part but becomes poorer upwards.

The interval is also represented by two samples analysed for calcareous nannofossils (at 16.6 and 13.82 m). The low diversity assemblage in the lower sample is dominated by Watznaueria barnesiae. Watznaueria fossacincta and Crucibiscutum salebrosum are also common. In addition, Watznaueria britannica, Watznaueria ovata, Retecapsa schizobrachiata, Retecapsa crenulata, Rotelapillus crenulatus, Sollasites horticus, Staurolithites stradneri, Assipetra infracretacea, Tegumentum stradneri, Rhagodiscus asper, Zeugrhabdotus fissus and Nannoconus concavus are present. The upper sample has an assemblage dominated by Crucibiscutum salebrosum and Watznaueria barnesiae. Also present are Assipetra infracretacea, Diazomatolithus lehmanii, Retecapsa crenulate, Rhagodiscus asper, Watznaueria fossacincta, Watznaueria britannica, Watznaueria manivitiae, Retecapsa angustiforata, Zeugrhabdotus embergeri, Cyclagelosphaera margerelii, Staurolithites stradneri, Stradnerlithus silvaradius, Tegumentum stradneri, Zeugrhabdotus erectus, Tripinnilithus shetlandensis, Zeugrhabdotus fissus and Thoracosphaera spp.

Biostratigraphy. O. complex appears for the first time at the Ryazanian-Valanginian boundary in north-western Europe (Riding & Thomas 1992), and in the top Ryazanian of North-East Greenland, Peregrinoceras albidum Zone (Stefan Piasecki unpublished data). The highest occurrence of Gochteodinia villosa villosa and Palaecysta palmula is in the lower Valanginian (Davey 1982; Riding & Thomas 1992). Poulsen & Riding (2003) correlate the last occurrence of G. villosa villosa with the top of the P. albidum Zone in North-West Europe, but this taxon is present into the lower Valanginian in the Rødryggen-1 core. The highest occurrence of Palaecysta palmula is at the top of the Paratollia Zone, upper lower Valanginian, in North-West Europe (Costa & Davey 1992) and at the top of the 'EKZ6 zone' in BioStrat (2018; mid-lower Valanginian). Nelchinopsis kostromiensis is first recorded at 10.17 m, corresponding to the

last occurrence of P. palmula (Costa & Davey 1992). However, in North-East Greenland, N. kostromiensis occurs for the first time in the upper Valanginian (Nøhr-Hansen et al. 2020). The calcareous nannofossil stratigraphy agrees fairly well with the palynostratigraphy. It indicates late Ryazanian to early Valanginian ages from high abundances of C. salesbrosum and Watznaueria spp. co-occuring with S. horticus in the upper Ryazanian to lower Valanginian of the North Sea area (Jeremiah 2001) and offshore mid-Norway (Mutterlose & Kessels 2000). R. crenulata has its first occurrence in the upper upper Ryazanian (Jakubowski 1987). The presence of Nannoconus concavus and Tripinnilithus shetlandensis in the absence of Micrantholithus speetonensis indicates the lower Valanginian nannofossil subzone BC3b (Bown et al. 1998). Pauly et al. (2012a) documented the first occurence (FO) of Crucibiscutum spp., Rhagodiscus asper and Watznaueria spp. in the upper Ryazanian of North-East Greenland.

Age. Early Valanginian, Early Cretaceous.

*Organic matter.* The organic content is very low. The presence of marine plankton, albeit scarce, indicates marine conditions. The organic terrestrial material is heavily oxidised into carbonised, angular to rounded black grains.

### 5.18 Upper *Oligosphaeridium complex* zone (NEG Cr 2; 10.17–1.10 m)

Fossils. The interval is recognised based on its content of dinoflagellate cysts. The base is placed at the first occurrence of *Nelchinopsis kostromiensis* (10.17 m), followed by the last occurrences of *Palaecysta palmula* (9.00 m) and *G. villosa villosa* (6.59 m), and the highest record of *Lagenorhytis delicatula* (1.10 m). The top of the zone is not recorded.

The dinoflagellate cyst assemblage is very poor, and the presence or absence of several species may reflect random occurrences. However, *Oligosphaeridium complex* dominates the assemblage, and *Cassiculosphaeridium magnum, Circulodinium distinctum, Epiplosphaera* spp. and *Downiesphaeridium tribuliferum* are common locally. The dinoflagellate cysts are fairly well preserved but constitute a very small fraction of the organic matter.

The interval also contains one sample analysed for its calcareous nannofossil content. The nannofossil assemblage has a low diversity dominated by *Watznaueria barnesiae*. Also present are *Watznaueria fossacincta*, *Calculites*? sp.1, *Tranolithus gabalus*, *Staurolithites stradneri*, *Rhagodiscus asper*, *Watznaueria britannica* and *Thoracosphaera* spp. *C. salesbrosum* is absent.

*Biostratigraphy*. The occurrence of *Nelchinopsis kostromiensis* indicates a late Valanginian age based on reports from the Arctic (Davies 1983; Nøhr-Hansen *et al.* 2020; Ingrams *et al.* 2021) in contrast to North-West Europe where it appears in lower Valanginian strata (e.g. Heilmann-Clausen

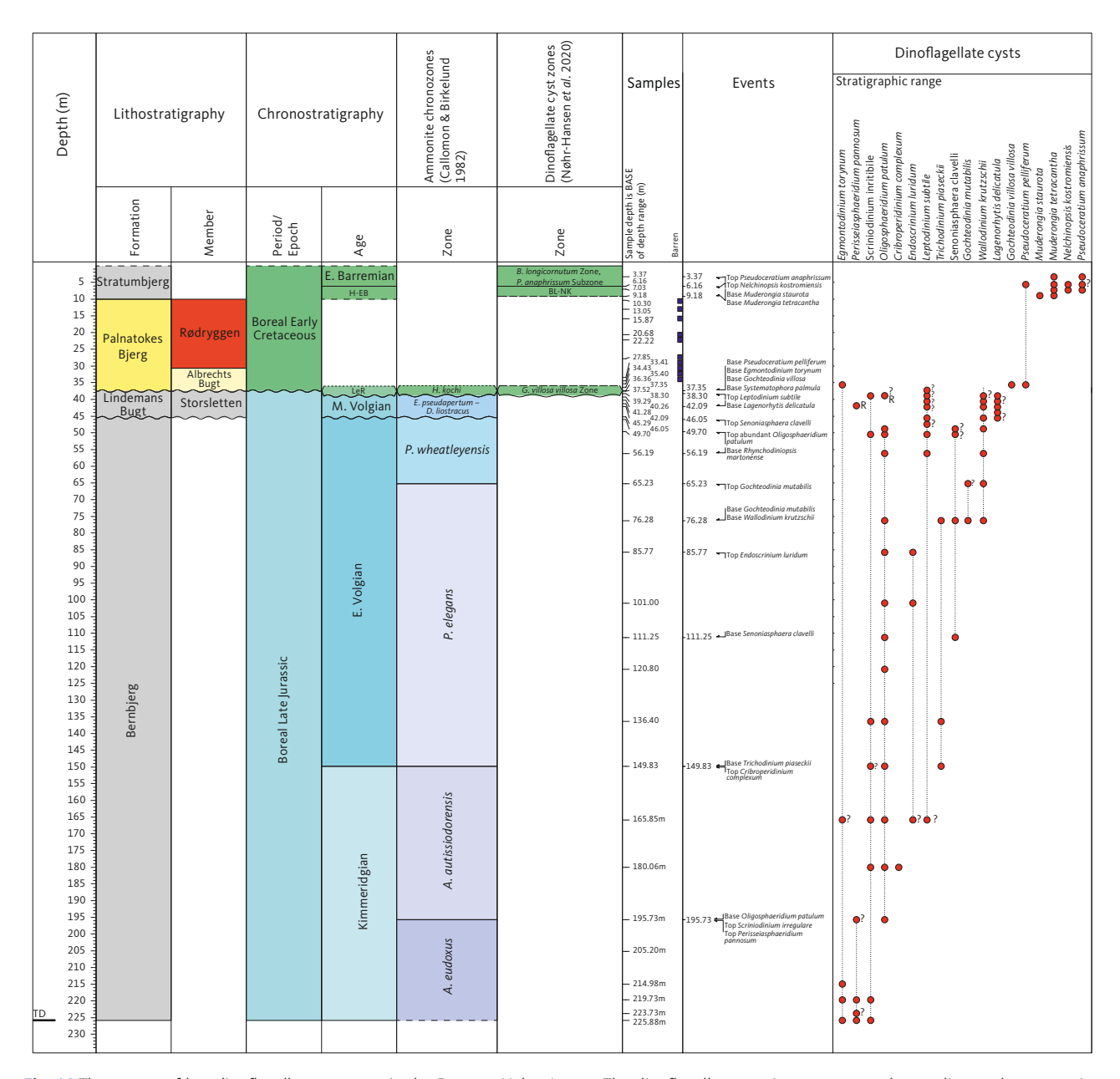


Fig. 16 The ranges of key dinoflagellate cyst taxa in the Brorson Halvø-1 core. The dinoflagellate species are arranged according to the succession of their lowest occurrences. Question mark (?): uncertainty in taxonomic identification. R: reworked or redeposited. A range chart showing all taxa recorded in the core is available in Supplementary Data File 2. H-EB: Hauterivian – Early Barremian. LeR: Latest early Ryazanian. BL-NK: B. longicornutum Zone – N. kostromiensis Subzone. E.: early. M.: middle.

& Birkelund 1987; Costa & Davey 1992; BioStrat 2018). The last occurrences of *Gochteodinia villosa villosa* and *P. palmula* and the continuous presence of *Lagenorhytis delicatula* in the uppermost core sample may suggest upper Valanginian strata as recorded in North-West Europe (Davey 1982; Riding & Thomas 1992).

The calcareous nannofossils *T. gabalus, R. asper* and *Watznaueria* spp. range from the upper Ryazanian in the North Sea (Jakubowski 1987; Jeremiah 2001), North-East Greenland (Pauly *et al.* 2012a) and off mid-Norway in the northern North Atlantic (Mutterlose & Kessels 2000). *Calculites*? sp.1 was described in Bown *et al.* (1998) as ranging from the Early Hauterivian? to the Early? Barremian, albeit in Tunisia and Bulgaria. Of note is the absence of

*C. salesbrosum.* In North-East Greenland, this species has its last appearance datum in the late Hauterivian (Pauly *et al.* 2012a) and a little later in the North Sea (Jakubowski 1987). However, the absence of this species is probably an artefact of preservation, since the age suggested by its apparent absence is too young compared with the palynostratigraphy of the interval, as well as the ammonite stratigraphy obtained in an outcrop study of the Albrechts Bugt Member at the drill site (Alsen 2006).

Age. Late Valanginian, Early Cretaceous.

Organic matter. The interval is characterised by a low organic content with little marine plankton and no

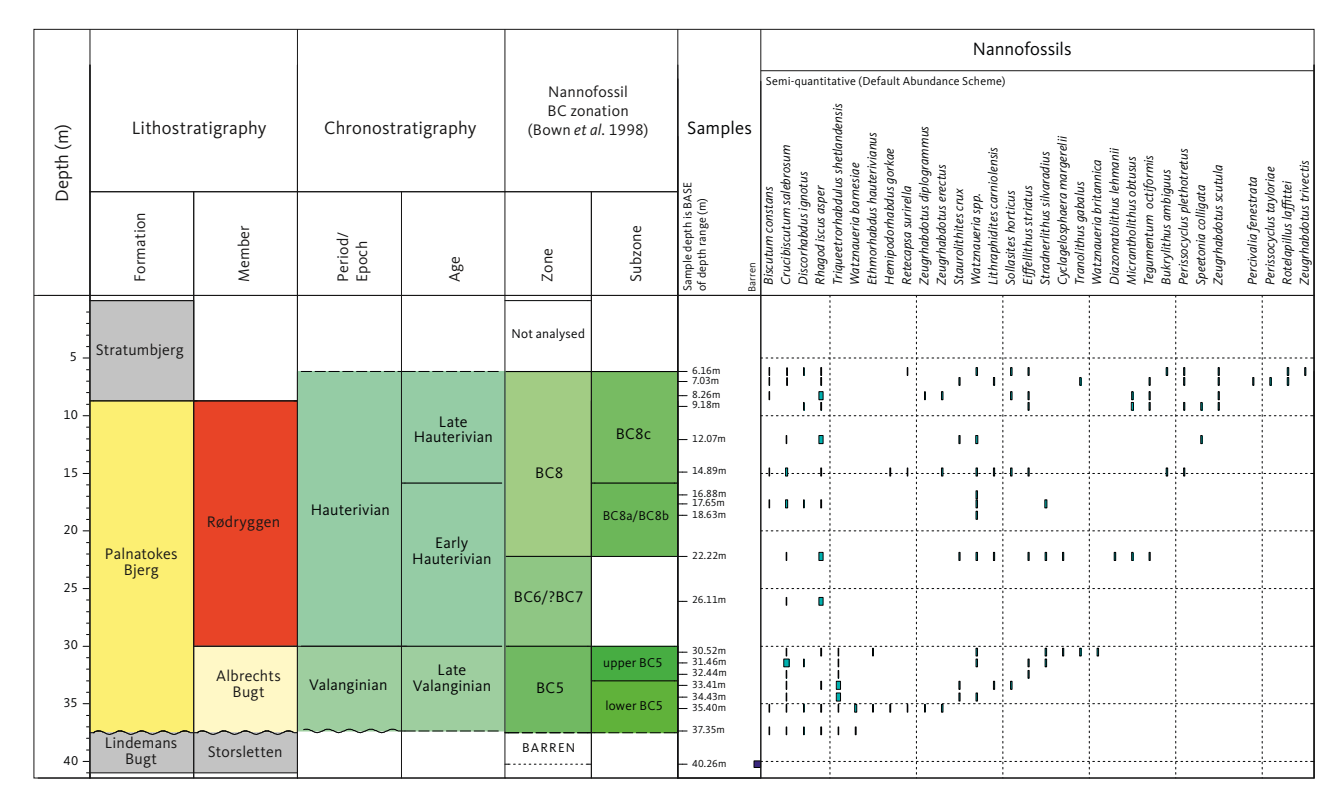


Fig. 17 The distribution of calcareous nannofossils in the Brorson Halvø-1 core.

recognisable terrestrial organic material. Marine conditions are indicated by the macrofauna and calcareous flora.

### 6. Biostratigraphy of the Brorson Halvø-1 core

The biostratigraphic subdivision of the Brorson Halvø-1 core is described from TD at 225.7 m upwards. The location of bulk-rock samples is seen in the charts, illustrating the distributions and ranges of dinoflagellate cyst and calcareous nannofossil taxa (Figs 16, 17). Selected dinoflagellate cysts are figured in Fig. 13.

### 6.1 *Aulacostephanus eudoxus* Chronozone (225.7 m (TD) – 195.73 m)

Fossils. The recognition of the zone is based on the dinoflagellate cyst record. The base of the zone is placed at the base of the core (at TD 225.7 m). The dinoflagellate cyst assemblage is generally poor, and dinoflagellate cysts are not common; Gonyaulacysta jurassica, G. dualis, Sirmiodinium grossii and Scriniodinium irregulare are locally common. Perisseiasphaeridium pannosum is rare to common, but not as abundant as normally recorded in East Greenland.

*Biostratigraphy. P. pannosum* occurs in the lowermost analysed sample at 225.88 m and is common at the top, at 195.73 m, where it coincides with the appearance of common to abundant *Oligosphaeridium patulum*. This

indicates an interval corresponding to the ammonite horizons M 20 – M 22, *A. eudoxus* Zone (Piasecki 1996). No other recorded dinoflagellate cysts indicate correlation to zones below the *A. eudoxus* Chronozone, and the succession correlates, therefore, with the *A. eudoxus* Chronozone. The dinoflagellate cysts *Atopodinium haromense*, *Dingodinium minutum*, *Nannoceratopsis pelucida*, *Paragonyaulacysta capillosa* and *Taeniophora iunctispina* occur scattered throughout this zone.

Age. Kimmeridgian, Late Jurassic.

Organic matter. Amorphous kerogene dominates together with terrestrial, organic material from higher land plants, especially sporomorphs and black woody material. The woody material is physically degraded to rounded and angular grains in the lower levels of the succession; the grains become lath-shaped and larger upwards. The presence of dinoflagellate cysts indicates a marine environment, and the dominance of AOM is suggestive of oxygen-deficient bottom conditions.

Remarks. The interpreted late Kimmeridgian age at the base of the well agrees with the find of an ammonite in a measured outcrop section, c. 200 m below the Albrechts Bugt Member, Palnatokes Bjerg Formation (M. Bjerager, pers. comm. 2022). The ammonite is identified as Amoeboceras subkitchini from the upper lower Kimmeridgian Rasenia cymodoce Zone (Figs 14, 18).

### 6.2 Aulacostephanus autissiodorensis Chronozone (195.73–149.83 m)

Fossils. The recognition of the zone is based on its dinoflagellate cyst record. The base of the zone is placed at the first appearance of common to abundant *Oligosphaeridium patulum* (195.73 m) and its top at the first appearance of *Trichodinium piaseckii* coincident with the last occurrence of *Cribroperidinium complexum* (149.83 m).

The dinoflagellate cyst assemblage is generally poor but is characterised by common to abundant *Oligosphaeridium patulum* and *Paragonyaulacysta capillosa*. *Atopodinium* spp., *Circulodinium* spp., *Pareodinia* spp. and *Sirmiodinium grossii* are common locally. The assemblage is mostly of low diversity and low abundance, probably due to the abundance of organic matter in the samples.

Biostratigraphy. Common to abundant *O. patulum* appears between ammonite horizons M 22 – M 23 in Milne Land near the boundary between the *A. eudoxus* and *A. autissiodorensis* Zones (Piasecki 1996; Alsen & Piasecki 2018). *T. piaseckii* appears below ammonite fauna horizon M 25, *P. wheatleyensis* Zone (Piasecki 1996). The succession is, therefore, correlated with the *A. autissiodorensis* and *P. elegans* Zones.

Age. Kimmeridgian, Late Jurassic.

*Organic matter*. The interval contains amorphous kerogen together with abundant terrestrial organic material from



**Fig. 18** Amoeboceras subkitchini (MGUH 34201 from GEUS 469823) ammonite from upper lower Kimmeridgian Rasenia cymodoce Zone. Collected stratigraphically c. 200 m below the Albrecht Bugt Member (Palnatokes Bjerg Fm) in an outcrop section measured along a small ravine from the Brorson Halvø-1 drill site and towards the west. The specimen is housed in the Palaeontology Type Collection at the Natural History Museum of Denmark and labelled with an MGUH number – Museum Geologica Universitas Hafniensis.

higher land plants, especially sporomorphs and black, lathshaped woody material. The presence of dinoflagellate cystsindicates a marine environment, and the dominance of AOM is suggestive of oxygen-deficient bottom conditions.

### 6.3 *Pectinatites elegans* Chronozone (149.83–65.23 m)

Fossils. The zone is based on the dinoflagellate cyst record. The base of the zone is recognised at the first occurrence of *Trichodinium piaseckii* coincident with the last occurrence of *Cribroperidinium complexum*.

The dinoflagellate cyst assemblage is dominated by *Cribroperidinium* spp., *Circulodinium* spp., *Oligosphaeridium patulum*, *Pareodinia* sp., *Paragonyaulacysta borealis* and *P. capillosa* in the lower part of the zone. *Cassiculosphaeridium magnum*, *Gochteodinia mutabilis*, *Oligosphaeridium patulum*, *Paragonyaulacysta capillosa*, *Sirmiodinium grossii*, *Tenua hystrix*, *Tubotuberella* spp. and the acritarch *Wallodinium krutschi* are more common in the upper part of the zone. The assemblage is relatively diverse and abundant.

Biostratigraphy. The first occurrence of *T. piaseckii* is coincident with the last occurrence of *C. complexum* in this core and in the Rødryggen-1 core, where it correlates with the lower boundary of the *P. elegans* Zone. The first occurrence of *T. piaseckii* is followed successively by the first occurrences of *Senoniasphaera clavellii* and *Gochteodinia mutabilis* and the last occurrence of common *O. patulum*. All these events are located below ammonite horizon M 25, Wheatleyensis Zone, in Milne Land (Piasecki 1996) suggesting correlation with the *P. elegans* Zone. These events coincide in the relatively condensed succession in Milne Land, whereas they occur in succession in both Rødryggen-1 and Brorson Halvø-1 cores.

Age. Early Volgian, Late Jurassic.

Organic matter. Abundant amorphous kerogen dominates together with abundant terrestrial organic material from higher land plants, especially sporomorphs and brown and black woody material. The presence of dinoflagellate cysts indicates a marine environment, and the dominance of AOM is suggestive of oxygen-deficient bottom conditions.

### 6.4 *Pectinatites wheatleyensis* Chronozone (65.23–45.5 m)

Fossils. The zone is based on the dinoflagellate cyst record. The base of this zone is placed at the last occurrence of common *Gochteodinia mutabilis*. The top of the zone is bounded by an unconformity marking a significant hiatus.

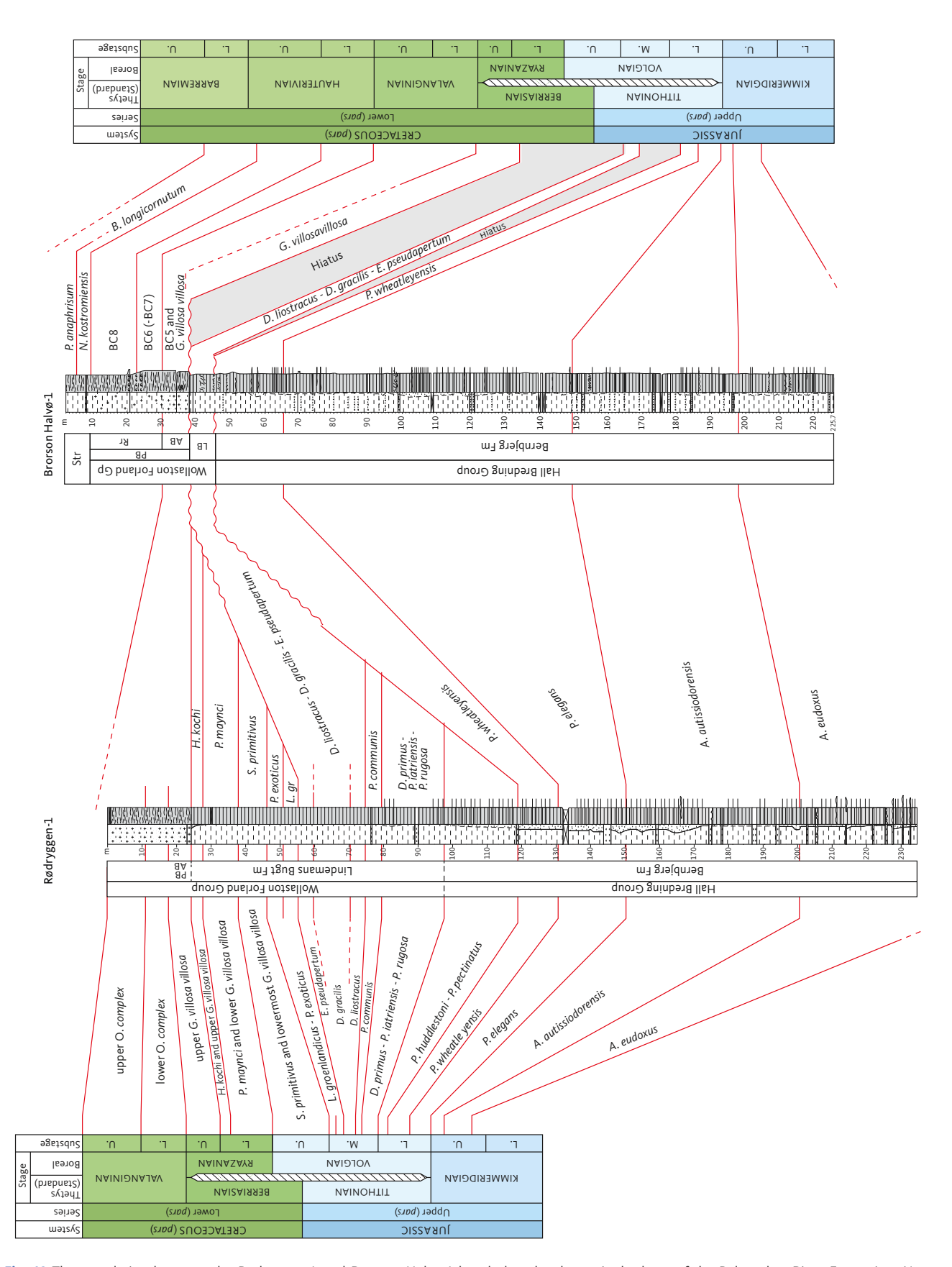


Fig. 19 The correlation between the Rødryggen-1 and Brorson Halvø-1 boreholes; the datum is the base of the Palnatokes Bjerg Formation. Note the complete stratigraphy in the Rødryggen-1 well compared to the significant hiatuses within the Volgian–Ryazanian in the Brorson Halvø-1 core. The zones that are present in the Rødryggen-1 well and absent in the Brorson Halvø-1 well are here shown schematically to onlap the unconformity. Although it could be argued that these zones were also represented in the Brorson Halvø-1 area and subsequently removed by erosion of the crest during tilting of the fault block, the lack of redeposited palynomorphs of these ages in the Rødryggen-1 core favours an onlap model. AB: Albrechts Bugt Mb. LB: Lindemans Bugt Formation. PB: Palnatokes Bjerg Fm. Rr: Rødryggen Member. Str: Stratumbjerg Formation. See Fig. 4 for legend and grain size.

Biostratigraphy. Common *G. mutabilis* characterises the dinoflagellate cyst assemblage in the uppermost *P. elegans* Zone in Milne Land and ammonite faunal horizon M 25, and *P. wheatleyensis* Zone correlates with the top of this interval (Piasecki 1996). The last occurrences of abundant *O. patulum* and *S. clavellii* occur in the upper part of the interval, followed by a change in composition of the dinoflagellate cyst assemblage in overlying strata.

Age. Early Volgian, Late Jurassic.

Organic matter. Abundant amorphous kerogen together with dinoflagellate cysts dominates; terrestrial plant material is less significant, occurring mainly as sporomorphs but also some black woody material. The presence of dinoflagellate cysts indicates a marine environment, and the dominance of AOM is suggestive of oxygen-deficient bottom conditions.

#### 6.5 Unconformity (45.5 m)

The occurrence of the *D. liostracus – E. pseudapertum* Zones immediately overlying the *P. wheatleyensis* Zone defines a significant stratigraphic break. The unconformity corresponds to the *P. huddlestoni – P. communis* Zones, spanning the upper lower Volgian to lower middle Volgian. Biostratigraphically, the unconformity is located between 42.09 and 46.05 m and placed at the lithostratigraphic boundary at 45.5 m.

## 6.6 Dorsoplanites liostracus – Epipallasiceras pseudapertum Chronozones undiff. (45.5–37.50 m)

Fossils. The zone is based on the dinoflagellate cyst record and correlated with the succession in the Rødryggen-1 core from the first appearance of Lagenorhytis delicatula (42.09 m) to the top of Leptodinium subtile (38.30 m). Cribroperidinium spp. dominates the assemblage, and Rhynchodiniopsis spp. is common. The lower boundary, however, is placed at the inferred unconformity at the lithostratigraphic boundary at 45.5 m. The assemblage is relatively diverse and abundant.

Biostratigraphy. The unusual appearance of Lagenorhytis delicatula as stratigraphically low as the middle Volgian strata is recorded in the Rødryggen-1 core (this study). In contrast, the last occurrence of Leptodinium subtile is a well-known stratigraphic marker in North-West Europe, where it has its highest occurrence in the Progalbanites albani (ammonite) Zone (Riding & Thomas 1992). The upper P. albani Zone is correlated with the E. pseudapertum Zone in the East Greenland ammonite zonation (Birkelund et al. 1984). The top occurrence of L. subtile

just below the ammonite *Epipalliceras pseudapertum* in the Rødryggen-1 core (this study) supports this correlation. Characteristic Boreal, uppermost Jurassic species, e.g. *Paragonyaulacysta borealis*, *P. capillosa* and the acritarch *Wallodinium krutzschii*, that are common in the lower core interval disappear in this zone and are absent throughout the rest of the overlying uppermost Jurassic interval.

Age. Middle Volgian, Late Jurassic.

Organic matter. The interval contains abundant amorphous kerogen with little terrestrial plant material, mainly sporomorphs and a limited content of dinoflagellate cysts. The presence of dinoflagellate cysts indicates a marine environment, and the dominance of AOM is suggestive of oxygen-deficient bottom conditions.

#### 6.7 Unconformity (37.50 m)

The *G. villosa* villosa dinoflagellate cyst Zone, here equivalent to the *H. kochi* ammonite Chronozone, directly overlies the *P. liostracus – E. pseudapertum* Zones. It marks a major stratigraphic break with a hiatus corresponding to the *C. anguinus – P. maynci* Zones interval, spanning the middle middle Volgian to the lower Ryazanian (Fig. 14).

## 6.8 Gochteodinia villosa villosa Zone (NEG Cr 1) and Calcareous Nannofossil Zone BC5 (37.35–30.52 m)

Fossils. The palynozone is recognised only in one sample at 37.35 m. The assemblage is poor, low density, but due to hardly any other organic matter in this sample, the whole assemblage is recovered in one slide. The assemblage is characterised by a high diversity, especially compared to the organic-rich samples analysed from deeper levels in the core. The interval is barren of dinoflagellate cysts in the upper part (36.36–30.52 m).

The calcareous nannofossil zone BC5 has its base at 37.35 m, 15 cm above the base of the calcareous Albrecht Bugt Member (Fig. 17). The upper boundary is placed at 30.52 m, where the assemblage is characterised by very low diversity without age-diagnostic nannofossils. The assemblage of BC5 consists of common to abundant *Crucibiscutum salebrosum*, *Watznaueria* spp., few *Biscutum constans*, *Rhagodiscus asper*, *Triquerhabdulus shetlandensis*, *Staurolitithes* crux, *Zeugrhabdotus* spp., *Cretarhabdus* spp. and *Discorhabdus* spp. (Fig. 17).

Biostratigraphy. The combined presence of dinoflagellate cysts Rotosphaeropsis thule and Palaecysta palmula indicates a Lower Cretaceous, mid-Ryazanian assemblage. R. thule has its range top in uppermost lower Ryazanian, H. kochi Zone in the Rødryggen-1 core. P. palmula is reported to appear in the top of the H. kochi Zone, uppermost lower Ryazanian in North-West Europe (Riding & Thomas 1992) and in the Rødryggen-1 core (this study), where it appears just above an H. kochi ammonite. The absence of abundant Oligosphaeridium complex supports the Ryazanian age, since its first appearance is in the lowermost Valanginian as reported both in North-West Europe (Riding & Thomas 1992) and in the Rødryggen-1 well (this study) as well as in the P. albidum ammonite Zone, uppermost Ryazanian on Store Koldewey, northern East Greenland (Nøhr-Hansen et al. 2020). The G. villosa villosa Zone thus correlates with the *H. kochi* (ammonite) Zone.

The calcareous nannofossil assemblage suggests the presence of the calcareous nannofossil zone BC5 of Bown *et al.* (1998). Common *T. shetlandensis* and the high abundance of *C. salebrosum* in the lower four samples and the co-occurrence of *Eiffellithus striatus* with *T. shetlandensis* in the upper three samples further suggest subdivision of the interval and the identification of the lower and upper BC5-zonal intervals, respectively (Fig. 17).

Age. Latest early Ryazanian - Valanginian. The dinoflagellate cysts indicate the base of the interval to be latest early Ryazanian. The calcareous nannofossil assemblages, on the other hand, indicate a late Valanginian age that is somewhat younger than the palynostratigraphic age derived from the basal sample of the interval. Previous studies of the ammonite assemblage collected from outcrops of the Albrechts Bugt Member at the drill site suggested a late Ryazanian - late early Valanginian age (Alsen 2006). A late Valanginian age based on the BC5 zone also significantly differs from the BC1 zone and late Ryazanian age of the base of the Albrechts Bugt Member in the Wollaston Forland area (Pauly et al. 2012a). A slight revision of stratigraphic ranges of Ryazanian-Valanginian calcareous nannofossil zones in the Boreal scheme was based on Sr-isotope and C-isotope stratigraphy (Möller et al. 2015). The offset in ages obtained from dinoflagellate cysts and calcareous nannofossils observed is, however, far beyond the smaller adjustments recorded by Möller et al. (2015).

Organic matter. A very little organic content comprising rounded to angular, carbonised grains with some dinoflagellate cysts and hardly any terrestrial plant material. This abrupt change in the nature of the organic fraction in the Brorson Halvø-1 core reflects a significant hiatus, whereas a corresponding rapid environmental change in the Rødryggen-1 well takes place over approximately 1 m of transitional beds in the Upper Ryazanian (this study).

### 6.9 Calcareous nannofossil Zones BC6-BC7? (30.52-22.22 m)

Fossils. This interval is characterised by the lack of age-diagnostic calcareous nannofossils hampering a precise age assessment. The interval is barren of dinoflagellate cysts. The absence of the calcareous nannofossils *T. shetlandensis*, *Eprolithus antiquus* and *Tegumentum octiformis* indicates the possible presence of the zones BC6–BC7, and the interval is tentatively assigned to BC6–BC7? (Fig. 17).

Age. The BC6 and BC7 zones are considered early Hauterivian in age (Bown et al. 1998).

*Organic matter*. The interval has a very low organic content of angular to rounded carbonised grains.

### 6.10 Calcareous nannofossil Zone BC8 (22.22–9.18 m)

Fossils. The assemblage contains common to abundant Watznaueria spp., R. asper, B. constans, Zeugrhabdotus spp. as well as few D. ignotus, Eiffellithus striatus, Perissocyclus spp. and rare Sollasites horticus, C. salebrosum, Bukrylithus ambiguus and pentaliths; all are characteristic of the higher Rødryggen Member. The interval is barren of dinoflagellate cysts.

Biostratigraphy. The assemblage suggests the presence of the BC8 Zone. E. striatus, T. octiformis, a few Stradner-lithus silvaradius and rare C. salebrosum in the lower part indicate the presence of the BC8a-b Subzone; Perissocyclus plethotretus and Z. scutula in the upper part indicate the overlying BC8c Subzone (Fig. 17).

Age. Late early Hauterivian – early late Hauterivian. In contrast to the conflicting ages obtained for the underlying Albrechts Bugt Member (interval 37.50–30.52 m), the calcareous nannofossil age indicated for this interval, the upper part of the Rødryggen Member, agrees well with the previously recorded age of the Rødryggen Member (Alsen 2006; Alsen & Mutterlose 2009; Pauly *et al.* 2012a).

*Organic matter*. The interval has a very low organic content of angular to rounded carbonised grains.

#### 6.11 Batioladinium longicornutum Zone (I), N. kostromiensis palyno Subzone (I1) and calcareous nannofossil Zone BC9 (9.18–6.16 m)

Fossils. The base of the zone is placed at the first occurrence of the palynomorphs *Nelchinopsis kostromiensis*, *Muderongia staurota* and *M. tetracantha*. The index fossil of the subzone is thus present, whereas the index of the

Batioladinium longicornutum longicornutum Zone was absent. The dinoflagellate cyst assemblage is characterised by Oligosphaeridium asterigerum, Oligosphaeridium complex, Circulodinium distinctum, Clesistosphaeridium aciculare, Muderongia staurota and M. tetracantha. Oligosphaeridium asterigerum and Circulodinium distinctum dominate the assemblage (Supplementary Data File 2). The assemblage is relatively poor in the lower part but becomes diverse and abundant upwards.

The calcareous nannofossil assemblage is characterised by common to abundant *Watznaueria* spp., *R. asper, B. constans* and *Zeugrhabdotus* spp. It contains few *D. ignotus, Eiffellithus striatus* and *Perissocyclus* spp., and rare *Sollasites horticus, C. salebrosum, Bukrylithus ambiguus* and *pentaliths*.

Biostratigraphy. Muderongia staurota and M. tetracantha have their first occurrences in the upper Hauterivian S. gottschei ammonite Zone according to Costa & Davey (1992) and Duxbury (2001). The highest occurrence of Nelchinopsis kostromiensis is in the upper Hauterivian? – lower Barremian Nelchinopsis kostromiensis Subzone (I1) in Nøhr-Hansen (1993) and Nøhr-Hansen et al. (2020).

The presence of the calcareous nannofossils *E. striatus*, *P. plethotretus*, *P. tayloriae*, *T. octiformis*, *S. colligata* and *Z. scutula* combined with the absence of *C. salebrosum*, *S. silvaradius*, *Tegulalithus septentrionalis* and *Clepsilithus maculosus* suggest the BC9 Zone (Fig. 17).

Age. Late Hauterivian to early Barremian based on palynostratigraphy. Calcareous nannofossils indicate a late Hauterivian age.

Organic matter. The interval is characterised by a very low organic content that is dominated by black angular to rounded carbonised grains with few dinoflagellate cysts; the latter testify to a marine depositional environment.

Remarks. It is noteworthy that this interval, which is in the lower part of the Stratumbjerg Formation, yields calcareous nannofossils despite a return to black mudstone deposition. Calcareous nannofossils are thus not restricted to the marls of the underlying Albrechts Bugt and Rødryggen Members. Despite a sharp boundary between the Palnatokes Bjerg Formation and the Stratumbjerg Formation observed in the field (Figs 5, 6), there appears to be a gradual transition between the two units in terms of palaeoecology and calcareous nannoplankton production.

### 6.12 Batioladinium longicornutum Zone (I), *P. anaphrissum* Subzone (I2) (6.16–0 m)

Fossils. The subzone is based on the dinoflagellate cyst record in one sample (Fig. 16; Supplementary Data File 2).

The base of the subzone is recognised at the last occurrence of *Nelchinopsis kostromiensis*. The subzone ranges to the last occurrences of *Pseudoceratium anaphrissum*. *Oligosphaeridium asterigerum*, *Oligosphaeridium complex*, *Circulodinium distinctum*, *Clesistosphaeridium aciculare* and *Muderongia tetracantha* dominate the assemblage.

Biostratigraphy. The highest occurrence of Nelchinopsis kostromiensis is in upper Hauterivian? to lower Barremian, Nelchinopsis kostromiensis Subzone (I1) in Nøhr-Hansen (1993). The highest occurrences of Batioladinium longicornutum and Hystrichodinium aborispinum are in the upper Barremian, whereas the highest occurrence of Pseudoceratium anaphrissum is in the upper part of the lower Barremian Pseudoceratium anaphrissum Subzone (I2) in Nøhr-Hansen (1993) and Nøhr-Hansen et al. (2020).

Age. Early Barremian, Early Cretaceous.

*Organic matter*. The interval has a very low organic content dominated by black, angular, carbonised grains with few dinoflagellate cysts, the latter of which indicate a marine depositional environment.

#### 7. Discussion

### 7.1 The Jurassic-Cretaceous boundary in (North-East) Greenland

The Jurassic system is characterised by a highly detailed subdivision by means of ammonite zones, which form the standard biostratigraphic and chronostratigraphic framework. Ammonite provincialism in some intervals hampers direct correlation to the standard ammonite zonation (established in North-West Europe), and secondary standards are then established locally. Difficulties in ammonite correlation are particularly pronounced around the Jurassic-Cretaceous boundary leading to separate chronostratigraphic divisions even at the Stage level in separate faunal provinces. The ammonite zonation for most of the Upper Jurassic in East Greenland is mainly based on the ammonite successions in Milne Land and Jameson Land (Callomon & Birkelund 1982; Birkelund et al. 1984; Birkelund & Callomon 1985). The Oxfordian ammonite zonation used in East Greenland belongs to the Boreal and Subboreal faunal provinces (Sykes & Callomon 1979; Birkelund et al. 1984; Zeiss 2003). Less provincialism during the Kimmeridgian allows the ammonite succession in Greenland to be referred to the standard ammonite zonation of North-West Europe (Birkelund & Callomon 1985; Zeiss 2003). Provincialism increased progressively during the latest Jurassic. The lower Volgian ammonite zonation in Greenland is adopted from England, whereas a separate Boreal zonation was

established for the middle Volgian in Greenland, allowing only few correlation levels to the Subboreal zonation of England (Callomon & Birkelund 1982; Zeiss 2003).

The Milne Land area is characterised by a gap in the sedimentary succession between the middle Volgian and the lowermost Cretaceous, whereas the upper Volgian in southern Jameson Land is documented by scattered biostratigraphic data. Further to the north, a more complete Jurassic-Cretaceous boundary succession exists in the Wollaston Forland - Kuhn Ø area. The thick, coarse-grained succession represents synrift deposition and contains only sporadic levels with ammonites. The ammonite succession was documented by Maync (1949), Donovan (1964) and Surlyk (1978) providing a zonation that covers the middle Volgian to Ryazanian. Only one zone (Praechaetaites tenuicostatus Zone) has been assigned to the upper Volgian; this has since been referred to the uppermost middle Volgian (Rogov 2020). However, the presence of Subcraspedites (Swinnertonia) from Kuhn Ø (Casey 1973) and a record of this genus in the present study indicate the presence of the Subboreal Subcraspedites primitivus Zone in Greenland, providing a correlation of the base upper Volgian from Greenland to North-West Europe.

The ammonite zonation of the Upper Jurassic to Lower Cretaceous interval of relevance to the present study is shown in Fig. 14. Note the usage of Boreal Stage names and the position of the Boreal Upper Jurassic – Lower Cretaceous boundary at the Volgian–Ryazanian boundary. The Jurassic–Cretaceous boundary in the standard chronostratigraphy established in the Tethyan Realm is placed at the Tithonian–Berriasian boundary. That level probably corresponds to the middle–upper Volgian boundary, implying that the uppermost Boreal Jurassic is to be considered lowermost Cretaceous in an international sense.

The definition of the base of the Cretaceous System in terms of a GSSP still remains unresolved. It is agreed that the GSSP should be located in the Tethyan Realm, but it remains to be determined what proxies (e.g. calpionelid microfossils and magnetostratigraphy) are most appropriate for defining the boundary. Once formal recognition is achieved, correlation with the Boreal and Arctic regions can be undertaken. The sedimentary cores recovered at Rødryggen-1 and Brorson Halvø-1 may thus become important reference sections for the Jurassic–Cretaceous boundary in the Boreal Realm as they record a succession across the boundary. In this regard, Rødryggen-1 is particularly significant with its biostratigraphically nearly unbroken section (Fig. 19).

#### 7.2 Basin evolution

Deposition of the Palnatokes Bjerg Formation marked an abrupt end to the Late Jurassic dysoxic-anoxic-euxinic

basin environment and black, organic-rich mudstone deposition (the Bernbjerg Formation and the Storsletten Member of the Lindemans Bugt Formation). The Palnatokes Bjerg Formation was deposited in the final, waning phase of rifting, during which the tilted and rotated Jurassic fault blocks possibly underwent a last phase of faulting, which led to an even finer subdivision of the blocks. The differences in lithology and thickness observed in the Albrechts Bugt and Rødryggen Members reflect strong local control on deposition. For example, the Albrechts Bugt Member at the Rødryggen-1 and Brorson Halvø-1 well sites at Stratumbjerg and at Perisphinctes Ravine (Kuhn Ø) is characterised by highly condensed, relatively carbonate-rich mudstones that were deposited on local submarine highs (Surlyk 1978; Alsen 2006). The carbonate content is mainly derived from calcareous nannofossils (Pauly et al. 2012a). The member is markedly thicker, less condensed and carbonate poor at, for example, Kuhnpasset and Niesen (Surlyk 1978), reflecting greater accommodation space and higher sedimentation rates in deeper parts of the basin. This probably reflects a change from half-graben basins on a rotated, westerly-tilted block during the Middle Jurassic to Volgian to greater fragmentation in the late Ryazanian to Hauterivian, when deposition occurred in smaller horst and graben systems.

The light grey and red sediments of the condensed Albrechts Bugt and Rødryggen Members, deposited on submarine highs, reflect well-oxygenated conditions related to a period of cold climate (Alsen 2006). Oceanographic changes driven by deep-water formation in the northern proto-North Atlantic or in the Boreal Arctic Sea resulted in a palaeo-Gulf Stream that allowed for the immigration of several Tethyan faunal and floral elements to eastern Greenland (Ager 1971; Alsen 2006; Pauly et al. 2012b). Time-equivalent units, which are compositionally similar to the calcareous Albrechts Bugt and Rødryggen Members, occur scattered in the northern North Atlantic and the Arctic, for example, on Andøya, on the Norwegian shelf, in the Barents Sea and at Svalbard (Kong Karls Øya). These units show that oceanic currents ventilated the sea water throughout the Greenland-Norwegian rift basin and the Arctic Sea during the late Ryazanian-Valanginian-Hauterivian. The Palnatokes Bjerg Formation is overlain by the Stratumbjerg Formation, which marks the return to grey, dark mudstone deposition. Deposition of the Stratumbjerg Formation reflects the rising sea level during postrift thermal subsidence. In most places, the base of the formation is in the Barremian (Bjerager et al. 2020), but at some localities, including the Brorson Halvø-1 core, the transition from the red mudstones of the Rødryggen Member to the grey mudstones of the Stratumbjerg Formation occurs in the upper Hauterivian (Bjerager *et al.* 2020; Nøhr-Hansen *et al.* 2020).

#### 8. Conclusions

The Rødryggen-1 core (234.4 m thick) is assigned to the Bernbjerg Formation (234.4 (TD) - 97 m), the Lindemans Bugt Formation (97-24.40 m) and the Palnatokes Bjerg Formation (24.40-0 m). The Lindemans Bugt Formation is represented by a new member, the Storsletten Member, which records deposition of dark mudstones on the Permpas Block. This region is detached from the coarse-grained depositional system of the western fault blocks fringing the main riftbasin bounding fault. The age of the cored succession is determined from integrated ammonite, palynofossil and calcareous nannofossil stratigraphy and ranges from the upper Kimmeridgian A. eudoxus ammonite Zone to the upper Valanginian O. complex dinoflagellate cyst Zone. There are essentially no biostratigraphic gaps in the succession.

The Brorson Halvø-1 core (225.70 m thick) is assigned to the Bernbjerg Formation (225.7 (TD) - 45.5 m), the Lindemans Bugt Formation (Storsletten Member; 45.5–37.5 m), the Palnatokes Bjerg Formation, including the Albrechts Bugt (37.5-30 m) and Rødryggen Members (30-8.7 m), and the Stratumbjerg Formation (8.7-0 m). The age of the cored succession is determined from integrated ammonite, palynofossil and calcareous nannofossil stratigraphy and ranges from the late Kimmeridgian A. eudoxus ammonite Zone to the lower Barremian B. longicornutum dinoflagellate cyst Zone or *P. anaphrisum* Subzone. The succession is characterised by two major biostratigraphic gaps representing unconformities in the succession that bound the Storsletten Member. They reflect rotation of the Permpas Block and uplift of the block crest during the middle Volgian rift climax, which resulted in repeated non-deposition in contrast to the deeper basin setting of Rødryggen-1.

Both cores, but in particular, the stratigraphically complete Rødryggen-1 core, provide key stratigraphic reference sections for the Jurassic–Cretaceous boundary interval in Greenland, with wider implications in the Arctic and North Atlantic regions.

#### **Acknowledgements**

A. Ryge and D. Samuelsen prepared the palynofossil slides and calcareous nannofossil slides. J. Halskov and M.C. Porse did the drafting. Data were collected under the auspices of GEUS' Petroleum Geological Studies, Data and Services in East and North-East Greenland, a collaboration project between GEUS and several industry companies (Bojesen-Koefoed *et al.* 2014). We acknowledge the useful reviews by S. Schneider and C. Schröder-Adams, and editorial comments from Jon R. Ineson and Jørgen A. Bojesen-Koefoed.

#### **Additional information**

#### **Funding statement**

Core drilling and fieldwork were undertaken during the Geological Survey of Denmark and Greenland (GEUS) field and drilling campaign in North-East Greenland in 2009 and 2010. The subsequent study was funded by a consortium of industry energy companies and the GEUS.

#### **Author contributions**

PAL: Concept. Writing – original draft (lead), ammonites and stratigraphy, lithostratigraphy, discussion, editing

SPI: Concept. Writing – original draft (second lead), palynostratigraphy Jurassic interval

HNH: Writing - palynostratigraphy Cretaceous interval

ES: Writing – calcareous nannofossil stratigraphy Rødryggen-1 core SPA: Writing – calcareous nannofossil stratigraphy Brorson-1 core JH: Writing – lithostratigraphy

#### **Competing interests**

The authors declare no competing interests.

#### **Additional files**

Two figures are available as supplementary files at <a href="https://doi.org/10.22008/FK2/KTPO5R">https://doi.org/10.22008/FK2/KTPO5R</a>. Supplementary Data File 1: A full range chart for palynomorphs in the Rødryggen-1 core is provided to supplement Fig. 7. Supplementary Data File 2: A full range chart for palynomorphs in the Brorson Halvø-1 core is provided to supplement Fig. 16.

#### References

Ager, D.V. 1971: Space and time in brachiopod history. In: Middlemiss, F.A., Rawson, P.F. & Newall, G. (eds): Faunal provinces in space and time. Geological Journal Special Issue **4**, 95–110.

Alsen, P. 2006: The Early Cretaceous (Late Ryazanian – Early Hauterivian) ammonite fauna of North-East Greenland: taxonomy, biostratigraphy, and biogeography. Fossils & Strata **53**, 1–229. https://doi.org/10.18261/9781405180146-2006-01

Alsen, P. & Mutterlose, J. 2009: The early Cretaceous of North-East Greenland: a crossroads of belemnite migration. Palaeogeography, Palaeoclimatology, Palaeoecology 280, 168–182. https://doi.org/10.1016/j.palaeo.2009.06.011

Alsen, P. & Piasecki, S. 2018: Biostratigraphy of the Hareelv Formation (Upper Jurassic) in the Blokelv-1 core, Jameson Land, central East Greenland. In: Ineson, J.R. & Bojesen-Koefoed, J.A. (eds): Petroleum geology of the Upper Jurassic – Lower Cretaceous of East and North-East Greenland: Blokelv-1 borehole, Jameson Land Basin. Geological Survey of Denmark and Greenland Bulletin 42, 15–37. https://doi.org/10.34194/geusb.v42.4308

Alsen, P. & Rawson, P.F. 2005: The Early Valanginian (Early Cretaceous) ammonite *Delphinites (Pseudogarnieria)* from East Greenland. Bulletin of the Geological Society of Denmark **52**, 201–212. https://doi.org/10.37570/bgsd-2005-52-15

Alsgaard, P.C., Felt, V.L., Vosgerau, H. & Surlyk, F. 2003: The Jurassic of Kuhn Ø, North-East Greenland. In: Ineson, J.R. & Surlyk, F. (eds): The Jurassic of Denmark and Greenland. Geological Survey of Denmark and Greenland Bulletin 1, 865–892. https://doi.org/10.34194/geusb.v1.4691

Bailey, D., Miller, P. & Varney, T. 1997: Some dinoflagellate cysts from the Kimmeridge Clay Formation in North Yorkshire and Dorset, UK. Proceedings of the Yorkshire Geological Society **51**, 235–245. https:// doi.org/10.1144/pygs.51.3.235

Birkelund, T. & Callomon, J.H. 1985: The Kimmeridgian ammonite faunas of Milne Land, central East Greenland. Grønlands Geologiske Undersøgelse Bulletin **153**, 56 pp. + 23 plates. https://doi.org/10.34194/bullggu. v153.6695

Birkelund, T., Callomon, J.H. & Fürsich, F.T. 1984: The stratigraphy of the Upper Jurassic and Lower Cretaceous sediments of Milne Land,

- central East Greenland. Grønlands Geologiske Undersøgelse Bulletin **147**, 1–56. https://doi.org/10.34194/bullggu.v147.6689
- BioStrat 2018: Early and Late Cretaceous Zonation. https://www.biostrat.org.uk (accessed September 2019).
- Bjerager, M., Alsen, P., Bojesen-Koefoed, J.A., Nielsen, T., Piasecki, S. & Pilgaard, A. 2018: Late Jurassic evolution of the Jameson Land Basin, East Greenland implications of the Blokelv-1 borehole. In: Ineson, J.R. & Bojesen-Koefoed, J.A. (eds): Petroleum geology of the Upper Jurassic Lower Cretaceous of East and North-East Greenland: Blokelv-1 borehole, Jameson Land Basin. Geological Survey of Denmark and Greenland Bulletin 42, 149–168. https://doi.org/10.34194/geusb.v42.4325
- Bjerager, M. *et al.* 2020: Cretaceous lithostratigraphy of Northeast Greenland. Bulletin of the Geological Society of Denmark **68**, 37–93. https://doi.org/10.37570/bgsd-2020-68-04
- Bojesen-Koefoed, J.A., Alsen, P., Bjerager, M., Hovikoski, J., Ineson, J.R., Johannessen, P.N., Olivarius, M., Piasecki, S. & Vosgerau, H. 2023a: The Rødryggen-1 and Brorson Halvø-1 fully cored boreholes (Upper Jurassic Lower Cretaceous), Wollaston Forland, North-East Greenland an introduction. GEUS Bulletin **55**, 8350 (this volume). https://doi.org/10.34194/geusb.v55.8350
- Bojesen-Koefoed, J.A., Alsen, P., Bjerager, M., Hovikoski, J., Johannessen, P.N., Nøhr-Hansen, H., Petersen, H.I., Piasecki, S. & Vosgerau, H. 2023b: Organic geochemistry of an Upper Jurassic Lower Cretaceous mudstone succession in a narrow graben setting, Wollaston Forland Basin, North-East Greenland. GEUS Bulletin **55**, 8320 (this volume). https://doi.org/10.34194/geusb.v55.8320
- Bojesen-Koefoed, J.A., Alsen, P. & Christiansen, F.G. 2014: Six years of petroleum geological activities in North-East Greenland (2008–2013): projects and a view of the future. In: Bennike, O. *et al.* (eds): Review of survey activities 2013. Geological Survey of Denmark and Greenland Bulletin **31**, 59–62. https://doi.org/10.34194/geusb.v31.4661
- Bown, P. & Young, J. 1998: Techniques. In: Bown, P.R. (ed): Calcareous nannofossil biostratigraphy, 16–28. British Micropalaeontological Society Publications Series. London: Chapman & Hall.
- Bown, P.R., Rutledge, D.C., Crux, J.A. & Gallagher, L.T. 1998: Lower Cretaceous. In: Bown, P.R. (ed): Calcareous nannofossil biostratigraphy, 86–131. British Micropalaeontological Society Publications Series. London: Chapman & Hall.
- Burnett, J.A. 1998: Upper Cretaceous. In: Bown, P.R. (ed): Calcareous nannofossil biostratigraphy, 132–199. British Micropalaeontological Society Series. London: Chapman & Hall/Kluwer Academic.
- Callomon, J.H. & Birkelund, T. 1982: The ammonite zones of the Boreal Volgian (Upper Jurassic) in East Greenland. In: Embry, A.F. & Balkwill, H.R. (eds): Arctic geology and geophysics. Canadian Society of Petroleum Geologists Memoir **8**, 349–369.
- Casey, R. 1973: The ammonite succession at the Jurassic–Cretaceous boundary in eastern England. In: Casey, R. & Rawson, P.F. (eds): The boreal Lower Cretaceous. Geological Journal Special Issue **5**, 193–266. Liverpool: Seel House Press.
- Costa, L. & Davey, R.J. 1992: Dinoflagellate cysts of the Cretaceous system. In: Powell, A. (ed): A stratigraphic index of dinoflagellate cysts, 99–153. British Micropalaeontological Society Publication Series. London: Chapman & Hall. https://doi.org/10.1007/978-94-011-2386-0\_3
- Davey, R.J. 1982: Dinocyst stratigraphy of the latest Jurassic to Early Cretaceous of the Haldager No. 1 borehole, Denmark. Danmarks Geologiske Undersøgelse, Serie B 6, 1–57. https://doi.org/10.34194/serieb.v6.7061
- Davies, E.H. 1983: The dinoflagellate Oppel-zonation of the Jurassic-Lower Cretaceous Sequence in the Sverdrup Basin, Arctic Canada. Geological Survey of Canada Bulletin 359, 1–59. https://doi. org/10.4095/119736
- Donovan, D.T. 1964: Stratigraphy and ammonite fauna of the Volgian and Berriasian rocks of East Greenland. Meddelelser om Grønland **154**(4), 1–34.
- Duxbury, S. 2001: A palynological zonation scheme for the Lower Cretaceous United Kingdom Sector, Central North Sea. Neues Jahrbuch für Geologie und Paläontologie Abhandlungen **219**(1–2), 95–137. https://doi.org/10.1127/njgpa/219/2001/95
- Fensome, R.A. & Williams, G.L. 2004: Lentin and Williams index of fossil dinoflagellates 2004 edition. AASP Contribution Series Number 42, 1–909.

- Gale, A.S., Mutterlose, J., Batenburg, S., Gradstein, F.M., Agterberg, F.P., Ogg, J.G. & Petrizzo, M.R. 2020: The Cretaceous period. In: Gradstein, F.M. *et al.* (eds): Geological time scale 2020, 1023–1086. Amsterdam: Flsevier
- Hammer, Ø., Hryniewicz, K., Hurum, J.H., Høyberget, M., Knutsen, E.M. & Nakrem, H.A. 2013: Large onychites (cephalopod hooks) from the Upper Jurassic of the Boreal Realm. Acta Palaeontologica Polonica 58, 827–835. https://doi.org/10.4202/app.2012.0020
- Harper, D.A.T., Alsen, P., Owen, E. & Sandy, M.R. 2005: Early Cretaceous brachiopods from North-East Greenland: biofacies and biogeography. Bulletin of the Geological Society of Denmark **52**, 213–225. https://doi.org/10.37570/bgsd-2005-52-16
- Heilmann-Clausen, C. & Birkelund, T. 1987: Lower Cretaceous dinoflagellate biostratigraphy in the Danish Central Trough. Danmarks Geologiske Undersøgelse Serie A 17, 1–89. https://doi.org/10.34194/seriea.v17.7036
- Hovikoski, J., Ineson, J.R., Olivarius, M., Bojesen-Koefoed, J.A., Piasecki, S. & Alsen, P. 2023a: Upper Jurassic Lower Cretaceous of eastern Wollaston Forland, North-East Greenland: a distal marine record of an evolving rift. GEUS Bulletin 55, 8349 (this volume). https://doi.org/10.34194/geusb.v55.8349
- Hovikoski, J. *et al.* 2023b: Late Jurassic Early Cretaceous marine deoxygenation in NE Greenland. Journal of the Geological Society, London **180**, 1–16. *https://doi.org/10.1144/jgs2022-058*
- Ilovaisky, D. 1917: Les ammonites du Jurassique supérior du pays de Liapine. Ouvrages de la Section Géologique de la Société Imperiale des Amis des Sciences Nalurelles de Moscou I(1–2), 1–180.
- Ineson, J.R. & Bojesen-Koefoed, J.A. (eds) 2018: Petroleum geology of the Upper Jurassic Lower Cretaceous of East and North-East Greenland: Blokelv-1 borehole, Jameson Land Basin. Geological Survey of Denmark and Greenland Bulletin 42, 1–168. https://doi.org/10.34194/geusb.v42
- Ingrams, S., Jolley, D.W. & Schneider, S. 2021: High latitude stratigraphical palynology of the Jurassic-Cretaceous boundary interval, Sverdrup Basin, Arctic Canada. Cretaceous Research **126**, 104922, 1–15. https://doi.org/10.1016/j.cretres.2021.104922
- Jakubowski, M. 1987: A proposed Lower Cretaceous Calcareous Nannofossil Zonation Scheme for the Moray Firth Area of the North Sea. Abhandlungen der Geologischen Bundesanstalt A **39**, 99–119.
- Jeremiah, J. 2001: A Lower Cretaceous nannofossil zonation for the North Sea Basin. Journal of Micropalaeontology 20(1), 45–80. https:// doi.org/10.1144/jm.20.1.45
- Kelly, S.R.A., Gregory, J., Braham, W., Strogen, D.P. & Whitham, A.G. 2015: Towards an integrated Jurassic biostratigraphy for eastern Greenland. Volumina Jurassica XIII(1), 43–64.
- Koch, L. & Haller, J. 1971: Geological map of East Greenland 72°–76°N. Lat. (1:250 000). Meddelelser om Grønland **183**, 1–26.
- Maync, W. 1947: Stratigraphie der Jurabildungen Ostgrönlands zwischen Hochstetterbugten (75°N.) und den Kejser Franz Joseph Fjord (73°N). Meddelelser om Grønland, **132**, 1–223.
- Maync, W. 1949: The Cretaceous beds between Kuhn Island and Cape Franklin (Gauss Peninsula), northern East Greenland. Meddelelser om Grønland **133**(3), 1–291.
- Meledina, S.V., Alfirov, A.S. & Shurygin, B.N. 2010: On position of the Praechetaites exooticus Zone in the Volgian Stage. Stratigraphy and Geological Correlation 18, 550–554. https://doi.org/10.1134/ s0869593810050060
- Mikhailov, N.P. 1966: Boreal Jurassic ammonites (Dorsoplanitinae) and zonal subdivision of the Volgian Stage. Academy of sciences of the USSR, Geological Institute, Transactions, Nauka **151**, 1–110.
- Möller, C., Mutterlose, J. & Alsen, P. 2015: Integrated stratigraphy of Lower Cretaceous sediments (Ryazanian–Barremian) North-East Greenland. Palaeogeography, Palaeoclimatology, Palaeoecology 437, 85–97. https://doi.org/10.1016/j.palaeo.2015.07.014
- Mutterlose, J. & Kessels, K. 2000: Early Cretaceous calcareous nannofossils from high latitudes: implications for palaeobiogeography and palaeoclimate. Palaeogeography, Palaeoclimatology, Palaeoecology 160, 347–372. https://doi.org/10.1016/s0031-0182(00)00082-1
- Nøhr-Hansen, H. 1993: Dinoflagellate cyst stratigraphy of the Barremian to Albian, Lower Cretaceous, North-East Greenland. Grønlands Geologiske Undersøgelse Bulletin **166**, 1–171. https://doi.org/10.34194/bullggu.v166.6722

- Nøhr-Hansen, H., Piasecki, S. & Alsen, P. 2020: A Cretaceous dinoflagellate cyst zonation for NE Greenland. Geological Magazine **157**, 1658–1692. https://doi.org/10.1017/S0016756819001043
- Olivarius, M., Kazerouni, A.M., Weibel, R., Kokfelt, T.F. & Hovikoski, J. 2023: Mudstone diagenesis and sandstone provenance in an Upper Jurassic Lower Cretaceous evolving half-graben system, Wollaston Forland, North-East Greenland. GEUS Bulletin **55**, 8309 (this volume). https://doi.org/10.34194/geusb.v55.8309
- Pauly, S., Mutterlose, J. & Alsen, P. 2012a: Lower Cretaceous (upper Ryazanian–Hauterivian) chronostratigraphy of high latitudes (North-East Greenland). Cretaceous Research 34, 308–326. https://doi. org/10.1016/j.cretres.2011.11.011
- Pauly, S., Mutterlose, J. & Alsen, P. 2012b: Early Cretaceous palaeoceanography of the Greenland-Norwegian Seaway evidenced by calcareous nannofossils. Marine Micropalaeontology 90-91, 72-85 https:// doi.org/10.1016/j.marmicro.2012.04.004
- Pauly, S., Mutterlose, J. & Alsen, P. 2013: Depositional environments of Lower Cretaceous (Ryazanian-Barremian) sediments from Wollaston Forland and Kuhn Ø, North-East Greenland. Bulletin of the Geological Society of Denmark 61, 19–36. https://doi.org/10.37570/bgsd-2013-61-02
- Piasecki, S. 1996: Boreal dinoflagellate cyst stratigraphy of Middle to Upper Jurassic sediments of Milne Land, East Greenland. In: Piasecki, S. *et al.* (eds): Formation of source and reservoir rocks in a sequence stratigraphic framework, Jameson Land, East Greenland. Energy Research Programme EFP-93, Projects 1313/93 & 00171996/30, Vol. I & II. Danmarks og Grønlands Geologiske Undersøgelse Rapport, **1966/30**, Vol. II, Appendix 13, 100 pp. Copenhagen: GEUS.
- Poulsen, N.E. & Riding, J.B. 2003: The Jurassic dinoflagellate cyst zonation of Subboreal Northwest Europe. Geological Survey of Denmark and Greenland Bulletin 1, 115–144. https://doi.org/10.34194/geusb.v1.4650
- Repin, Y.S., Zakharov, V.A., Meledina, S.V. & Nalnyaeva, T.I. 2006: Atlas of the molluscs of the Pechora Jurassic. Bulletin of the VNIGRI 3, 1–262.
- Riding, J.B. & Thomas, J.E. 1992: Dinoflagellate cysts of the Jurassic System. In: Powell, A.J. (ed): A stratigraphic index of dinoflagellate cysts, 7–97. London: Chapman & Hall.
- Riding, J.B., Fedorova, V.A. & Ilyina, V.I. 1999: Jurassic and lowermost Cretaceous dinoflagellate cyst biostratigraphy of the Russian Platform and northern Siberia, Russia. AASP Contribution Series **36**, 1–179.
- Riding, J.B., Poulsen, N.E. & Bailey, D.A. 2000: A taxonomic study of the dinoflagellate cyst *Muderongia simplex* Alberti 1961 and related species. Palynology **24**, 21–35. https://doi.org/10.2113/0240021
- Rogov, M. 2010: New data on ammonites and stratigraphy of the Volgian Stage in Spitzbergen. Stratigraphy and Geological Correlation 18, 505–531. https://doi.org/10.1134/s0869593810050047
- Rogov, M. 2020: Infrazonal ammonite biostratigraphy, paleobiogeography and evolution of Volgian craspeditid ammonites. Paleontological Journal 54(10), 1189–1219. https://doi.org/10.1134/s0031030120100068
- Rogov, M. & Zakharov, V.A. 2009: Ammonite- and bivalve-based biostratigraphy and Panboreal correlation of the Volgian Stage. Science in China Series D: Earth Sciences 52, 1890–1909. https://doi.org/10.1007/s11430-009-0182-0
- Rogov, M. & Zakharov, V.A. 2011: The Volgian Praechetaites Zone: Geochronological range, stratigraphic position and interregional correlation (a response to the paper by S.V. Meledina et al. 'On the position of the Praechetaites exoticus Zone in the Volgian Stage'). Stratigraphy and Geological Correlation 19, 102–107. https://doi.org/10.1134/s0869593811010047
- Shulgina, N.I. 1967: Tithonian ammonites of northern Siberia. In: Problems of paleontological substantiation of detailed Mesozoic Stratigraphy of Siberia and Far East, 131–149. Leningrad: Nauka.
- Spath, L.F. 1936: The Upper Jurassic invertebrate faunas of Cape Leslie, Milne Land. II. Upper Kimmeridgian and Portlandian. Meddelelser om Grønland **99**(3), 1–180.
- Spath, L.F. 1952: Additional observations on the invertebrates (chiefly ammonites) of the Jurassic and Cretaceous of East Greenland. II.

- Some Infra-Valanginian ammonites from Lindemans Fjord, Wollaston Forland; with a note on the base of the Cretaceous. Meddelelser om Grønland **133**(4), 1–40.
- Surlyk, F. 1977: Stratigraphy, tectonics and palaeogeography of the Jurassic sediments of the areas north of Kong Oscars Fjord, East Greenland. Grønlands Geologiske Undersøgelse Bulletin **123**, 1–56. https://doi.org/10.34194/bullggu.v123.6665
- Surlyk, F. 1978: Submarine fan sedimentation along fault scarps on tilted fault blocks (Jurassic-Cretaceous boundary, East Greenland). Grønlands Geologiske Undersøgelse Bulletin 128, 1–108. https://doi. org/10.34194/bullggu.v128.6670
- Surlyk, F. 1991: Sequence stratigraphy of the Jurassic lower-most Cretaceous of East Greenland. American Association of Petroleum Geologists Bulletin **75**, 1468–1488. https://doi.org/10.1306/0c9b296b-1710-11d7-8645000102c1865d
- Surlyk, F. 2003: The Jurassic of East Greenland: thermal subsidence, onset and culmination of rifting. In: Ineson, J.R. & Surlyk, F. (eds): The Jurassic of Denmark and Greenland. Geological Survey of Denmark and Greenland Bulletin 1, 659–722. https://doi.org/10.34194/geusb.v1.4674
- Surlyk, F. & Clemmensen, L.B. 1983: Rift propagation and eustacy as controlling factors during Jurassic inshore and shelf sedimentation in northern East Greenland. Sedimentary Geology 34, 119–143. https:// doi.org/10.1016/0037-0738(83)90083-0
- Surlyk, F., Callomon, J.H., Bromley, R.G. & Birkelund, T. 1973: Stratigraphy of the Jurassic–Lower Cretaceous sediments of Jameson Land and Scoresby Land, East Greenland. Grønlands Geologiske Undersøgelse Bulletin **105**, 1–76. https://doi.org/10.34194/bullggu.v105.6646
- Surlyk, F. & Zakharov, V.A. 1982: Buchiid bivalves from the Upper Jurassic and Lower Cretaceous of East Greenland. Palaeontology 25(4), 727–753.
- Surlyk, F. et al. 2021: Jurassic stratigraphy of East Greenland. GEUS Bulletin 46, 6521. https://doi.org/10.34194/geusb.v46.6521
- Sykes, R.M. & Callomon, J.H. 1979: The *Amoeboceras* fauna of the Boreal Upper Oxfordian. Palaeontology **22**, 839–903.
- Sykes, R.M. & Surlyk, F. 1976: A revised ammonite zonation of the Boreal Oxfordian and its application in northeast Greenland. Lethaia **9**, 421–436. https://doi.org/10.1111/j.1502-3931.1976.tb00984.x
- Vischer, A. 1943: Die Postdevonische Tektonik von Ostgrönland zwischen 74° und 75° n. Br. Meddelelser om Grønland **133**(1), 1–195.
- Wimbledon, W.A.P. et al. 2020: The proposal of a GSSP for the Berriasian Stage (Cretaceous System): Part 1. Volumina Jurassica XVIII(1), 53–106. https://doi.org/10.7306/vj.18.5
- Wright, C.W., Callomon, J.H. & Howarth, M.K. 1996: Mollusca 4, Cretaceous Ammonoidea. In: Kaesler, R.L. (ed): Treatise on invertebrate palaeontology, Part L, Revised, 1–362. Boulder, CO: The Geological Society of America.
- Woollam, R. & Riding, J.B. 1983: Dinoflagellate cyst stratigraphy of the English Jurassic. Institute of Geological Sciences, Report **83**(2),
- Zakharov, V.A. & Mesezhnikov, M.S. 1974: The Volgian Stage of the Subarctic Ural. Academy of Sciences of the USSR, Siberian Branch, Transactions of the Institute of Geology and Geophysics 196, 1–214.
- Zakharov, V.A. & Rogov, M. 2006: New data on Jurassic-Cretaceous sediments in the Arctic Region (Nordvik Peninsula, northern Siberia). In: Proceedings of the Third All-Russian Meeting 'Cretaceous System of Russia and adjacent regions: problems of stratigraphy and paleogeography', Sept. 26–30. Saratov 528, 61–63.
- Zakharov, V.A. & Rogov, M. 2008: The upper Volgian substage in Northeast Siberia (Nordvik Peninsula) and its panboreal correlation based on ammonites. Stratigraphy and Geological Correlation **16**, 423–436. https://doi.org/10.1134/s0869593808040059
- Zeiss, A. 2003: The Upper Jurassic of Europe: its subdivision and correlation. In: Ineson, J.R. & Surlyk, F. (eds): The Jurassic of Denmark and Greenland. Geological Survey of Denmark and Greenland Bulletin 1, 75–114. https://doi.org/10.34194/geusb.v1.4649



Contrasts in sedimentation. The upper photograph illustrates the coarse conglomeratic nature of the proximal marine sediments at the rift-basin margin (Niesen, northern Wollaston Forland; photo: Peter Alsen) whereas the lower photograph shows the contemporaneous black, organic-rich mudstones (Rødryggen-1 borehole; photo: John Boserup) that accumulated distally in structurally isolated sub-basins, as documented in this bulletin.

### **GEUS Bulletin**



# **Upper Jurassic – Lower Cretaceous of eastern Wollaston Forland, North-East Greenland: a distal marine record of an evolving rift**

Jussi Hovikoski<sup>1,2</sup>, Jon R. Ineson<sup>1</sup>, Mette Olivarius<sup>3</sup>, Jørgen A. Bojesen-Koefoed<sup>4</sup>, Stefan Piasecki<sup>1,5,6</sup>, Peter Alsen<sup>3</sup>

<sup>1</sup>Department for Geophysics and Sedimentary Basins, Geological Survey of Denmark and Greenland (GEUS), Copenhagen, Denmark; <sup>2</sup>Geological Survey of Finland (GTK), Espoo, Finland; <sup>3</sup>Department for Geo-energy and Storage, Geological Survey of Denmark and Greenland (GEUS), Copenhagen, Denmark; <sup>4</sup>Department for Mapping and Mineral Resources, Geological Survey of Denmark and Greenland (GEUS), Copenhagen, Denmark; <sup>5</sup>Globe Institute, University of Copenhagen, Copenhagen, Denmark; <sup>6</sup>Retired

#### **Abstract**

Two drill cores spanning the Upper Jurassic - Lower Cretaceous succession in Wollaston Forland, North-East Greenland, offer an insight into mud accumulation in an evolving distal fault block. Previous studies have revealed the presence of long-lasting black mudstone accumulation extending through the oxygen-restricted early rift and rift climax phases (Bernbjerg and Lindemans Bugt Formations). Here, we present a detailed description of the sedimentary succession extending into the late syn-rift settings (Palnatokes Bjerg and Stratumbjerg Formations). The results indicate that the Kimmeridgian – lower Volgian early rift-phase was characterised by suspension settling and millimetre-scale event deposition in a tectonically affected, prodeltaic offshore setting. The event-related depositional processes are recorded by starved wave ripples, scour-and-fill structures, putative mud-floccule ripples and mud-dominated gravity-flow deposits. During the middle Volgian - Ryazanian rift climax, the depositional environment evolved into a narrow half-graben that was detached from the proximal depocentre flanking the deltaic coastline, itself dominated by coarse sediment. The correlative sedimentary facies in the detached half-graben are bioclastic and pyrite-rich black mudstones, which document suspension settling and gravityflow or mass-wasting deposition in sub-storm wave-base slope and basin-floor environments. Black mudstone sedimentation ended abruptly in the late Ryazanian when the accumulation of condensed, bioturbated deep marine marls coincided with broader oceanographic reorganisation concomitant with waning rift activity in the west. Deposition of red bioclastic mudstones with a common gravity-flow component characterised the Hauterivian, potentially representing final draping of the submerged fault block crest. The top of the cored succession is demarcated by dark grey bioturbated mudstones of Barremian age, reflecting the onset of regionally continuous deep marine mud accumulation in thermally subsiding basins. Although superficially monotonous, the mudstone-dominated succession reveals a highly dynamic depositional system that reflects changing sediment transport processes during almost a full rift cycle.

#### 1. Introduction

Although mudstones form most of the Earth's sedimentary record, they remain less understood than most other rock types (Schieber *et al.* 2007). This is unfortunate because mudstones form important archives of Earth's climatic and oceanographic processes and crises and are economically valuable, hosting petroleum source rocks and hydrocarbons and forming seals in hydrocarbon, groundwater and carbon storage reservoirs (Potter *et al.* 2005). Traditionally, mud has been regarded as being deposited via suspension settling under low-energy conditions (Potter *et al.* 1980). However, particularly since the early 2000s, flume-tank experiments and detailed observations from the modern sea floor, and from ancient successions, have revealed that mud accumulation can take place during much

\*Correspondence: jussi.hovikoski@gtk.fi

Received: 03 Mar 2023 Revised: 12 Sep 2023 Accepted: 26 Sep 2023 Published: 21 Dec 2023

**Keywords:** Late Jurassic, Early Cretaceous, Bernbjerg Formation, Lindemans Bugt Formation, Palnatokes Bjerg Formation, Stratumbjerg Formation, mudstone, Greenland

Abbreviations

API: American Petroleum Institute units BI: bioturbation index GR: gamma ray

WEGF: wave-enhanced gravity-flow

GEUS Bulletin (eISSN: 2597-2154) is an open access, peer-reviewed journal published by the Geological Survey of Denmark and Greenland (GEUS). This article is distributed under a *CC-BY 4.0* licence, permitting free redistribution, and reproduction for any purpose, even commercial, provided proper citation of the original work. Author(s) retain copyright.

**Edited by:** Karen Dybkjær (GEUS, Denmark)

**Reviewed by:** Guy Plint (Western University, Canada) and Paul Smith (Oxford University Museum of Natural History, UK)

Funding: See page 70

Competing interests: See page 70

Additional files: None

more varied hydrodynamic conditions than previously thought (Kineke et al. 1996; Wright et al. 2001; Bentley & Nittrouer 2003; Macquaker & Bohacs 2007; Schieber et al. 2007; Ichaso & Dalrymple 2009; Schieber & Southard 2009; Schieber & Yawar 2009; Macquaker et al. 2010; Ghadeer & Macquaker 2011; Plint et al. 2012; Plint 2014; Yawar & Schieber 2017). Most notably, such studies have shown that mud can be transported as, and deposited from, bedload transport, which can generate subtle sedimentary structures (e.g. crosslamination, normally graded lamina sets, structureless ungraded mud laminae and convergent lamination) that remain overlooked in the sedimentary record. This can be particularly true in outcrop studies where mudstone successions are typically poorly exposed relative to coarser facies and tend to appear homogenous due to weathering.

The Upper Jurassic - Lower Cretaceous depositional record of eastern Wollaston Forland, North-East Greenland (Fig. 1), provides an exceptional window into mudstone deposition under changing paleoenvironmental conditions. The area experienced a protracted rift phase that started in the Middle Jurassic, reached a climax during the Late Jurassic and waned progressively during Jurassic-Cretaceous boundary times and through the Early Cretaceous (Surlyk 1978, 1990, 2003). As a result of rift evolution, the basin geometry changed from a regionally continuous suboxic shelf setting to a series of narrow half-grabens that were subsequently affected by thermal subsidence and transgression. Whilst the fill of the proximal half-grabens was coarse-grained, being characterised by major conglomeratic submarine fandelta systems (Surlyk 1978, 2003; Henstra et al. 2016), the distal fault blocks were mud-filled, stagnated and

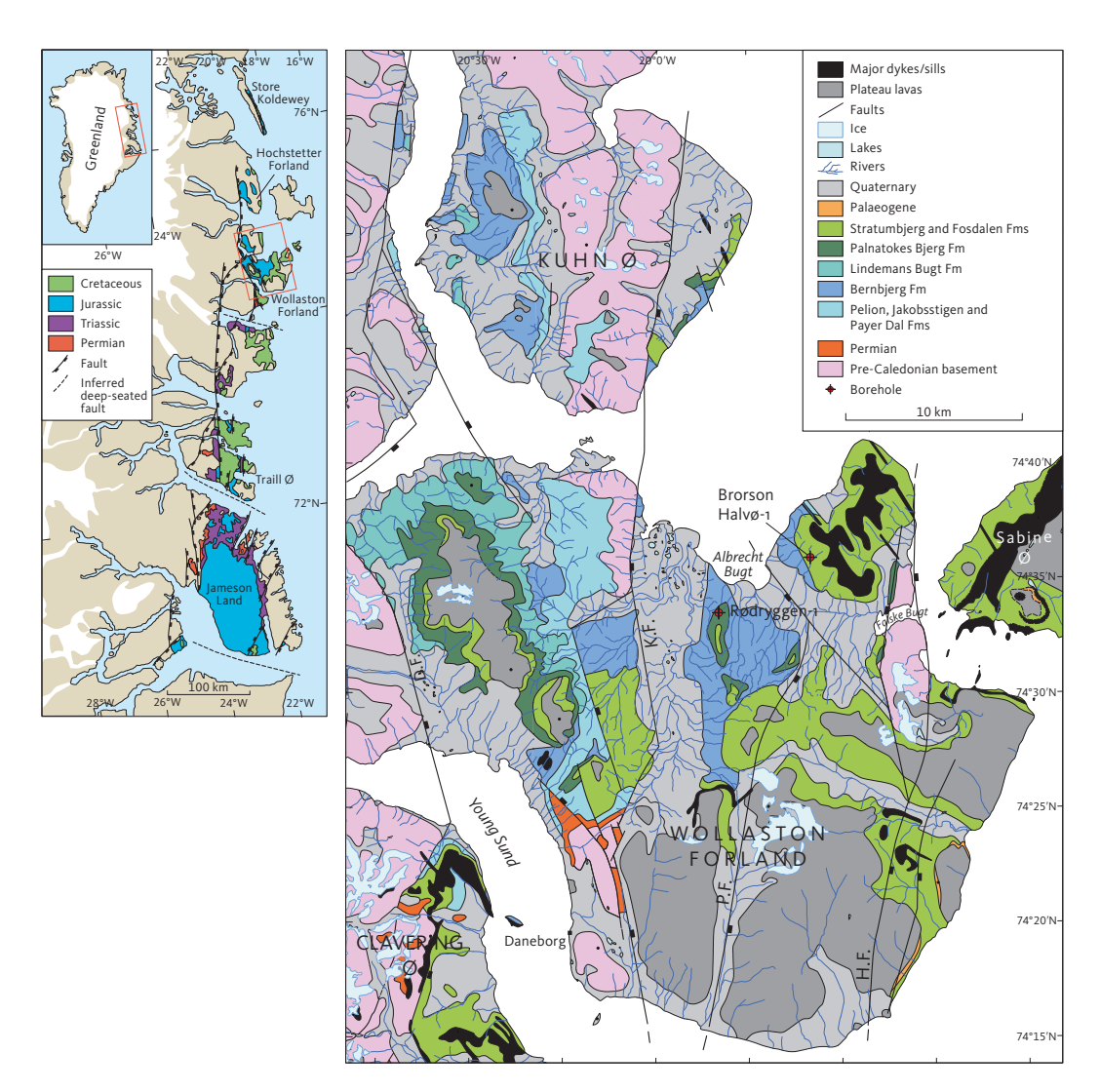


**Fig. 1** Location maps. **Left**: Geological overview map of East and North-East Greenland showing the location of the study area (red box) and the dominant Late Jurassic – Early Cretaceous faults. **Right**: Simplified geological map of Wollaston Forland showing the positions of the Rødryggen-1 and Brorson Halvø-1 boreholes. **K.F.**: Kuhn fault. **P.F.**: Permpas Fault. **H.F.**: Hühnerbjerg Fault. **D.F.**: Dombjerg Fault. The position of the coastline was primarily dictated by the Dombjerg Fault during the Late Jurassic, whilst the Kuppel and Hühnerbjerg Faults were the most important structures controlling the distal half-graben architecture. Reproduced from Bojesen-Koefoed *et al.* (2023a, this volume, fig. 1).

detached from the coastal gravity-flow systems (Pauly et al. 2013; Hovikoski et al. 2023; Bojesen-Koefoed et al. 2023, this volume; Olivarius et al. 2023, this volume). The subsequent rift waning and thermal subsidence were associated with improved ventilation and deposition of deep marine mudstones.

All these tectonostratigraphic phases are recorded in the fully cored boreholes Rødryggen-1 and Brorson Halvø-1, which were drilled in two contrasting locations within a distal half-graben (Figs 1, 2). Full core recovery has yielded pristine preservation of the Kimmeridgian to lower Barremian mudstone-dominated succession, allowing detailed documentation of the sedimentary facies of the dominant, organic-rich black mudstone succession (Bernbjerg and Lindemans Bugt Formations), as well as the gradation to upper Ryazanian bioturbated mudstones (Palnatokes Bjerg and Stratumbjerg Formations). The sedimentary facies of the black mudstone interval were recently summarised in Hovikoski *et al.* (2023) in which the wider implications

of this subsurface record are developed with respect to the development of anoxia in the region during rifting. The aim of this complementary paper is to present a comprehensive description of the depositional facies and processes in this unexposed and previously unknown distal marine setting.

#### 2. Stratigraphy and depositional setting

The cored section covered by the Rødryggen-1 and Brorson Halvø-1 boreholes spans the Kimmeridgian to lower Barremian interval, which is divided into four formations: (1) the Bernbjerg Formation, (2) the Lindemans Bugt Formation (the new Storsletten Member; Alsen *et al.* 2023, this volume), (3) the Palnatokes Bjerg Formation (the Albrechts Bugt Member and the Rødryggen Member) and (4) the Stratumbjerg Formation (Fig. 2).

The age of the Bernbjerg Formation is late Oxfordian to early Volgian, and it comprises a thick black

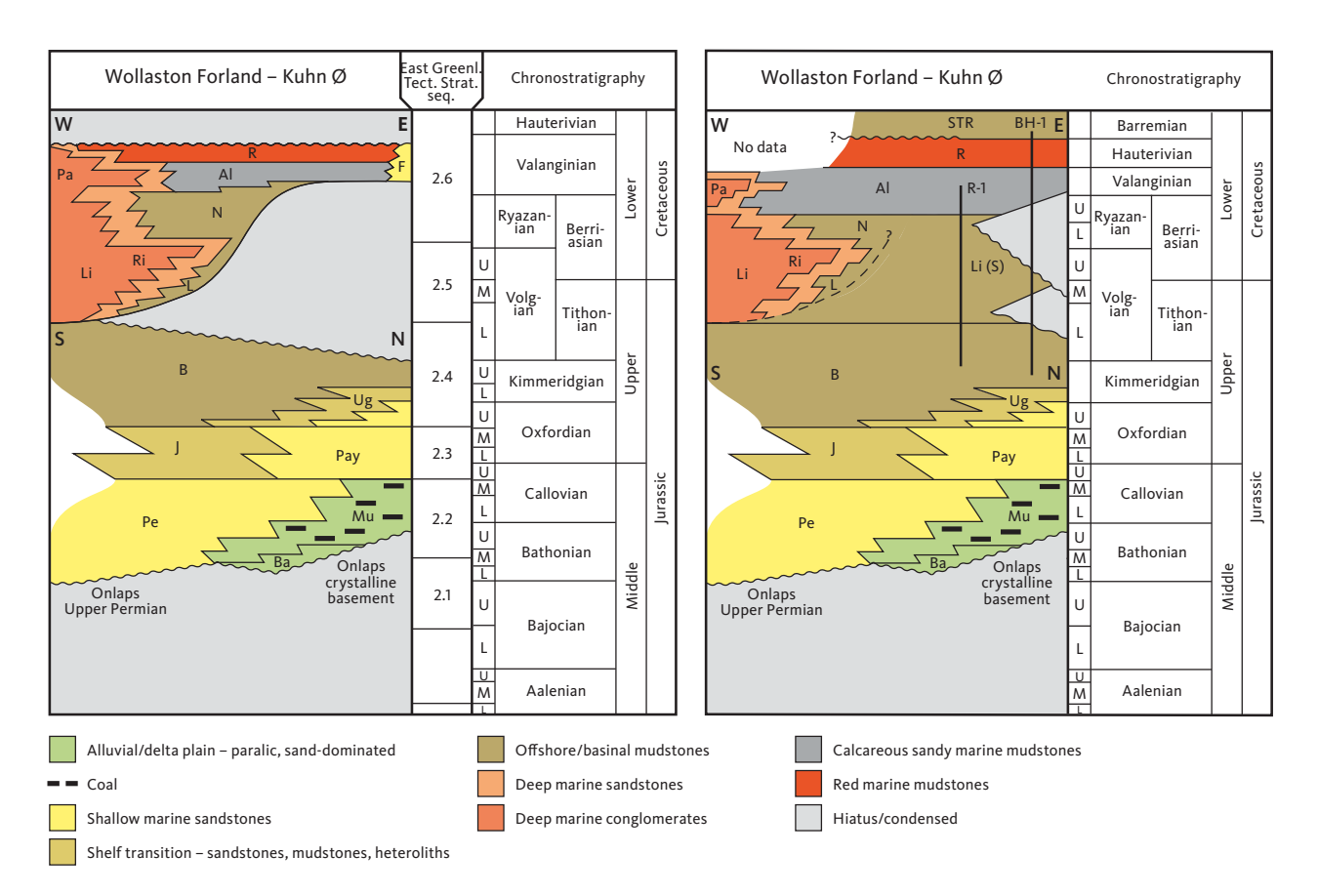


Fig. 2 Stratigraphic models of the Wollaston Forland – Kuhn Ø area. Left: the conceptual stratigraphic scheme of Surlyk (2003) based on outcrop study. Right: the revised scheme after drilling of the Rødryggen-1 and Brorson Halvø-1 boreholes and incorporating changes introduced by Surlyk et al. (2021). The revised succession is much more complete and richer in marine mudstone (brown colour) than previously envisaged. East Greenl. Tect. Strat. Seq.: East Greenland Tectono-stratigraphic sequence. U: Upper/upper. M: Middle/middle. L: Lower/lower. Lithostratigraphic abbreviations are as follows: Al: Albrechts Bugt Member. B: Bernbjerg Formation. Ba: Bastians Dal Formation. F: Falskebugt Member. J: Jakobsstigen Formation. L: Laugeites Ravine Member. Li: Lindemans Bugt Formation. Li (S): Lindemans Bugt Formation (Storsletten Member). Mu: Muslingebjerg Formation. N: Niesen Member. Pa: Palnatokes Bjerg Formation (Young Sund Member). Pay: Payer Dal Formation. Pe: Pelion Formation. R: Rødryggen Member. Ri: Rigi Member. Str: Stratumbjerg Formation. Ug: Ugpik Ravine Member. Black vertical lines indicate the schematic location and stratigraphic extent of the Rødryggen (R-1) and Brorson Halvø-1 (BH-1) boreholes. Reproduced from Bojesen-Koefoed et al. 2023b (this volume).

mudstone shale succession (500-600 m) that accumulated in a tectonically influenced shelf setting (Sykes & Surlyk 1976; Surlyk et al. 2021). Previous sedimentological studies of outcrop sections have reported the presence of a dysoxic to anoxic or euxinic shelf setting with occasional storm influence during Oxfordian-Volgian times (Surlyk & Clemmensen 1975, 1983). Similarly, the previous core-based study pointed to a generally sub-oxic prodeltaic shelf environment (Hovikoski et al. 2023). Rifting intensified during the Volgian, which dissected the basin into a series of narrow, 10-30 km wide, westward tilted, fjord-like half-grabens (Vischer 1943; Surlyk 1978). Major conglomeratic submarine fan-delta systems (Lindemans Bugt Formation, Rigi Member; Surlyk 1978; Henstra et al. 2016) developed in the most proximal fault blocks reaching a maximum thickness of 2 km. The coeval paleoenvironmental development in more distal, eastern fault blocks remained poorly understood due to the lack of outcrops, but is well-recorded in the cores described here, which indicate deep basinal sedimentation and isolation from the coarsegrained proximal systems (Hovikoski et al. 2023). The mudstone-dominated succession that accumulated in this setting is referred to the new Storsletten Member of the Lindemans Bugt Formation (Alsen et al. 2023, this volume).

The rift climax started to wane in the west during the late Ryazanian, leading to the deposition of the Palnatokes Bjerg Formation (Surlyk 1978, 1984, 1990, 2003). The formation changes coincided with transgression and improved ventilation in the water column and oceanographic change with improved communication between the Boreal and Tethyan realms (Pauly et al. 2013). Sand-dominated gravity-flow deposits (Palnatokes Bjerg Formation, Young Sund Member) continued to accumulate in the proximal fault block, whereas fossiliferous mudstones (Albrechts Bugt and Rødryggen Members) accumulated in basinal areas and on submarine block crests (Surlyk 1978; Hovikoski et al. 2018). The Rødryggen-1 and Brorson Halvø-1 cores penetrate both the latter, fine-grained members, and new biostratigraphic data indicate a late Ryazanian to Hauterivian age for these deposits (Alsen et al. 2023, this volume). In the Brorson Halvø-1 core, the Palnatokes Bjerg Formation is gradationally overlain by a thin interval of uppermost Hauterivian - Barremian, sub-storm and wave-base bioturbated mudstones of the Stratumbjerg Formation (Bjerager et al. 2020). This formation crops out from Traill Ø in the south to Store Koldewey in the north and reaches its maximum thickness of 270 m in the Brorson Halvø area; the Stratumbjerg Formation was previously referred to as the 'Mid-Cretaceous sandy shale sequence' (Nøhr-Hansen 1993).

#### 3. Methods

The Rødryggen-1 and Brorson Halvø-1 cores were sedimentologically and ichnologically described at a scale of 1:100. The sedimentological description included descriptions of lithology, grain size (visual estimation) and trends in grain size, primary and secondary sedimentary structures, bedding contacts and the identification of important stratigraphic surfaces. Diagenesis and authigenic minerals are described in Olivarius et al. (2023, this volume) and are integrated in facies descriptions. Ichnological data comprise description of ichnogenera, trace-fossil assemblage, cross-cutting relationships and bioturbation index (BI of Taylor & Goldring 1993). The BI provides a description of the degree to which original sedimentary fabric has been destroyed due to biogenic processes. This classification scheme allocates a numerical value ranging from 0 to 6 - the values correspond to the percentage of bioturbation (cf. Taylor & Goldring 1993). Undisturbed or non-bioturbated sedimentary fabrics are classified as BI 0 (0% reworked), while pervasively bioturbated media (100% reworked) are classified as BI 6. Intermediate levels of bioturbation are characterised using BI 1-5 and are defined as follows: BI 1, 1-4% reworked; BI 2, 5-30% reworked; BI 3, 31-60% reworked; BI 4, 61-90% reworked; BI 5, 91-99% reworked (Taylor & Goldring 1993). Locally, a lack of lithological contrast hindered accurate estimation of the degree of bioturbation. The age of the sediments is based on the biostratigraphy of Alsen et al. (2023, this volume).

#### 4. Depositional facies

The two cored sections spanning the Bernbjerg, Lindemans Bugt, Palnatokes Bjerg and Stratumbjerg Formations are divided into seven facies (F1–7). The facies are grouped and described here according to the lithostratigraphic unit(s) in which they occur (Figs 3, 4), as follows:

- F1, F2, F3 and F7 Bernbjerg and Lindemans Bugt Formations
- F4 and F5: Palnatokes Bjerg Formation
- F6: Stratumbjerg Formation

#### 4.1 Bernbjerg and Lindemans Bugt Formations

The studied deposits of the Bernbjerg and Lindemans Bugt Formations are divided into four facies (F1, F2, F3 and F7) and five subfacies (F1A, F1B, F1C, F2A and F2B) based on their sedimentological and ichnological properties.

#### 4.1.1 Facies F1: mudstone

Three subfacies (F1A–C) are recognised in the mudstone facies (Fig. 5A–G).

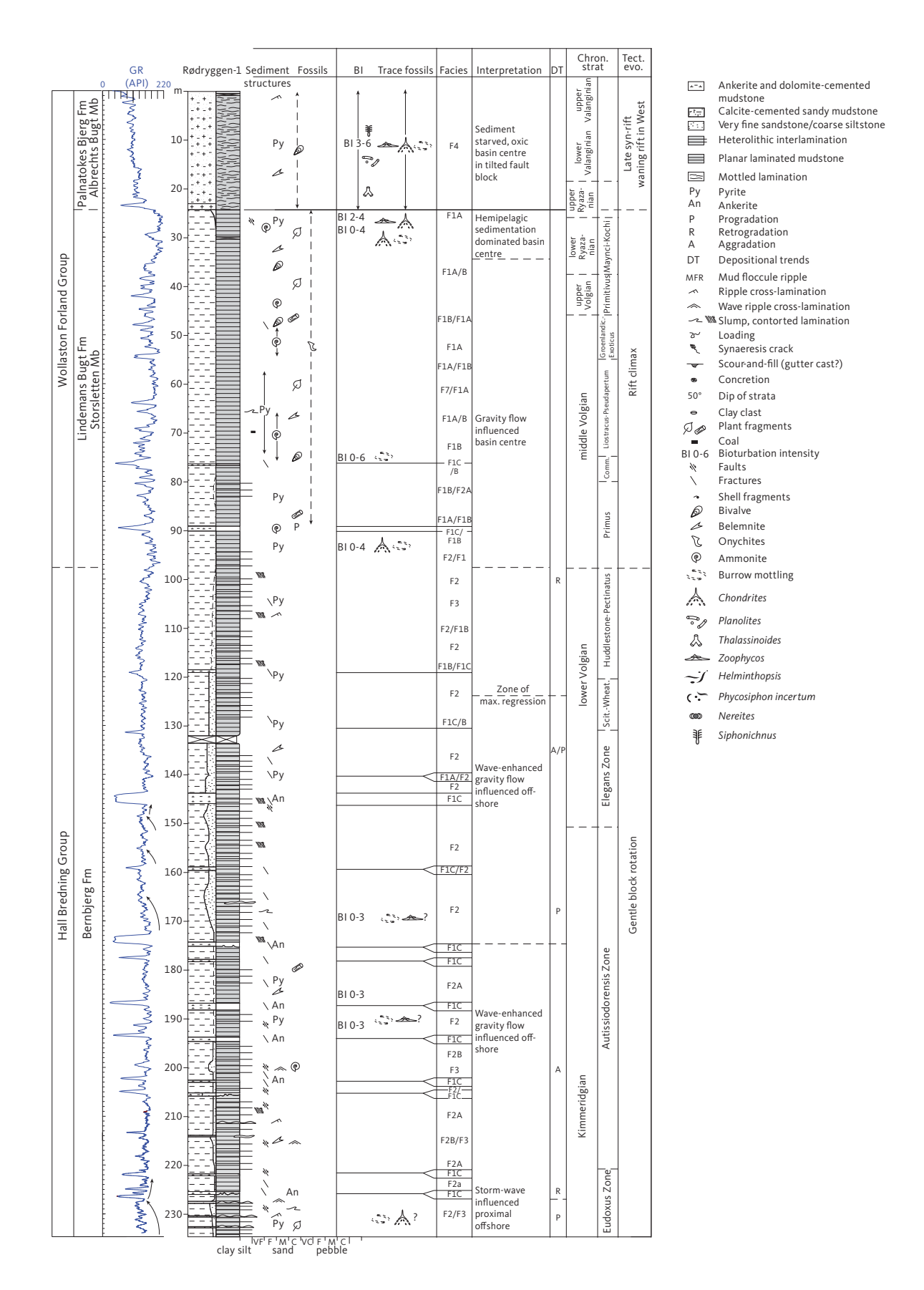


Fig. 3 Sedimentological log of the Rødryggen-1 core. Note that the ammonite zones are here indicated with chronozone terminology, whereas in the text, ammonite zones are used. Modified from Hovikoski *et al.* (2023). Chron. Strat.: chronostratigraphy. Tect. evo.: tectonic evolution. GR: gamma ray. Comm.: Comminus Zone. Scit.-Wheat.: Sciitulus-Wheatleyensis Zones. Groenlandic.: Groenlandicus Zone.

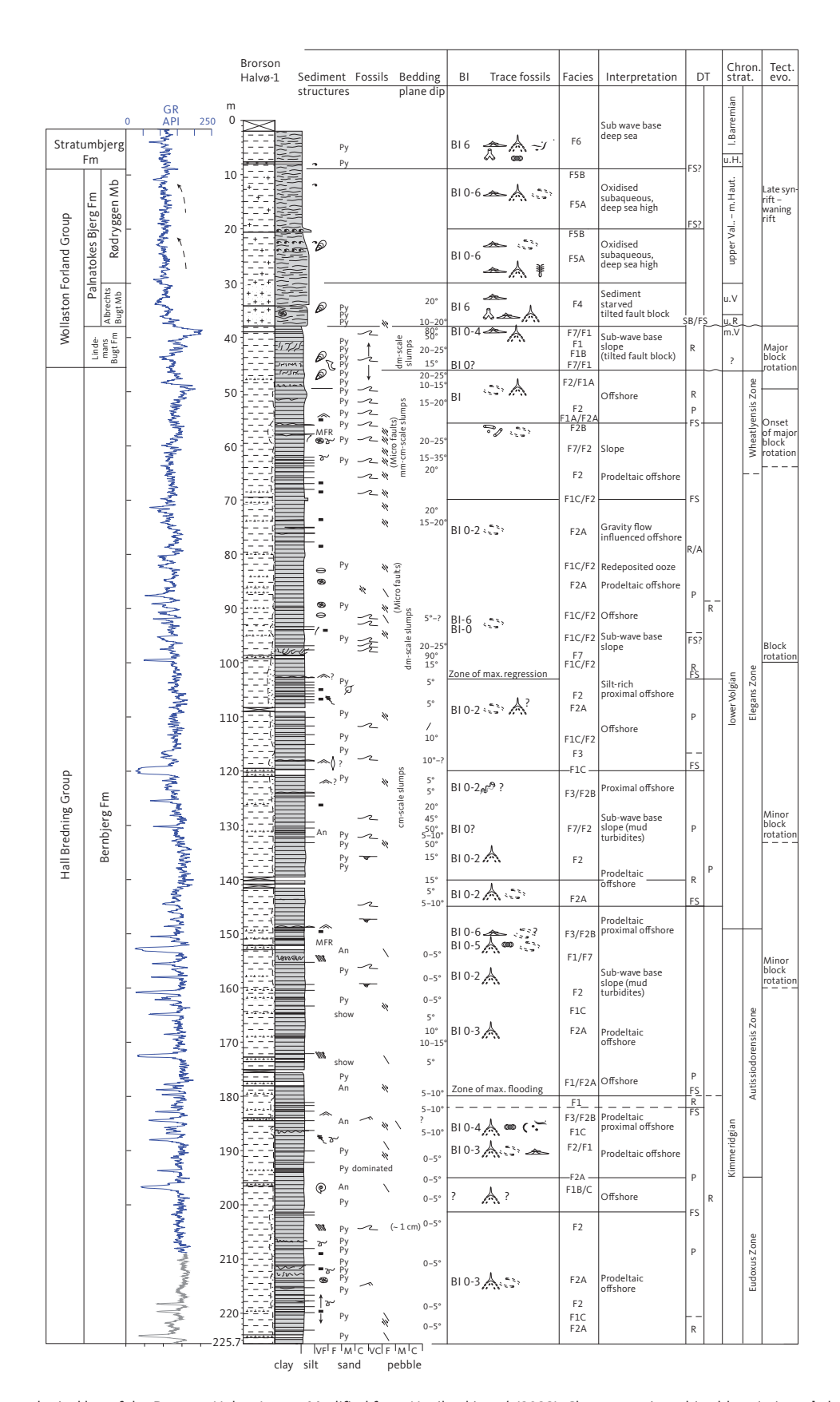


Fig. 4 Sedimentological log of the Brorson Halvø-1 core. Modified from Hovikoski *et al.* (2023). Chronostratigraphic abbreviations: **l.**: lower. **m.**: middle. **u.**: upper. **Vol**.: Volgian. **R.**: Ryazanian. **V./Val.**: Valanginian. **H./Haut**: Hauterivian. Legend in Fig. 3.

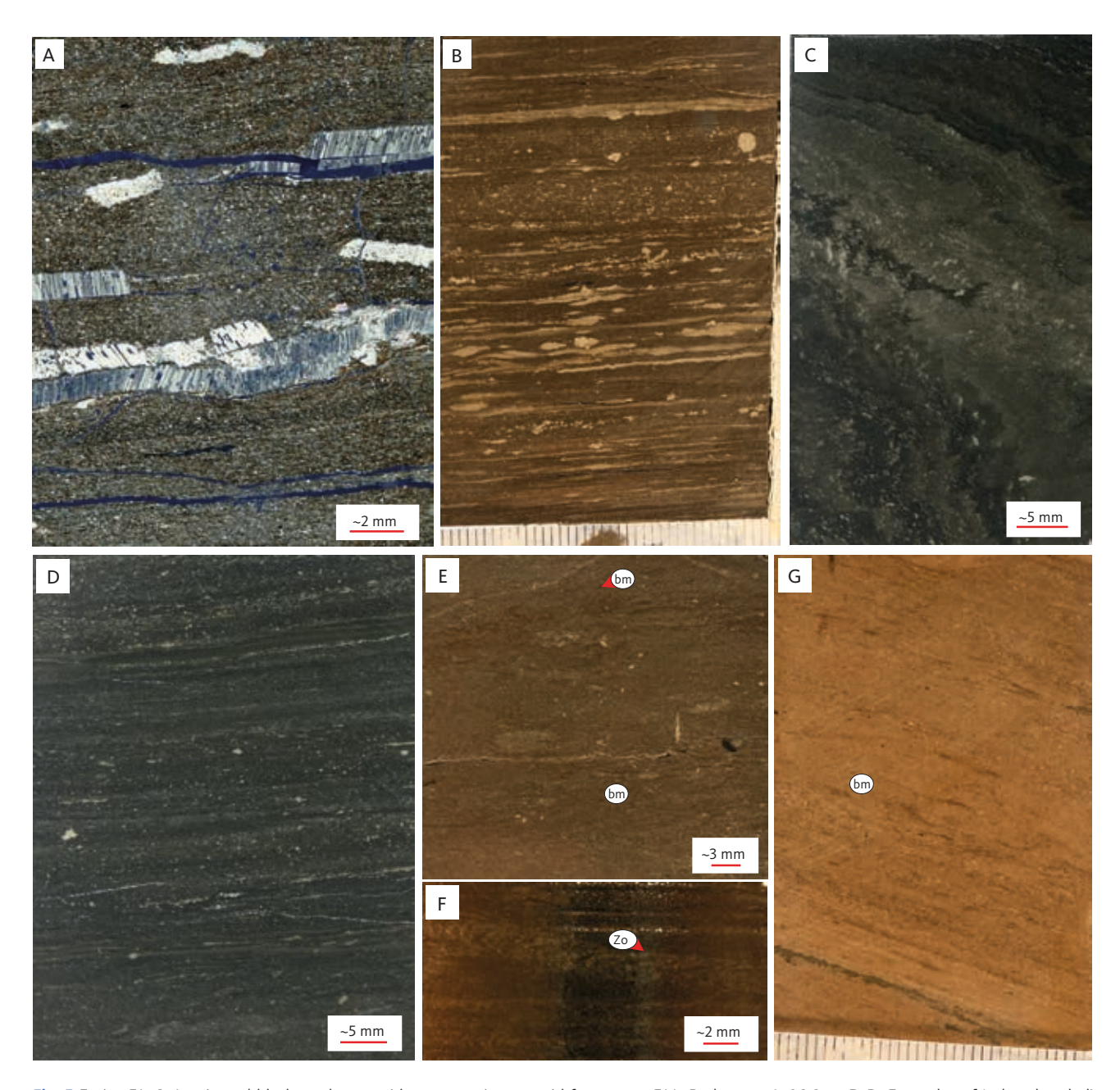


Fig. 5 Facies F1. **A**: Laminated black mudstone with common inoceramid fragments. F1A, Rødryggen-1, 26.6 m. **B-D**: Examples of 'colour-banded' pyrite-rich mudstone of F1B. Fig. 5C illustrates slump-folded ankerite- and pyrite-rich mudstone. **B**: Rødryggen-1, *c*. 64 m. **C**: Brorson Halvø-1, *c*. 47.5 m. **D**: Brorson Halvø-1, 46 m. **E**, **F**: Bioturbated examples of F1AB. **E**: Rødryggen-1, ~ 29 m. **F**: Rødryggen-1, ~ 25.5 m. Panel F represents a gradational interval from Lindemans Bugt to Palnatokes Bjerg Formation. **G**: Laminated to bioturbated ankerite- and dolomite-cemented mudstone. Subfacies F1C, Rødryggen-1, 76.6 m. **bm**: burrow mottling. **Zo**: *Zoophycos*.

### 4.1.1.1 Subfacies F1A: massive to laminated clayey mudstone

*Description*: F1A is a rare subfacies type occurring mainly in the Lindemans Bugt Formation (in the core intervals: Rødryggen-1 *c.* 97–24.4 m, Brorson Halvø-1 41–38 m; Figs 3, 4), where it typically forms centimetre- to metrescale successions. It commonly occurs in association with F7 (slumps) and F1B (colour-banded mudstone), and less commonly with F2 (clay-silt heteroliths) in the Bernbjerg Formation (Fig. 4, 178 m).

F1A has the finest grain size of the described facies and typically shows the highest gamma-ray (GR) values of

the succession (>180 API; American Petroleum Institute units). It consists of dark grey to black, apparently structureless or faintly laminated clayey mudstone (Fig. 5A). Pyrite is locally common. Generally, the deposits appear to be unbioturbated or contain rare diminutive *Chondrites, Zoophycos* and indistinct mottling (BI 0–3; Fig. 5E, F). The transitional occurrences (F1A/F2A) in the Bernbjerg Formation are more commonly intensively micro-bioturbated with millimetre to sub-millimetre scale indistinct traces that are typically visible as laminae disruptions (BI 0–5). The estimation of BI and recognition of trace fossils was locally hampered by lack of lithological contrast and

poorly preserved core (rubble). Finally, F1A is fossil-rich, bearing ammonites, belemnites and bivalves.

Interpretation: The lithology and sedimentary structures (e.g. laminated mud), concentration of marine fossils and ichnological properties are compatible with a marine, sub-storm wave-base, oxygen-deficient basinal environment characterised by hemipelagic suspension settling (see Hovikoski et al. 2023 for redox data). The close association with F7 (slumps) in the middle Volgian of the Brorson Halvø-1 section suggests a drowned slope setting in a tilted fault block at this location.

The bioturbated, intermediate occurrences in the Bernbjerg Formation are interpreted as dysoxic offshore sediments based on ichnological and sedimentological characteristics as well as the stratigraphic occurrence of the facies.

#### 4.1.1.2 Subfacies F1B: colour-banded mudstone

Description: Subfacies 1B is common in the Lindemans Bugt Formation in Rødryggen-1 (core depth 90–30 m). In the Brorson Halvø-1 core, F1B is rare, forming a thin interval in the middle Volgian (core depth 43 m). In addition, a single occurrence of F1B transitional to F1C was recorded at around 152 m in the Bernbjerg Formation. In both of the latter instances, the subfacies is also associated with slumps (F7).

F1B alternates gradationally with F1C and F1A, being an intermediate facies type between these two subfacies. On the GR log, F1B shows intermediate values commonly ranging between 100 and 150 API. This facies consists of interlaminated clayey mudstone, pyrite and ankerite-rich mudstone (see Olivarius et al. 2023, this volume), which leads to the characteristic colour banding of this facies (Fig. 5B, D). Moreover, lensoidal laminae and possible low-relief cross-lamination occur locally, but their conclusive documentation is hampered by soft-sedimentary deformation and concretionary structures (e.g. pyrite nodules) that obscure primary micro-facies. Bioclasts, consisting mainly of marine elements (e.g. onychites (belemnoid hooks), ammonites and bivalves), are also common. Pyrite is abundant. F1B typically appears to be unbioturbated (BI 0) and shows small-scale soft-sedimentary deformation structures (micro-slumps consisting of contorted lamination and micro-scale loading structures). The determination of bioturbation intensity is hampered locally, however, by lack of lithological contrast in black mudstone-dominated intervals.

Interpretation: Abundant small-scale soft sedimentary deformation, structureless mud laminae up to a few mm thick and local lenticular laminae suggest that deposition was probably partly derived from muddy gravity flows rather than being solely the result of hemipelagic

suspension fallout. Similarly, the alternation between stratified and structureless micro-facies suggests alternating transport processes, potentially driven by changing turbulence under decelerating mud flows (Plint 2014). The gravity flows were probably facilitated by the increasing depositional gradient due to late early Volgian – early Ryazanian fault block development (Surlyk 1978, 2003).

The localised ankeritic laminae probably reflect alteration of rare primary laminae rich in bioclasts (e.g. calcispheres; see Section 4.1.1.3; Olivarius *et al.* 2023, this volume). Considering the sedimentological and ichnological properties described here, coupled with the stratigraphic occurrence of the facies, F1B is interpreted to represent the accumulation of oxygen-deficient, basinal to slope mudstone in a tilted fault-block setting (see Section 5. Discussion).

### 4.1.1.3 Subfacies F1C: ankerite- and dolomite-rich mudstone

Description: F1C is a common facies type in both core sections in the Kimmeridgian and lower Volgian (Rødryggen-1 230–70 m, Brorson Halvø-1 220–48 m; Fig. 5G). It occurs most commonly as decimetre-scaled intervals. On the GR logs, F1C is readily identified by anomalously low GR peaks (<50 API) that sometimes occur within an interval of overall high GR readings (at the base of an upward-coarsening interval) or at the very top of coarsening-upward successions. In addition, F1C occurs in trendless successions.

F1C consists of ankerite- and dolomite-cemented mudstone, which characteristically shows interlaminated mudstone and bioclast-rich mudstone; the bioclasts are replaced by pyrite and ankerite (see Olivarius et al. 2023, this volume). Poorly preserved, their typical circular cross-section is suggestive of calcispheres, although some vase-shaped cross-sections resemble calpionellids. Locally, F1C shows soft sediment deformation. Pyrite and apatite are locally common (e.g. 89.8 m in Rødryggen-1; Olivarius et al. 2023, this volume).

Bioturbation intensity ranges from unbioturbated to intensive burrow-mottling (BI 0-6; e.g. Brorson Halvø-1, 150 m; Fig. 5G). Burrow mottling contains indistinct *c.* 1 mm wide, horizontal to sub-horizontal trace fossils, which produce a mottled fabric. These are tentatively assigned to *Zoophycos*, because of (1) locally visible chevron-shaped structures, which may point to the presence of spreite, and (2) despite their diminutive size, they can in places be followed laterally through the width of the core, suggesting the presence of a lobe rather than an individual burrow. Estimation of bioturbation intensity in F1C is locally hampered by concretionary structures related to ankerite and dolomite formation.

Interpretation: The enrichment of bioclastic material, authigenic minerals (phosphate) and locally high

bioturbation intensity is best explained by reduced sedimentation rates (condensation). This interpretation is supported by the occasional stratigraphic occurrence of F1C at the very top or base of parasequences, which could point to a reduced sedimentation rate during either transgressive events, tectonic reorganisation or both. However, local soft sediment deformation features and the close association with slumps (F7) suggest that some of the F1C layers (e.g. Brorson Halvø-1, 100–80 m) may represent redeposited calcareous ooze that was originally deposited as a pelagic drape on the eastern sediment-starved, incipient block crest, following the onset of block rotation.

### 4.1.2 Facies F2: interstratified claystone, siltstone and sandstone

Description: F2 is the dominant facies type in the Kimmeridgian - lower Volgian Bernbjerg Formation in the Rødryggen-1 cored section (234.5 to c. 97 m; Fig. 3), where it typically forms several metres thick aggradational (i.e. trendless) successions, and is also well-represented in this formation in the Brorson Halvø-1 core (225.7–45 m; Fig. 4). It is a transitional facies type with F3 (see Section 4.1.3) and can be gradationally or erosionally interbedded with F3. In addition, F2 is locally intercalated with F1C. On the GR log, F2 typically represents aggradational successions displaying relatively uniform GR values (c. 140–160 API). Locally, intervals dominated by F2 show stacked funnel-shaped GR patterns, a few metres thick (e.g. Rødryggen-1, 175-148 m; Fig. 3). F2 is most commonly unbioturbated, but locally, sporadic diminutive burrow mottling is recorded (BI 0-2).

F2 is subdivided into two subfacies: F2A, consisting of laminated mudstone (Fig. 6A, B), and F2B, which comprises interlaminated, very fine-grained sandstone or coarse siltstone and claystone and is characterised by lenticularity and basal erosional contacts (Figs 6C–H, 7A, B).

#### 4.1.2.1 Subfacies F2A: parallel-laminated clay and silt

Description: F2A is a common facies type in the Bernbjerg Formation. It forms millimetre- to centimetre-thick intervals occurring intergradationally between F1 and F2B. Together, these subfacies form aggradational (trendless) successions, or subtle, up to a few tens of metres thick, upward-coarsening successions (e.g. Rødryggen-1, 175–148 m; Brorson Halvø-1, 140–120 m).

F2A consists of fine-grained heterolithic interlamination, typically parallel-laminated siltstone and claystone (Fig. 6A). Lamina pinch-outs and erosional scours are rare or absent. Thin (c. 1 mm), tabular, normally graded siltstone–claystone couplets are present locally. Moreover, the transitional expressions (F2A–F2B gradation) show increasing silt content and lamina thickness, and the appearance of normally graded lamina sets a few

millimetres thick, which may laterally grade into scourbased, normally graded siltstone–claystone lamina sets (F2B). The deposits often appear unbioturbated or bear indistinct burrow mottling; rare diminutive *Zoophycos, Chondrites* and *?Phycosiphon* occur in places (BI 0–5; Fig. 6A, B). Disseminated pyrite and particularly coalified wood fragments are common locally. F2A differs from F2B in that it lacks (1) signs of erosion, (2) sandstone, (3) clear normal grading and (4) laminae convergence, pinch-outs or lenticularity.

Interpretation: In F2A parallel lamination dominates, with no indications of erosion. As in F1A, the deposits are bioturbated locally with possible diminutive Zoophycos, Chondrites and indistinct sub-millimetre scale burrow mottling, which is in line with a dysoxic, generally low energy environment (e.g. Martin 2004; Boyer & Droser 2011; Schieber & Wilson 2021; see also Hovikoski et al. 2023 for redox data). The normally graded, tabular siltstone-claystone couplets that lack erosional scour are interpreted as the most distal expression of thin mud-dominated gravity flows (see Section 4.1.2.2 Subfacies F2B). The transitional variants showing graded lamina couplets that may grade laterally into erosionally based siltstone-claystone lamina sets suggest that this type of interlamination is partly related to weak traction deposition. The interpreted depositional mechanism is the gravity-flow component of wave-enhanced gravity-flow (WEGF) currents as described by Macquaker et al. (2010; see Section 4.1.2.2 for discussion). These wave-initiated flows possibly extended some distance below storm wave base as slope-maintained gravity-flow currents.

In summary, considering the sedimentological and ichnological characteristics as well as the stratigraphic position, subfacies F2A is interpreted to record a low-energy dysoxic offshore environment that periodically experienced dilute, muddy gravity-flow events.

### 4.1.2.2 Subfacies F2B: cross-laminated – lenticularly laminated silt and clay

Description: F2B is a common subfacies type in the Brorson Halvø-1 core. It forms millimetre- to decimetre-scale successions and is commonly interbedded with F2A or F3. It usually occurs as a dominant subfacies in the top part of coarsening-upward successions (see Section 5. Discussion). F2B forms erosionally based upward-fining lamina sets a few millimetre thick, which may grade laterally into F2A over the width of the core. It is a broad subfacies dominated by interlaminated claystone-silt-stone and lenses of siltstone, characterised by lamina truncations, low-relief erosional scours, lamina pinchouts and down-lapping to top-lapping lamina contacts (Fig. 6C–H).

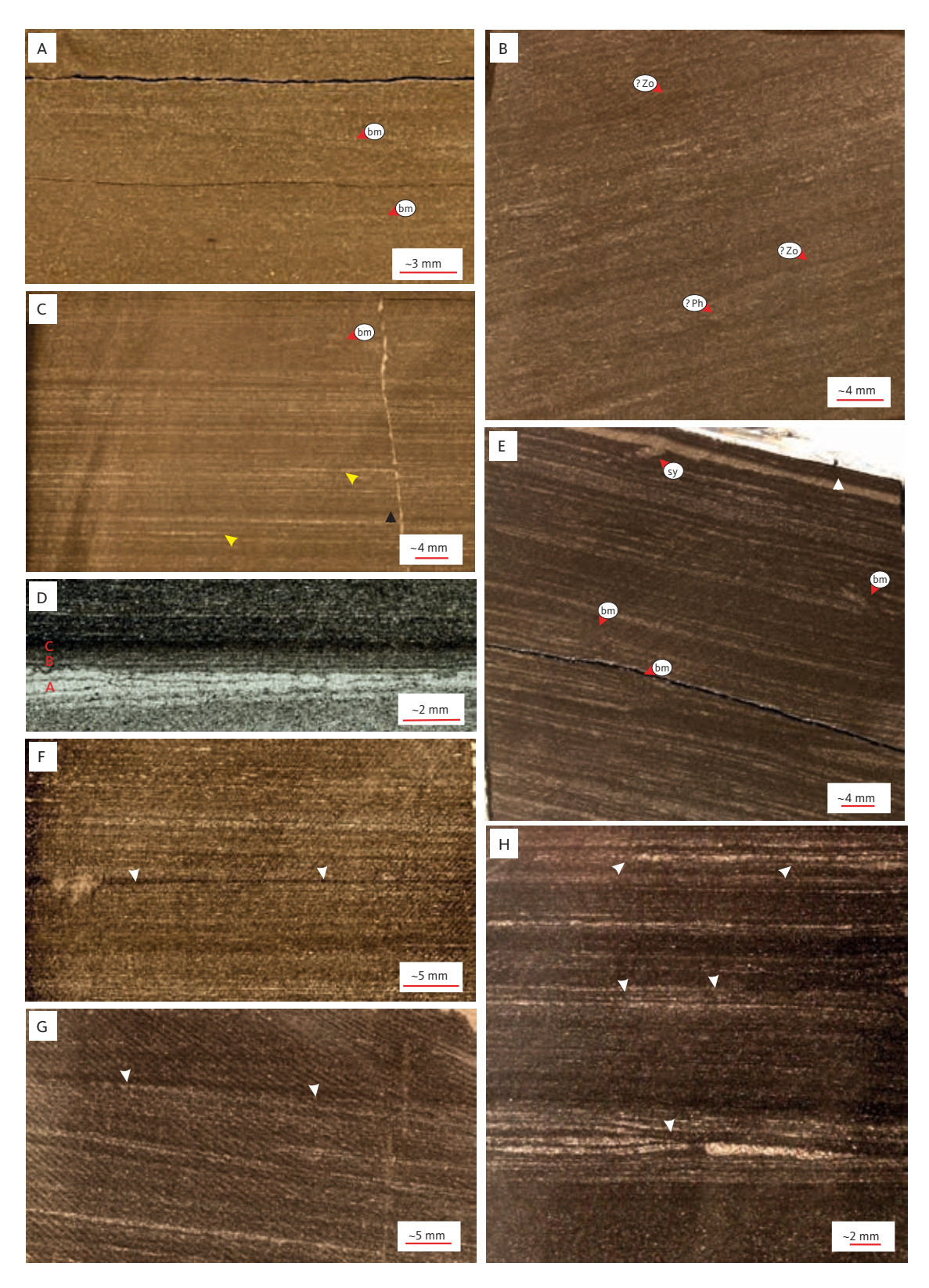


Fig. 6 Facies F2. A: Laminated mudstone with local burrow mottling (bm). F2A, Rødryggen-1, c. 190 m. B: Laminated to bioturbated mudstone (F2). Biogenic structures are interpreted to include diminutive Zoophycos (?Zo) and Phycosiphon (?Ph). Brorson Halvø-1, c. 186 m. C: Laminated silt and clay of F2B, showing normally graded laminae sets (black triangle), lenticular laminae and erosional contacts (yellow arrow). Top of photo shows an interval of F2A with burrow mottling. Rødryggen-1, c. 231.5 m. D: Thin section image illustrating a typical tripartite division of a normally graded laminae set: a basal, erosionally based, cross-laminated very fine-grained sand or coarse silt lamina (unit A), parallel laminated silt and clay (unit B) and a clay-rich mud layer (unit C). F2B, Rødryggen-1, 206.8 m. E: Burrow mottling, visible as laminae disruption, in heterolithic interlamination. Sy: synaeresis crack. White triangle: normally graded laminae set. Brorson Halvø-1, 106 m. F-H: Facies examples illustrating laminae terminations (white arrows) and convergent lamination in F2B, suggesting the presence of ripple cross-lamination in mudstone. The lowermost cross-lamination in H contains sand and thus represents a transient example to F3. F: Rødryggen-1, 232 m. G: Brorson Halvø-1, c. 150.5 m. H: Brorson Halvø-1, 215 m.

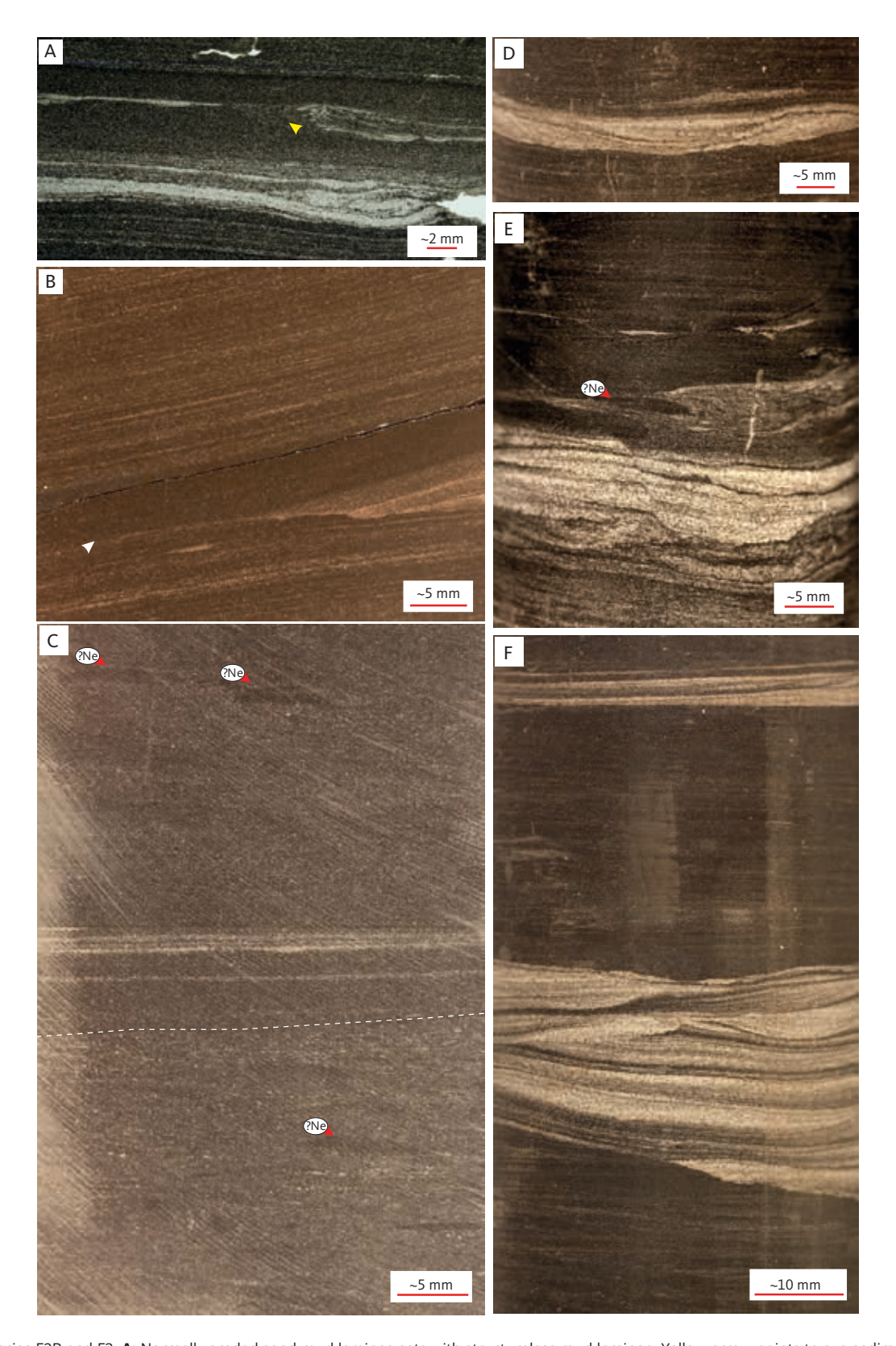


Fig. 7 Facies F2B and F3. A: Normally graded sand-mud laminae sets with structureless mud laminae. Yellow arrow points to syn-sedimentary deformation including small-scale slump folding. Rødryggen-1, 233.69 m. B: A sand-filled scour (F3) grading laterally into mud-on-mud contact. The scour is interbedded with laminated silt and clay of F2B. Brorson Halvø-1, 135 m. C: Mud-rich heteroliths (F2B), interbedded bioturbated intervals. White-dashed line marks the base of a structureless mud lamina. ?Ne: possible Nereites. Brorson Halvø-1, 185.5 m. D: Ripple cross-lamination showing laminae offshoots typical for wave ripples (F3). Brorson Halvø-1, 147 m. E: Cross-lamination with bioturbated top (F3). Brorson Halvø-1, 185 m. F: A scour-and-fill structure with ripple cross-laminated top (F3). The structure is interpreted as a storm wave-modified gravity deposit. Brorson Halvø-1, 183.5 m.

Two different types of erosionally based, normally graded lamina sets and beds are present. Type (1) comprises a few millimetre-thick siltstone-claystone couplets that show locally a tripartite microstructure: a basal micro-scoured contact below a millimetre-scale coarse siltstone or very fine-grained sandstone lamina (unit A; Fig. 6C, D). This basal lamina shows lateral thickness variability, pinch-outs and may contain inclined sub-millimetre thick mud drapes. The basal unit A is abruptly overlain by millimetre-thick parallel-laminated claystone and siltstone (unit B in Fig. 6D), which further grades into a structureless clayey mud-drape (unit C in Fig. 6D) that may contain pyrite. Type (2) comprises tabular, sharp-based siltstone-claystone laminae/beds. These beds are clay-dominated and appear to be composed of two components: a basal, c. 0.5-2 mm thick lenticular silt layer, which may contain inclined mud drapes and grades upwards into a structureless millimetre- to centimetre-scale clay bed. The basal contact in the Type 2 beds lacks evidence of prominent erosion.

In addition to the upward-fining lamina couplets and triplets, F2B shows subtle changes locally in lamina angle, lamina truncations and on-lapping or top-lapping lamina contacts, particularly where the facies is interbedded with cross-laminated sandstone (F3; Fig. 6F–H). Locally, silt–clay laminae sets show subtle changes in lateral thickness (Fig. 6H). Soft-sediment deformation is also very common and occurs as millimetres- to centimetre-scale micro-slump units (contorted Z-shaped lamina). Synaeresis cracks are rarely observed.

The deposits commonly appear unbioturbated, though exhibiting locally a low-density or diversity trace fossil fabric similar to that of subfacies F2A (Fig. 6E). The differences include lowered and fluctuating bioturbation intensity (BI 0–3) and increasing burrow diameter of burrow mottling in F2B (from sub-millimetre- to millimetre-scale). Moreover, in a few cases, an assemblage comprising *Nereites*, *?Chondrites* and *Phycosiphon* was observed at the top or in between event laminae or beds, at the gradation to F3 (Fig. 7C).

Interpretation: The deposits are interpreted to be mainly related to various gravity-flow and wave-modified gravity-flow processes, but an influence from more sustained current systems is also possible. The heterolithic interlamination showing subtle changes in lamina angle, lamina truncations and down-lapping to top-lapping lamina contacts (Figs 6G, H) suggests the presence of compacted, low relief mud-floccule ripples (Macquaker & Bohacs 2007; Schieber et al. 2007; Schieber & Southard 2009). The silt-clay interlamination with laminae pinch-outs and lenticularity (Fig. 6H) is similar to that generated by Yawar & Schieber (2017) in a flume tank experiment. Their results showed that such clay-silt interlamination can

form under similar flow velocity as mud-floccule ripples, but with a lower sedimentation rate.

The Type 1 erosionally based graded lamina set with the locally visible tripartite microstructure (Figs 6C, D) is very similar to the wave-enhanced gravity-flow deposits described by Macquaker et al. (2010). They proposed a three-phase flow model to explain the formation of these structures. In phase 1, wave-induced turbulence and resuspension form an erosionally based sand or coarse silt lamina (unit A). In phase 2, the increasing sediment concentration in the wave boundary layer damps turbulence, a pressure gradient develops and gravity flow begins. Shear mixing at the base of the laminar flow and mixing with sediment already in suspension results in the deposition of interlaminated silt and clay (unit B). In phase 3, the flow energy wanes, and the lutocline collapses (i.e. the suspended mud cloud), flow stops and the deposits grade into a clay-rich layer (unit C). Alternatively, such a structure could be deposited from a muddy gravity-flow current below wave base, which would also lead to turbulence damping as the flow decelerates and mud concentration increases (cf. Baas et al. 2011). The wave-enhanced gravity-flow interpretation is supported here by the fact that the deposits either grade into or are interbedded with, wave-rippled sandstone (F3) and gutter casts (see Section 4.1.3).

The Type 2 normally graded, tabular siltstone-claystone beds that lack prominent erosional scour at the base are interpreted as muddy gravity-flow deposits related to an increasing sea-floor gradient during episodes of block rotation. This interpretation is supported by the presence of intercalated slump deposits (F7). However, given the close association with deposits showing wave-influenced sedimentary structures, it is also possible that wave energy had a role in the formation of these deposits, and that the lack of unit B in these beds could be due to the dominance of clay, rapid flow deceleration or both.

The locally occurring *Nereites*-bearing ichnofabric and increasing burrow diameter suggest that oxygen levels increased at times during the deposition of F2B to F3. Fluctuating bioturbation intensity and soft-sediment deformation are also compatible with elevated depositional rates and common small-scale event deposition. The abundant coaly material and plant debris point to distal fluvial influence. This is corroborated by Hydrogen Index and C30 desmethyl sterane trends, which reveal an elevated input of terrigenous organic matter (Bojesen-Koefoed *et al.* 2023, this volume).

Additionally, considering the sedimentological and ichnological characteristics as well as the stratigraphic position of the facies above dysoxic offshore sediments (F2A), F2B is interpreted to reflect deposition in a wave-influenced and fluvially sourced and tectonically

active proximal offshore environment with a variable sea-floor gradient.

#### 4.1.3 Facies F3: cross-laminated sandstone

Description: F3 is a subordinate, but recurring facies type in both cores. It forms a few millimetres to a centimetre thick and is commonly interbedded with F2. It is typically present in the upper part of coarsening-upward successions (See 5. Discussion). F3 consists of ripple cross-stratified siltstone and very fine-grained sandstone. The ripples are characterised by asymmetrical to symmetrical profiles, irregular lower-bounding surfaces and common foreset offshoots that persist across the trough between ripples and peak again on the next ripple (Fig. 7D). Locally, the cross-laminated facies show a laterally variable erosional lower boundary forming scour-and-fill structures that are a few centimetres thick (Figs 7B, F). The basal contact may be overlain by parallel-laminated, cross-stratified siltstone or very fine-grained sandstone onlapping the laterally limited basal scour. At the top, the siltstone–sandstone unit may be overlain by clay-rich mud drapes up to 1 cm thick (Figs 7B, F). On the GR log, F3 is not always clearly expressed (due to the thin layers) but shows variable values of c. 80-120 API. F3 is commonly unbioturbated. In a single example, probable Nereites intensively burrow the overlying mud drape (BI 0-5).

Interpretation: Irregular lower bounding surfaces, bundling of laminae, foreset offshoots and locally occurring symmetrical ripple profiles suggest wave influence in the formation of the ripples (e.g. Reineck & Singh 1986). The laterally limited, relatively deep scour-and-fill structures showing onlapping lamina contacts over the basal erosional surface are interpreted to be storm-generated gutter casts (Myrow et al. 2002).

#### 4.1.4 Facies F7: slumps

*Description:* In the Brorson Halvø-1 core section, F7 is a common facies type in the lower Volgian of the Bernbjerg Formation and a dominant facies in the middle Volgian Lindemans Bugt Formation. It forms decimetre-to metre-scaled intervals and consists of slumped mudstone (F1) or heterolithic sediments (F2; Fig. 5C).

*Interpretation:* F7 is interpreted to record downslope mass wastage due to episodes of increased sea-floor gradients under block rotation.

#### 4.2 Palnatokes Bjerg Formation

The Palnatokes Bjerg Formation in the two cored boreholes consists of two facies: F4 of the Albrechts Bugt Member and F5 of the Rødryggen Member. The latter only occurs in the Brorson Halvø-1 borehole and is subdivided into two subfacies.

### 4.2.1 Facies F4: bioturbated calcareous mudstone

Description: F4 is a broad facies type, which forms the Albrechts Bugt Member interval. It is dominated by bioturbated fossiliferous mudstone, which has a variable amount of sand and calcite cement in the matrix. Locally, the deposits consist of variably bioturbated interlaminated grey mudstone and light grey calcareous mudstone. Near the top of the Albrechts Bugt Member, the facies appears structureless and contains shell fragments. F4 is generally characterised by a high fossil content. Buchia bivalves are especially common. Lithological accessories include abundant pyrite.

F4 is typically intensively bioturbated (BI 3–6) with a relatively low-diversity trace fossil assemblage dominated by *Zoophycos* and *Chondrites* of various sizes or cryptobioturbation (Fig. 8A, B). *Chondrites* cross-cut or reburrow other trace fossils. Secondary trace fossils include palimpsest grazing structures as well as rare *Siphonichnus* and *Thalassinoides* (Figs 8B, C).

Interpretation: The ubiquitous biogenic reworking in this facies precludes detailed process interpretation. However, given the depositional setting, grain size and the nature of the underlying succession, it is likely that hemipelagic settling and dilute gravity-flow processes were prevalent. The change from the unburrowed black mudstones of the Lindemans Bugt Formation to the fully bioturbated calcareous mudstones of the Albrechts Bugt Member points to an environmental shift from an anoxic basin to an oxic basin with limited input of clastic sediment. The very low clastic sediment input is interpreted to be due to the late syn-rift paleogeographic configuration (compartmentalised basin) and eustatic sea-level rise (Surlyk 1978). In summary, F4 is interpreted to represent sediment-starved deposits in a transgressed tilted fault-block setting.

#### 4.2.2 Facies F5: red calcareous mudstone

Description: F5 forms the Rødryggen Member interval in the Brorson Halvø-1 borehole. It consists of bioturbated red mudstone (Fig. 8D–G), which has a variable carbonate content in the matrix; earlier works have shown that the red colour is due to haematite (Alsen 2006). F5 is typically fully bioturbated (BI 6) exhibiting Zoophycos, Chondrites, Siphonichnus, ?Nereites and burrow mottling.

Facies F5 is divided into 2 subfacies. The first, F5A, consists of intensively bioturbated (burrow mottled), structureless red mudstone (Fig. 8F). Sand content is variable. The second subfacies, F5B, comprises bioclast-rich red mudstone and is characterised by a lower and fluctuating bioturbation intensity (BI 0–6). It contains sharp-based, shell hash beds that are a few centimetre thick (Fig. 8D). In addition, dispersed *Inoceramus* 

fragments with borings (Fig. 8G) and millimetre-scale rounded mud-clasts are very common locally.

Interpretation: The strongly composite biogenic fabric and the trace fossil assemblage point to a condensed, relatively deep, marine environment. The sharp-based shell-hash beds and locally incomplete bioturbation intensity in F5B are indicative of event deposition, probably due to gravity-flow events on a slope. Earlier fieldwork has demonstrated that the Rødryggen Member is restricted to fault-block crests (Surlyk 1978). Given the sedimentological and ichnological evidence discussed here, F5 is interpreted to record sedimentation on an oxygenated submarine high in a deep marine setting (See 5. Discussion).

#### 4.3 Stratumbjerg Formation

In the two borehole sections presented here, the Stratumbjerg Formation is represented only in the uppermost levels of the Brorson Halvø-1 core.

#### 4.3.1 Facies F6: bioturbated mudstone

Description: The interval referred to F6 in the Brorson Halvø-1 core is poorly preserved, consisting mainly of rubble. It comprises fully bioturbated (BI 6) light grey to greenish mudstone (Fig. 8G). The deposits contain *Chondrites* of different sizes, diminutive *Zoophycos*, palimpsest grazing structures (*Helminthopsis* and ?*Nereites*) and rare *Thalassinoides*. *Chondrites* commonly re-burrow other trace fossils. *Inoceramus* fragments and pyrite are common. The mudstone has a variable carbonate content, and concretionary beds are present locally.

Interpretation: The fine-grained lithology, the fully bioturbated fabric, the present ichnogenera and the lack of other forms suggest sub-storm wave-base basinal environment. The trace fossil content is not essentially different from that of the underlying Palnatokes Bjerg Formation. In outcrop, the Stratumbjerg Formation is characterised by a regionally extensive grey mudstone succession with occasional thin sandy turbidites (Bjerager et al. 2020). Thus, the F6 mudstone facies in the uppermost Brorson Halvø-1 core probably represents a transitional variant recording the initial change towards renewed clastic sediment deposition in the area.

#### 5. Discussion

The two drill cores provide an insight into mud accumulation in a distal fault block through almost a full rift cycle. Whereas most of the previous research in the area has concentrated on characterisation of the coarse-grained gravity-flow systems in the coast-attached proximal fault block (e.g. Surlyk 1978; Henstra *et al.* 2016), the coeval sediments in distal areas have remained poorly

documented. Notably, distal sediments corresponding to the rift-climax phase were practically unknown prior to this drilling program.

The facies recorded in the cores are diverse, reflecting sedimentation in the following settings: (1) storm-affected, oxygen-depleted deltaic shelf (Bernbjerg Formation; Fig. 9A); (2) basin floor and slope in a dysoxic-anoxic half-graben (Lindemans Bugt Formation; Fig. 9B) and (3) sediment-starved deep half-graben under oxic conditions (Palnatokes Bjerg Formation). Finally, the top Brorson Halvø-1 core extends into the Barremian, which records the gradation to (4) regionally continuous basinal mud accumulation under waning rifting (Stratumbjerg Formation).

Recently, Hovikoski *et al.* (2023) summarised the depositional and tectonostratigraphic evolution of the black mudstone succession and broad-scale changes in bottom oxygenation during the rifting. Here, we revisit the depositional evolution and further discuss the main facies.

### 5.1 Bernbjerg Formation (Kimmeridgian – lower Volgian)

The sedimentary facies indicate that the Bernbjerg Formation represents an essentially aggradational muddy shelf succession that was fed by fine-grained fluvial systems (Fig. 9A; see also Surlyk & Clemmensen 1983). In addition to macroscopic observations of common coalified wood fragments and plant debris, the prodeltaic nature is well-documented by organic geochemistry data, which indicate a prominent input of terrigenous organic matter (Bojesen-Koefoed et al. 2023, this volume; Hovikoski et al. 2023). The seaway was influenced by south-orientated axial currents (Hovikoski et al. 2023), which allowed along-coast dispersal of the river-supplied sediments. The Upper Cretaceous Dunvegan Formation of Canada represents an analogous scenario (Plint 2014). Water depth ranged from a sub-storm wave-base offshore setting (F1; mainly laminated mudstone) to proximal offshore (F2B, F3; cross-laminated heteroliths and sandstone) and incipient slope environments (F7; slumps) below and above storm wave-base. The slope environment started to evolve, especially during the early Volgian when rifting accelerated. Elemental redox data and the distribution of bioturbation indicate fluctuating redox conditions in a generally hypoxic setting (see Hovikoski et al. 2023).

Facies alternations occur on several scales ranging from millimetre- to centimetre-scale facies alternations to depositional or tectonic cycles up to several tens of metres thick. The formation consists of several subtle, irregular transgressive-regressive and regressive cycles c. 10–30 m thick that individually comprise apparently chaotic facies alternations and rare, poorly developed higher-frequency depositional successions some metres

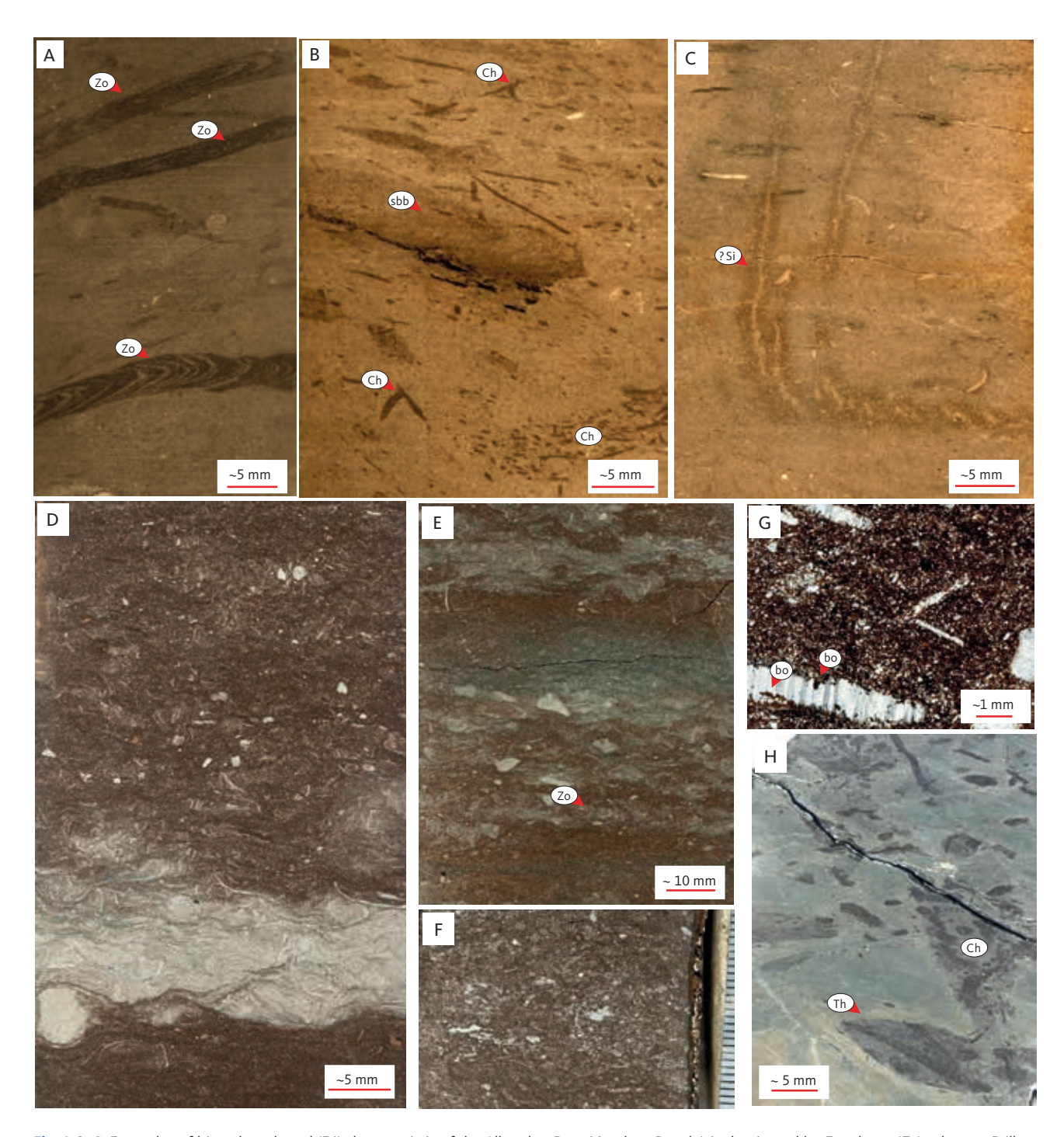


Fig. 8 A-C: Examples of bioturbated marl (F4) characteristic of the Albrechts Bugt Member. Panel A is dominated by *Zoophycos* (*Zo*), whereas B illustrates common *Chondrites* (*Ch*) that cross-cut and re-burrow palimpsest traces. sbb: – spreite-bearing burrow potentially representing *Rhizocorallium*. C shows potential pyritised *Siphonichnus* (*?Si*). A and B from Rødryggen-1, interval around 20.5 m; C from Rødryggen-1, 10.5 m. D-G: Facies examples of red bioclast-rich mudstones of the Rødryggen Member (F5). Panels D and E show occasional shell beds and scattered shell fragments in variably burrow-mottled fabric (F5B). Visible traces include *Zoophycos*. F illustrates intensively bioturbated structureless red mudstone (F5A). Panels D, E and F from Brorson Halvø-1, 20 m, 22 m and 28 m, respectively. Panel G is a thin section micrograph illustrating bored (bo) inoceramid fragments in sandy mudstone. Brorson Halvø-1, 9.7 m. H: Bioturbated grey mudstone (F6) from the basal part of the Stratumbjerg Formation. Two size classes of Chondrites reburrowing *Thalassinoides* (*Th*). Brorson Halvø-1, 6.5 m.

thick. An ideal, major upward-coarsening succession consists of F1, F2A, F2B and F3, reflecting progradation from dominantly low-energy dysoxic offshore conditions to proximal offshore with a higher frequency of depositional events. This ideal coarsening-upward trend is complicated by syntectonic influence, which affected

depositional rate, bottom gradient, water depth and sediment source areas. Particularly from the lower Volgian and on, contrasting depositional rates are recorded by the two cores: The *P. elegans – P. wheatleyensis* ammonite chronozone interval is *c.* 30 m thick in the Rødryggen-1 core, whereas the corresponding interval in the

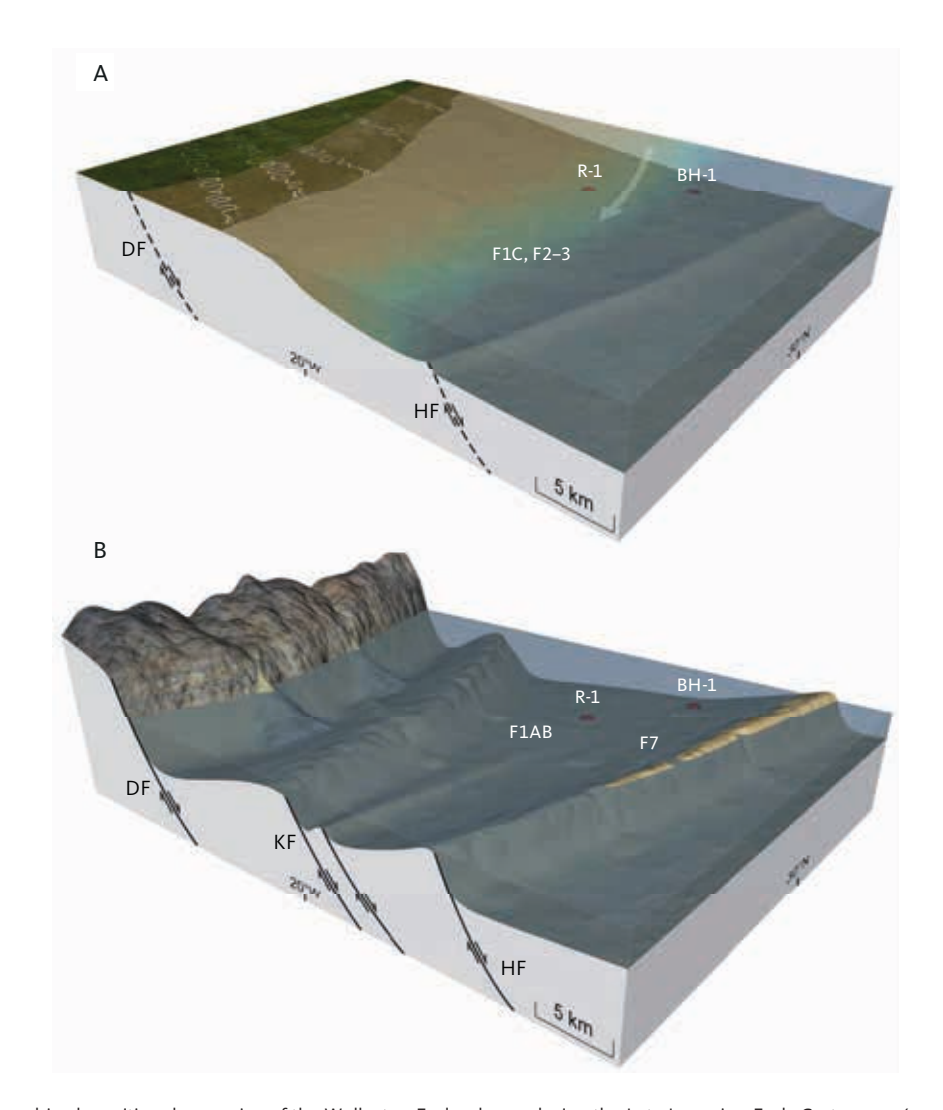


Fig. 9 Tectonostratigraphic-depositional scenarios of the Wollaston Forland area during the Late Jurassic – Early Cretaceous (modified from Hovikoski et al. in 2023). A: Kimmeridgian fluvially-sourced shelf influenced by along-coast sediment dispersal. The arrow indicates the main sediment transport direction, and red dots indicate borehole positions. DF: Dombjerg fault. HF: Hühnerbjerg fault. B: Middle Volgian – Ryazanian half-graben. The model shows major uplift along the Dombjerg fault and the development of the coarse-grained fan deltas of the Rigi Member (Lindemans Bugt Formation) in the coastal fault block (Surlyk 1978, 2003). The fan delta-related gravity flows were blocked by the uplifted Kuppel fault (KF) crest, which defined the western margin of the Permpas/Hühnerbjerg block(s). The hiatuses present in the Brorson Halvø-1 core indicate coeval uplift pulses along the Hühnerbjerg block crest. R-1: Rødryggen-1 borehole. BH-1: Brorson Halvø-1 borehole. Subfacies F1C and F1AB along with facies F2-3 and F7 are shown.

Brorson Halvø-1 core is >100 m thick (Alsen *et al.* 2023, this volume). Due to these factors, as well as increasing clay laminae thickness in higher energy facies (F3), the coarsening-upward successions are commonly poorly expressed on the GR log.

Fining-upward successions related to transgressive phases are best developed in the lower part of the Bernbjerg Formation (Kimmeridgian). These successions characteristically contain F1C beds, interbedded with F1B or F2. On the GR log, the successions are only weakly developed but are identifiable as serrated, generally increasing GR trends, punctuated by recurrent beds with low GR values (e.g. Brorson Halvø-1, 202–195 m). The stacking patterns of the major cycles suggest a maximum flooding zone in the upper part of the Kimmeridgian, around 178 m in the Brorson Halvø-1 core. This is followed by an overall progradational trend, the zone

of maximum regression being situated at around 100 m, in the lower Volgian *P. elegans* zone.

#### 5.1.1 Sedimentary event beds and laminae

Although the lithology of the Bernbjerg Formation is generally fine-grained, indications of erosion, laminae-scale event deposition and traction currents are widespread. Event deposition is recorded as wave ripples, scour-and-fill structures (gutter casts), convergent lamination pointing towards putative mud floccule ripples (Schieber *et al.* 2007) and associated silt-clay interlamination with pinchouts and lenticular laminae (Figs 6, 7; Yawar & Schieber 2017). Furthermore, normally graded siltstone-claystone beds, interpreted as muddy gravity flows, and probable wave-enhanced gravity-flow deposits occur frequently (Macquaker *et al.* 2010; Plint 2014). Although similar structures may result from pure gravity-flow processes

below wave-base, their close association with gutter casts and wave ripples points to the involvement of storm-wave processes. Such structures are also missing from the Lindemans Bugt Formation, which is interpreted to represent a sub-storm wave-base basinal and slope environment (see Section 5.2).

Clay-rich mud layers can be up to 1 cm thick at the top of normally graded event beds. Their structureless and seemingly ungraded nature coupled with common soft sedimentary deformation features (loading, slump-folding) suggest high water content and probably a fluid mud component in sedimentation.

Many sand-bearing event beds such as gutter casts pinch-out rapidly and are laterally equivalent to mudon-mud contacts. The mud-rich ripples range from well-defined cross-lamination with sand interlaminae (Fig. 6H) to subtle silt-clay laminae sets showing lateral thickness variations and convergent laminae (Fig. 6F, G). Such occurrences are commonly observed adjacent to small, laminae-confined slump intervals, which may suggest that an increased slope gradient enhanced the mud-ripple development.

Overall, the observed facies are similar to those reported from other storm-affected Mesozoic mudstone successions, including the Cretaceous Dunvegan Formation (Plint 2014) and the Mowry shale (Macquaker et al. 2010; Lazar et al. 2022) from the Western Interior Seaway. Other examples include the Jurassic Cleveland Ironstone Formation, the Whitby Mudstone Formation (Ghadeer & Macquaker 2011) and some intervals of the Kimmeridge Clay Formation, UK (e.g. Wignall 1989; Macquaker & Gawthorpe 1993).

### 5.2 Lindemans Bugt Formation (middle Volgian – late Ryazanian)

In the Brorson Halvø core, the base of the Lindemans Bugt Formation is marked by a major hiatus or stratigraphic condensation as indicated by biostratigraphic data (Alsen et al. 2023, this volume). Similarly, the upper boundary of the formation is demarcated by a hiatus spanning from the middle Volgian to the late Ryazanian. These unconformities testify to further intensified tectonic activity in the Wollaston Forland area during the middle Volgian (Surlyk 1978, 2003). This rift climax resulted in tilted faultblock development and basin segmentation, lasting until the early late Ryazanian. The Brorson Halvø-1 borehole is situated near the elevated hanging-wall crest of the Permpas fault block about 30 km east of the main fault zone (the Dombjerg fault). During the middle Volgian, major conglomeratic fan deltas developed east of the Dombjerg fault (Surlyk 1978; Henstra et al. 2016). The eastern limit of the submarine fan delta deposits was controlled by the Kuppel Fault, which defined the western margin of the Permpas block (Figs 1 and 9B). Due to basin segmentation and changes in sediment source areas, the Permpas block became isolated from the main focus of deltaic sedimentation and received progressively less terrestrial clastic sediment during rifting. This is directly reflected in the sedimentary facies exhibited by the Brorson Halvø-1 core, which suggest transformation into a non-deltaic, drowned oxygen-restricted slope (F7: slump) sub-storm wave-base slope (F1A, B: structureless to laminated mudstone) during the middle Volgian. The presence of the two major hiatuses resulted from reduced accommodation caused by uplift of the block crest.

### 5.3 Palnatokes Bjerg and Stratumbjerg Formations

The change from the Lindemans Bugt Formation to the Albrechts Bugt Member (Palnatokes Bjerg Formation) in the Rødryggen-1 core is gradational, occurring within 1 m of this boundary—a major hiatus in the Brorson Halvø-1 section. Above this boundary, the clastic sediment input decreased, and the environment became oxygenated as indicated by bioturbation and elemental redox proxies (Hovikoski *et al.* 2023). The change from black mudstone deposition to a ventilated basin with calcareous sedimentation is recognised supraregionally as an oceanographic change accompanied by the appearance of nannofossils with Tethyan influence (Pauly *et al.* 2013).

The interpretation of limited clastic input and low sedimentation rate is supported by the increased fossil content, increased bioturbation intensity, composite ichnofabrics (cross-cutting, re-burrowing) and the nature of the ichnofauna (*Zoophycos-* and *Chondrites-*dominated, low diversity ichnofabric). Moreover, the estimated bulk depositional rates are low (Hauterivian depositional rate c. 5.6 m/Myr; Hovikoski *et al.* 2023). In comparison to coeval outcrop data from the proximal fault block (Hovikoski *et al.* 2018), land-derived turbidites are absent, indicating continued detachment from coastal depositional systems in the studied fault block.

In the Brorson Halvø-1 section, the Albrechts Bugt Member grades into the Rødryggen Member at around 30 m depth, marked by a shift in the sedimentary facies to red bioclastic mudstones. Sedimentary facies suggest a more common gravity-flow component than in the Albrechts Bugt Member suggestive of an increasing slope gradient and a rift pulse or multiple rift pulses.

Piasecki *et al.* (2020) recently described coarse clastic sediments of the Falske Bugt Member (Palnatokes Bjerg Formation) near the Falkebjerg ridge, some kilometres east of the Brorson Halvø-1 drill site (Fig. 1), indicative of intensified rift activity in this region during the Valanginian–Barremian. Barremian syn-rift conglomerates are

not known from western fault systems (e.g. Dombjerg Fault), potentially suggesting that the rift climax persisted longer in the east. Unlike the deposits of the Falske Bugt Member, the coeval gravity flows of the Rødryggen Member comprise bioclasts and mud-clasts pointing to a limited or absent extraformational sediment source. This observation is compatible with localised footwall uplift and a compartmentalised basin.

The setting gradually returned to an oxygen-restricted, sub-storm wave-base, deep basinal environment during the late Hauterivian (basal Stratumbjerg Formation, F6). The sediments record decreasing biogenic carbonate accumulation and the renewed increase in clastic sediment input. In outcrop, the basal boundary of the Stratumbjerg is variably developed, being either conformable, as observed in the Brorson Halvø-1 core, or hiatal, eroding into the Bernbjerg Formation (Bjerager *et al.* 2020). In Wollaston Forland, this contact records waning rift activity, increased thermal subsidence and disappearance of rift-basin morphology.

#### 6. Conclusions

The Rødryggen-1 and Brorson Halvø-1 drill cores offer an insight into marine mud accumulation in an evolving distal fault block. The full core recovery, almost pristine preservation of the facies, stratigraphic continuity and the well-established biostratigraphic framework make the cores one of the best stratigraphic-sedimentological data points of the Jurassic-Cretaceous boundary and Kimmeridge Clay equivalent in northern high latitude regions. In particular, the Kimmeridgian – lower Volgian hypoxic shelf setting allowed exceptional preservation of subtle sedimentary structures in very thinly bedded mudstones recording distinct depositional events and traction currents and contributing to a general understanding of the processes governing mud accumulation.

The cores document that black mudstone accumulation extended through the Kimmeridgian – early Ryazanian (late) early rift and rift climax phases (Bernbjerg and Lindemans Bugt Formations). The facies suggest that the early rift hypoxic prodeltaic shelf was characterised by suspension settling, starved wave ripples, scour-and-fill structures, putative mud floccule ripples and mud-dominated gravity-flow deposits. During the rift climax phase, the depositional environment evolved into a narrow half-graben characterised by bioclastic and pyrite-rich black mudstones. These deposits document hemipelagic suspension settling and gravity-flow or mass-wasting deposition in sub-storm wave-base, dysoxic, anoxic to euxinic slope and basin-floor environments.

The Ryazanian–Valanginian late syn-rift setting experienced a supra-regional oceanographic change and improved ventilation, which is reflected in the deposition

of deep marine marls (Albrechts Bugt Member, Palnatokes Bjerg Formation). Condensed, red bioclastic mudstones with a common gravity-flow component characterised the Hauterivian, which probably recorded an eastward shift in fault activity and final blanketing of the submerged fault-block crest (Rødryggen Member, Palnatokes Bjerg Formation). The top of the cored succession is marked by the appearance of dark grey bioturbated mudstones of Barremian age, recording the onset of regionally continuous deep marine clastic mud accumulation in thermally subsiding basins.

Thus, although superficially monotonous, detailed facies analysis of the mudstone-dominated succession exhibited by the Rødryggen-1 and Brorson Halvø-1 boreholes reveals a highly dynamic depositional system that reflects shifting marine processes under varied hydrodynamic conditions, at different water depths and varied levels of bottom oxygenation during almost a full rift cycle.

#### **Acknowledgements**

Jette Halskov, Stefan Solberg and Jacob L. Bendtsen are thanked for professional graphic support. Guy Plint and Paul Smith are thanked for constructive and insightful reviews.

#### **Additional information**

#### **Funding statement**

Funding for drilling of the Rødryggen-1 and Brorson Halvø-1 boreholes and studies of the cores was provided by a consortium of oil companies and the Geological Survey of Denmark and Greenland (GEUS).

#### **Author contributions**

JH: wrote the paper in co-operation with other authors. JH and JI: sedimentology. MO: Mineralogy and diagenesis. JBK: organic geochemistry. SP and PA: biostratigraphy.

#### **Competing interests**

The authors declare no competing interests.

#### **Additional files**

None provided.

#### References

Alsen, P. 2006: The Early Cretaceous (Late Ryazanian – Early Hauterivian) ammonite fauna of North-East Greenland: Taxonomy, biostratigraphy, and biogeography. Fossils & Strata **53**, 229 pp. https://doi.org/10.18261/9781405180146-2006-01

Alsen, P., Piasecki, S., Nøhr-Hansen, H., Pauly, S., Sheldon, E. & Hovikoski, J. 2023: Stratigraphy of the Upper Jurassic to lowermost Cretaceous in the Rødryggen-1 and Brorson Halvø-1 boreholes, Wollaston Forland, North-East Greenland. GEUS Bulletin 55, 8342 (this volume). https://doi.org/10.34194/geusb.v55.8342

Baas, J.H., Best, J.L. & Peakall, J. 2011: Depositional processes, bedform development and hybrid bed formation in rapidly decelerated cohesive (mud-sand) sediment flows. Sedimentology 58, 1953–1987. https://doi.org/10.1111/j.1365-3091.2011.01247.x

Bentley, S.J. & Nittrouer, C.A. 2003: Emplacement, modification, and preservation of event strata on a flood-dominated continental shelf:

- Eel Shelf, northern California: Continental Shelf Research 23(19), 1465–1493. https://doi.org/10.1016/j.csr.2003.08.005
- Bjerager, M. et al. 2020: Cretaceous lithostratigraphy of North-East Greenland. Bulletin of the Geological Society of Denmark **68**, 37–93. https://doi.org/10.37570/bgsd-2020-68-04
- Bojesen-Koefoed, J.A, Alsen, P., Bjerager, M., Hovikoski, J., Ineson, J.R., Johannessen, P., Olivarius, M., Piasecki, S. & Vosgerau, H. 2023a: The Rødryggen-1 and Brorson Halvø-1 fully cored boreholes (Upper Jurassic Lower Cretaceous), Wollaston Forland, North-East Greenland an introduction. GEUS Bulletin **55**, 8350 (this volume). https://doi.org/10.34194/geusb.v55.8350
- Bojesen-Koefoed, J.A., Alsen, P., Bjerager, M., Hovikoski, J., Johannessen, P., Nøhr-Hansen, H., Petersen, H.I., Piasecki, S. & Vosgerau, H. 2023b: Organic geochemistry of an Upper Jurassic Lower Cretaceous mudstone succession in a narrow graben setting, Wollaston Forland Basin, North-East Greenland. GEUS Bulletin 55, 8320 (this volume). https://doi.org/10.34194/geusb.v55.8320
- Boyer, D. & Droser, M. 2011: A combined trace- and body-fossil approach reveals high-resolution record of oxygen fluctuations in Devonian seas. Palaios 26, 500–508. https://doi.org/10.2110/palo.2010.p10-073r
- Ghadeer, S. & Macquaker, J. 2011: Sediment transport processes in an ancient mud-dominated succession: A comparison of processes operating in marine offshore settings and anoxic basinal environments. Journal of the Geological Society (London) 168, 1121–1132. https://doi.org/10.1144/0016-76492010-016
- Henstra, G.A. *et al.* 2016: Depositional processes and stratigraphic architecture within a coarse-grained rift margin turbidite system: The Wollaston Forland Group, East Greenland. Marine and Petroleum Geology **76**, 187–209. https://doi.org/10.1016/j.marpetgeo.2016.05.018
- Hovikoski, J., Uchman, A., Alsen, P. & Ineson, J. 2018: Ichnological and sedimentological characteristics of submarine fan deposits in a half-graben, Lower Cretaceous Palnatokes Bjerg Formation, NE Greenland. Ichnos 26(1), 28–57. https://doi.org/10.1080/10420940.2017.1396981
- Hovikoski, J. *et al.* 2023: Late Jurassic–Early Cretaceous marine deoxygenation in NE Greenland. Journal of the Geological Society **180**(3), jgs2022-058. https://doi.org/10.1144/jgs2022-058
- Ichaso, A.A. & Dalrymple, R.W. 2009: Tide- and wave-generated fluid mud deposits in the Tilje Formation (Jurassic), offshore Norway. Geology **37**, 539–542. https://doi.org/10.1130/g25481a.1
- Kineke, G.C., Sternberg, R.W., Trowbridge, J.H. & Geyer, W.R. 1996: Fluid mud processes on the Amazon continental shelf. Continental Shelf Research 16. 667–696.
- Lazar, O.R., Bohacs, K.M., Schieber, J., Macquaker, J.H.S. & Demko, T.M. 2022: Laminae, laminasets, beds, and bedsets. In: Bohacs, K.M. & Lazar, O.R. (eds): Sequence stratigraphy: Applications to fine-grained rocks. AAPG Memoir 126, 89–106.
- Macquaker, J. & Bohacs, K. 2007: On the accumulation of mud. Science **318**, 1734–1735. https://doi.org/10.1126/science.1151980
- Macquaker, J., Bentley, S. & Bohacs, K. 2010: Wave-enhanced sediment-gravity flows and mud dispersal across continental shelves: Reappraising sediment transport processes operating in ancient mudstone successions. Geology 38, 947–950. https://doi.org/10.1130/g31093.1
- MacQuaker, J.H.S. & Gawthorpe, R.L. 1993: Mudstone lithofacies in the Kimmeridge Clay Formation, Wessex Basin, southern England; implications for the origin and controls of the distribution of mudstones. Journal of Sedimentary Research 63(6), 1129–1143. https://doi. org/10.1306/D4267CC1-2B26-11D7-8648000102C1865D
- Martin, K.D. 2004: A re-evaluation of the relationship between trace fossils and dysoxia. In: McIlroy, D. (ed.): The Application of Ichnology to Palaeoenvironmental and Stratigraphic Analysis. Geological Society (London), Special Publications 228, 141–156. https://doi.org/10.1144/gsl.sp.2004.228.01.08
- Myrow, P., Fischer, W. & Goodge, J. 2002: Wave-modified turbidites: Combined-flow shoreline and shelf deposits, Cambrian, Antarctica. Journal of Sedimentary Research **72**, 641–656. https://doi.org/10.1306/022102720641
- Nøhr-Hansen, H. 1993: Dinoflagellate cyst stratigraphy of the Barremian to Albian, Lower Cretaceous, North-East Greenland. Grønlands Geologiske Undersøgelse Bulletin **166**, 171 pp. https://doi.org/10.34194/bullggu.v166.6722

- Olivarius, M., Kazerouni, A.M., Weibel, R., Kokfelt, T.F. & Hovikoski, J. 2023: Mudstone diagenesis and sandstone provenance in an Upper Jurassic Lower Cretaceous evolving half-graben system, Wollaston Forland, North-East Greenland. GEUS Bulletin **55**, 8309 (this volume). https://doi.org/10.34194/geusb.v55.8309
- Pauly, S., Mutterlose, J. & Alsen, P. 2013: Depositional environments of Lower Cretaceous (Ryazanian–Barremian) sediments from Wollaston Forland and Kuhn Ø, North-East Greenland. Bulletin of the Geological Society of Denmark 61, 19–36. https://doi.org/10.37570/ bgsd-2013-61-02
- Piasecki, S., Bojesen-Koefoed, J.A. & Alsen, P. 2020: Geology of the Lower Cretaceous in the Falkebjerg area, Wollaston Forland, northern East Greenland. Bulletin of the Geological Society of Denmark **68**, 155–169. https://doi.org/10.37570/bgsd-2020-68-07
- Plint, A.G., Macquaker, J.H.S. & Varban, B.L. 2012: Shallow-water, storm-influenced sedimentation on a distal, muddy ramp: Upper Cretaceous Kaskapau Formation, Western Canada foreland basin. Journal of Sedimentary Research 82, 801–822.
- Plint, G. 2014: Mud dispersal across a Cretaceous prodelta: storm-generated, wave-enhanced sediment gravity flows inferred from mudstone microtexture and microfacies. Sedimentology **61**, 609–647. https://doi.org/10.1111/sed.12068
- Potter, P.E., Maynard, J.B. & Depetris, P.J. 2005: Mud and Mudstones: Introduction and Overview. 297 pp. Berlin: Springer-Verlag. https://doi.org/10.2113/gsecongeo.100.7.1469
- Potter, P.E., Maynard, J.B. & Pryor, W.A. 1980: Sedimentology of Shale Study Guide and Reference Source. 306 pp. New York: Springer. https://doi.org/10.1007/978-1-4612-9981-3
- Reineck, H. & Singh, I. 1986: Sedimentary Depositional Environments. 683 pp. Berlin: Springer-Verlag. https://doi.org/10.1016/0033-5894(81)90023-5
- Schieber, J. & Southard, J.B. 2009: Bedload transport of mud by flocule ripples Direct observation of ripple migration processes and their implications. Geology **37**, 483–486. https://doi.org/10.1130/g25319a.1
- Schieber, J. & Wilson, R. 2021: Burrows without a trace How meioturbation affects rock fabrics and leaves a record of meiobenthos activity in shales and mudstones. Paläontologische Zeitschrift 95, 767–791.
- Schieber, J. & Yawar, Z. 2009: A new twist on mud deposition Mud ripples in experiment and rock record. The Sedimentary Record 7, 4–8. https://doi.org/10.2110/sedred.2009.2.4
- Schieber, J., Southard, J. & Thaisen, K. 2007: Accretion of mudstone beds from migrating floccule ripples. Science **318**, 1760–1763. https://doi.org/10.1126/science.1147001
- Surlyk, F. 1978: Submarine fan sedimentation along fault scarps on tilted fault blocks (Jurassic-Cretaceous boundary, East Greenland). Bulletin Grønlands Geologiske Undersøgelse 128, 108 pp. https://doi. org/10.34194/bullggu.v128.6670
- Surlyk, F. 1984: Fan-delta to submarine fan conglomerates of the Volgian-Valanginian Wollaston Forland Group, East Greenland. In: Koster, E.H. & Steel, R.J. (eds): Sedimentology of gravel and conglomerates. Canadian Society of Petroleum Geologists Memoir 10, 359–382.
- Surlyk, F. 1990: A Jurassic sea-level curve for East Greenland. Palaeo-geography, Palaeoclimatology, Palaeoecology 78, 71–85. https://doi.org/10.1016/0031-0182(90)90205-l
- Surlyk, F. 2003: The Jurassic of East Greenland: A sedimentary record of thermal subsidence, onset and culmination of rifting. In: Ineson, J.R. & Surlyk, F. (eds): The Jurassic of Denmark and Greenland. Geological Survey of Denmark and Greenland Bulletin 1, 659–722. https://doi. org/10.34194/geusb.v1.4674
- Surlyk, F. & Clemmensen, L.B. 1975: A Valanginian turbidite sequence and its palaeogeographical setting (Kuhn Ø, East Greenland). Bulletin of the Geological Society of Denmark **24**, 61–73
- Surlyk, F. & Clemmensen, L.B. 1983: Rift propagation and eustacy as controlling factors during Jurassic inshore and shelf sedimentation in northern East Greenland. Sedimentary Geology **34**, 119–143. https://doi.org/10.1016/0037-0738(83)90083-0

- Surlyk, F. et al. 2021: Jurassic stratigraphy of East Greenland. GEUS Bulletin **46**, 6521. https://doi.org/10.34194/geusb.v46.6521
- Sykes, R.M. & Surlyk, F. 1976: A revised ammonite zonation of the Boreal Oxfordian and its application in northeast Greenland. Lethaia **9**, 421–436. https://doi.org/10.1111/j.1502-3931.1976.tb00984.x
- Taylor, A.M. & Goldring, R. 1993: Description and analysis of bioturbation and ichnofabric. Journal of the Geological Survey (London) **150**, 141–148. https://doi.org/10.1144/gsjgs.150.1.0141
- Vischer, A. 1943: Die Postdevonische Tektonik von Ostgrönland zwischen  $74^\circ$  und  $75^\circ$  n. Br. Meddelelser om Grønland 133(1), 195 pp.
- Wignall, P.B. 1989: Sedimentary dynamics of the Kimmeridge Clay: Tempests and earthquakes. Journal of the Geological Society **146**(2), 273–284. https://doi.org/10.1144/gsjgs.146.2.0273
- Wright, L.D., Friedrichs, C.T., Kim, S.C. & Scully, M.E. 2001: Effects of ambient currents and waves on gravity-driven sediment transport on continental shelves. Marine Geology 175, 25–45. https://doi.org/10.1016/s0025-3227(01)00140-2
- Yawar, Z. & Schieber, J. 2017: On the origin of silt laminae in laminated shales. Sedimentary Geology **360**, 22–34. https://doi.org/10.1016/j. sedgeo.2017.09.001

# **GEUS Bulletin**



# Mudstone diagenesis and sandstone provenance in an Upper Jurassic – Lower Cretaceous evolving half-graben system, Wollaston Forland, North-East Greenland

Mette Olivarius<sup>1</sup>, Afsoon M. Kazerouni<sup>2</sup>, Rikke Weibel<sup>1</sup>, Thomas F. Kokfelt<sup>3</sup>, Jussi Hovikoski<sup>4,5</sup>

<sup>1</sup>Department for Geo-energy and Storage, Geological Survey of Denmark and Greenland (GEUS), Copenhagen, Denmark; <sup>2</sup>Geological Survey of Denmark and Greenland (GEUS), Copenhagen, Denmark; <sup>3</sup>Department for Mapping and Mineral Resources, Geological Survey of Denmark and Greenland (GEUS), Copenhagen, Denmark; <sup>4</sup>Department for Geophysics and Sedimentary Basins, Geological Survey of Denmark and Greenland (GEUS), Copenhagen, Denmark; <sup>5</sup>Geological Survey of Finland (GTK), Espoo, Finland

# **Abstract**

The influence of rifting on the composition of Kimmeridgian to Barremian mudstones from northern Wollaston Forland, North-East Greenland is investigated by petrographic and mineralogical analyses of the Brorson Halvø-1 and Rødryggen-1 cores, and provenance analysis by zircon U-Pb age dating of nearby sandstones. Mudstone composition varies systematically as a function of the timing of rifting progression and position in the half-graben depositional system. Pyrite primarily precipitated in the early rift to rift climax phases. Euhedral pyrite overgrowths on framboids formed only during the rift climax phase (Lindemans Bugt Formation). Dolomite is the dominant carbonate cement, except for the sediments deposited in the early waning rift phase (Palnatokes Bjerg Formation) where calcite is dominant, and in the late waning rift phase (Stratumbjerg Formation) where siderite dominates. The highest-temperature reactions with precipitation of illite, quartz, ankerite and barite signify sediment burial depths of >2 km prior to exhumation. Uplift-induced fracturing occurred mainly in the early rift to rift acceleration succession (Bernbjerg Formation). Mudstones in the proximal part of the half-graben (Rødryggen-1) include more detrital kaolinite than the distal mudstones (Brorson Halvø-1), which contain more mixed-layer illite-smectite and illite. Vermiculite was deposited only in the proximal part of the basin in the rift climax and waning rift successions. Chlorite was deposited proximally and distally during the waning rift phase, though supply began earlier in the distal part. Fine-grained sediment in the distal part of the half-graben was therefore probably supplied by axial transport from Palaeoproterozoic crystalline rocks and Meso- to Neoproterozoic metamorphic rocks located to the north and north-west. This agrees with the zircon provenance signature from outcropping sand-rich facies, where zircon grains with U-Pb ages of 2.0-1.6 Ga are dominant, in addition to common 1.6-0.9 Ga ages, and fewer 2.8-2.6 Ga and 0.47-0.36 Ga ages.

### 1. Introduction

The archetypal half-graben setting has an ample sediment supply and can be divided into several sedimentation zones related to proximity to bounding faults and rift evolution (Surlyk 1978; Gawthorpe & Leeder 2000). This subdivision contributes to evaluations of sediment distribution in basins. Moreover, when knowledge of structural evolution is combined with information on basement rocks in a hinterland area and sediment delivery systems, changes in sediment composition can be linked to source changes over time.

Possible trends in sediment composition are not well-known in distal marine half-grabens that may be largely isolated from coarse-grained clastic input by coast-parallel submarine rift shoulders. Such a setting results in axial sediment transport and mudstone deposition, particularly in basins detached from the coastal area. Therefore, the Rødryggen-1 and Brorson Halvø-1 cores from northern Wollaston Forland in North-East Greenland (Fig. 1) were used in this study to investigate the proximal versus distal development of a mudstone-dominated half-graben succession deposited during Late Jurassic to Early Cretaceous rifting. Organic-rich black shales

\*Correspondence: mol@geus.dk

Received: 03 Jan 2022 Revised: 03 Oct 2023 Accepted: 03 Oct 2023 Published: 21 Dec 2023

**Keywords:** diagenetic processes, mudstone mineralogy, petrography, provenance analysis, rifting

#### Abbreviations:

BSE: backscattered electrons EDS: energy dispersive X-ray spectrometry GEUS: Geological Survey of Denmark and Greenland K-S: Kolmogorov-Smirnov

LA-ICP-MS: laser ablation inductively coupled plasma mass spectroscopy MDS: multidimensional scaling SE: secondary electrons

SEM: scanning electron microscopy TOC: total organic carbon

XRD: X-ray diffraction

GEUS Bulletin (eISSN: 2597-2154) is an open access, peer-reviewed journal published by the Geological Survey of Denmark and Greenland (GEUS). This article is distributed under a *CC-BY 4.0* licence, permitting free redistribution, and reproduction for any purpose, even commercial, provided proper citation of the original work. Author(s) retain copyright.

**Edited by:** Jon Ineson & Jørgen A. Bojesen-Koefoed (GEUS, Denmark)

**Reviewed by:** Chris L. Kirkland (Curtin University, Australia), Kevin Taylor (The University of Manchester, UK)

Funding: See page 92

Competing interests: See page 92

Additional files: See page 92

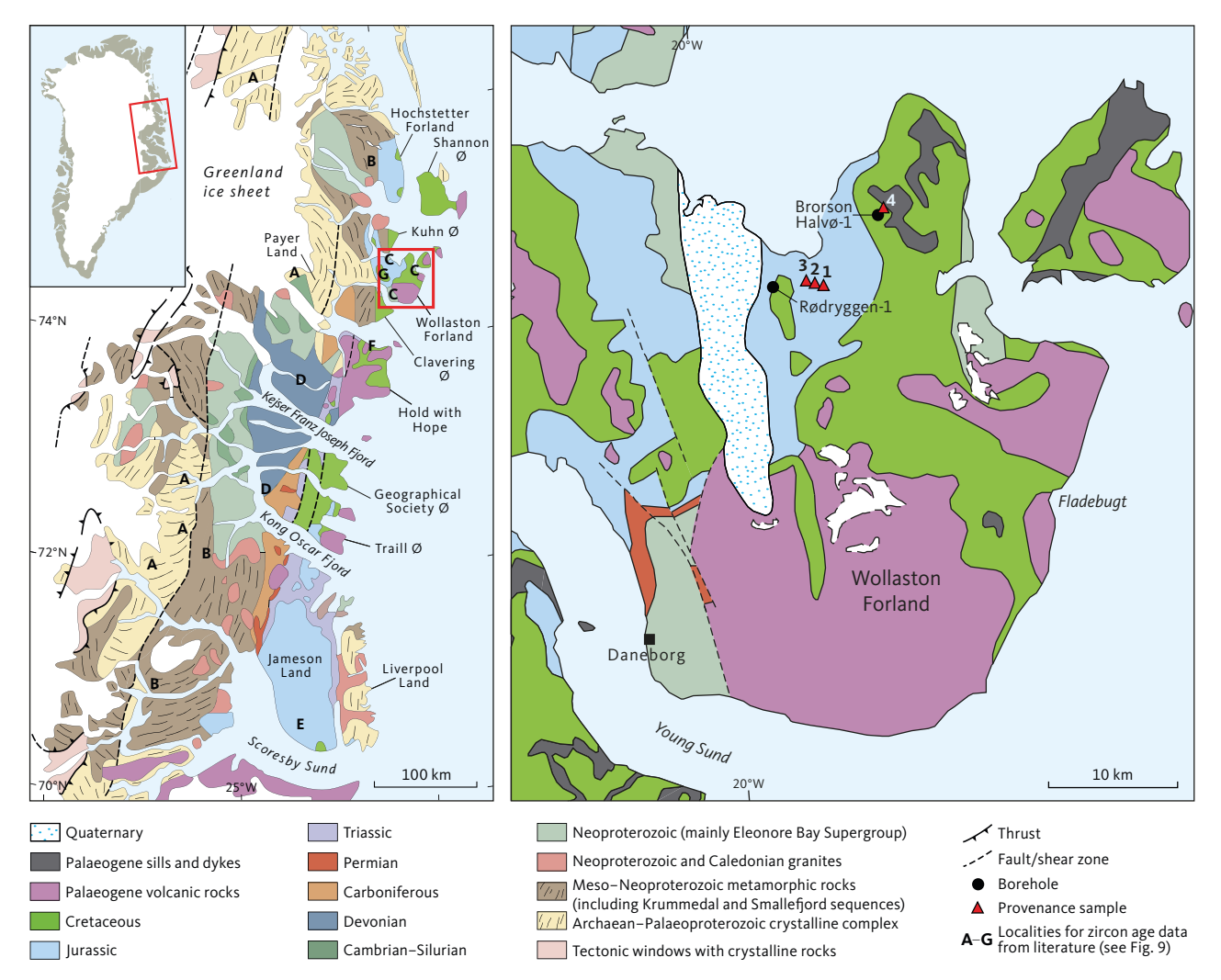


Fig. 1 Geological map of North-East Greenland based on Stemmerik et al. (1997), Henriksen et al. (2008) and Kalsbeek et al. (2008a). Detailed map of Wollaston Forland based on the digital Greenland geological map at a scale of 1:500 000 and the printed map series at a scale of 1:100 000. The locations of the Rødryggen-1 and Brorson Halvø-1 boreholes and the samples for zircon U-Pb age dating are shown.

have accumulated in many contemporaneous basins, especially in the northern hemisphere (Langrock *et al.* 2003; Mutterlose *et al.* 2003; Rogov *et al.* 2020), so the findings of this study facilitate the prediction of mudstone composition in such basins.

The Rødryggen-1 and Brorson Halvø-1 boreholes were drilled in 2009–2010 to depths of 234.5 and 225.7 m, respectively, covering Kimmeridgian to Barremian sediments (Fig. 2) that represent prolonged mudstone deposition in an evolving half-graben setting. The studied half-graben was bounded by north-south-orientated fault crests delimiting this basin from the rest of the rift system and from the palaeo-coast to the west (Surlyk 1978). Late Jurassic – Early Cretaceous rifting was widespread along the Norwegian–Greenland Seaway, which connected the proto-Arctic to the proto-North Atlantic (e.g. Stoker *et al.* 2017).

We aim to address two main research questions in this study: (1) How do the different phases of halfgraben development (i.e. early rift, rift acceleration, rift climax, waning rift) affect the composition of the deposited sediment in a mudstone-dominated environment? (2) To what extent does the sediment composition differ between the two cores that represent the proximal versus distal parts of the half-graben system?

### 2. Geological setting

The Greenlandic craton consists mainly of crystalline basement, which is exposed at the rim of the Greenland ice sheet and in tectonic windows in the Caledonides (Fig. 1; Henriksen *et al.* 2008; Kalsbeek *et al.* 2008a). The sediment source areas relevant for this study are present within the East Greenland Caledonian fold belt, which originated from the Laurentia–Baltica continental collision that took place in late Cambrian to early Devonian time (McKerrow et al. 2000; Smith & Rasmussen 2008). The orogenesis caused westwards thrusting of crystalline complexes of Archaean to Palaeoproterozoic age, metasediments of the Krummedal and Smallefjord sequences of Mesoproterozoic to early Neoproterozoic age, metasediments of the Eleonore

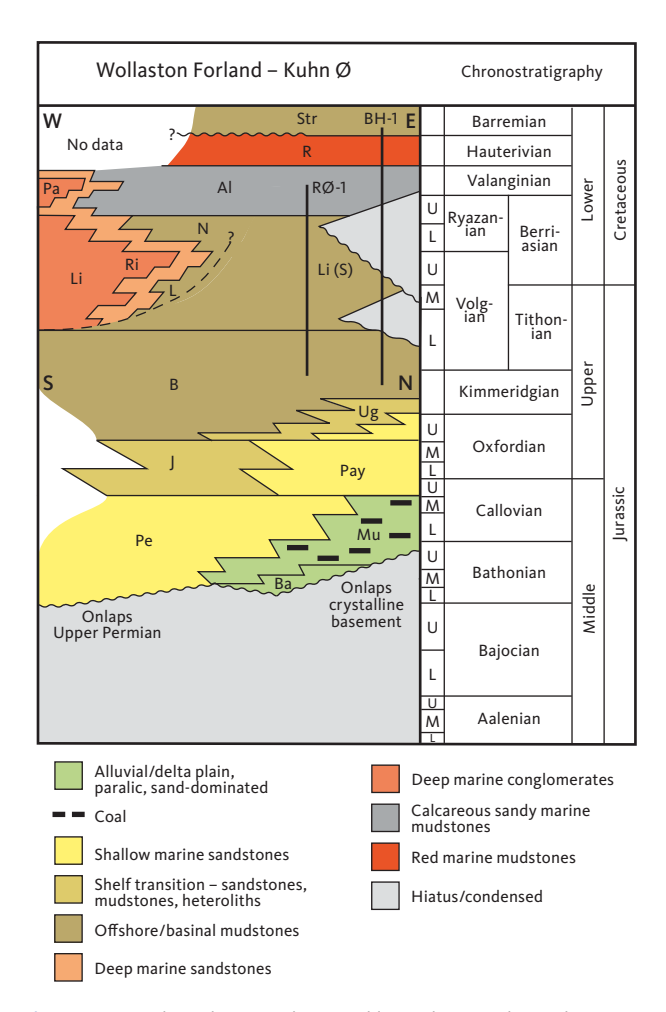


Fig. 2 Stratigraphic scheme with vertical lines showing the Rødryggen-1 (RØ-1) and Brorson Halvø-1 (BH-1) cored successions. Al: Albrechts Bugt Mb. B: Bernbjerg Fm. Ba: Bastians Dal Fm. J: Jakobsstigen Fm. L: Laugeites Ravine Mb. Li: Lindemans Bugt Formation. Li (S): Lindemans Bugt Fm (Storsletten Mb). Mu: Muslingebjerg Fm. N: Niesen Mb. Pa: Palnatokes Bjerg Fm (Young Sund Mb). Pay: Payer Dal Fm. Pe: Pelion Fm. R: Rødryggen Mb. Ri: Rigi Mb. Str: Stratumbjerg Fm. Ug: Ugpik Ravine Mb. Modified from Bojesen-Koefoed et al. 2023a, this volume).

Bay Supergroup of Neoproterozoic age and sediments of Neoproterozoic to Silurian age (Kalsbeek *et al.* 2000, 2008b; Watt *et al.* 2000; Thrane 2002; Higgins *et al.* 2004).

Caledonian metamorphism, migmatization and granite intrusion took place in Ordovician to Silurian times, and the crustal thickening resulted in continental sedimentation during the Devonian, followed by post-Caledonian terrestrial and marine sedimentation in the Carboniferous to Palaeogene (Stemmerik *et al.* 1992; Kalsbeek *et al.* 2001; Gilotti *et al.* 2008; Larsen *et al.* 2008). Late Triassic – Middle Jurassic thermal subsidence in the sedimentary basins was followed by Middle Jurassic rifting that was succeeded by transgression in the Late Jurassic and then renewed rifting, which culminated in the latest Jurassic – earliest Cretaceous (Surlyk 2003).

The Wollaston Forland peninsula provides one of the most complete stratigraphic records of the Jurassic and Early Cretaceous in North-East Greenland (Fig. 1). The cored section covers the Kimmeridgian to lower Barremian interval,

which is divided into four formations: (1) the Bernbjerg Formation, (2) the Lindemans Bugt Formation (Storsletten Member), (3) the Palnatokes Bjerg Formation (Albrechts Bugt and Rødryggen Members) and (4) the Stratumbjerg Formation (Fig. 2). The Bernbjerg Formation spans the late Oxfordian to the early Volgian and forms an up to 500-600 m thick black mudstone - shale succession that accumulated in a tectonically-affected shelf setting (e.g. Surlyk et al. 2021). Rifting intensified during the Volgian, fragmenting the basin into a series of narrow, 10-30 km wide, westward tilted, fjord-like half-grabens. Major conglomeratic submarine fan-delta systems (Lindemans Bugt Formation, Rigi Member) developed in the most proximal fault block reaching a maximum thickness of 2 km (Surlyk 1978; Henstra et al. 2016). The coeval palaeoenvironmental development in more distal fault blocks has remained poorly understood due to lack of outcrops but is well-recorded in the studied cores. The new data indicate deep basinal sedimentation (distal part of Lindemans Bugt Formation) and detachment of the Permpas-Hühnerbjerg Blocks (in which the studied boreholes are located) from the coastal deltaic systems (Hovikoski et al. 2023a (this volume), b).

The rift climax lasted until the Valanginian and was followed by waning rift activity and transgression in the western part of the study area (Surlyk 1978, 1984, 1990, 2003). An up to 600 m thick succession of gravity-flow deposits with conglomerates and sandstones (Palnatokes Bjerg Formation, Young Sund Member) accumulated in the proximal fault block, whereas fossiliferous mudstones (Albrechts Bugt and Rødryggen Members) were deposited in basinal areas and on submarine block crests (Surlyk 1978, 1984, 2003; Surlyk & Korstgård 2013; Hovikoski et al. 2018). The Rødryggen-1 and Brorson Halvø-1 cores penetrate both mudstone members. New biostratigraphic data (Nøhr-Hansen et al. 2020; Alsen et al. 2023, this volume) suggest a Valanginian to Hauterivian age for these deposits. Towards the east, fault activity continued until the Barremian and led to the deposition of the coarse-grained Falskebugt Member (Piasecki et al. 2020). During the late Hauterivian, deposits of the Palnatokes Bjerg Formation were drowned and succeeded by sub-storm wave-base bioturbated mudstones of the Stratumbjerg Formation (Bjerager et al. 2020). A several metres thick upper Hauterivian to lower Barremian interval of the lowermost Stratumbjerg Formation is recorded at the top of the Brorson Halvø-1 core (Alsen et al. 2023, this volume) and younger parts of the formation of Barremian to Albian age are present in outcrops near the drill site (Piasecki et al. 2020).

# 3. Methodology

# 3.1 Petrography

The petrographic and mineralogical characteristics of cemented and laminated mudstones in the

Rødryggen-1 and Brorson Halvø-1 cores were studied by transmitted and reflected light microscopy as well as by scanning electron microscopy (SEM). Samples of fracture fillings and sandy intervals were also examined. Polished thin sections were prepared from selected intervals in the cores representing diagenetic features characteristic of the different types of lithologies. The thin sections were impregnated with blue epoxy to ease identification of open pore space. Half of each thin section was etched and stained with sodium cobaltinitrite to facilitate K-feldspar identification. The SEM analyses were performed at the Geological Survey of Denmark and Greenland (GEUS) using a Philips XL40 SEM equipped with a ThermoNoran Energy Dispersive X-ray spectrometry (EDS) detector that was used to analyse the chemistry. Selected samples were studied with a backscattered electron (BSE) detector on carbon-coated thin sections and with a secondary electron (SE) detector on gold-coated rock chips. The mineralogy of each type of lithology present in the Rødryggen-1 and Brorson Halvø-1 cores was analysed by X-ray diffraction (XRD) at the University of Copenhagen, Denmark, and GEUS. The edge of the core was removed to avoid contamination. The bulk mineralogy was measured on a Bruker Advance D8 diffractometer with a Lynx-Eye detector using samples crushed to <63 µm applying the Bragg-Brentano method. Semi-quantification of the bulk mineralogy was obtained by the Rietveld method (Rietveld 1969; McCusker et al. 1999). The clay fraction analysis was carried out on a Philips 1050 goniometer with fixed divergence, anti-scatter slits and Co-Ka radiation (pulse high selection and Fe-filter). Chemical pre-treatment with NaOCl at pH 9.0 was used to remove organic matter. The samples were dispersed ultrasonically in distilled water to acquire the clay fraction (<2  $\mu$ m). The >30  $\mu$ m fraction was removed by density separation and the intermediate fraction by centrifugation in a centrifugal particle size analyser (Slater & Cohen 1962). The suspensions were flocculated in 1 M NaCl, and excess salt was removed by centrifugation and washing with water and ethanol. Three orientated specimens were made for each sample by the pipette method, comprising Mg-saturated air-dry, Mg-saturated with glycerol, and K-saturated air-dry heated at 300°C for 1 h. An X-ray diffractogram was produced for each of the saturated specimens on which the discrete minerals were identified from peak positions (Hillier 2000) and semi-quantified by application of correction factors.

### 3.2 Zircon U-Pb geochronology

The Rødryggen-1 and Brorson Halvø-1 cores did not contain sufficiently coarse material to apply detrital

zircon U-Pb age dating methods. Instead, outcrop samples collected from three locations east of the Rødryggen-1 drill site and a location situated north-east of the Brorson Halvø-1 drill site were used for the provenance analysis (Fig. 1). The samples collected near the Rødryggen-1 drill site consist of silty sandstone to sandy siltstone belonging to the Bernbjerg Formation, corresponding to the lower part of the cored succession. The sandstone sampled near the Brorson Halvø-1 drill site belongs to the Albian part of the Stratumbjerg Formation, so it is younger than the part of the formation encountered in the Brorson Halvø-1 core. The detrital zircon U-Pb age analyses were performed by laser ablation inductively coupled plasma mass spectroscopy (LA-ICP-MS) at GEUS. Samples were crushed and sieved to retrieve the grain-size fraction <500 µm. A water-shaking Wilfley table was used to obtain heavy mineral concentrates. Zircon grains were hand-picked in a random way to ensure that a range of grain sizes, shapes and colours were included. The polished epoxy mount with the zircon grains was cleaned in an ultrasonic bath with propanol and loaded into the sample cell of the laser ablation system for radiometric age dating. The data were acquired with a single spot analysis on individual zircon grains. A beam diameter of 30 µm and a crater depth of c. 15-20 µm were used. The amount of ablated material was c. 200-300 ng for the ablation time of 30 sec. The ablated material was analysed on an Element2 (Thermo Finnigan) single-collector, double focusing, magnetic sector-field, inductively coupled plasma mass spectrometer with a fast-field regulator for increased scanning speed. The total acquisition time was 60 sec for each analysis, of which the first 30 sec were used to measure the gas blank. The instrument was tuned to give large, stable signals for the 206Pb and 238U peaks, low background count rates (typically around 150 counts per second for <sup>207</sup>Pb) and low oxide production rates (238U16O/238U generally below 2.5%). 202Hg, <sup>204</sup>(Pb+Hg), <sup>206</sup>Pb, <sup>207</sup>Pb, <sup>208</sup>Pb, <sup>232</sup>Th and <sup>238</sup>U intensities were determined through peak jumping using electrostatic scanning in low resolution mode and with the magnet resting at 202Hg. Mass 202Hg was measured to monitor the 204Hg interference on 204Pb where the  $^{202}$ Hg/ $^{204}$ Hg  $\equiv$  4.36, which can be used to correct significant common Pb contributions using the model Pb composition of Stacey & Kramers (1975).

Standard-sample bracketing using the GJ-1 zircon (Jackson *et al.* 2004) was used to correct the elemental fractionation induced by the laser ablation and the instrumental mass bias on measured isotopic ratios. Long-term external reproducibility was monitored by repeated analyses of the Plešovice zircon standard (Sláma *et al.* 2008). The reported ages are based on

<sup>207</sup>Pb/<sup>206</sup>Pb derived ages for the >0.8 Ga (billion years) analyses and <sup>206</sup>Pb/<sup>238</sup>U ages for the <0.8 Ga analyses, since the latter is more precise for the younger age range, and a natural gap between age populations exists. The propagation of the analytical errors follows the principles of Sambridge & Lambert (1997). Age measurements were discarded if they lacked a stable <sup>207</sup>Pb/<sup>206</sup>Pb plateau or for U/Pb or Pb/Pb error >10%. A correction for common Pb was applied on a small fraction (≤7%) of the concordant analyses from each sample. The data are plotted using kernel density estimation (Vermeesch 2012) employing analyses with <10% discordance. The analytical data are reported in Supplementary File S1.

# 4. Results

# 4.1 Lithology

The studied succession was deposited during a protracted rifting episode that is differentiated into four discrete rift phases: (1) early rifting during the Kimmeridgian part of the Bernbjerg Formation, (2) rift acceleration during the Volgian part of the Bernbjerg Formation, (3) rift climax during deposition of the Lindemans Bugt Formation and (4) waning rifting during deposition of the Palnatokes Bjerg Formation (Figs 3 and 4; Surlyk 1978, 2003). These major rift phases resulted in significant shifts in depositional conditions that are reflected in the lithological characteristics observed in the different stratigraphic units in the Rødryggen-1 and Brorson Halvø-1 cores.

In the cored sections, the Bernbjerg Formation comprises dark grey mudstones with interlaminated coarse siltstones to very fine sandstones in some intervals (Fig. 5A). The Lindemans Bugt Formation consists of dark grey clayey mudstones (Fig. 5C) with a larger content of fossils and pyrite than in the Bernbjerg Formation. The Albrechts Bugt Member of the Palnatokes Bjerg Formation comprises light grey mudstones (Fig. 5D) that differ from the Lindemans Bugt Formation in being more calcareous, sandy and bioturbated. The Rødryggen Member of the Palnatokes Bjerg Formation consists of red hematitic mudstones with intercalated sandy mudstones (Fig. 5E). The Stratumbjerg Formation contains bioturbated grey mudstones (Fig. 5F). The sedimentological characteristics are described in more detail by Hovikoski et al. (2023a, this volume).

Carbonate-cemented intervals occur in all the stratigraphic units and are characterised by lower gamma-ray values (Figs 3, 4) and lighter colours (Fig. 5B). The lighter colours are also evident in the microscopic appearance of the cemented mudstones due to the lower clay mineral content as compared to the uncemented mudstones (Figs 6A, 6B). Pyrite is evident in many core intervals as well as various macrofossils, deformation structures, faults and fractures (Figs 3 and 4).

# 4.2 Detrital components

The mineralogy of the Rødryggen-1 and Brorson Halvø-1 cores based on XRD analyses is presented in Figs 3 and 4 for the 27 analysed mudstones and two samples of cemented fractures. Quartz is the most abundant mineral amounting to 12-48 wt% with an average of 29 wt%, which is present as silt- and sand-sized grains in the mudstones (Fig. 6C). K-feldspar and plagioclase/albite occurs in amounts of up to 11 and 18 wt%, respectively, and each of them are present as 6 wt% on average. Petrographic analysis of the K-feldspar grains reveals that they are generally well-preserved, whereas the plagioclase and albite grains are often partially dissolved (Fig. 6D). Apatite is found as detrital clasts (Fig. 6E) in amounts of 4 wt% on average with the highest contents up to 16 wt% occurring in a condensed interval in the lower part of Lindemans Bugt Formation in the Rødryggen-1 core.

Calcite is present as detrital clasts, including bioclasts in the Palnatokes Bjerg Formation, in both the Albrechts Bugt and Rødryggen Members. The Bernbjerg and Lindemans Bugt Formations are rich in organic matter including some coal fragments. Detrital heavy minerals are found in accessory amounts and comprise primarily ilmenite, leucoxene, rutile, magnetite, zircon and garnet in the form of almandine. Muscovite could not be differentiated from illite by XRD but was observed in thin section. The mica minerals primarily consist of muscovite with subordinate biotite. The micas are generally aligned parallel to the lamination and are often cleaved into thin sheets and bend around less ductile grains (Fig. 6C).

Most of the clay minerals are detrital as testified by the absence of growth structures and by their tangential orientation around the other detrital minerals (Fig. 6F). Kaolinite is present in the matrix of all the mudstones and occurs in higher amounts in the Rødryggen-1 core than in the Brorson Halvø-1 core (Figs 3, 4). Kaolinite is found in amounts up to 17 wt% with an average of 10 wt%. Mixed-layer illite-smectite is found in amounts of 7 wt% on average with the highest contents occurring in the Brorson Halvø-1 core and especially in the sample from the Stratumbjerg Formation where it constitutes 28 wt%. Illite occurs with an average of 13 wt% and is more abundant overall in the Brorson Halvø-1 core than in the Rødryggen-1 core. The smallest illite contents within each well occur in the Palnatokes Bjerg Formation and the highest contents of up to 25 wt% are present in the Bernbjerg Formation. Some of the illite is authigenic as evident by its morphology, but the proportion of detrital to authigenic illite cannot be quantified.

Chlorite is found in all samples from the Brorson Halvø-1 core (Fig. 6F), except the two deepest samples from the Bernbjerg Formation, and its content increases

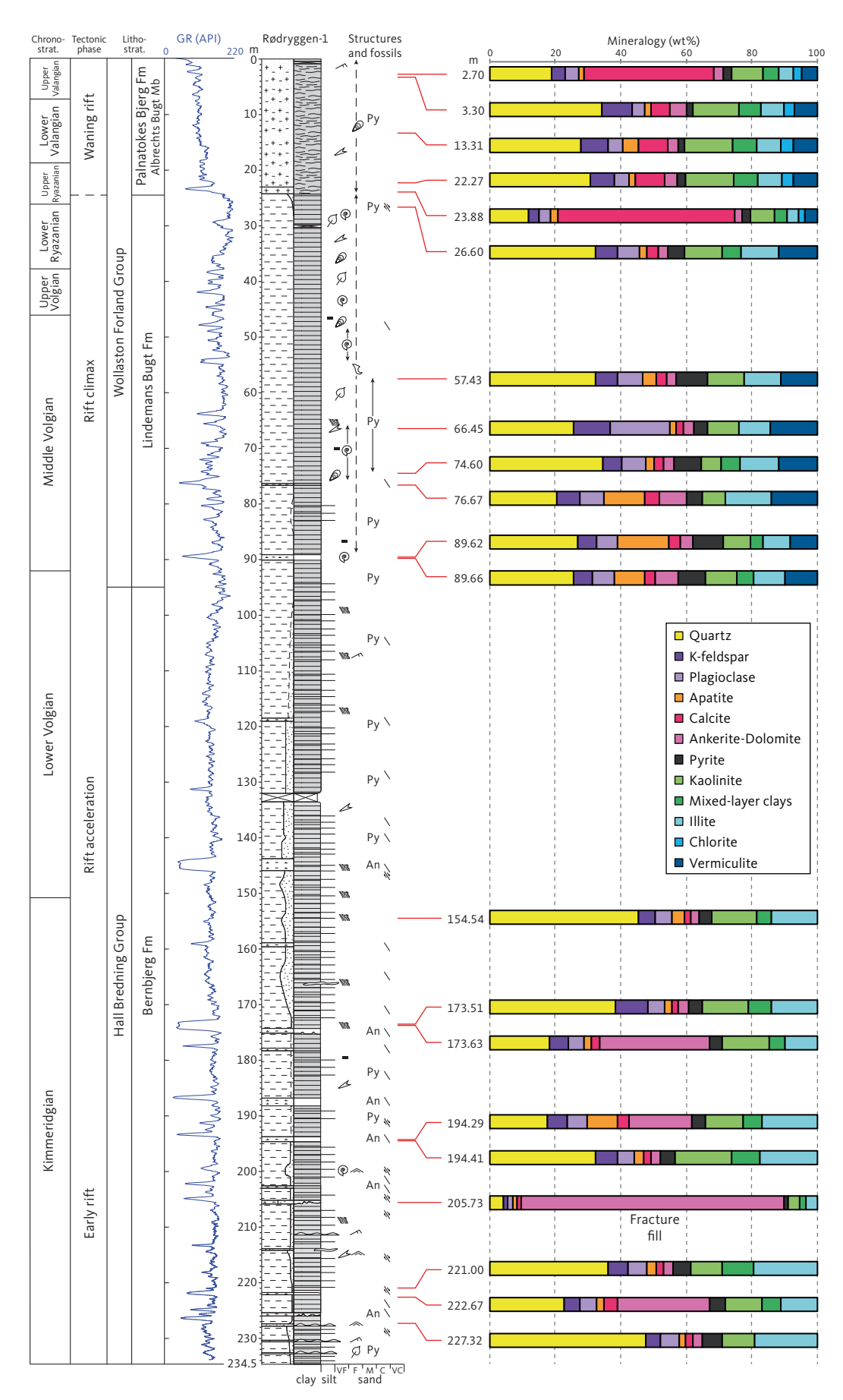


**Fig. 3** Mineralogy from XRD of the Rødryggen-1 core plotted with the sedimentological log. Chronostratigraphy from Alsen *et al.* (2023, this volume). See Fig. 4 for legend. **Chronostrat.**: chronostratigraphy. **Lithostrat.**: lithstratigraphy. **GR**: gamma ray. **API**: American Petroleum Units.

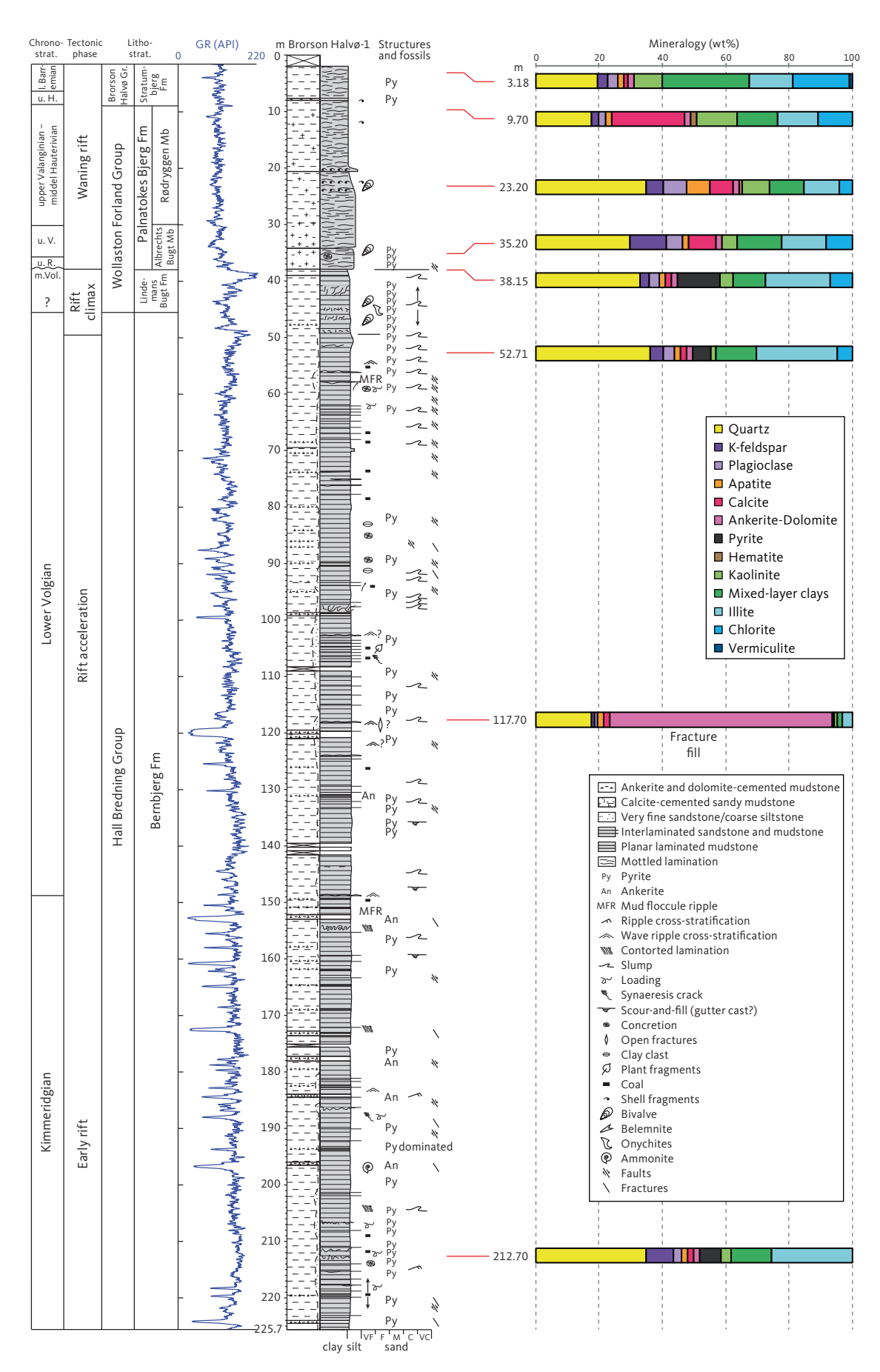


Fig. 4 Mineralogy from XRD of the Brorson Halvø-1 core shown alongside the sedimentological log. Chronostratigraphy from Alsen *et al.* (2023, this volume). **Chronostrat.**: chronostratigraphy. **Lithostrat.**: lithstratigraphy. **GR**: gamma ray. **API**: American Petroleum Units.

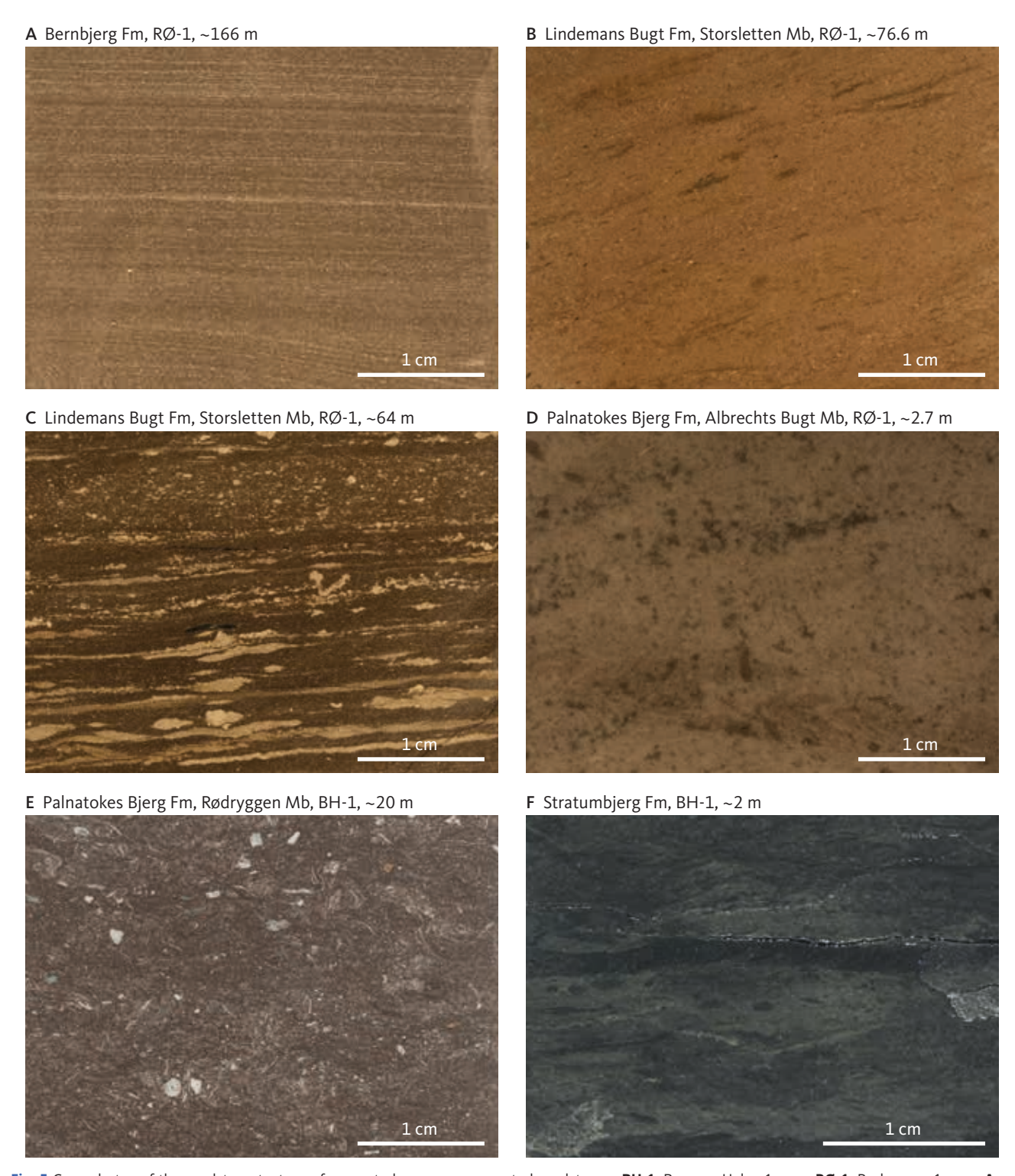


Fig. 5 Core photos of the mudstone texture of cemented versus uncemented mudstones. **BH-1**: Brorson Halvø-1 core. **RØ-1**: Rødryggen-1 core. **A**: Laminated sandy mudstone. **B**: Cemented mudstone. **C**: Laminated pyritic mudstone. **D**: Bioturbated mudstone. **E**: Bioclastic hematitic cemented mudstone. **F**: Bioturbated mudstone.

upwards with the highest amount of 18 wt% occurring in the Stratumbjerg Formation (Figs 3, 4). In the Rødryggen-1 core, chlorite is only present in the Palnatokes Bjerg Formation where it occurs in amounts of 2–4 wt%. Vermiculite is not present in the mudstones from the Brorson Halvø-1 core except for a small content (1 wt%) in the Stratumbjerg Formation. In the Rødryggen-1 core,

vermiculite is present in all samples from the Lindemans Bugt and Palnatokes Bjerg Formations in contents of 4–14 wt%, whereas it is absent in the Bernbjerg Formation.

# 4.3 Authigenic minerals

Pyrite is on average 5 wt% and it was the first mineral that precipitated in the sediments. Pyrite is present

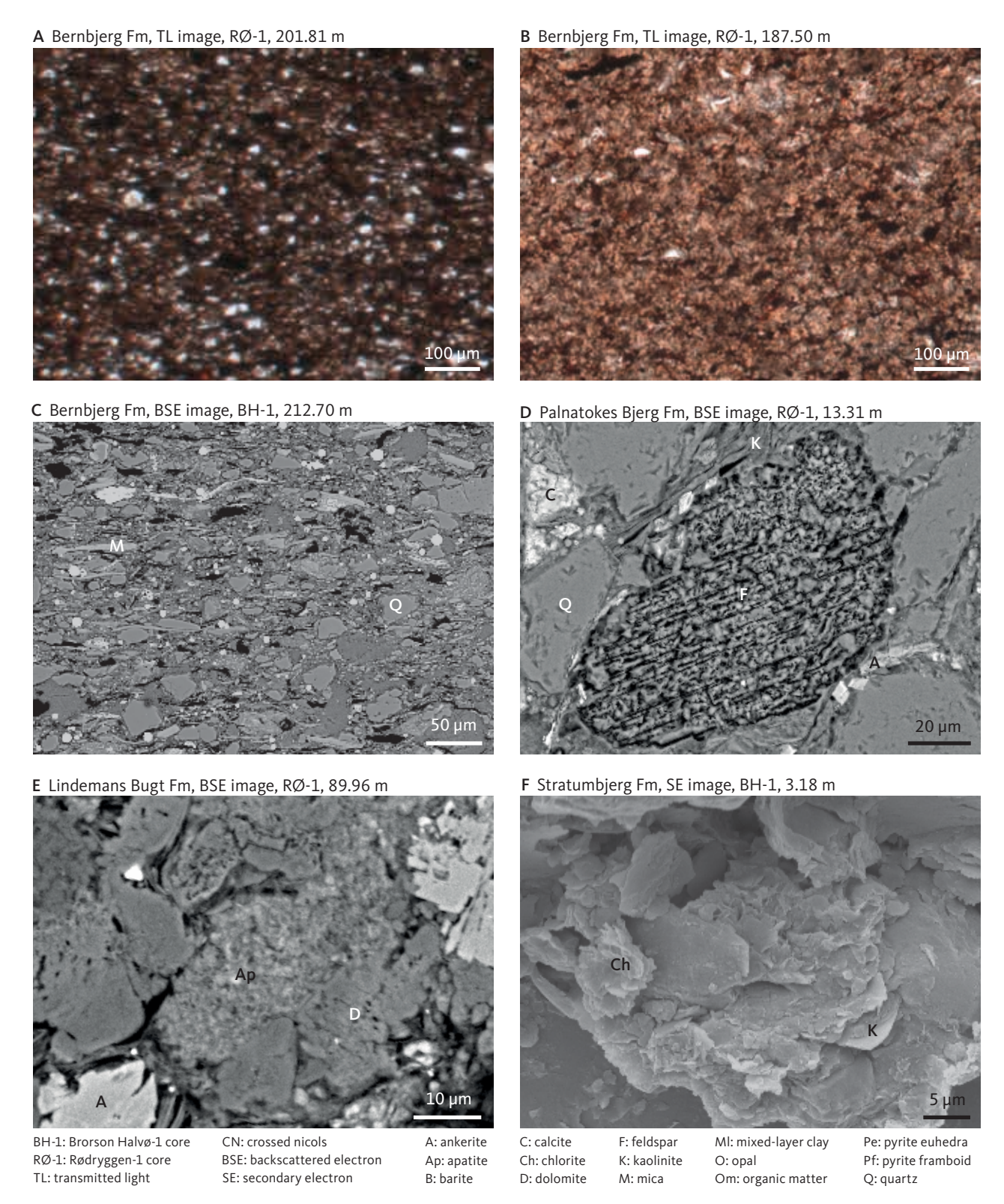
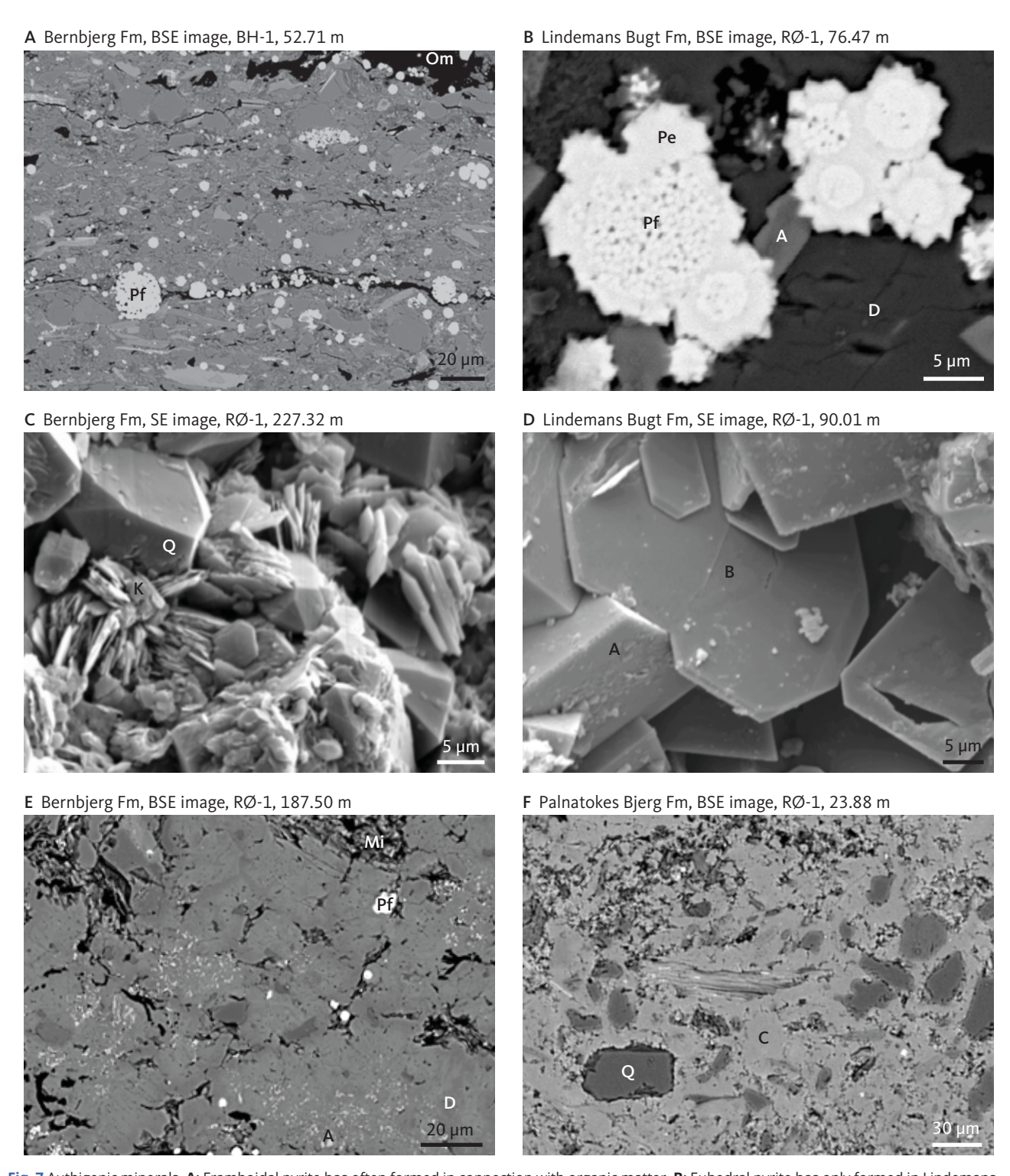


Fig. 6 Texture and detrital phases. A: Typical mudstone texture. B: Cemented mudstone texture. C: Quartz occurs as silt- and sand-sized grains in the mudstones. D: Partially dissolved albite grain. E: Apatite occurs as detrital clasts. F: Most clay minerals are detrital such as chlorite.

in all formations except some parts of the Stratumbjerg and Palnatokes Bjerg Formations in the Brorson Halvø-1 core (Figs 3, 4). It is often found in association with organic matter (Fig. 7A). The highest amounts (4–14 wt%) are found in the Lindemans Bugt Formation where the pyrite framboids are often overgrown by euhedral pyrite (Fig. 7B). Only framboidal pyrite is present in the remaining formations where it constitutes 4–7 wt% in the Bernbjerg Formation and 0–3 wt% in the Palnatokes Bjerg Formation.

Although the kaolinite crystals have euhedral shapes, they are likely to have been transported before



**Fig. 7** Authigenic minerals. **A**: Framboidal pyrite has often formed in connection with organic matter. **B**: Euhedral pyrite has only formed in Lindemans Bugt Formation where it has overgrown pyrite framboids. **C**: Quartz has overgrown detrital kaolinite. **D**: Barite has overgrown ankerite rhombs. **E**: Dolomite is the dominant carbonate cement in Bernbjerg and Lindemans Bugt Formations. **F**: Calcite is the dominant carbonate cement in Palnatokes Bjerg Formation. See Fig. 6 for abbreviations.

deposition since they do not occur in well-defined booklets (Fig. 7C). However, some detrital grains have been kaolinised, including some of the muscovite and feldspar grains, which must have happened within the sediment since they would have disintegrated during transport. It is often difficult to distinguish unambiguously between the detrital and authigenic clay minerals,

but the morphology of the mixed-layer illite-smectite and illite indicate that part of it is authigenic. Fibrous and hairy illite was observed using SEM. Thin quartz overgrowths have mainly precipitated in the coarser-grained intervals (Fig. 7C) and overgrow pyrite and kaolinite. Barite has precipitated in some of the mudstones where it formed as the last authigenic phase.

It occurs as string-like precipitations and as euhedral crystals overgrowing ankerite (Fig. 7D). Barite was identified by EDS but has formed in such small amounts that it could not be estimated by XRD analysis.

Pervasive carbonate cementation of the mudstones is found in some intervals of all the studied formations, and these intervals are characterised by low gamma-ray values in the natural gamma log (Figs 3, 4). High concentrations of bioclasts or micrite are present in the carbonate-cemented intervals, except for those with siderite. Dolomite is the dominant carbonate mineral in the Bernbjerg and Lindemans Bugt Formations, whereas calcite is dominant in the Palnatokes Bjerg Formation and siderite is dominant in the Stratumbjerg Formation.

Dolomite and ankerite could not be clearly discriminated by XRD so they have been grouped as ankeritedolomite in the XRD results (Figs 3, 4). However, both minerals are present since they were identified by EDS. They are found in all formations with the highest abundance in the Bernbjerg Formation (maximum 34 wt%) followed by Lindemans Bugt Formation (maximum 8 wt%). Poikilotopic dolomite occurs in highest abundance, whereas ankerite occurs mostly as smaller rhombs (Fig. 7E). Ankerite is often precipitated between exfoliated mica flakes. An outwards increase in Fe content is observed in both the dolomite and ankerite crystals.

Calcite occurs in amounts of 2–4 wt% in the samples from the Bernbjerg and Lindemans Bugt Formations, reaching 6–54 wt% in the Palnatokes Bjerg Formation comprising both detrital and authigenic calcite that is poikilotopic and micritic (Fig. 7F). A calcite content of 1 wt% is found in the sample from the Stratumbjerg Formation. This sample does not contain siderite, but it is present in other samples from this stratigraphic unit where it has precipitated as an early phase.

# 4.4 Bioclasts

The Bernbjerg and Lindemans Bugt Formations contain numerous calpionellids that are most abundant in the cemented mudstones. The calpionellids and other shell material in the Bernbjerg and Lindemans Bugt Formations are recrystallised, but moulds of molluscs and ammonites have been found (Alsen et al. 2023). Calpionellids are calcareous microfossils of uncertain affinity. They have oblong shells which have been filled with either dolomite or micritic calcite and often also ankerite and pyrite (Fig. 8A). Pyrite precipitated mostly along shell rims though sometimes filling most of the internal cavity. Ankerite formed small euhedral crystals, most of which precipitated on the exterior of the bioclasts. Poikilotopic dolomite crystals precipitated in most of the remaining cavity, but some porosity is often preserved (Fig. 8B).

Fossils in the Palnatokes Bjerg Formation include ostracods, brachiopods, foraminifera and inoceramid bivalves (Alsen *et al.* 2023). The formation contains abundant calcispheres, especially in the cemented intervals. They have not been recrystallised as seen by the characteristic test (Fig. 8C) and by the extinction pattern following the growth structure in other fossils. These calcispheres are probably calcareous dinoflagellate cysts and have a spherical test. Calcite has precipitated in the interior, and small ankerite crystals have sometimes formed within the calcite (Fig. 8D).

#### 4.5 Fractures

Small fractures are present in most of the core and are most evident in the cemented intervals where they cut through the carbonate-cemented fabrics. Opal has often formed along the rims of the fractures where it radiates in multiple layers and forming spherical layers around a protruding matrix (Fig. 8E). The remaining parts of the fractures are filled with dolomite in which the Fe content decreases towards the middle of the fractures (Fig. 8F). The dolomite has occasionally replaced some of the opal along its outer rim (Fig. 8E).

XRD analyses have been made of fracture fills comprising one sample selected from each well in the Bernbjerg Formation where fractures are most abundant, and show that dolomite is the dominant fracture-filling cement (Figs 3, 4). Fracturing has happened several times as seen by the cross-cutting relationships of the fracture generations, where each of them became cemented prior to the next generation of successively wider fractures. The largest encountered fractures are up to a few centimetres wide. The last generation of fractures were not filled by any minerals and thus increased the porosity and permeability.

# 4.6 Zircon U-Pb ages

The detrital zircon U-Pb ages of the four outcrop samples from Wollaston Forland (Fig. 1) cover a broad Mesoarchaean to Palaeozoic age span (Fig. 9). The discordant ages (comprising 21–28%) are not plotted but included in Supplementary File S1. The three samples from the Bernbjerg Formation (samples 1–3, Fig. 9) all contain a pronounced Archaean zircon age population with peak ages at 2.75–2.65 Ga (comprising 7–10% in each sample), whereas only a single Archaean zircon grain was found in the sample from the Stratumbjerg Formation (sample 4, Fig. 9).

The dominant age populations of the samples are present within the 2.0–1.6 Ga interval (comprising 42–75% in each sample), although the relative proportions between the age populations vary. In the

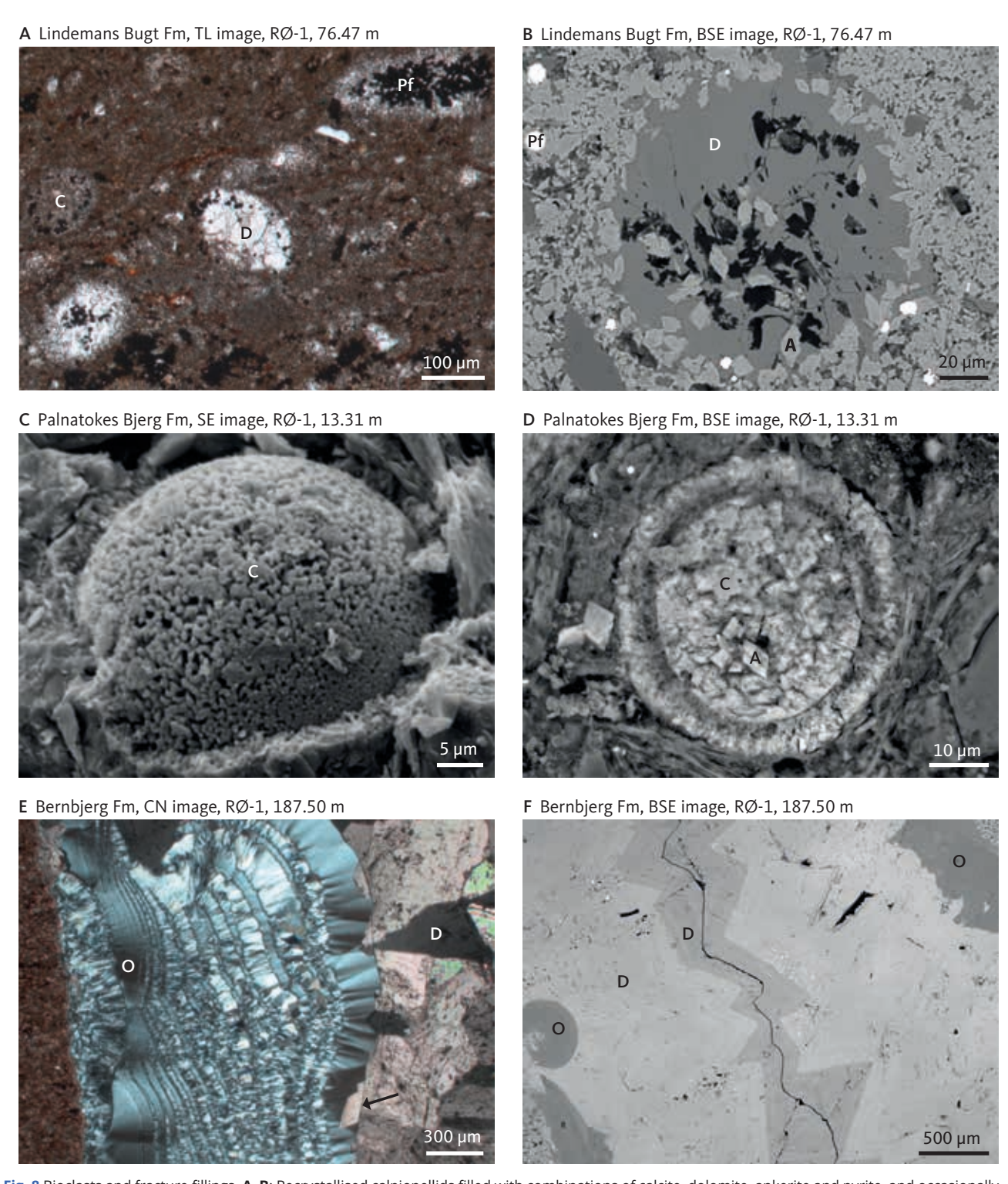
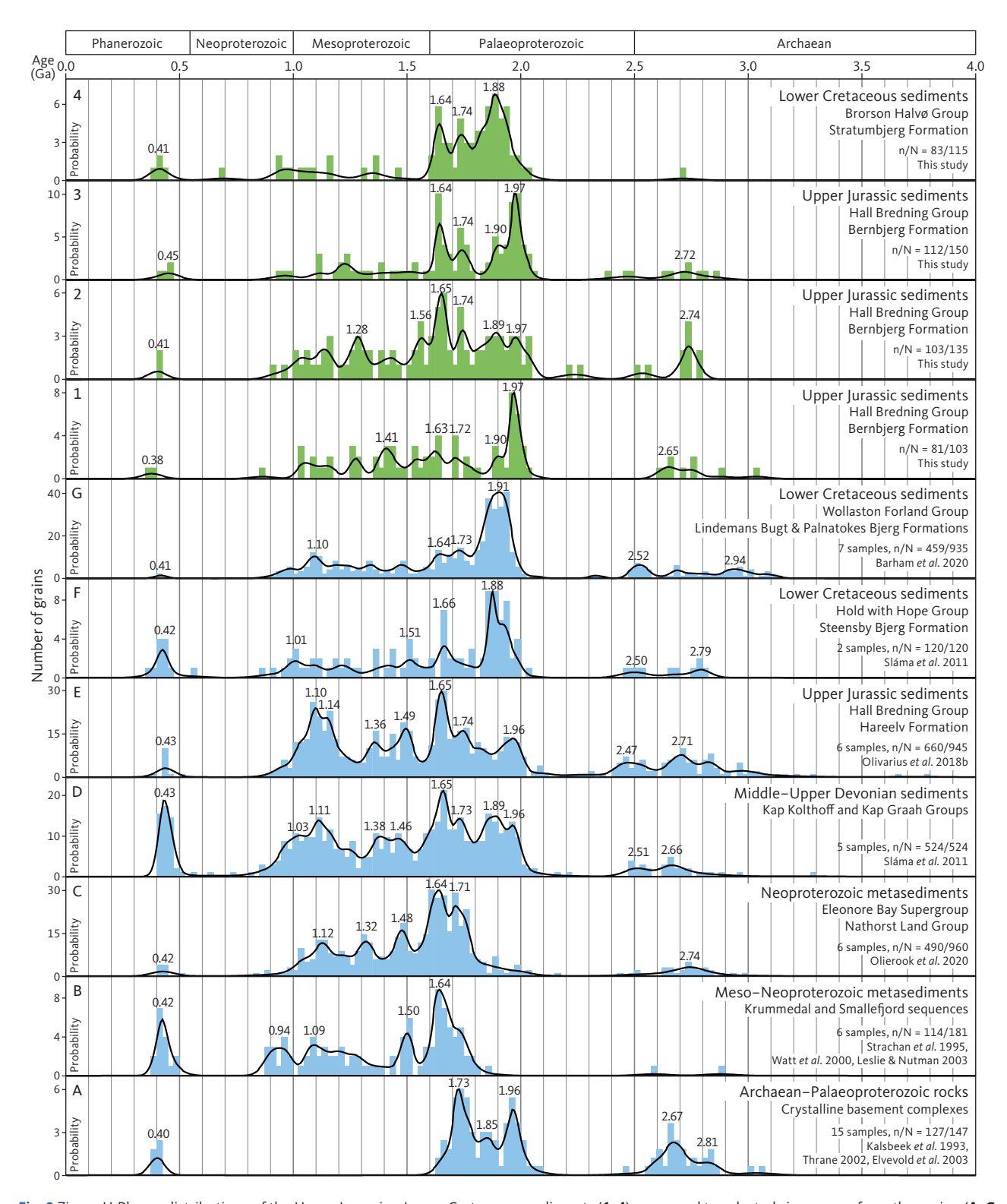


Fig. 8 Bioclasts and fracture fillings. **A-B**: Recrystallised calpionellids filled with combinations of calcite, dolomite, ankerite and pyrite, and occasionally with internal porosity. Calpionellids are present in Bernbjerg and Lindemans Bugt Formations. **C-D**: Well-preserved calcispheres filled with calcite and small ankerite rhombs. Calcispheres are present in Palnatokes Bjerg Formation. **E**: Opal precipitated in several zones in a fracture and succeeded by dolomite, which has replaced some opal along the contact (**arrow**). **F**: Opal along fracture rims and succeeded by dolomite with lower Fe content in the middle. Fractures are most abundant in Bernbjerg Formation. See Fig. 6 for abbreviations.

Bernbjerg Formation, an age population with peak age at 1.97 Ga is dominant in two of the samples (samples 1 and 3, comprising 23–24%) and evident in the third (sample 2, comprising 10%), but not in the sample from the Stratumbjerg Formation. The dominant age population in the Stratumbjerg Formation sample has peak

age at 1.88 Ga (sample 4, comprising 39%), and this population is less pronounced and slightly older in the Bernbjerg Formation samples. An age population with peak ages at 1.65–1.63 Ga is pronounced in the sample from Stratumbjerg Formation (sample 4, comprising 17%) and in two of the samples from the Bernbjerg



**Fig. 9** Zircon U-Pb age distributions of the Upper Jurassic – Lower Cretaceous sediments (**1-4**) compared to selected zircon ages from the region (**A-G**: Strachan *et al.* 1995; Watt *et al.* 2000; Thrane 2002; Elvevold *et al.* 2003; Kalsbeek *et al.* 1993; Leslie & Nutman 2003; Sláma *et al.* 2011; Olivarius *et al.* 2018b; Barham *et al.* 2020; Olierook *et al.* 2020). The Phanerozoic zircon ages in A-C are from the intruded Caledonian granites. The sampling locations are shown in Fig. 1. The ages are plotted using kernel density estimation (Vermeesch 2012) and histograms with a bin interval of 25 million years. Zircon ages with <10% discordancy are plotted. "**n/N**" denotes the number of concordant analyses out of the total number of analyses. See Fig. 1 for locations.

Formation (samples 2 and 3, both comprising 16%). A population with peak age of 1.74 Ga is slightly less prominent in the same three samples (comprising 9–14% in each sample), whereas both age populations

are less prominent in the last sample from the Bernbjerg Formation (sample 1; Fig. 9).

A wide range of Mesoproterozoic zircon ages are found in all four samples (comprising 11-38% in each

sample) with less pronounced age populations as compared to the Palaeoproterozoic populations. Few Neoproterozoic zircons are encountered (comprising 1–6% in each sample), and an age gap occurs at 0.9–0.5 Ga except for a few grains (Fig. 9). Small Palaeozoic age populations of 2–4 grains are found in all samples with peak ages varying between 0.45 and 0.38 Ga (comprising 2–5% in each sample). The oldest and youngest of these Ordovician–Devonian zircons, with ages of 474  $\pm$  14 Ma and 364  $\pm$  3 Ma, respectively, are both from the Bernbjerg Formation.

# 5. Discussion

# **5.1 Provenance analysis**

The Mesoarchaean to Palaeozoic zircon age populations found in the four analysed samples of Upper Jurassic - Lower Cretaceous sediments from Wollaston Forland are comparable (Fig. 9). The age distributions of the studied sediments are all characterised by a dominance of 2.0-1.6 Ga ages and by containing the full range of zircon ages within this time interval, although the relative proportion between the probabilities of the age populations varies. Therefore, the sediments presumably have the same overall provenance in which the proportion between the Palaeoproterozoic zircon ages varies. However, some of the differences in age distributions between the samples may possibly be the result of bias related to mineral separation with handpicking of grains for analysis (e.g. Sláma & Košler 2012; Dröllner et al. 2021). Selected zircon age data from the literature are plotted in Fig. 9 to facilitate comparison with possible sediment source rocks.

As in the studied sediments, zircon age populations with a dominance of 2.0-1.6 Ga ages occur in Lower Cretaceous and Lower Triassic sediments from northern Hold with Hope, c. 80 km south-south-west of the study area (Fig. 1; Fonneland et al. 2004; Sláma et al. 2011). These sediments also contain Archaean, Mesoproterozoic and Palaeozoic age populations with low probabilities, although the Palaeozoic peak age is more pronounced than in the studied sediments (Fig. 9). The age populations of Upper Jurassic sediments from southern Jameson Land c. 450 km south-south-west of the study area are similar overall to the studied sediments, but with significantly larger relative proportions of the Archaean and Mesoproterozoic age populations (Olivarius et al. 2018b). Lower Jurassic sediments from southern Jameson Land have a significantly different age distribution; they exhibit a limited number of peak ages reflecting their local provenance from the Liverpool Land High that was elevated at the time (Sláma et al. 2011).

The zircon age populations of Carboniferous and Devonian sediments along Kong Oscar Fjord and inner Kejser Franz Joseph Fjord (Moskusokse Fjord) are comparable to those in the studied sediments, except that the Mesoproterozoic and Palaeozoic populations are more prominent in these older sediments; furthermore, Archaean ages are more common in the Carboniferous sediments (Sláma et al. 2011). The Neoproterozoic Lyell Land Group and Nathorst Land Group of the Eleonore Bay Supergroup have age distributions that are distinctly different from each other (Watt et al. 2000; Dhuime et al. 2007; Sláma et al. 2011; Olierook et al. 2020). Late Mesoproterozoic zircons are dominant in the Lyell Land Group along inner Kong Oscar Fjord (Segelsellskapet Fjord) with subordinate early Mesoproterozoic zircons, so these sediments show poor resemblance to the studied Upper Jurassic - Lower Cretaceous sediments. The Nathorst Land Group is dominated by late Palaeoproterozoic age populations and additionally contains several Mesoproterozoic age populations in addition to a smaller Archaean population; a sample of the intruded granites is included in Fig. 9 to show their Palaeozoic age (Olierook et al. 2020). The metasediments of the Nathorst Land Group on Wollaston Forland are thus comparable to the studied sediments, except that the metasediments contain a higher proportion of Mesoproterozoic zircons and no significant age populations in the 2.0–1.8 Ga interval.

The Meso-Neoproterozoic metasediments of the Krummedal supracrustal sequence and Smallefjord sequence have dominant zircon age populations of late Palaeoproterozoic age and additionally contain Mesoproterozoic, early Neoproterozoic and Palaeozoic populations (Strachan et al. 1995; Watt et al. 2000; Leslie & Nutman 2003). Thus, they are lacking 2.0-1.8 Ga age populations but otherwise resemble the age distributions of the studied sediments rather well. Archaean and Palaeoproterozoic crystalline basement complexes of the East Greenland Caledonides have age populations of 2.9-2.5 and 2.0-1.7 Ga (Kalsbeek et al. 1993; Thrane 2002; Elvevold et al. 2003). These are comparable to the oldest age populations found in the studied sediments, although the proportion of Palaeoproterozoic ages relative to Archaean ages is higher in the sediments than in the basement complexes.

Comparison between the samples analysed in this study and other sediments and possible sediment sources is made by multivariate statistical analysis by multidimensional scaling (MDS) visualised in an MDS diagram (Fig. 10). Here, similarities between samples are highlighted by solid lines revealing their proximity in Kolmogorov-Smirnov space, whereas dashed lines show smaller similarities. The sediments from this study have largest similarities to other Upper Jurassic and

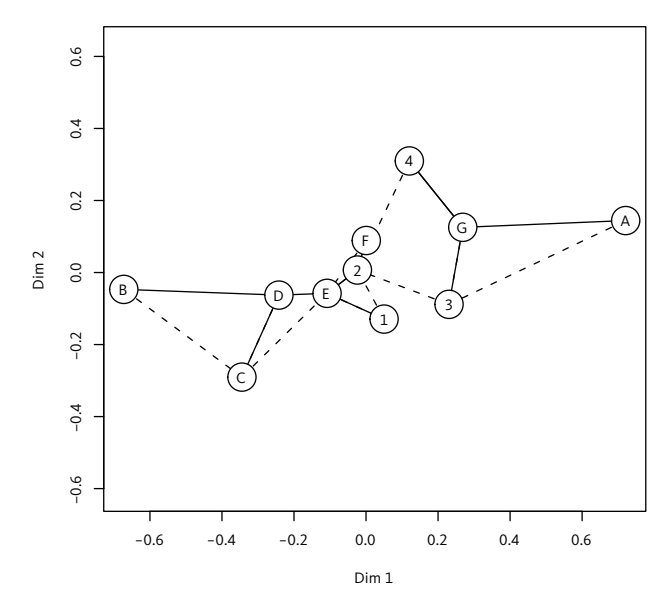


**Fig. 10** Multidimensional scaling (MDS) diagram of zircon U-Pb age data. Plotted using Kolmogorov-Smirnov (K-S) dissimilarity (Vermeesch *et al.* 2016). The nearest neighbours in K-S space are shown by solid lines and the second nearest by dashed lines. See Fig. 10 for sample information.

Lower Cretaceous sediments, though some of these are as far away as Jameson Land. The largest differences are found between the end members comprising the Archaean–Palaeoproterozoic rocks and the Meso–Neoproterozoic metasediments, indicating that a mixture of these is necessary to explain the range of ages encountered in the sediments.

# 5.2 Sediment transport

An overall north-south change in provenance in the upper Palaeozoic to Mesozoic succession in East Greenland is evident in the concentration of Palaeoproterozoic zircons in sediments on Wollaston Forland and Hold with Hope compared with sediments farther south, which contain a higher proportion of Mesoproterozoic zircons (Fig. 9). In particular, 2.0–1.8 Ga zircons are abundant in the central and northern parts of East Greenland in Triassic, Jurassic and Cretaceous sediments (Fonneland et al. 2004; Sláma et al. 2011; this study). This implies that there must be pronounced differences between either age or extent, or both, of the various sediment source rocks in the northern versus southern parts of the Caledonides. Factors such as zircon fertility, sediment routing, recycling and methodological bias may also affect the provenance signal (e.g. Dröllner et al. 2021).

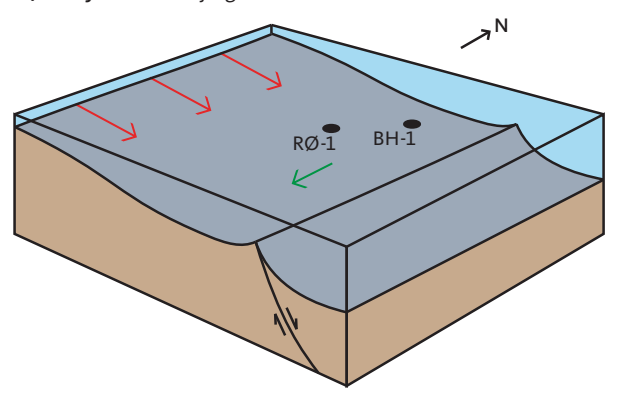
The primary source of the Upper Jurassic – Lower Cretaceous sediments on Wollaston Forland comprised the crystalline rocks of the East Greenland Caledonides or their derived sediments, or both. The Archaean and Palaeoproterozoic ages of the basement in Payer Land (Elvevold *et al.* 2003) match the oldest age populations of the studied sediments, so they may have been supplied

from the crystalline complexes present west of Wollaston Forland (Fig. 1). An additional sediment source is necessary to account for the late Palaeoproterozoic peak age of 1.65–1.63 Ga and the range of Mesoproterozoic ages present in the studied sediments (Fig. 9), so this input must originate from erosion of Meso-Neoproterozoic metasediments or Palaeozoic sediments, or both.

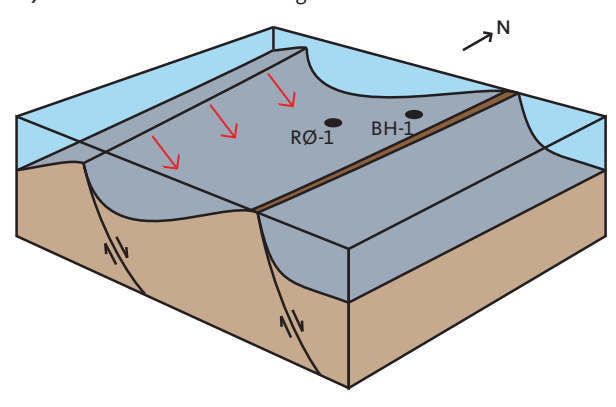
The peak zircon age of 1.66-1.63 Ga is evident and often dominant in the sediments and metasediments of the East Greenland Caledonides (Fig. 9), except for the Lyell Land Group in which the peak ages are restricted to 1.5 and 1.1 Ga (Sláma et al. 2011). Peak ages of 1.5 and 1.1 Ga are also present in the Krummedal supracrustal sequence, the Nathorst Land Group and younger sediments such as the Devonian and Carboniferous, but are not pronounced in the studied sediments. However, these peak ages are distinct in the Upper Jurassic sediments on Jameson Land that are age-equivalent to the Bernbjerg Formation (Fig. 9). This is due to the lower proportion of Mesoproterozoic zircon ages in the northern part of the East Greenland Caledonides and in the studied sediments, which makes the individual age populations in this interval less distinct. Some change in the drainage pattern must have occurred between the Kimmeridgian – early Volgian and the Albian, since the distinct Archaean and 1.97 Ga populations in the Bernbjerg Formation are not evident in the Stratumbjerg Formation where a 1.88 Ga population is dominant, as observed in Aptian sediments on northern Hold with Hope. Ages corresponding to these populations are present in different crystalline basement complexes (Fig. 9).

Zircon age distributions of the Bernbjerg, Lindemans Bugt, Palnatokes Bjerg and Stratumbjerg Formations from western Wollaston Forland are comparable to each other (Barham et al. 2020) and broadly comparable to the new results from northern Wollaston Forland (Fig. 9). However, the pronounced peak age of 1.97 Ga in the three samples from the Bernbjerg Formation in northern Wollaston Forland is not present in samples from the west. Likewise, Caledonian zircons are also virtually absent in the west in contrast to the northern part of Wollaston Forland. Thus, although much of the sediment on northern Wollaston Forland has been produced from reworking of sediment from western Wollaston Forland (Fig. 11), there must also have been an additional source that supplied sediment to the half-graben in which the Rødryggen-1 and Brorson Halvø-1 boreholes are situated. This additional sediment was probably supplied by axial transport from the north in accordance with the general depositional pattern in the Late Jurassic (Surlyk 2003). This is compatible with the abundance of Palaeoproterozoic basement to the north

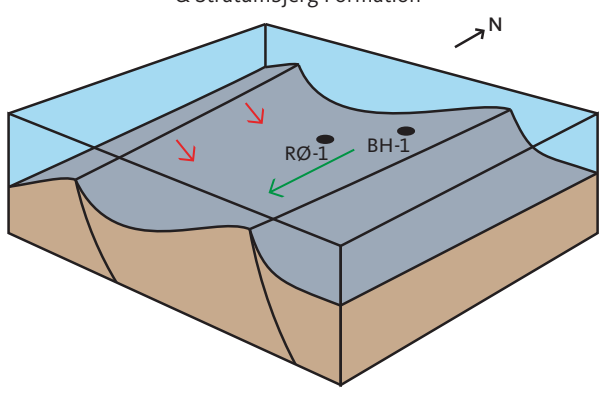
### A) Early rift: Bernbjerg Formation



B) Rift climax: Lindemans Bugt Formation



C) Waning rift: Palnatokes Bjerg Formation & Stratumbjerg Formation



7

Basinwards sediment transport



**Fig. 11** Inferred structural setting of northern Wollaston Forland in Late Jurassic to Early Cretaceous time when submarine deposition of mudstones took place during (**A**) early rifting, (**B**) rifting climax and (**C**) waning rifting in west (not waning in east, i.e. Falskebugt Member). Locations of the Rødryggen-1 (**RØ-1**) and Brorson Halvø-1 (**BH-1**) boreholes are shown as well as sediment transport directions.

and the presence of Caledonian granites in this area, though it is unknown if these granites were exposed in the Mesozoic.

Changes in sediment composition are also evident in the clay mineral composition where chlorite and

vermiculite were added upwards in the succession (Figs 3, 4). Another difference between the Bernbjerg Formation and the younger deposits is evident in the zircon age distributions from northern Wollaston Forland where the Stratumbjerg Formation lacks the Archaean and 1.97 Ga age populations that are present in the Bernbjerg Formation (Fig. 9). Thus, the rifting activity probably changed the erosional pattern resulting in altered sediment transport pathways. The kaolinite that is overgrown by authigenic quartz in the mudstones must comprise detrital kaolinite since they do not occur in well-defined booklets (Fig. 7C). The climate was humid subtropical at the time of deposition (Surlyk 2003), so kaolinite is the most likely clay mineral to have formed in the hinterland (Rateev et al. 2008), which explains its abundance in the mudstones. The presence of detrital kaolinite with preserved euhedral shapes points to a short transport distance from source area to place of deposition. This agrees with the interpreted proximity to the deltaic coast of North-East Greenland (Hovikoski et al. 2023b) with high mountains consisting of readily erodible material in the immediate hinterland (Henriksen & Higgins 2008).

# 5.3 Tectonic regime

Comparing the mineralogy of the carbonate-cemented mudstones with uncemented mudstones shows that the mudstones had similar initial mineralogical compositions, with the exception of the carbonate bioclasts, which represent the only additional component occurring in the cemented intervals (Figs 3, 4). Thus, in general, sediments with similar composition were supplied to the basin during deposition of the studied stratigraphic units, although the proportion between grains and clay minerals varies in relation to the grain size (Figs 3, 4). Other differences in the detrital mineralogy include the varying content of apatite clasts and the addition of vermiculite and chlorite to the clay mineral assemblages upwards in the succession. The variations in detrital mineralogy and grain size of the studied sediments are the results of (1) changing tectonic regime of the depositional setting that changed the sediment transport pathways and sea-bottom topography, and (2) rotational block faulting that caused increasing basin depth and sediment starvation up through the succession (Hovikoski et al. 2023a, this volume). Rifting also influenced the amount of deoxygenation and thereby the diagenetic evolution of the sediments as reflected in the varying amount of precipitated pyrite. The calcareous bioclast abundance is largest in transgressive intervals and in some condensed intervals as is also the case for apatite clasts.

The marine shelf setting of the Bernbjerg Formation with sediment supply from the deltaic coastline to the west (Fig. 11A) is reflected in the sandy component of the

mudstones with storm-wave influence in the lower part of the cored succession and in the presence of abundant silt and fine sand-sized quartz grains (Fig. 6C). Faulting intensified (Surlyk 2003), linked to the onset of coarse marine sedimentation proximally (Lindemans Bugt Formation). At the culmination of rotational block faulting, a fault was created west of the study area resulting in westwards tilting of the resulting basin (Fig. 11B; Hovikoski et al. 2023b). The submarine fault scarp west of this half-graben blocked sediment input from the mainland, but some sediment was supplied into the basin by gravity flows originating at the fault scarp. The fairly short distance to the fault scarp resulted in the input of some silt-sized detrital grains despite the relatively sediment-starved environment. Clasts of quartz, feldspar, mica and apatite (Fig. 6E) were supplied by mass flows in addition to the detrital clay minerals.

Vermiculite is absent in the Bernbjerg Formation in the Rødryggen-1 core but is found in all samples of the Lindemans Bugt and Palnatokes Bjerg Formations (Fig. 3). The cause of this change is not clear, but it may reflect the changed setting caused by block faulting whereby sediment supplied to the Rødryggen-1 drill site was sourced by the submarine fault scarp to the west during rift climax, and this input mixed with sediment supplied by axial transport during the waning rift phase (Fig. 11C). The high gamma-ray values of the Lindemans Bugt Formation in the Rødryggen-1 borehole (Fig. 3) are compatible with the fine-grained nature of the deposits in the centre of the half-graben where fine-crystalline vermiculite is dominant and coarse-crystalline kaolinite becomes less abundant, whereas the formation is only thinly preserved farther to the east in the Brorson Halvø-1 borehole (Fig. 4). Vermiculite does not occur in the succession in the Brorson Halvø-1 core, except for minor amounts in the uppermost sample from Stratumbjerg Formation. This is compatible with the larger distance to the submarine fault crest to the west that primarily fed vermiculite to the proximal part of the half-graben.

The Palnatokes Bjerg Formation is more sediment-starved than the Lindemans Bugt Formation due to transgression and waning of active rifting (Fig. 11C; Surlyk 2003). This is reflected in the high calcareous content suggestive of slow clastic deposition. The presence of occasional muddy sandstones, however, implies that gravity-flow processes were still operative. In the Brorson Halvø-1 core, chlorite occurs in the rift climax and waning rift samples, whereas it is only found in waning rift samples in the Rødryggen-1 core, and in smaller amounts (Figs 3, 4). This indicates that chlorite was supplied from the north-north-west by axial transport and deposited primarily in the distal part of the half-graben since the proximal part was mainly fed by the submarine

fault scarp to the west. The abundance of chlorite may have resulted from erosion of the Meso-Neoproterozoic metamorphic rocks north-west of Wollaston Forland that were exposed due to rift faulting, since chlorite often originates from such lithologies (Nielsen *et al.* 2015).

The provenance signature of the Stratumbjerg Formation near the Brorson Halvø-1 drill site is also indicative of a change in source area since the Archaean zircon age population is absent, in contrast to the Bernbjerg Formation (Fig. 9), which signifies a change in sediment source from the crystalline rocks to the west to the metamorphic and crystalline rocks to the north-west of the half-graben. This change is not evident in the zircon age distributions of the Palnatokes Bjerg and Lindemans Bugt Formations reported by Barham *et al.* (2020) because their samples were taken from localities within the proximal halfgraben that were linked directly to the coastline.

# 5.4 Diagenetic evolution

Textural relationships in sediments of the Rødryggen-1 and Brorson Halvø-1 cores have been used to determine the diagenetic sequence. A diagenetic process scheme is established to highlight the relative importance of each process (Fig. 12), as discussed next. The sedimentary succession in the cores has poor reservoir quality since the few sandstone intervals are thin and muddy. The reservoir properties are poorest in the intervals with pervasive carbonate cementation. The formation of secondary porosity by partial dissolution of bioclasts and feldspars and by fracture formation has only had a minor influence on the total porosity. The permeability is only slightly affected by the dissolution process since it was restricted to local clasts. The open fractures, however, have presumably increased the permeability significantly.

# 5.4.1 Eogenetic processes

Pyrite framboids precipitated early in the sediments in association with bacterial sulphate reduction of organic matter (Fig. 7A). The membrane of organic matter in shells probably promoted early pyrite formation within many of the bioclasts (Fig. 8A). Euhedral pyrite formed only during the rift climax, corresponding primarily to the Lindemans Bugt Formation where the largest amounts of pyrite are found (Figs 3, 4, 5C, 7B). The small euhedral crystals suggest syngenetic formation of pyrite indicating that the chemocline moved above the sediment-water interface and anoxic conditions may have prevailed during the rift climax phase (Tribovillard et al. 2006) or the crystals may have formed later diagenetically. Dysoxic conditions were dominant when the rifting was still at an initial stage during deposition of the Bernbjerg Formation, and when rifting was waning as seen by the increased bioturbation and low

| Diagenetic process | Sulphate<br>reduction                         | Bioclast<br>alteration       | Smectite<br>illitization | Carbonate<br>transformation | Fracture<br>formation  | Meteoric<br>water flushing  |  |
|--------------------|---|------------------------------|--------------------------|-----------------------------|--|-----------------------------|--|
| Diagenetic regime  | agenetic regime Eogenesis Eogen               |                              | Mesogenesis              | Mesogenesis                 | Telogenesis  | Telogenesis                 |  |
| Temperature        | depositional depositional                     |                              | >80°C                    | 80-100°C                    | <65°C  | <50°C                       |  |
| Dissolution        | organic matter,<br>Fe-minerals                | bioclasts,<br>carbonate ooze | smectite,<br>K-feldspar  | dolomite,<br>smectite       | feldspar,<br>mica  |                             |  |
| Precipitation      | <b>Precipitation</b> pyrite calcite, dolomite |                              | illite,<br>quartz        | ankerite,<br>barite         | opal,<br>dolomite  | kaolinite                   |  |
| Porosity           | Permeability decreased dec                    |                              | decreased                | decreased                   | increased<br>slightly  | increased<br>slightly       |  |
| Permeability       |   |                              | decreased                | decreased                   | increased  | decreased<br>slightly       |  |
| Requirements       | S from<br>seawater                            | Mg from<br>seawater          | detrital<br>smectite     | Ba from initial seawater    | source of<br>water   | supply of<br>meteoric water |  |
| Morphology         | PF<br>Pe-                                     | •                            |                          |                             | The state of the s |                             |  |

Fig. 12 Diagenetic process scheme of the authigenic changes that have occurred in the Rødryggen-1 and Brorson Halvø-1 successions. See Section 5.4 for explanation.

pyrite content of the Palnatokes Bjerg and Stratumbjerg Formations. During sulphidic bottom-water conditions, the reactivity and abundance of Fe minerals control the amount of pyrite that can form, whereas pyrite formation is controlled by the reactivity and abundance of organic matter during oxygenated bottom-water conditions (Berner 1985). Thus, the low amounts (0–1%) of total organic carbon (TOC) present in the Palnatokes Bjerg and Stratumbjerg Formations largely precluded pyrite precipitation, whereas higher TOC (2–6%) in the Bernbjerg and Lindemans Bugt Formations (Bojesen-Koefoed *et al.* 2023b, this volume) will have favoured this process.

The calcite and dolomite cements probably formed shortly after deposition. The sparry carbonate cement within calpionellids in Bernbjerg and Lindemans Bugt Formations must have formed early after deposition since the calpionellids have not been deformed by mechanical compaction (Fig. 8A, B). The presence of bioclasts is important for the precipitation of dolomite and ankerite (e.g. Hendry *et al.* 2000; Burns *et al.* 2005) since they act both as nucleation sites for the crystals and as a source of carbonate. The Palnatokes Bjerg Formation was sediment-starved so pelagic lime mud formed a significant component of the sediment that accumulated on the sea floor, and the pelagic carbonate resulted in micritic calcite matrix (Fig. 7F).

In the Bernbjerg and Lindemans Bugt Formations, the laminated mudstones signify reducing conditions during deposition as also reflected in the relatively

high content of organic matter. In the Palnatokes Bjerg Formation, the bioturbation intensity reveals more oxygenated depositional conditions, and many of the bioclasts were preserved in this formation (Figs 8C, D). Partial dissolution of calpionellids and other bioclasts in the Bernbjerg and Lindemans Bugt Formations resulted in carbonate-cemented layers with a large bioclast content, caused by a primary heterogeneity (Fig. 7E). These layers possibly represent bioclast concentrations produced by reworking at discrete flooding surfaces (e.g. Burns et al. 2005). This is also suggested by the cemented mudstones that typically occur at the top of a few metres of upward-coarsening successions or in the finest grained intervals at the base of upward-coarsening cycles. The fewer cemented intervals in the Lindemans Bugt Formation in comparison to the Bernbjerg Formation (Fig. 3) are thus in accordance with the progressive deepening of the setting, where the influence of minor relative sea-level fluctuations decreased steadily.

### 5.4.2 Mesogenetic processes

The presence of authigenic mixed layer illite-smectite and illite in the studied mudstones indicates that illitisation of smectite has occurred, thereby providing silica and cations for other mineral reactions such as the formation of quartz and ankerite (Fig. 12). Significant illitisation may, however, be contradicted by the presence of K-feldspar in the investigated mudstones, as K-feldspar disappears in shales from most wells below 2.5 km in the northern North Sea due to the illitisation

of smectite (Pearson & Small 1988). If the deposited clay minerals were rich in illite, however, the pore fluids may not have been undersaturated with respect to potassium and consequently less aggressive towards K-feldspar during early diagenesis. Hence, K-feldspar may have survived until deep burial. The iron necessary to form ankerite may have been provided by smectite illitisation and it may have formed at the expense of dolomite cement. Barite is typically a late authigenic phase because the pore fluids need to be very concentrated before they contain sufficient Ba for barite formation. As expected, barite formed late in the studied sediments as seen by the crystal habit of barite as euhedral overgrowths (Fig. 7D), and the string-like occurrence of the precipitated barite identifies the transport route of the last pore fluid.

The diagenetic alteration of the mudstones is indicative of the maximum burial depths to which they have been exposed prior to structural inversion. The presence of quartz overgrowths shows that the sediments must have been exposed to temperatures of at least c. 80°C that is necessary for the growth onset and less than c. 100°C since they are thin and scattered (Bjørlykke & Jahren 2015). Precipitation of quartz in mudstones can be sourced by the smectite to illite transformation, which generally occurs at temperatures of 60-100°C (Thyberg et al. 2009) and is likely to have happened in the studied sediments. Barite precipitated after quartz and ankerite in the mudstones as the last mineral phase during deep burial, a process that has been found to occur at temperatures of 83-105°C in sandstones (Burley et al. 1989). Thus, the precipitation temperatures of the authigenic phases that formed at deepest burial correspond to maximum burial depths of c. 2.1-2.6 km assuming a surface temperature of 20°C and a palaeogeothermal gradient of 30°C/km (Japsen et al. 2021). This is less than the estimated uplift of c. 2.8 km based on thermochronological data from Upper Jurassic sediments from Jameson Land c. 450 km towards south-south-west, in which the diagenesis has progressed further (Green & Japsen 2018; Olivarius et al. 2018a).

# *5.4.3 Telogenetic processes*

The fracturing that has occurred in the sediments must have happened late during uplift since the thin fractures cross-cut the authigenic phases in the sediments. Fracturing is presumed to have accompanied exhumation and pressure release since cooling of the sediments was necessary to decrease their elasticity enough for fracturing (e.g. Gale *et al.* 2014). The fractures formed mainly in the cemented intervals because they had least elasticity. The late timing of the fracturing is also testified by the opal infill, which requires low temperatures of <65°C for precipitation (Weibel *et al.* 2010). The pore fluids must

have been oversaturated with silica in the beginning since opal often formed along the rim of the fractures (Fig. 8E). Formation of Fe-rich dolomite then took over in accordance with the expected composition of the pore fluid since the fractured mudstones are cemented with dolomite and ankerite. The pore fluid became depleted in Fe, so the last dolomite that precipitated was Fe-poor (Fig. 8F). The last fracturing episode happened so late during exhumation that no mineral phases were precipitated in the fractures, which thus contribute minor secondary porosity. However, it is difficult to differentiate natural open fractures, formed in the subsurface, from artefacts produced during drilling and drying of the core.

Introduction of meteoric water is a common mechanism for kaolinite formation (Bjørlykke 1998), as this process could not take place after deposition in the marine environment. The partially dissolved feldspar grains have not been deformed so the secondary porosity has been preserved (Fig. 6D), which indicates that the dissolution and kaolinisation of detrital phases may have happened late during the exhumation (Fig. 12). The fracturing that has occurred during late uplift may have caused a flow of meteoric water through the sediment that was sufficient for kaolinite formation. This may also explain why the latest generation of fractures is not cemented since the pore fluids had a low saturation.

# 5.5 Implications for sediment composition in the Norwegian–Greenland Seaway

The presence of Archaean zircon grains in the Norwegian Sea is often considered diagnostic of sediment supply from East Greenland since Archaean zircons are scarce in sediment eroded off the Fennoscandian Shield (e.g. Morton et al. 2008). Only a single Archaean zircon grain was retrieved from the sample from the Stratumbjerg Formation on Wollaston Forland (Fig. 9). However, the absence or scarcity of Archaean zircons cannot be considered unambiguous proof of a Fennoscandian source in the offshore sediments. This is particularly the case in sediment derived from the central or northern part of the East Greenland Caledonides where Palaeoproterozoic basement is most abundant, whereas Archaean basement is more abundant in the southern Caledonides (Thrane 2002). This is reflected in the geographical differences evident in the zircon age distributions of post-Caledonian sediments in East Greenland (Sláma et al. 2011; Olivarius et al. 2018b).

In sediments with an East Greenland source, the present results highlight how a high proportion of Mesoproterozoic and latest Palaeoproterozoic zircon ages testifies to a provenance from the southern East Greenland Caledonides, whereas a higher proportion of late Palaeoproterozoic (2.0–1.7 Ga) ages is indicative of a more northern sediment source. This is reflected in the distribution of zircon age populations in sediments in the western part of the Norwegian Sea such as in the Upper Cretaceous – Paleocene succession (Fonneland *et al.* 2004; Morton *et al.* 2005).

Time-equivalent sediments in the Norwegian Sea have presumably experienced some of the same diagenetic reactions as the studied sediments, specifically, initial sulphate reduction causing pyrite precipitation, eogenetic bioclast alteration causing calcite-dolomite cementation, mesogenetic smectite illitisation and quartz precipitation and carbonate transformation into ankerite (Fig. 12).

# 6. Conclusions

This study illustrates that changes in mudstone composition can be induced by half-graben evolution and that the composition may also vary in relation to the position in the rift basin and the sea-bottom topography. This knowledge can be applied to predict variations in sediment composition in underexplored half-graben settings.

The diagenetic evolution includes processes related to the different diagenetic regimes that the mudstones have experienced. During early diagenesis, sulphate reduction caused pyrite formation, and bioclast alteration resulted in precipitation of calcite and dolomite. During burial diagenesis, illite and quartz formed due to smectite illitisation, and ankerite and barite precipitated because of carbonate transformation. During uplift, opal and dolomite precipitated in the earliest fractures, and kaolinite formed due to meteoric water flushing.

The provenance analysis of sand-rich intervals shows that the zircon age patterns of the studied sediments are most similar to other Upper Jurassic – Lower Cretaceous sandstones from East and North-East Greenland. This is revealed by MDS where it is evident that the Archaean–Palaeoproterozoic crystalline basement complexes and the Meso–Neoproterozoic metasediments comprise two end members, so their derived detritus must have been mixed to produce the Mesozoic sediments.

# **Acknowledgements**

Technical assistance by Helene Almind, Kirsten Fries, John Boserup, Fiorella F. Aguilera, Mojagan Alaei, Michael S. Nielsen and Jette Halskov is much appreciated. Valuable advice was provided by Emma Sheldon, Jon Ineson, Henrik Vosgerau, Holger Lindgreen and Tonci Balic-Zunic. The authors would like to thank the reviewers Chris Kirkland and Kevin Taylor for insightful comments that helped improve the manuscript.

# **Additional information**

### **Funding statement**

Funding for drilling of the Rødryggen-1 and Brorson Halvø-1 boreholes and studies of the cores was provided by a consortium of oil companies and the Geological Survey of Denmark and Greenland (GEUS).

#### **Author contributions**

MO: wrote the manuscript in cooperation with the other authors. MO, AK, RW: performed the mineralogical and petrographic work. TK: processed the radiometric analyses. JH: carried out the sedimentological work.

### **Competing interests**

None.

#### **Additional files:**

The full table of zircon U-Pb data is provided as Supplementary File S1, available at https://doi.org/10.22008/FK2/KEL0A6.

# References

- Alsen, P., Piasecki, S., Nøhr-Hansen, H., Pauly, S., Sheldon, E. & Hovikoski, J. 2023: Stratigraphy of the Upper Jurassic to lowermost Cretaceous in the Rødryggen-1 and Brorson Halvø-1 boreholes, Wollaston Forland, North-East Greenland. GEUS Bulletin 55, 8342 (this volume). https:// doi.org/10.34194/geusb.v55.8342
- Barham, M., Kirkland, C.L., Hovikoski, J., Alsen, P., Hollis, J. & Tyrrell, S. 2020: Reduce or recycle? Revealing source to sink links through integrated zircon-feldspar provenance fingerprinting. Sedimentology 68, 531–556. https://doi.org/10.1111/sed.12790
- Berner, R.A. 1985: Sulphate reduction, organic matter decomposition and pyrite formation. Royal Society of London, Series A **315**, 25–38. https://doi.org/10.1098/rsta.1985.0027
- Bjerager, M. et al. 2020: Cretaceous lithostratigraphy of North-East Greenland. Bulletin of the Geological Society of Denmark **68**, 37–93. https://doi.org/10.37570/bgsd-2020-68-04
- Bjørlykke, K. 1998: Clay mineral diagenesis in sedimentary basins a key to the prediction of rock properties. Examples from the North Sea Basin. Clay Minerals 33, 15–34. https://doi.org/10.1180/claymin.1998.033.1.03
- Bjørlykke, K. & Jahren, J. 2015: Sandstones and Sandstone Reservoirs. In: Bjørlykke, K. (ed.): Petroleum Geoscience: From Sedimentary Environments to Rock Physics 119–149. Berlin, Heidelberg: Springer. https://doi.org/10.1007/978-3-642-34132-8\_4
- Bojesen-Koefoed, J.A., Alsen, P., Bjerager, M., Hovikoski, J., Ineson, J.R., Johannessen, P.N., Olivarius, M., Piasecki, S. & Vosgerau, H. 2023a: The Rødryggen-1 and Brorson Halvø-1 fully cored boreholes (Upper Jurassic Lower Cretaceous), Wollaston Forland, North-East Greenland an introduction. GEUS Bulletin **55**, 8350 (this volume). https://doi.org/10.34194/geusb.v55.8350
- Bojesen-Koefoed, J.A., Alsen, P., Bjerager, M., Hovikoski, J., Johannessen, P.N., Nøhr-Hansen, H., Petersen, H.I., Piasecki, S. & Vosgerau, H. 2023b: Organic geochemistry of an Upper Jurassic Lower Cretaceous mudstone succession in a narrow graben setting, Wollaston Forland Basin, North-East Greenland. GEUS Bulletin **55**, 8320 (this volume). https://doi.org/10.34194/geusb.v55.8320
- Burley, S.D., Mullis, J. & Matter, A. 1989: Timing diagenesis in the Tartan reservoir (UK North Sea): Constraints from combined cathodoluminescence microscopy and fluid inclusion studies. Marine and Petroleum Geology **6**, 98–120. https://doi.org/10.1016/0264-8172(89)90014-7
- Burns, F.E., Burley, S.D., Gawthorpe, R.L. & Pollard, J.E. 2005: Diagenetic signatures of stratal surfaces in the Upper Jurassic Fulmar Formation, Central North Sea, UKCS. Sedimentology **52**, 1155–1185. https://doi.org/10.1111/j.1365-3091.2005.00729.x
- Dhuime, B., Bosch, D., Bruguier, O., Caby, R. & Pourtales, S. 2007: Age, provenance and post-deposition metamorphic overprint of detrital zircons from the Nathorst Land group (NE Greenland) A LA-ICP-MS and SIMS study. Precambrian Research **155**, 24–46. https://doi.org/10.1016/j.precamres.2007.01.002
- Dröllner, M., Barham, M., Kirkland, C.L. & Ware, B. 2021: Every zircon deserves a date: Selection bias in detrital geochronology. Geological Magazine 158, 1135–1142. https://doi.org/10.1017/S0016756821000145
- Elvevold, S., Thrane, K. & Gilotti, J.A. 2003: Metamorphic history of high-pressure granulites in Payer Land, Greenland

- Caledonides. Journal of Metamorphic Geology **21**, 49–63. https://doi. org/10.1046/j.1525-1314.2003.00419.x
- Fonneland, H.C., Lien, T., Martinsen, O.J., Pedersen, R.B. & Košler, J. 2004: Detrital zircon ages: A key to understanding the deposition of deep marine sandstones in the Norwegian Sea. Sedimentary Geology **164**, 147–159. https://doi.org/10.1016/j.sedgeo.2003.09.005
- Gale, J.F.W., Laubach, S.E., Olson, J.E., Eichhubl, P. & Fall, A. 2014: Natural fractures in shale: A review and new observations. AAPG Bulletin 98, 2165–2216. https://doi.org/10.1306/08121413151
- Gawthorpe, R.L. & Leeder, M.R. 2000: Tectono- sedimentary evolution of active extensional basins. Basin Research **12**, 195–218. https://doi.org/10.1111/j.1365-2117.2000.00121.x
- Gilotti, J.A., Jones, K.A. & Elvevold, S. 2008: Caledonian metamorphic patterns in Greenland. Geological Society of America Memoir **202**, 201–225. https://doi.org/10.1130/2008.1202(08)
- Green, P.F. & Japsen, P. 2018: Burial and exhumation history of the Jameson Land Basin, East Greenland, estimated from thermochronological data from the Blokelv-1 core. Geological Survey of Denmark and Greenland Bulletin 42, 133–147. https://doi.org/10.34194/geusb. v42 4324
- Hendry, J.P., Wilkinson, M., Fallick, A.E. & Haszeldine, R.S. 2000: Ankerite cementation in deeply buried Jurassic sandstone reservoirs of the Central North Sea. Journal of Sedimentary Research **70**, 227–239. https://doi.org/10.1306/2DC4090D-0E47-11D7-8643000102C1865D
- Henriksen, N. & Higgins, A.K. 2008: Geological research and mapping in the Caledonian orogen of East Greenland, 70°N–82°N. In: Higgins, A.K. *et al.* (eds): The Greenland Caledonides: Evolution of the Northeast Margin of Laurentia. Geological Society of America Memoirs **202**, 1–27.
- Henriksen, N., Higgins, A.K., Gilotti, J.A. & Smith, M.P. 2008: Introduction The Caledonides of Greenland. The Geological Society of America, Memoir **202**, v–xv. https://doi.org/10.1130/2008.1202(00)
- Henstra, G.A. *et al.* 2016: Depositional processes and stratigraphic architecture within a coarse-grained rift-margin turbidite system: The Wollaston Forland Group, east Greenland. Marine and Petroleum Geology **76**, 187–209. https://doi.org/10.1016/j.marpetgeo.2016.05.018
- Higgins, A.K. *et al.* 2004: The foreland-propagating thrust architecture of the East Greenland Caledonides 72°–75°N. Journal of the Geological Society **161**, 1009–1026. *https://doi.org/10.1144/0016-764903-141*
- Hillier, S. 2000: Accurate quantitative analysis of clay and other minerals in sandstones by XRD: comparison of a Rietveld and a reference intensity ratio (RIR) method and the importance of sample preparation. Clay Minerals **35**, 291–302. https://doi.org/10.1180/000985500546666
- Hovikoski, J., Uchman, A., Alsen, P. & Ineson, J. 2018: Ichnological and sedimentological characteristics of submarine fan-delta deposits in a half-graben, Lower Cretaceous Palnatokes Bjerg Formation, NE Greenland. Ichnos 26(1), 28–57. https://doi.org/10.1080/10420940.20 17.1396981
- Hovikoski, J., Ineson, J.R., Olivarius, M., Bojesen-Koefoed, J.A., Piasecki, S. & Alsen, P. 2023a: Upper Jurassic Lower Cretaceous of eastern Wollaston Forland, North-East Greenland: a distal marine record of an evolving rift. GEUS Bulletin 55, 8349 (this volume). https://doi.org/10.34194/geusb.v55.8349
- Hovikoski, J. *et al.* 2023b: Late Jurassic Early Cretaceous marine deoxygenation in NE Greenland. Journal of the Geological Society **180**, jgs2022–058. *https://doi.org/10.1144/jgs2022-058*
- Jackson, S.E., Pearson, N.J., Griffin, W.L. & Belousova, E.A. 2004: The application of laser ablation-inductively coupled plasma-mass spectrometry to in situ U-Pb zircon geochronology. Chemical Geology 211, 47–69. https://doi.org/10.1016/j.chemgeo.2004.06.017
- Japsen, P., Green, P.F., Bonow, J.M., Bjerager, M. & Hopper, J.R. 2021: Episodic burial and exhumation in North-East Greenland before and after opening of the North-East Atlantic. GEUS Bulletin 45(2). 5299. https://doi.org/10.34194/geusb.v45.5299
- Kalsbeek, F., Nutman, A.P. & Taylor, P.N. 1993: Palaeoproterozoic basement province in the Caledonian fold belt of North-East Greenland. Precambrian Research 63, 163–178. https://doi.org/10.1016/0301-9268(93)90010-Y
- Kalsbeek, F., Thrane, K., Nutman, A.P. & Jepsen, H.F. 2000: Late Mesoproterozoic to early Neoproterozoic history of the East Greenland

- Caledonides: Evidence for Grenvillian orogenesis? Journal of the Geological Society (London) **157**, 1215–1225. https://doi.org/10.1144/jgs.157.6.1215
- Kalsbeek, F., Jepsen, H.F. & Nutman, A.P. 2001: From source migmatites to plutons: Tracking the origin of ca. 435 Ma S-type granites in the East Greenland Caledonian orogen. Lithos **57**, 1–21. https://doi.org/10.1016/S0024-4937(00)00071-2
- Kalsbeek, F., Thrane, K., Higgins, A.K., Jepsen, H.F., Leslie, A.G., Nutman, A.P. & Frei, R. 2008a: Polyorogenic history of the East Greenland Caledonides. Geological Society of America Memoir 202, 55–72.
- Kalsbeek, F., Higgins, A.K., Jepsen, H.F., Frei, R. & Nutman, A.P. 2008b: Granites and granites in the East Greenland Caledonides. Geological Society of America Memoir 202, 227–249. https://doi. org/10.1130/2008.1202(09)
- Langrock, U., Stein, R., Lipinski, M. & Brumsack, H.-J. 2003: Late Jurassic to Early Cretaceous black shale formation and paleoenvironment in high northern latitudes: Examples from the Norwegian-Greenland Seaway. Paleoceanography **18**, 1074. https://doi.org/10.1029/2002PA000867
- Larsen, P.-H., Olsen, H. & Clack, J.A. 2008: The Devonian basin in East Greenland – Review of basin evolution and vertebrate assemblages. Geological Society of America Memoir 202, 273–292. https://doi. org/10.1130/2008.1202(11)
- Leslie, A.G. & Nutman, A.P. 2003: Evidence for Neoproterozoic orogenesis and early high temperature Scandian deformation events in the southern East Greenland Caledonides. Geological Magazine 140, 309–333.
- McCusker, L.B., Von Dreele, R.B., Cox, D.E., Louer, D. & Scardi, P. 1999: Rietveld refinement guidelines. Journal of Applied Crystallography **32**, 36–50. https://doi.org/10.1107/S0021889898009856
- McKerrow, W.S., Mac Niocaill, C. & Dewey, J.F. 2000: The Caledonian Orogeny redefined. Journal of the Geological Society (London) **157**, 1149–1154. https://doi.org/10.1144/jgs.157.6.1149
- Morton, A.C., Whitham, A.G. & Fanning, C.M. 2005: Provenance of Late Cretaceous to Paleocene submarine fan sandstones in the Norwegian Sea: Integration of heavy mineral, mineral chemical and zircon age data. Sedimentary Geology 182, 3–28. https://doi.org/10.1016/j. sedgeo.2005.08.007
- Morton, A., Fanning, M. & Milner, P. 2008: Provenance characteristics of Scandinavian basement terrains: Constraints from detrital zircon ages in modern river sediments. Sedimentary Geology **210**, 61–85.
- Mutterlose, J. et al. 2003: The Greenland-Norwegian Seaway: A key area for understanding Late Jurassic to Early Cretaceous paleoenvironments. Paleoceanography 18, 1010. https://doi.org/10.1029/2001PA000625
- Nielsen, O.B., Rasmussen, E.S. & Thyberg, B.I. 2015: Distribution of clay minerals in the northern North Sea Basin during the Paleogene and Neogene: A result of source-area geology and sorting processes. Journal of Sedimentary Research 85, 562–581. https://doi.org/10.2110/jsr.2015.40
- Nøhr-Hansen, H., Piasecki, S. & Alsen, P. 2020: A Cretaceous dinoflagellate cyst zonation for NE Greenland. Geological Magazine **157**, 1658–1692. https://doi.org/10.1017/S0016756819001043
- Olierook, H.K.H., Barham, M., Kirkland, C.L., Hollis, J. & Vass, A. 2020: Zircon fingerprint of the Neoproterozoic North Atlantic: Perspectives from East Greenland. Precambrian Research **342**, 105653. https://doi.org/10.1016/j.precamres.2020.105653
- Olivarius, M., Weibel, R., Schovsbo, N.H., Olsen, D. & Kjøller, C. 2018a: Diagenesis of Upper Jurassic sandstones of the Blokelv-1 core in the Jameson Land Basin, East Greenland. Geological Survey of Denmark and Greenland Bulletin 42, 65–84. https://doi.org/10.34194/geusb.v42.4310
- Olivarius, M., Bjerager, M., Keulen, N., Knudsen, C. & Kokfelt, T.F. 2018b: Provenance of basinal sandstones in the Upper Jurassic Hareelv Formation, Jameson Land Basin, East Greenland. Geological Survey of Denmark and Greenland Bulletin 42, 115–126. https://doi.org/10.34194/geusb.v42.4317
- Pearson, M.J. & Small, J.S. 1988: Illite-smectite diagenesis and palaeo-temperatures in northern North Sea Quaternary to Mesozoic shale sequences. Clay Minerals 23, 109–132. https://doi.org/10.1180/claymin.1988.023.2.01
- Piasecki, S., Bojesen-Koefoed, J.A. & Alsen, P. 2020: Geology of the Lower Cretaceous in the Falkebjerg area, Wollaston Forland, northern East Greenland. Bulletin of the Geological Society of Denmark **68**, 155–170.

- Rateev, M.A., Sadchikova, T.A. & Shabrova, V.P. 2008: Clay minerals in recent sediments of the world ocean and their relation to types of lithogenesis. Lithology and Mineral Resources **43**, 125–135. https://doi.org/10.1134/S002449020802003X
- Rietveld, H.M. 1969: A profile refinement method for nuclear and magnetic structures. Journal of Applied Crystallography **2**, 65–71. https://doi.org/10.1107/S0021889869006558
- Rogov, M.A., Shchepetova, E.V. & Zakharov, V.A. 2020: Late Jurassic Earliest Cretaceous prolonged shelf dysoxic–anoxic event and its possible causes. Geological Magazine **157**, 1622–1642. https://doi.org/10.1017/S001675682000076X
- Sambridge, M. & Lambert, D.D. 1997: Propagating errors in decay equations: Examples from the Re-Os isotopic system. Geochimica et Cosmochimica Acta **61**, 3019–3024.
- Sláma, J. & Košler, J. 2012: Effects of sampling and mineral separation on accuracy of detrital zircon studies. Geochemistry, Geophysics, Geosystems 13, Q05007. https://doi.org/10.1029/2012GC004106
- Sláma, J. et al. 2008: Plešovice zircon A new natural reference material for U–Pb and Hf isotopic microanalysis. Chemical Geology **249**, 1–35. https://doi.org/10.1016/j.chemgeo.2007.11.005
- Sláma, J., Walderhaug, O., Fonneland, H., Kosler, J. & Pedersen, R.B. 2011: Provenance of Neoproterozoic to upper Cretaceous sedimentary rocks, eastern Greenland: Implications for recognizing the sources of sediments in the Norwegian Sea. Sedimentary Geology 238, 254–267. https://doi.org/10.1016/j.sedgeo.2011.04.018
- Slater, C. & Cohen, L. 1962: A centrifugal particle size analyser. Journal of Scientific Instrumentation 39, 614–617.
- Smith, M.P. & Rasmussen, J.A. 2008: Cambrian–Silurian development of the Laurentian margin of the lapetus Ocean in Greenland and related areas. Geological Society of America Memoir **202**, 137–167. https://doi.org/10.1130/2008.1202(06)
- Stacey, J.S. & Kramers, J.D. 1975: Approximation of terrestrial lead isotope evolution by a two-stage model. Earth and Planetary Science Letters 26, 207–221. https://doi.org/10.1016/0012-821X(75)90088-6
- Stemmerik, L., Christensen, F.G., Piasecki, S., Jordt, B., Marcussen, C. & Nøhr-Hansen, H. 1992: Depositional history and petroleum geology of the Carboniferous to Cretaceous sediments in the northern part of East Greenland. Norwegian Petroleum Federation, Special Publication 2, 67–87. https://doi.org/10.1016/B978-0-444-88943-0.50009-5
- Stemmerik, L., Clausen, O.R., Korstgård, J., Larsen, M., Piasecki, S., Seidler, L., Surlyk, F. & Therkelsen, J. 1997: Petroleum geological investigations in East Greenland: Project 'Resources of the sedimentary basins of North and East Greenland'. Geological Survey of Greenland Bulletin 176, 29–38. https://doi.org/10.34194/ggub.v176.5058
- Stoker, M.S. *et al.* 2017: An overview of the Upper Palaeozoic–Mesozoic stratigraphy of the NE Atlantic region. Geological Society, London, Special Publications **447**, 11–68. *https://doi.org/10.1144/SP447.2*
- Strachan, R.A., Nutman, A.P. & Friderichsen, J.D. 1995: SHRIMP U-Pb geochronology and metamorphic history of the Smallefjord sequence,

- NE Greenland Caledonides. Journal of the Geological Society **152**, 779–784.
- Surlyk, F. 1978: Submarine fan sedimentation along fault scarps on tilted fault blocks (Jurassic-Cretaceous boundary, East Greenland). Geological Survey of Greenland Bulletin 128, 108 pp. https://doi.org/10.34194/ bullggu.v128.6670
- Surlyk, F. 1984: Fan-delta to submarine fan conglomerates of the Volgian-Valanginian Wollaston Forland Group, East Greenland. Canadian Society of Petroleum Geologists Memoir 10, 359–382.
- Surlyk, F. 1990: A Jurassic sea-level curve for East Greenland. Palaeogeography, Palaeoclimatology, Palaeoecology 78, 71–85. https://doi. org/10.1016/0031-0182(90)90205-L
- Surlyk, F. 2003: The Jurassic of East Greenland: A sedimentary record of thermal subsidence, onset and culmination of rifting. Geological Survey of Denmark and Greenland Bulletin 1, 659–722. https://doi.org/10.34194/geusb.v1.4674
- Surlyk, F. & Korstgård, J. 2013: Crestal unconformities on an exposed Jurassic tilted fault block, Wollaston Forland, East Greenland as an analogue for buried hydrocarbon traps. Marine and Petroleum Geology 44, 82–95. https://doi.org/10.1016/j.marpetgeo.2013.03.009
- Surlyk, F. et al. 2021: Jurassic stratigraphy of East Greenland. GEUS Bulletin **46**, 6521. https://doi.org/10.34194/geusb.v46.6521
- Thrane, K. 2002: Relationships between Archaean and Palaeoproterozoic crystalline basement complexes in the southern part of the East Greenland Caledonides: An ion microprobe study. Precambrian Research 113, 19–42. https://doi.org/10.1016/ S0301-9268(01)00198-X
- Thyberg, B., Jahren, J., Winje, T., Bjørlykke, K. & Faleide, J.I. 2009: From mud to shale: Rock stiffening by micro-quartz cementation. First Break 27, 27–33. https://doi.org/10.3997/1365-2397.2009003
- Tribovillard, N., Algeo, T.J., Lyons, T. & Riboulleau, A. 2006: Trace metals as paleoredox and paleoproductivity proxies: An update. Chemical Geology **232**, 12–32. https://doi.org/10.1016/j.chemgeo.2006.02.012
- Vermeesch, P. 2012: On the visualisation of detrital age distributions. Chemical Geology 312-313, 190-194. https://doi.org/10.1016/j. chemgeo.2012.04.021
- Vermeesch, P., Resentini, A. & Garzanti, E. 2016: An R package for statistical provenance analysis. Sedimentary Geology 336, 14–25. https://doi.org/10.1016/j.sedgeo.2016.01.009
- Watt, G.R., Kinny, P.D. & Friderichsen, J.D. 2000: U–Pb geochronology of Neoproterozoic and Caledonian tectonothermal events in the East Greenland Caledonides. Journal of the Geological Society **157**, 1031–1048. https://doi.org/10.1144/jgs.157.5.1031
- Weibel, R., Friis, H., Kazerouni, A.M., Svendsen, J.B., Stokkendal, J. & Poulsen, M.L.K. 2010: Development of early diagenetic silica and quartz morphologies. Sedimentary Geology 228, 151–170. https://doi. org/10.1016/j.sedgeo.2010.04.008

# **GEUS Bulletin**



# Organic geochemistry of an Upper Jurassic – Lower Cretaceous mudstone succession in a narrow graben setting, Wollaston Forland Basin, North-East Greenland

Jørgen A. Bojesen-Koefoed¹\* , Peter Alsen² , Morten Bjerager³ , Jussi Hovikoski³,⁴ ,
Peter N. Johannessen⁵, Henrik Nøhr-Hansen² , Henrik I. Petersen² , Stefan Piasecki³,6,7 , Henrik Vosgerau³

<sup>1</sup>Department for Mapping and Mineral Resources, Geological Survey of Denmark and Greenland (GEUS), Copenhagen, Denmark; <sup>2</sup>Department for Geo-energy and Storage, Geological Survey of Denmark and Greenland (GEUS), Copenhagen, Denmark; <sup>3</sup>Department for Geophysics and Sedimentary Basins, Geological Survey of Denmark and Greenland (GEUS), Copenhagen, Denmark; <sup>4</sup>Geological Survey of Finland (GTK), Espoo, Finland; <sup>5</sup>Geological Survey of Denmark and Greenland (GEUS), now retired; <sup>6</sup>Globe Institute, University of Copenhagen, Copenhagen, Denmark; <sup>7</sup>Retired

### **Abstract**

The Oxfordian-Ryazanian was a period of widespread deposition of marine organic-rich mudstones in basins formed during the early phases of the rifting that heralded the formation of the present-day North Atlantic. Occasionally, uninterrupted deposition prevailed for 20 million years or more. Today, mudstones of this time interval are found on the shelves bordering the North Atlantic and adjacent areas from Siberia to the Netherlands. Here, we report data on two fully cored boreholes from Wollaston Forland (North-East Greenland, approx. 74° N), which represent an unin $terrupted\ succession\ from\ the\ upper\ Kimmeridgian\ to\ the\ Hauterivian.\ The\ boreholes\ record\ basin$ development at two different positions within an evolving halfgraben, located at the margin of the main rift, and thus partially detached from it. Although the overall depositional environment remained an oxygen-restricted deep-shelf setting, rifting-related changes can be followed through the succession. The Kimmeridgian was a period of eustatic highstand and records the incipient rifting with a transgressive trend straddling the transition to the lower Volgian by a gradual change from deposits with high levels of total organic carbon (TOC) and kerogen rich in allochthonous organic matter to deposits with lower TOC and a higher proportion of autochthonous organic matter. This is followed by a slight regressive trend with lower TOC and increased proportions of allochthonous organic matter until rifting culminated in the middle Volgian-Ryazanian, indicated by increasing autochthonous organic matter and higher TOC, which prevailed until basin ventilation occurred towards the end of the Ryazanian. The properties of the reactive kerogen fraction remained rather stable irrespective of TOC, underlining the effect of terrigenous matter input for TOC. These variations are also captured by biological markers and stable carbon isotopes. The deposits are very similar to equivalent successions elsewhere in the proto-North Atlantic region, albeit the proportion of terrigenous kerogen is greater.

**Reviewed by:** Erdem Idiz (University of Oxford, UK), Iain Scotchman (Scotchman Geochemistry Services Ltd, UK)

Funding: See page 116

Competing interests: See page 116

Additional files: None provided

1. Introduction

Marine shales of Oxfordian–Ryazanian age constitute the most important source rocks for petroleum in the prospective basins of the North Atlantic region, which include the basins of the greater North Sea area, the Barents Shelf, and the basins west of Ireland and the Shetland Islands as well as the basins of western Siberia. On the western side of the Atlantic this also includes

\*Correspondence: jbk@geus.dk Received: 20 Apr 2022

Revised: 06 Jan 2023 Accepted: 10 Jan 2023 Published: 21 Dec 2023

**Keywords:** North-East Greenland, organic geochemistry, paleogeography, source rock, Upper Jurassic

# Abbreviations:

b. rfl.: below reference level GC: gas chromatography GEUS: Geological Survey of Denmark and Greenland

HI: Hydrogen Index

 $\ensuremath{\mathsf{HI}_{\mathsf{live}}}\xspace$  average HI of the live kerogen fraction MS: mass spectrometry

mmboe: million barrels of oil equivalent NSO: nitrogen, sulphur and oxygen

PI: Production Index

SRA: Source Rock Analyzer

TC: total carbon

TD: total depth

 $T_{
m max}$ : temperature at maximum rate of pyrolysate generation during Rock-Eval or SRA analysis (°C)

TOC: total organic carbon

TS: total sulphur

UEG: Ultimate Expulsion Gas

UEO: Ultimate Expulsion Oil

UEP: Ultimate Expulsion Potential

GEUS Bulletin (eISSN: 2597-2154) is an open access, peer-reviewed journal published by the Geological Survey of Denmark and Greenland (GEUS). This article is distributed under a *CC BY 4.0* licence, permitting free redistribution, and reproduction for any purpose, even commercial, provided proper citation of the original work. Author(s) retain copyright.

Edited by: Jon R. Ineson (GEUS, Denmark)

the Jeanne d'Arc and Flemish Pass basins off eastern Canada, and probably untested basins off East and North-East Greenland. These deposits have been extensively studied (e.g. Von der Dick et al. 1989; Miller 1990; Chakhmakhchev et al. 1994; Klemme 1994; Telnæs et al. 1994; Fowler & McAlpine 1995; Isaksen & Ledje 2001; Ineson et al. 2003; Justwan & Dahl 2005; Justwan et al. 2005, 2006a,b; Petersen et al. 2010; Scotchman et al. 2016). Ageequivalent deposits crop out onshore North-East Greenland. However, irrespective of their importance for the general understanding of the most important petroleum system of Northwest Europe, published in-depth studies of the nature and petroleum potential of the equivalent North-East Greenland succession are scarce. Exceptions include papers by Requejo et al. (1989), Christiansen et al. (1992), Strogen et al. (2005) and Bojesen-Koefoed et al. (2018).

Over the years 2008-2010, the Geological Survey of Denmark and Greenland (GEUS) drilled three fully cored boreholes to depths of more than 200 m to penetrate the Upper Jurassic - Lower Cretaceous mudstone succession in East and North-East Greenland. The successions drilled are partially time equivalents of the Kimmeridge Clay Formation of the Wessex Basin, UK, as well as of the Upper Jurassic - Lower Cretaceous petroleum source-rock successions of the North Sea and North Atlantic basins, where they are known under a variety of different local names, see for instance Ineson et al. (2003). The Kimmeridge Clay Formation has been penetrated by cored boreholes close to its type section in Dorset (Morgans-Bell et al. 2001). However, the East and North-East Greenland boreholes offer an opportunity to study nearly the full Oxfordian to Ryazanian succession in an area remote from other studied outcrops and wells. The first of these boreholes to be drilled was the Blokelv-1 in Jameson Land, which covers the succession from the Oxfordian to the lower Volgian (see Ineson & Bojesen-Koefoed 2018). The second and third of the planned boreholes, the Rødryggen-1 and Brorson Halvø-1, respectively, were drilled in northern Wollaston Forland, North-East Greenland in 2009 and 2010, respectively. The Brorson Halvø-1 drill site is situated approximately 10 km north-east of the Rødryggen-1 drillsite, near the uplifted eastern crest of the fault block defined by the Permpas fault to the west and the Hühnerbjerg fault to the east (Fig. 1; Surlyk 1978). The Rødryggen-1 borehole is located near the centre of the same block.

The main target of the drilling in both cores was the same Kimmeridgian–Ryazanian black mudstone succession with the primary objective being to delineate the lateral development in facies of the Upper Jurassic – Lower Cretaceous mudstone succession in an evolving half-graben system in the Wollaston Forland area. The objective of this paper is to present an overview of the organic geochemistry of the Upper Jurassic – Lower Cretaceous mudstone succession in the Wollaston Forland Basin,

based on new evidence from the Rødryggen-1 and Brorson Halvø- 1 boreholes (Fig. 1). Details of the drilling, sedimentology and stratigraphy of the Rødryggen-1 and Brorson Halvø- 1 boreholes can be found in Bojesen-Koefoed *et al.* (2023, this volume), Hovikoski *et al.* (2023b, this volume) and Alsen *et al.* (2023, this volume).

# 2. Geological setting and stratigraphy of the drilled succession

The Jurassic–Cretaceous Wollaston Forland Basin developed in response to rifting in the proto-North Atlantic to the east of the basin. The Wollaston Forland Basin is overall a system of westerly tilted fault blocks or half-grabens bounded to the west by the Dombjerg Fault and to the east by the Hühernbjerg Fault (Figs 1, 2; Surlyk, 1978, 2003; Fyhn *et al.* 2021a). The basin is internally segmented into several subbasins defined by roughly north–south trending normal faults, which were active during various phases of the basin development (Fyhn *et al.* 2021a,b; Hovikoski *et al.* 2023a,b and references therein).

The two drill-cores penetrate the Kimmeridgian – lower Barremian succession, which includes four lithostratigraphic units (Fig. 3): (1) the Bernbjerg Formation, (2) the Lindemans Bugt Formation, Storsletten Member (Alsen *et al.* 2023, this volume), (3) the Palnatokes Bjerg Formation (the Albrechts Bugt Member and the Rødryggen Member), and (4) the Stratumbjerg Formation (Bjerager *et al.* 2020; Surlyk *et al.* 2021).

The upper Oxfordian - lower Volgian Bernbjerg Formation is up to 500-600 m thick and represents a tectonically affected muddy shelf succession that crops out from Store Koldewey in the north to Traill Ø (Ø meaning island) in the South (Surlyk & Clemmensen 1983; Surlyk 2003; Surlyk et al. 2021). A major rift episode starting in the Volgian terminated the regionally continuous shelf accumulation and resulted in accelerated tilted fault-block development and basin segmentation that lasted until the Barremian in the western part of the area (Surlyk 1978, 1984, 1990, 2003; Piasecki et al. 2020). As a result, the basin geometry changed into a series of narrow, 10-30 km wide, S-N-oriented basins that were strongly westwards tilted. In the most proximal fault block, the Volgian-Ryazanian syn-rift interval is characterised by major conglomeratic submarine fandelta systems (Lindemans Bugt Formation; Rigi Member; Surlyk 1978; Henstra et al. 2016), which graded into heterolithic and mud-dominated deposits in more distal areas (the Laugeites Ravine, Niesen and Storsletten Members). The areal distribution of the Lindemans Bugt Formation is limited to north-eastern Clavering Ø, north-western Wollaston Forland, eastern Th. Thomsen Land (named for the ethnographer Thomas Thomsen, known as Th. Thomsen (Higgins 2010)) and south-west

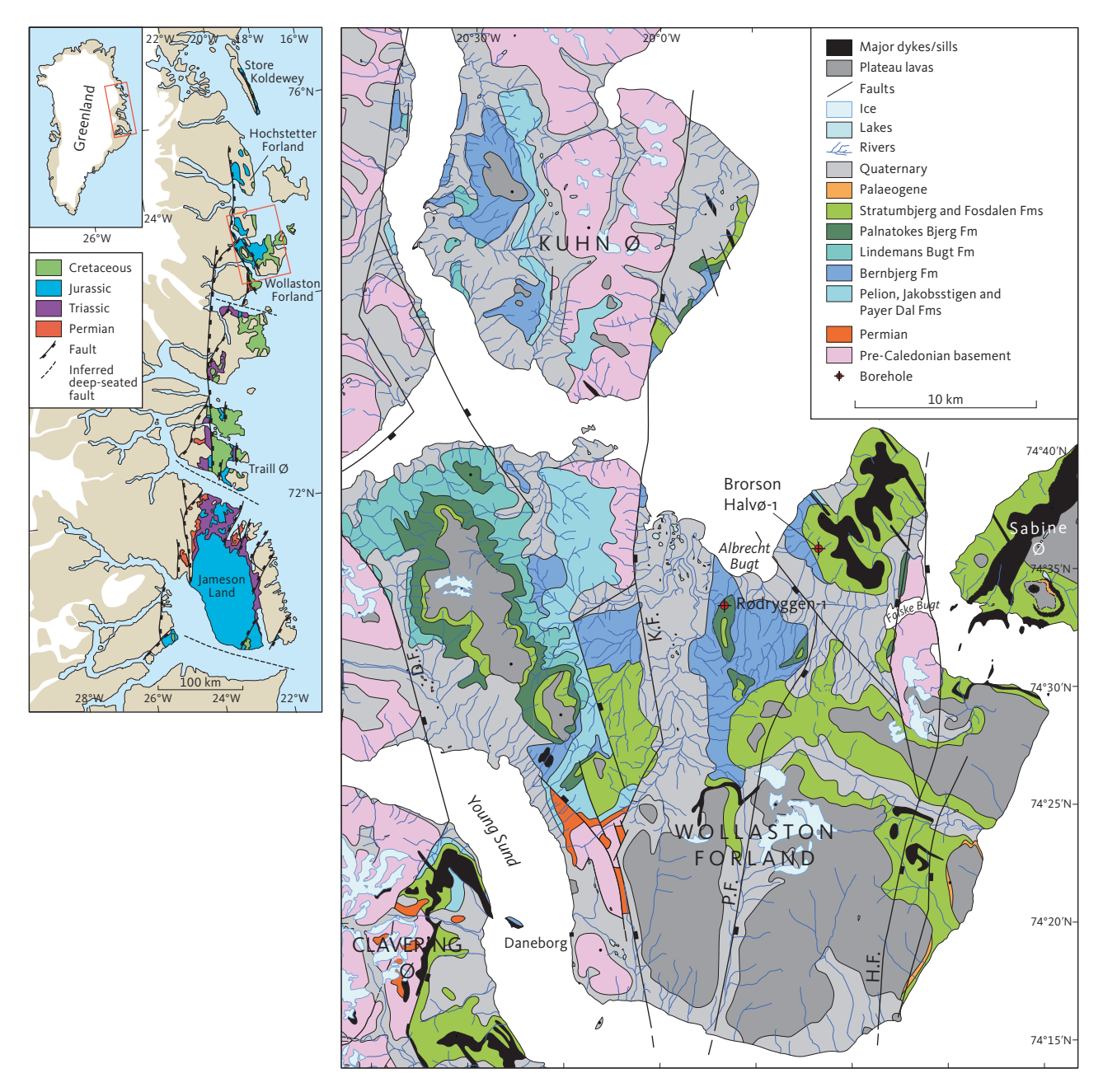


**Fig. 1** Location maps. Overview map (**left**). Positions of the Rødryggen-1 and Brorson Halvø-1 boreholes on Wollaston Forland are shown on a simplified geological map (**right**). **K.F.**: Kuhn fault; **P.F.**: Permpas Fault; **H.F.**: Hühnerbjerg Fault; **D.F.**: Dombjerg Fault. The Dombjerg Fault was the main fault to control the position of the coastline during the Late Jurassic. The Permpas–Hühnerbjerg block(s) was bounded by the Kuppel and Hühnerbjerg Faults, which probably represented the main controlling faults in the block that is studied here, during the Late Jurassic. Reproduced from Bojesen-Koefoed *et al.* (2023, this volume).

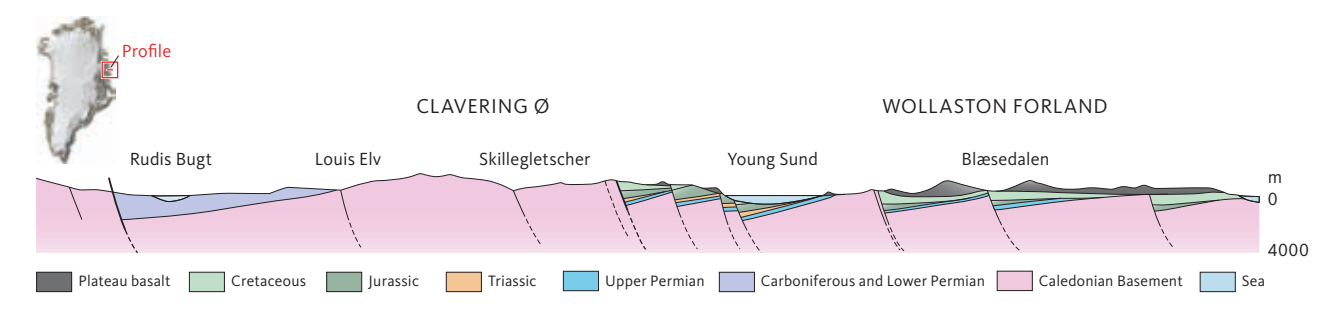


Fig. 2 Conceptual, approximately SW–NE-oriented cross-section of Clavering Ø – Wollaston Forland, showing multiple westward-tilted fault blocks. Modified from Birkelund & Perch-Nielsen (1976) and Vischer (1943).

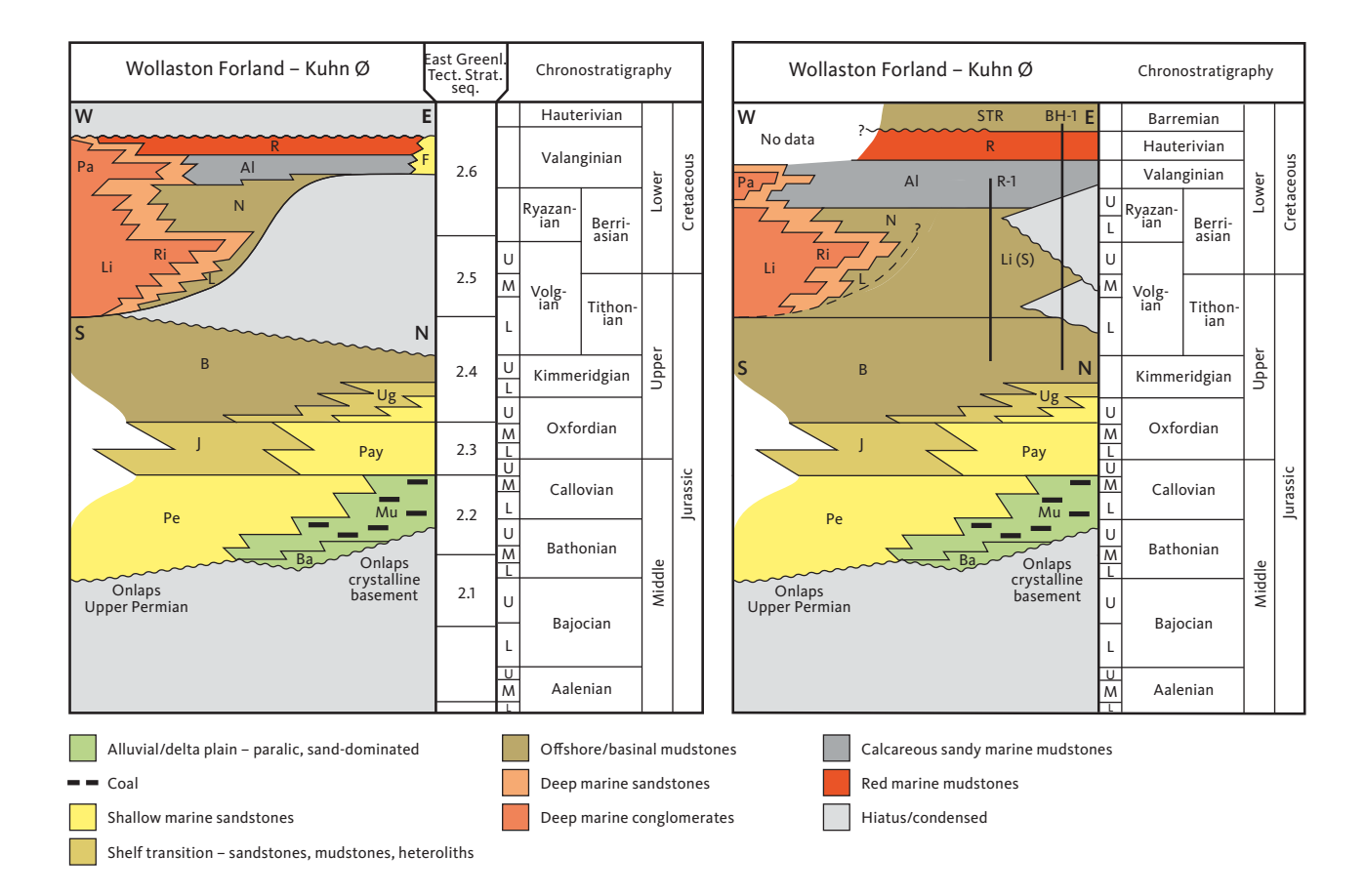


Fig. 3 Stratigraphic models of the Wollaston Forland – Kuhn Ø area. Left: the original stratigraphy by Surlyk (2003). Right: the revised stratigraphy after drilling of the Rødryggen-1 and Brorson Halvø-1 boreholes and incorporating changes introduced by Surlyk et al. (2021). The revised succession is much more complete and richer in mudstone than suggested by the original. East Greenl. Tect. Strat. Seq.: East Greenland Tectono-stratigraphic sequence. U: Upper. M: Middle. L: Lower. Abbreviations for geology are as follows: STR: Stratumbjerg Formation. R: Rødryggen Member. F: Falske Bugt Member. Pa: Palnatokes Bjerg Formation (Young Sund Member). Al: Albrechts Bugt Member. N: Niesen Member. Li: Lindemans Bugt Formation. Li (S): Lindemans Bugt Formation (Storsletten Member). Ri: Rigi Member. L: Laugeites Ravine Member. B: Bernbjerg Formation. Ug: Ugpik Ravine Member. J: Jakobsstigen Formation. Pay: Payer Dal Formation. Pe: Pelion Formation. Mu: Muslingebjerg Formation. Ba: Bastians Dal Formation. Black dashes indicate uncertain contact. Black vertical lines indicate boreholes, R-1: Rødryggen-1; BH-1: Brorson Halvø-1.

Kuhn Ø (Surlyk 1978; Surlyk et al. 2021). The formation is wedge-shaped in a west–east direction and is estimated to reach a maximum thickness of 2 km.

The Valanginian stage is characterised by waning rift activity in the study area (late syn-rift) and transgression, whereas rifting continued in the axial areas to the east (Surlyk 1978, 1984, 2003; Surlyk & Korstgård 2013; Hovikoski et al. 2018). The Palnatokes Bjerg Formation was deposited during this period. The Formation crops out in Wollaston Forland, Kuhn Ø, Hochstetter Forland and Traill Ø (Surlyk 1978; Surlyk et al. 2021). Like the Lindemans Bugt Formation, the formation shows variable thickness in west-east transect and reaches a maximum thickness of 600 m. It includes the coarse-grained gravity flow deposits of the Young Sund and Falskebugt Members, and the fossiliferous fine-grained Albrechts Bugt and Rødryggen Members. The cored interval penetrates both fine-grained members and the recent biostratigraphic data suggest a Valanginan to Hauterivian age for these deposits (Alsen & Mutterlose 2009; Pauly et al. 2012; Möller et al. 2015).

In the Brorson Halvø core, the Palnatokes Bjerg Formation is gradationally overlain by a thin interval of upper Hauterivian sub-storm-wave-base bioturbated mudstones of the Stratumbjerg Formation (Bjerager *et al.* 2020). This formation crops out from Traill Ø in the south to Store Koldewey in the north and reaches its maximum thickness of 270 m in the Brorson Halvø area.

# 3. Samples and methods

Samples used for the present study include material from the fully cored Rødryggen-1 and Brorson Halvø-1 boreholes.

The Rødryggen-1 borehole reached a total depth (TD) of 234.66 m below terrain, with a core recovery of 99%. The lithostratigraphic units encountered include the Bernbjerg Formation (Kimmeridgian – lower Volgian), the Lindemans Bugt Formation (lower Volgian – upper Ryazanian) and the Palnatokes Bjerg Formation, Albrechts Bugt Member (upper Ryazanian – upper Valanginian; Alsen et al. 2023, this volume). The succession penetrated by

the borehole is stratigraphically complete and does not include any notable hiatuses. A total of 258 samples were subjected to total carbon (TC), total sulphur (TS), total organic carbon (TOC) and Rock-Eval type screening analyses, and subsets of these samples were selected for further analyses such as vitrinite reflectance analysis (12 samples), biological marker analysis (24 samples) and stable carbon isotopic analysis (20 samples).

The Brorson Halvø-1 borehole reached a TD of 225.88 m below terrain, with a core recovery of 99%. The lithostratigraphic units encountered include the Bernbjerg Formation (Kimmeridgian – lower Volgian), the Lindemans Bugt Formation (middle Volgian), the Palnatokes Bjerg Formation including the Albrechts Bugt Member (upper Ryazanian – upper Valanginian), and Rødryggen Member (Hauterivian) and the Stratumbjerg Formation (Barremian; Alsen et al. 2023, this volume). The succession penetrated by the borehole is stratigraphically incomplete and includes notable hiatuses with significant portions of the upper part of the lower Volgian and the lower part of the middle Volgian being absent. A significant portion of the upper part of the middle Volgian, the entire upper Volgian and lower Ryazanian successions are also missing (Fig. 3). A total of 232 samples were subjected to TC/TS/TOC-Rock-Eval type screening analyses, and subsets of these samples were selected for further analyses, such as vitrinite reflectance analysis (10 samples), biological marker analysis (18 samples) and stable carbon isotopic analysis (10 samples).

In addition to the borehole samples, a set of outcrop samples collected in the immediate vicinity of the Rødryggen-1 drill site were subjected to TC/TS/TOC-Rock-Eval type screening analyses. The sample set represents dense sampling of a c. 30 m thick profile of the uppermost part of the Storsletten Member (Lindemans Bugt Formation), extending stratigraphically downwards from the well-defined boundary between the Storsletten Member of the Lindemans Bugt Formation and the overlying Albrechts Bugt Member. The boundary thus serves as a datum for the sampling, which can also be recognised in the Rødryggen-1 core. The outcrop samples were collected from regular outcrops exposed by digging away the cover of loose shale debris.

Analytical procedures, summarised here, are detailed in full in Bojesen-Koefoed *et al.* (2018).

TC (wt%), TOC (wt%) and TS (wt%) were determined by combustion in a LECO CS-200 induction furnace. Petroleum potential was determined by Rock-Eval type pyrolysis using a Source Rock Analyzer (SRA) instrument, manufactured by Humble Instruments and Services and calibrated against the IFP160000 standard.

Particulate blocks for reflected light microscopy were prepared and measured for vitrinite reflectance according to international standards (Taylor *et al.* 1998). Several

samples were also qualitatively inspected in reflected white light and fluorescence-inducing blue light.

Solvent extraction (samples powdered to <250 µm) was carried out with methanol/dichloromethane 7:93 vol./vol. as solvent using a Soxtec $^{\text{TM}}$ . Asphaltenes were precipitated by addition of 40-fold excess n-pentane. Maltene fractions were separated into saturated, aromatic and NSO fractions (NSO: compounds containing nitrogen, sulphur and oxygen and other heteroatoms) by medium-pressure liquid chromatography (Radke *et al.* 1980).

Gas chromatography of saturated extract fractions was carried out using a Shimadzu GC-2010 instrument. Gas chromatography (GC) – mass spectrometry (MS) was carried out using an Agilent 6890N gas chromatograph connected to a Waters (Micromass) Quattro Micro GC tandem quadrupole-hexapole-quadrupole mass spectrometer.

# 4. Results

# 4.1 Thermal maturity

The thermal maturity of the successions penetrated by the Rødryggen-1 and Brorson Halvø-1 boreholes was assessed using a combination of several independent parameters including the temperature at the maximum rate of pyrolysate generation (°C)  $T_{\text{max}}$ and Production Index (PI) derived from Rock-Eval type pyrolysis, vitrinite reflectance (%Ro), and sterane isomerization ratios (Tables 1, 2, 4, 5). Fig. 4, upper panel, shows maturity data for both boreholes drilled versus depth. Fig. 4, lower panel, likewise shows maturity data versus depth but includes data on the stratigraphic breakdown and the presence of hiatuses in the Brorson Halvø-1 succession documented by Alsen et al. (2023, this volume). Hence, the Brorson Halvø-1 data are shifted to accommodate two major hiatuses, assuming the thickness of missing sections equals the thickness of corresponding sections in the Rødryggen-1 borehole. Despite this very simplistic approach, a surprisingly good match is obtained when considering detailed variations, see Fig. 5, which has been prepared in a similar way. In both boreholes, homohopane isomerization ratios have reached equilibrium distribution, and thus carry no information on the maturity gradient, but demonstrate that the burial temperature has exceeded that required for the equilibrium reaction to have been completed.

The Rødryggen-1 borehole shows clearly increasing trends with depth in all parameters (Fig. 4).  $T_{\rm max}$  increases from c. 420°C in the Ryazanian succession to 430°C in the Kimmeridgian succession at the base of the borehole. PI shows a parallel increase from c. 0.04 to 0.08, whereas the vitrinite reflectance increases from c. 0.48% Ro to 0.61% Ro, and sterane 20S/(20S+20R) isomerization ratio

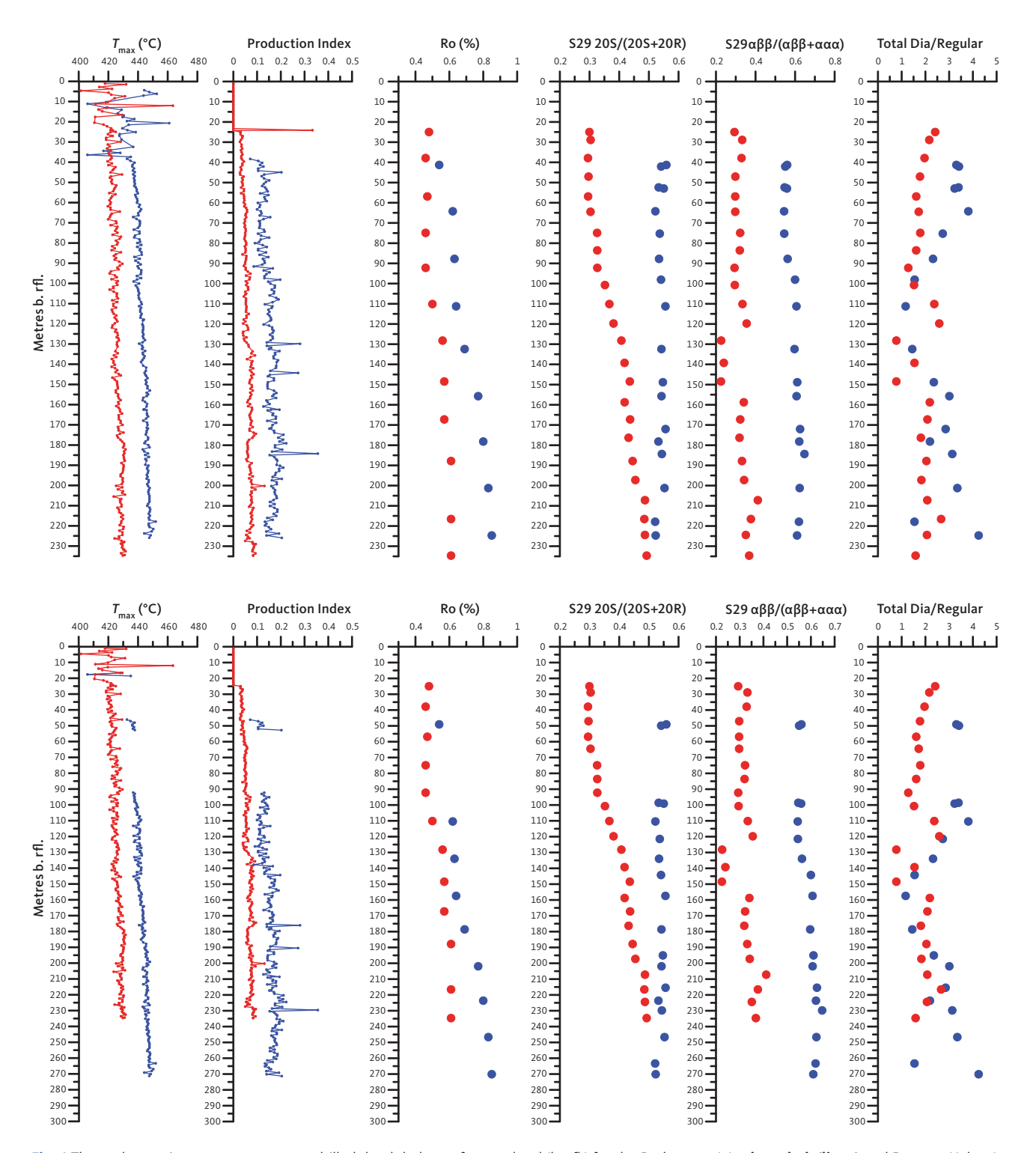


**Fig. 4** Thermal maturity parameters versus drilled depth below reference level (b. rfl.) for the Rødryggen-1 (**red symbols/lines**) and Brorson Halvø-1 (**blue symbols/lines**) boreholes (**upper panels**) and the Rødryggen-1 (**red symbols/lines**) and Brorson Halvø-1 (**blue symbols/lines**) boreholes taking into account stratigraphic information (**lower panels**; Alsen *et al.* 2023, this volume). Two hiatuses in the succession penetrated by the Brorson Halvø-1 borehole have been compensated for by assuming that the thickness of the missing section equals the equivalent section in the Rødryggen-1 borehole, which shows no hiatus. Hence, only samples of the Rødryggen-1 borehole show true drilled depths, while samples below the hiatus in the Brorson Halvø-1 section have been shifted to greater depths and may even appear deeper than the total depth (**TD**) of the Brorson Halvø-1 borehole.  $T_{max}$ : temperature of maximum rate of generation of pyrolysate during Rock-Eval type pyrolysis. **Production Index**: S1/(S1+S2) from Rock-Eval type pyrolysis. **Ro (%)**: vitrinite reflectance. **S29 20S/(20S+20R)**:  $C_{29}$  sterane  $20\alpha\alpha\alpha S/(20\alpha\alpha\alpha S+20\alpha\alpha\alpha R)$  isomer ratio. **S29**  $\alpha\beta\beta/(\alpha\beta\beta+\alpha\alpha\alpha)$ : C29 sterane  $20\alpha\beta\beta/(20\alpha\alpha\alpha+20\alpha\beta\beta)$  isomer ratio. **Total Dia/Regular:** total diasteranes to total regular steranes ratio.

goes from 0.30 to 0.49. Only the sterane  $\alpha\beta\beta/(\alpha\alpha\alpha+\alpha\beta\beta)$  isomerization ratio shows a slightly more irregular depth trend, but on average, this ratio increases from *c*. 0.29 to

0.36 over the succession penetrated by the Rødryggen-1 borehole. Combined, the maturity parameters agree in suggesting that the succession is thermally immature

with respect to petroleum generation but is approaching oil-window maturity at the base of the borehole. The existence of a clear maturity gradient over such a limited depth interval is unexpected, but a similar feature is found in the Blokelv-1 borehole in Jameson Land (Bojesen-Koefoed et al. 2018), and in the Brorson Halvø-1 borehole, situated approximately 10 km north-east of the Rødryggen-1 drill site. Over the succession penetrated by the Brorson Halvø-1 borehole,  $T_{\text{max}}$  increases from c. 435°C to 450°C with parallel increases in PI from c. 0.09 to 0.19, and in vitrinite reflectance from 0.54% Ro to 0.85% Ro. Sterane 20S/(20S+20R) isomerization ratios have reached equilibrium distribution in the entire succession, whereas the sterane  $\alpha\beta\beta/(\alpha\alpha\alpha+\alpha\beta\beta)$  isomer ratio increases from c. 0.55 to 0.62 with depth. Combined, the maturity parameters suggest that the upper part of the succession just enters the oil-generative window, which extends further towards the base of the borehole. Comparing the two panels of Fig. 4, the hiatus has little detectable effect on the maturity profile of the Brorson Halvø-1 borehole.

Despite the similar depth trends, which suggest a regionally high geothermal gradient, there is a notable difference in the level of thermal maturity observed in the two boreholes.

# 4.2 Petroleum potential and organic facies variations

The succession penetrated by the Rødryggen-1 borehole is stratigraphically complete with no notable hiatus. The Kimmeridgian and lower Volgian sections show a steady up-section decrease in TOC, from close to 6 wt% to c. 3 wt% at the transition to the middle Volgian (Fig. 5; Table 1). TS remains largely constant at c. 2.5 wt% over the same interval, whereas the S2-parameter displays some variation, which is shown by the derived Hydrogen Index (HI) that shows initial values close to 200 and a gradual upwards increase culminating locally with a HI of c. 300, some 35 m below the transition to the lower Volgian. The section above shows a decreasing trend with a minimum HI of c. 200 in the lowermost part of the lower Volgian section, followed by a notable increase towards the base of the middle Volgian to HI close to 350. Average HI remains largely constant at 300-350 in the middle Volgian and the lower portion of the Ryazanian sections, after which it essentially drops to zero. However, in general terms, the drilled succession shows only limited variation in kerogen type as defined by screening data, i.e. a gas-oil-prone kerogen type II/III (Fig. 6). Superimposed on the general trends described here are a number of subordinate trends. Both general and subordinate trends can often be tied to transgressive-regressive cycles indicated by detailed sedimentological analysis and various chemical proxies, and which in turn are linked to the tectonic evolution of the area as described by Hovikoski *et al.* (2023a,b).

The stratigraphically partly overlapping succession penetrated by the Brorson Halvø-1 borehole shows very similar detailed variations to the corresponding succession in the Rødryggen-1 borehole, except for the effects of increased thermal maturity, as shown by higher S1-values and lower S2-values and HI in the Brorson Halvø-1 borehole (Figs 5, 7; Table 2). Moreover, due to the presence of hiatuses, certain intervals are not present.

The uninterrupted sedimentary record demonstrated by the succession drilled by the Rødryggen-1 borehole and its low level of thermal maturity allow a more detailed assessment of the petroleum potential of the individual chronostratigraphic intervals. Using the method of Dahl et al. (2004), the average proportions of inert/dead carbon and the average HI of the live kerogen fraction (HI<sub>live</sub>) have been assessed (Fig. 8; Table 3). The results show that the Kimmeridgian, lower Volgian, middle Volgian and upper Volgian successions all include similar proportions of dead carbon, yielding values roughly in the range 1.5-2.0 wt%. Conversely, HI<sub>live</sub> tends to increase steadily up-section to culminate at a value of 610 in the upper Volgian section. The Ryazanian succession shows very low proportions of inert/dead carbon and slightly lower HI<sub>live</sub> than the upper Volgian section, but the data set is limited and includes non-source deposits.

Several biological marker parameters and stable carbon isotope ratio data ( $\delta^{13}$ C) show trends that follow those outlined for the screening data. Representative chromatograms and ion fragmentograms for both boreholes are shown in Figs 9 and 10. Key biological markers and  $\delta^{13}C$  data are listed in Tables 4 and 5, and selected biological marker parameters and  $\delta^{13}C$ data are shown versus depth for both boreholes in Fig. 11. With some scatter, the pristane/phytane ratio shows a slight, but clear upwards-decreasing trend over the entire drilled succession, with no clear differences between the two boreholes. The isohopane ratio (Nytoft 2011) shows a much better defined, but very similar trend, i.e. a clear decrease from the base of the succession until the base of the middle Volgian succession from where the ratio seems to become stable. The homohopane ratio (Peters et al. 2005 and references therein) shows a clear increase upwards through the succession until the middle Volgian where the ratio becomes invariant. The boreholes show identical trends, but the Brorson Halvø-1 data are shifted in the order of 5 percentage points towards higher values. The Gammacerane Index in the Rødryggen-1 borehole shows upwards-increase into the lower Volgian, followed by a decrease continuing into the middle Volgian and a sharp increase and stabilisation in

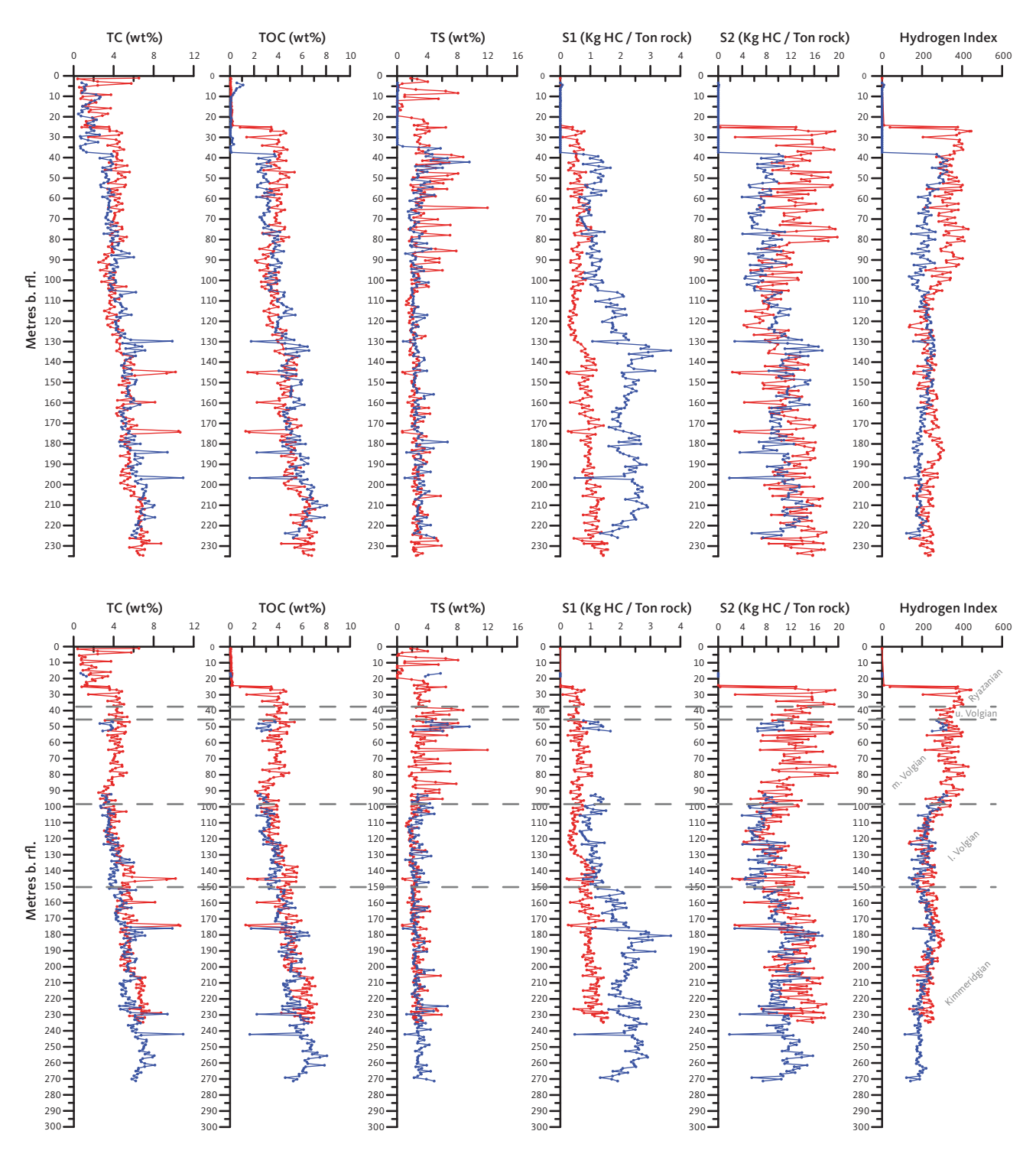


**Fig. 5** Organic geochemical screening parameters versus drilled depth below reference level (b. rfl.) for the Rødryggen-1 (**red symbols/lines**) and Brorson Halvø-1 (**blue symbols/lines**) boreholes (**upper panels**) and the Rødryggen-1 (**red symbols/lines**) and Brorson Halvø-1 (**blue symbols/lines**) boreholes taking into account stratigraphic information (**lower panels**; Alsen *et al.* 2023, this volume). Two hiatuses in the succession penetrated by the Brorson Halvø-1 borehole have been compensated for by assuming that the thickness of the missing section equals the equivalent section in the Rødryggen-1 borehole, which shows no hiatus. Hence, only samples of the Rødryggen-1 borehole show true drilled depths, while samples below the hiatuses in the Brorson Halvø-1 section have been shifted to greater depths and may even appear deeper than the total depth (**TD**) of the Brorson Halvø-1 borehole. Stratigraphic ages as defined by the Rødryggen-1 borehole.

the middle Volgian through the Ryazanian section. In the Brorson Halvø-1 borehole, no clear trends are observed. The proportion of  $C_{30}$  desmethyl steranes shows a steadily upwards-increasing trend throughout the entire penetrated successions with no obvious

differences observed between the two boreholes. The  $\delta^{13}C$  data shows a slight upwards-decrease in the Kimmeridgian section, which becomes more pronounced upwards through the lower Volgian section followed by stabilisation or even a slight increase in the middle

Table 1 Summary of organic geochemical data per stratigraphic interval of the Rødryggen-1 borehole

|                  |         | Ryazanian | upper Volgian | middle Volgian | lower Volgian | Kimmeridgian |
|------------------|---------|-----------|---------------|----------------|---------------|--------------|
|                  |         | (n = 23)  | (n = 9)       | (n = 55)       | (n = 55)      | (n = 97)     |
|                  | Minimum | 0.81      | 3.55          | 2.49           | 2.80          | 4.28         |
| TC               | Maximum | 5.03      | 5.36          | 5.60           | 10.19         | 10.66        |
|                  | Mean    | 3.14      | 4.39          | 4.07           | 4.55          | 6.00         |
|                  | Minimum | 0.02      | 2.52          | 1.58           | 0.73          | 0.70         |
| TS               | Maximum | 6.49      | 8.80          | 12.05          | 4.21          | 5.91         |
|                  | Mean    | 3.10      | 5.04          | 3.75           | 2.21          | 2.72         |
|                  | Minimum | 0.10      | 3.07          | 2.11           | 1.48          | 1.30         |
| TOC              | Maximum | 4.77      | 4.68          | 5.37           | 5.61          | 7.22         |
|                  | Mean    | 2.37      | 3.98          | 3.72           | 3.91          | 5.36         |
|                  | Minimum | 419       | 419           | 420            | 421           | 424          |
| T <sub>max</sub> | Maximum | 428       | 425           | 430            | 428           | 432          |
|                  | Mean    | 421       | 422           | 424            | 425           | 428          |
|                  | Minimum | 0.01      | 0.28          | 0.25           | 0.22          | 0.26         |
| S1               | Maximum | 0.80      | 0.60          | 1.05           | 1.20          | 1.58         |
|                  | Mean    | 0.46      | 0.47          | 0.64           | 0.60          | 1.01         |
|                  | Minimum | 0.33      | 8.93          | 5.39           | 2.36          | 2.77         |
| <b>S2</b>        | Maximum | 19.46     | 15.41         | 19.83          | 14.98         | 17.99        |
|                  | Mean    | 13.58     | 12.89         | 12.61          | 9.13          | 12.76        |
|                  | Minimum | 39        | 271           | 214            | 136           | 137          |
| HI               | Maximum | 445       | 363           | 431            | 342           | 308          |
|                  | Mean    | 355       | 324           | 335            | 231           | 238          |
|                  | Minimum | 0.03      | 0.03          | 0.03           | 0.04          | 0.05         |
| PI               | Maximum | 0.04      | 0.04          | 0.07           | 0.09          | 0.13         |
|                  | Mean    | 0.03      | 0.04          | 0.05           | 0.06          | 0.07         |

TC: Total Carbon (wt%). TS: Total Sulphur (wt%). TOC: Total Carbon (wt%).  $T_{max}$ :  $T_{max}$  (°C) from Rock-Eval pyrolysis, S1: Free hydrocarbons (mg/g) from Rock-Eval pyrolysis. S2: Pyrolytic hydrocarbons (mg/g) from Rock-Eval pyrolysis. HI: Hydrogen Index (100 × S2/TOC). PI: Production Index (S1/(S1+S2)).

 Table 2
 Summary of organic geochemical data per stratigraphic interval of the Brorson Halvø-1 borehole

|     |         | Ryazanian | middle Volgian | lower Volgian | Kimmeridgian |  |  |
|-----|---------|-----------|----------------|---------------|--------------|--|--|
|     |         | (n = 3)   | (n = 8)        | (n = 125)     | (n = 62)     |  |  |
|     | Minimum | 0.71      | 2.62           | 2.86          | 4.58         |  |  |
| гс  | Maximum | 1.28      | 3.93           | 3.91          | 10.95        |  |  |
|     | Mean    | 0.99      | 3.5 <b>4</b>   | 3.48          | 6.35         |  |  |
|     | Minimum | 3.76      | 2.44           | 2.44          | 1.03         |  |  |
| s   | Maximum | 5.79      | 9.63           | 9.63          | 6.72         |  |  |
|     | Mean    | 4.57      | 5.46           | 4.74          | 3.07         |  |  |
|     | Minimum | 0.04      | 2.23           | 1.76          | 1.64         |  |  |
| ос  | Maximum | 0.10      | 3.79           | 6.58          | 8.07         |  |  |
|     | Mean    | 0.06      | 3.08           | 4.05          | 5.74         |  |  |
|     | Minimum | 406       | 433            | 436           | 443          |  |  |
| max | Maximum | 435       | 438            | 438           | 452          |  |  |
|     | Mean    | 423       | 436            | 437           | 447          |  |  |
|     | Minimum | 0.00      | 0.76           | 0.76          | 0.48         |  |  |
| 1   | Maximum | 0.00      | 1.67           | 1.67          | 2.91         |  |  |
|     | Mean    | 0.00      | 1.19           | 1.25          | 2.23         |  |  |
|     | Minimum | 0.00      | 6.52           | 6.52          | 1.87         |  |  |
| 2   | Maximum | 0.00      | 10.94          | 10.94         | 15.77        |  |  |
|     | Mean    | 0.00      | 9.07           | 8.61          | 10.64        |  |  |
|     | Minimum | 0         | 250            | 250           | 114          |  |  |
| II  | Maximum | 0         | 324            | 325           | 220          |  |  |
|     | Mean    | 0         | 294            | 303           | 184          |  |  |
|     | Minimum | n.a.      | 0.07           | 0.10          | 0.13         |  |  |
| PI  | Maximum | n.a.      | 0.20           | 0.20          | 0.36         |  |  |
|     | Mean    | n.a.      | 0.12           | 0.13          | 0.18         |  |  |

TC: Total Carbon (wt%). TS: Total Sulphur (wt%). TOC: Total Carbon (wt%).  $T_{max}$ :  $T_{max}$  (°C) from Rock-Eval pyrolysis. S1: Free hydrocarbons (mg/g) from Rock-Eval pyrolysis. S2: Pyrolytic hydrocarbons (mg/g) from Rock-Eval pyrolysis. HI: Hydrogen Index (100 × S2/TOC). PI: Production Index (S1/(S1+S2)).

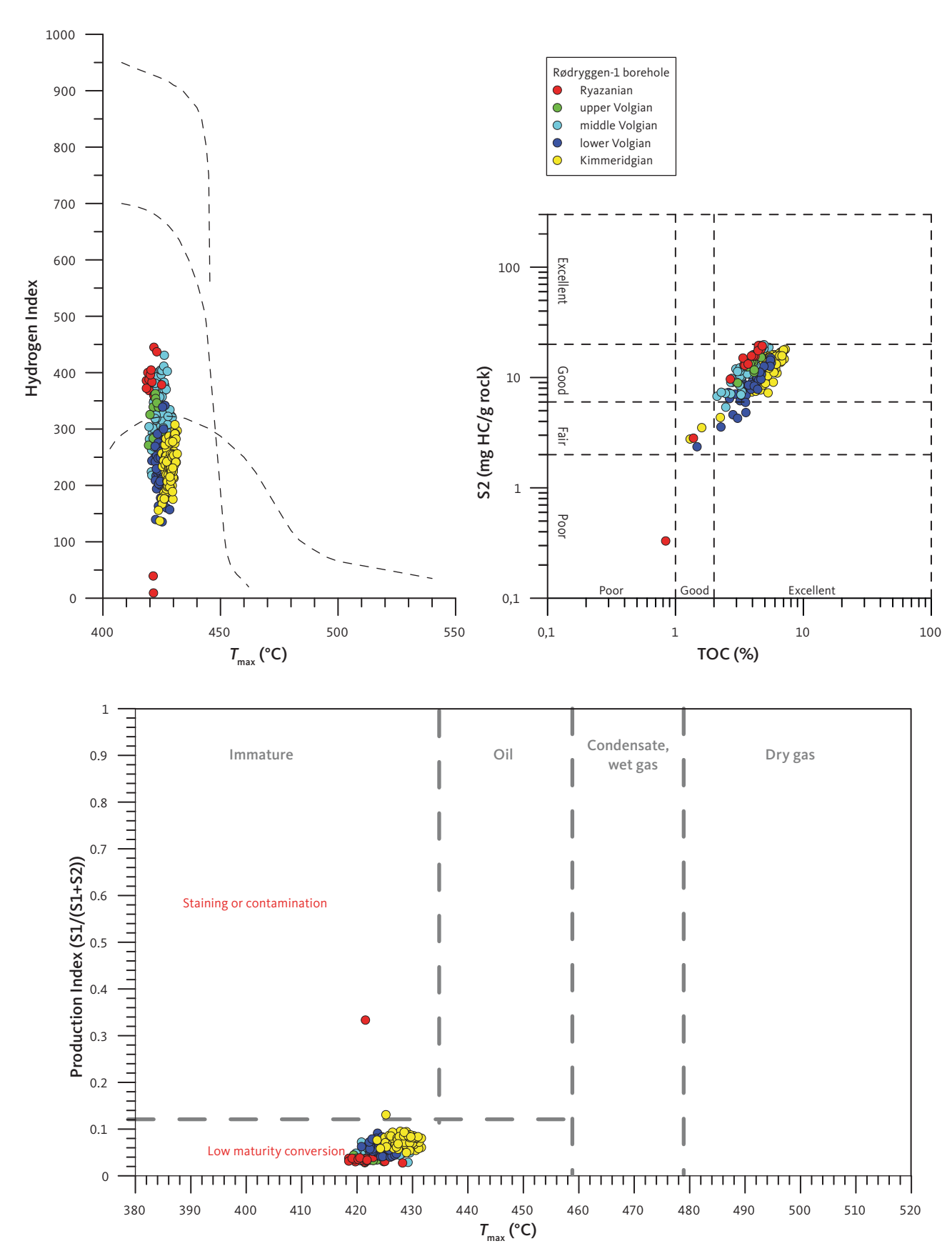


Fig. 6 Standard plots of organic geochemical screening data from the Rødryggen-1 borehole.

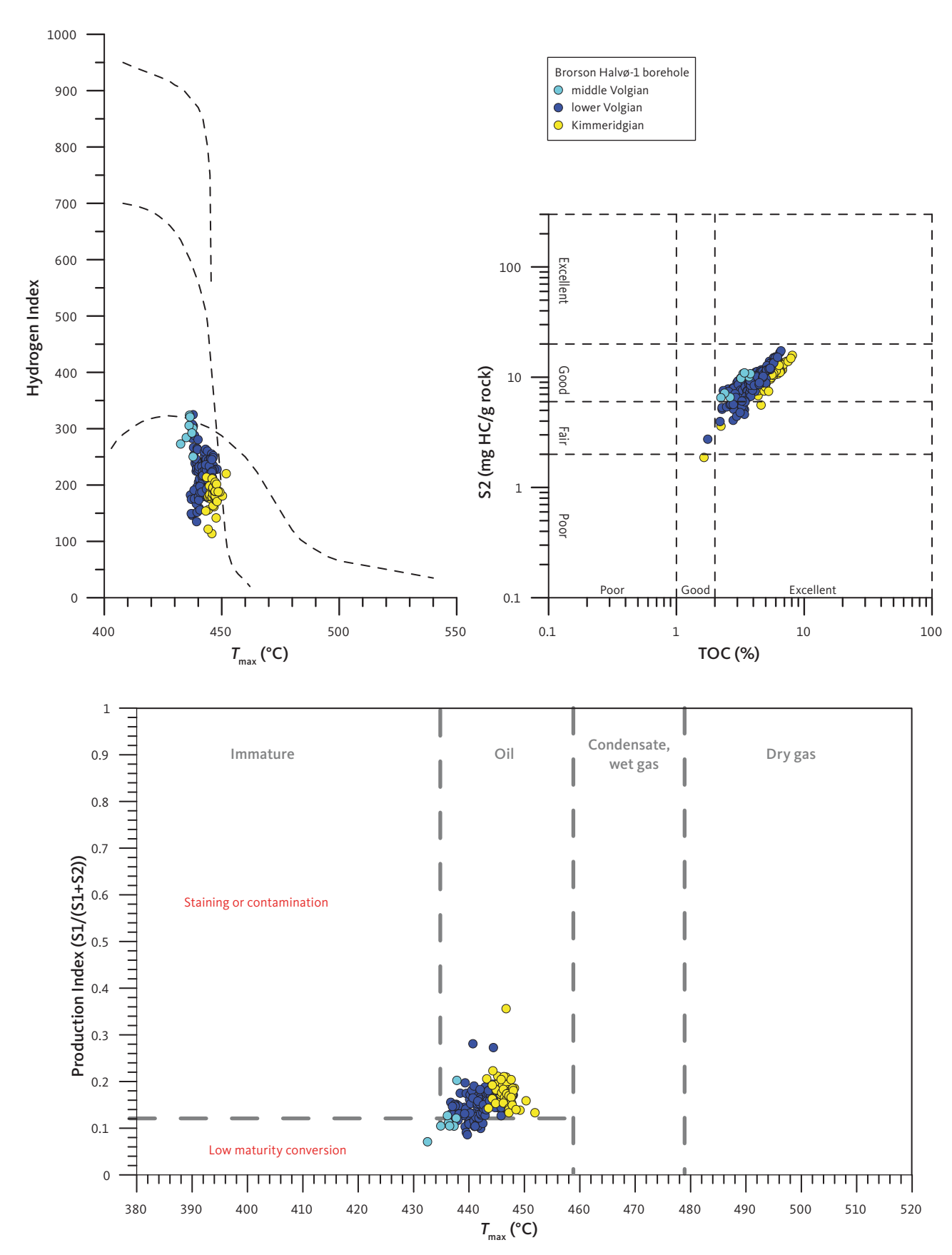


Fig. 7 Standard plots of organic geochemical screening data from the Brorson Halvø-1 borehole.

Volgian through Ryazanian section. Overall, the  $\delta^{13}$ C trend is mirrored in the homohopane ratio, the isohopane ratio and the proportion of  $C_{30}$  desmethyl steranes. Moreover,  $\delta^{13}$ C and the pristane/phytane ratio is reasonably well correlated, with increasing isotopic depletion and decreasing average pristane/phytane ratio up-section (Fig. 12).

Superimposed on the general trends described here, minor trends can be observed in several data sets, which combined with detailed sedimentology and main and trace element data are reported by Hovikoski *et al.* (2023a).

# 4.3 Outcrop versus borehole samples: weathering effects

The proximity of the sampled outcrop profile to the Rødryggen-1 drill site allows a close comparison of borehole versus outcrop data and thus assessment of weathering effects. Key data for outcrop and correlative borehole samples are shown in Fig. 13. The contents of TOC, and hence roughly the concentration of organic matter, do not show conspicuous differences between outcrop and borehole samples, but the quality of the organic matter, using HI as a proxy, is remarkably different. With only one exception, represented by a low-value spike on the drill-core sample data curve, the HI values are consistently and significantly lower in outcrop samples compared to drill-core samples. On average, borehole data show HI values (average HI 343) that are a factor of three to four greater than the values yielded in corresponding outcrop samples (average HI 102). TS concentrations in outcrop samples (average TS = 2.4%), which due to the clayey nature of the sediments can be safely assumed to primarily represent pyritic sulphur, are approximately half of the values observed in fresh drill-core samples (average TS = 4.3%).

# 5. Discussion

#### 5.1 Thermal maturity

The presence of clear and consistent gradients in several independent thermal maturity indicators over such limited depth intervals as represented by the drilled successions of the Rødryggen-1 and Brorson Halvø-1 boreholes is remarkable, but a similar trend was observed in the Blokelv-1 borehole in Jameson Land (Bojesen-Koefoed et al. 2018). The trend can be explained by considering the processes of thermal maturation and the amount of uplift and erosion that has taken place in the Wollaston Forland region. Based on apatite fission track data, Bonow & Japsen (2021) estimate that 2–3 km of sediments and volcanic deposits have been removed by erosion, which

with a slightly higher than normal geothermal gradient suggests that the succession was near to or within the 'oil window' during the time of maximum burial. Assuming a higher-than-normal geothermal gradient seems reasonable considering rifting and magmatic activity in the area. The processes associated with thermal maturation and the conversion of kerogen into petroleum are not linear but include several 'thresholds', known as 'coalification jumps' in coal-petrographic nomenclature (Taylor et al. 1998). Such coalification jumps are defined by rapid changes in the rates of the maturation processes. Incipient petroleum generation or the start of the oil window coincides with the first coalification jump at which point several processes related to petroleum generation accelerate. This causes the non-linearity of maturation profiles commonly seen in exploration wells entering or penetrating the oil-generative window. The thermal maturity of the Rødryggen-1 and Brorson Halvø-1 successions includes the transition into or remains within, respectively, the oil-generative window. Due to rapid uplift and erosion, which removed the overlying succession, petroleum generation ceased while leaving the unusual maturity gradient. The pronounced difference in thermal maturity between the two boreholes cannot readily be explained, but it may be speculated if the Brorson Halvø area was more affected by magmatic intrusions than the central parts of the basin where the Rødryggen-1 borehole is situated. Basaltic lavas and magmatic intrusions of various sizes crop out in the Brorson Halvø area whereas none are known in the immediate vicinity of the Rødryggen-1 borehole. The effects of magmatic intrusions and hydrothermal waters on encasing sedimentary rocks are well known (e.g. Searl 1994; Bojesen-Koefoed et al. 2018, 2020).

# 5.2 Petroleum potential and organic facies variations

The variations in organic facies reflect large-scale variations in depositional environment linked to relative sea-level changes, which in turn can be related to phases of the rifting in the region and tectonostratigraphic development. The overall trends are cursorily discussed further here, whereas a detailed account can be found in Hovikoski *et al.* (2023a,b), who also describe notable differences in the detailed sedimentology of the successions drilled by the two boreholes. However, since these have little impact on the general organic geochemical character of the deposits, they are not considered here.

The Kimmeridgian succession in general represents an oxygen-restricted depositional environment, receiving considerable amounts of allochthonous/terrigenous organic matter. Towards the end of the Kimmeridgian,

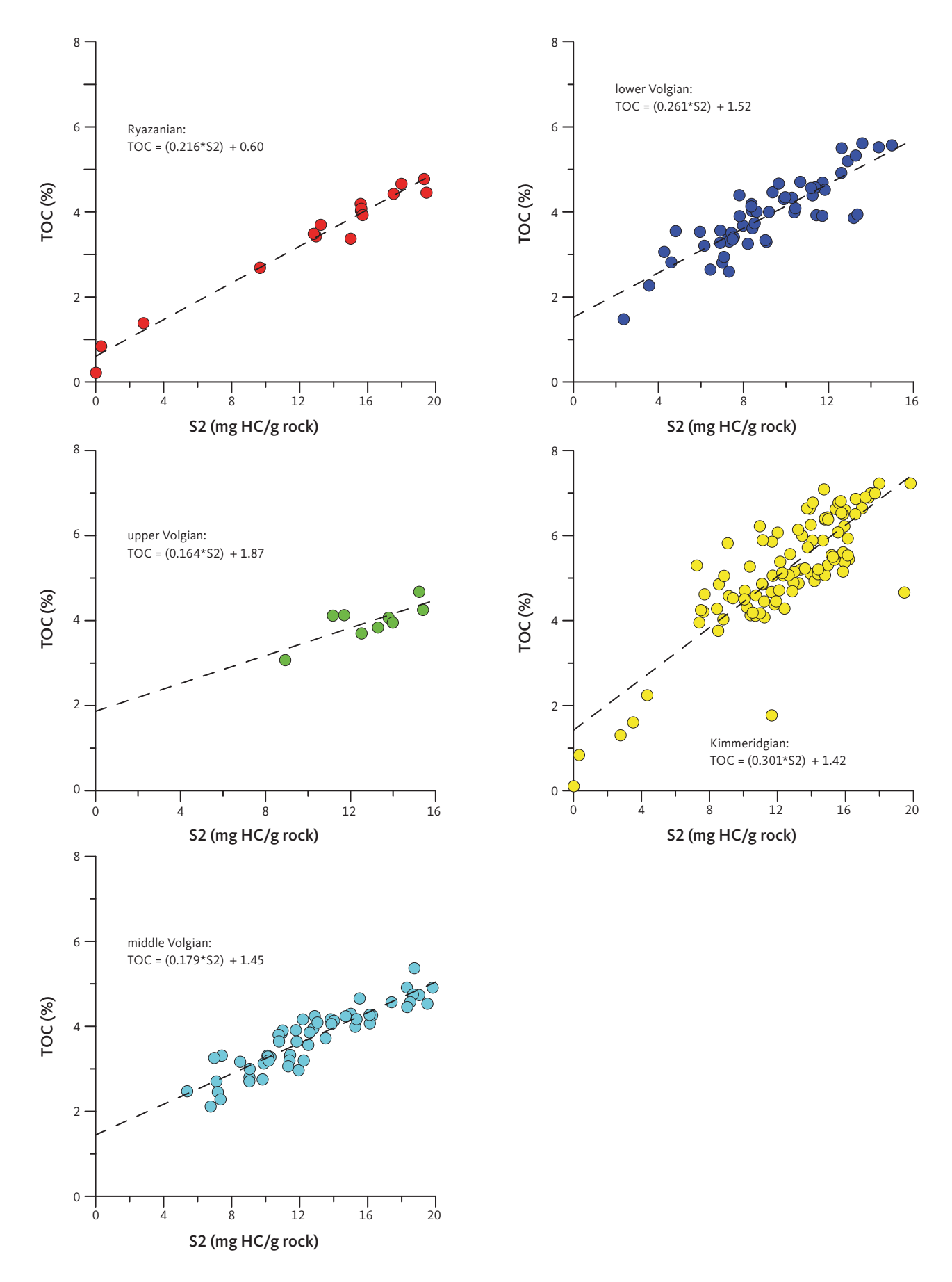


**Fig. 8** Assessment of HI<sub>live</sub> (i.e. HI of the actively petroleum-generating part of the kerogen) and dead carbon (i.e. the carbon fraction that is inert with respect to petroleum generation) per stratigraphic unit of the Rødryggen-1 borehole, following the procedure of Dahl *et al.* (2004). Data are listed in Table 3. **S2**: Pyrolytic hydrocarbons (mg/g) from Rock-Eval pyrolysis. **TOC**: Total organic carbon.

**Table 3** Average contents of inert carbon and hydrogen index values of the reactive kerogen fraction per stratigraphic interval of the Rødryggen-1 borehole. Calculated using the method of Dahl *et al.* (2004)

| Interval       | Inert C (%) | Live kerogen HI |
|----------------|-------------|-----------------|
| Ryazanian      | 0.60        | 463             |
| Late Volgian   | 1.87        | 610             |
| Middle Volgian | 1.45        | 559             |
| Lower Volgian  | 1.52        | 383             |
| Kimmeridgian   | 1.42        | 332             |

a gradual change occurs, pointing to increasing stagnation and reduced input of allochthonous/terrigenous organic matter and increasing proportions of autochthonous/marine organic matter in the sediments, corresponding to an overall transgression, probably eustatic in nature compounded by the effects of initial rifting (Hovikoski *et al.* 2023a). This is clearly demonstrated in the sediments by the decreasing levels of TOC, coinciding with steadily increasing values of HI. The transgressive trend is also manifest in decreasing pristane/ phytane and isohopane ratios, increasing proportions of marine  $C_{30}$  desmethyl steranes and slightly decreasing  $\delta^{13}C$  (Figs 5, 11).

After a period of stabilisation in the latest part of the Kimmeridgian, the lower Volgian succession records renewed transgression and further water column stagnation, extending well into the lower part of the middle Volgian. This is shown in the deposits by stable or slightly decreasing TOC paralleled by increasing HI, further decreases in pristane/phytane and isohopane ratios, increasing homohopane ratio and proportion of marine  $C_{30}$  desmethyl steranes plus further carbon isotopic depletion leading to decreasing  $\delta^{13}$ C (Figs 5, 11).

Overall, the succession from the lower part of the middle Volgian through the Ryazanian seems to represent a fairly stable highstand with sediments dominated by autochthonous organic matter with a background contribution of allochthonous terrigenous organics. Minor variations may perhaps be attributed to local development of the rift. Hence, most parameters remain stable or show only weak trends.

The general trends in relative sea level largely, albeit not fully, conform to the findings of Sneider *et al.* (1995) and Surlyk (2003), albeit with a shift in timing suggesting somewhat younger ages of the events recorded.

The Kimmeridgian through Ryazanian succession, however, overall records a development including a gradual decrease in terrigenous input, increasing stagnation and marine organic input. This is illustrated in Fig. 12, where  $\delta^{13}$ C and the pristane/phytane ratio both decrease upwards through the section. This is also depicted as a gradual transition from 'deltaic' sedimentation in the Kimmeridgian towards increasingly marine

sedimentation in the Volgian-Ryazanian. This development determines the petroleum-generation potential of the resulting deposits. The entire succession shows high potential for petroleum generation, developing from predominantly gas-oil-prone kerogen in the Kimmeridgian towards an increasingly oil-prone kerogen up-section (see also Section 5.4 Kinex™ modelling). This is also evident from the calculation of the average characteristics for partial sections defined by chronostratigraphic breakdown (Fig. 8; Table 3). The average HI shows a steady increase from the Kimmeridgian through the upper Volgian succession, and at the same time the proportion of inert carbon remains rather stable. The data on the Ryazanian are not fully representative for the petroleum potential since the data set also includes samples from the non-source section deposited after ventilation of the basin in the later part of the Ryazanian.

# 5.3 Outcrop versus borehole samples: weathering effects

Compared to correlative stratigraphic intervals in the greater North Atlantic area, outcrop samples of the Upper Jurassic - Lower Cretaceous succession in East and North-East Greenland often show surprisingly low petroleum potential (Requejo et al. 1989; Christiansen et al. 1992; Strogen et al. 2005; Bojesen-Koefoed et al. 2018). The exact reason for this is not fully understood but based on the data reported in this paper as well as the observations of Bojesen-Koefoed et al. (2018) an important cause may be the very large concentrations of finely disseminated pyrite present in the shales. Weathering of pyrite will ultimately generate sulphurous and sulphuric acids, which, by their oxidising nature, may attack kerogen and reduce its petroleum potential. In addition, decomposition through microbial sulphate reduction is conceivable since several strains of sulphate-reducing bacteria seem to be facultative anaerobes, and are thus able to survive or perhaps even proliferate in oxic environments (Sass & Cypionka 2007). In the present case, the true HI may be reduced by a factor of 3 or more due to weathering (Fig. 13). Hence, although the underlying reason is not fully clear, it can be concluded that in the present case, outcrop samples are unsuitable for assessing the true potential for petroleum generation of the deposits. A common sign of weathering of pyrite is encrustations of greenish-yellow jarosite on outcrop faces, and this occurs frequently in the succession studied here. Jarosite is a potassium-iron sulphate-mineral (KFe<sub>3</sub>(SO<sub>4</sub>)<sub>2</sub>(OH)<sub>6</sub>), characteristically formed by pyrite weathering. Several published studies report similar effects but with TOC levels often much more reduced than those observed here (Leythaeuser 1973; Clayton & Swetland 1978; Raiswell & Berner 1986;

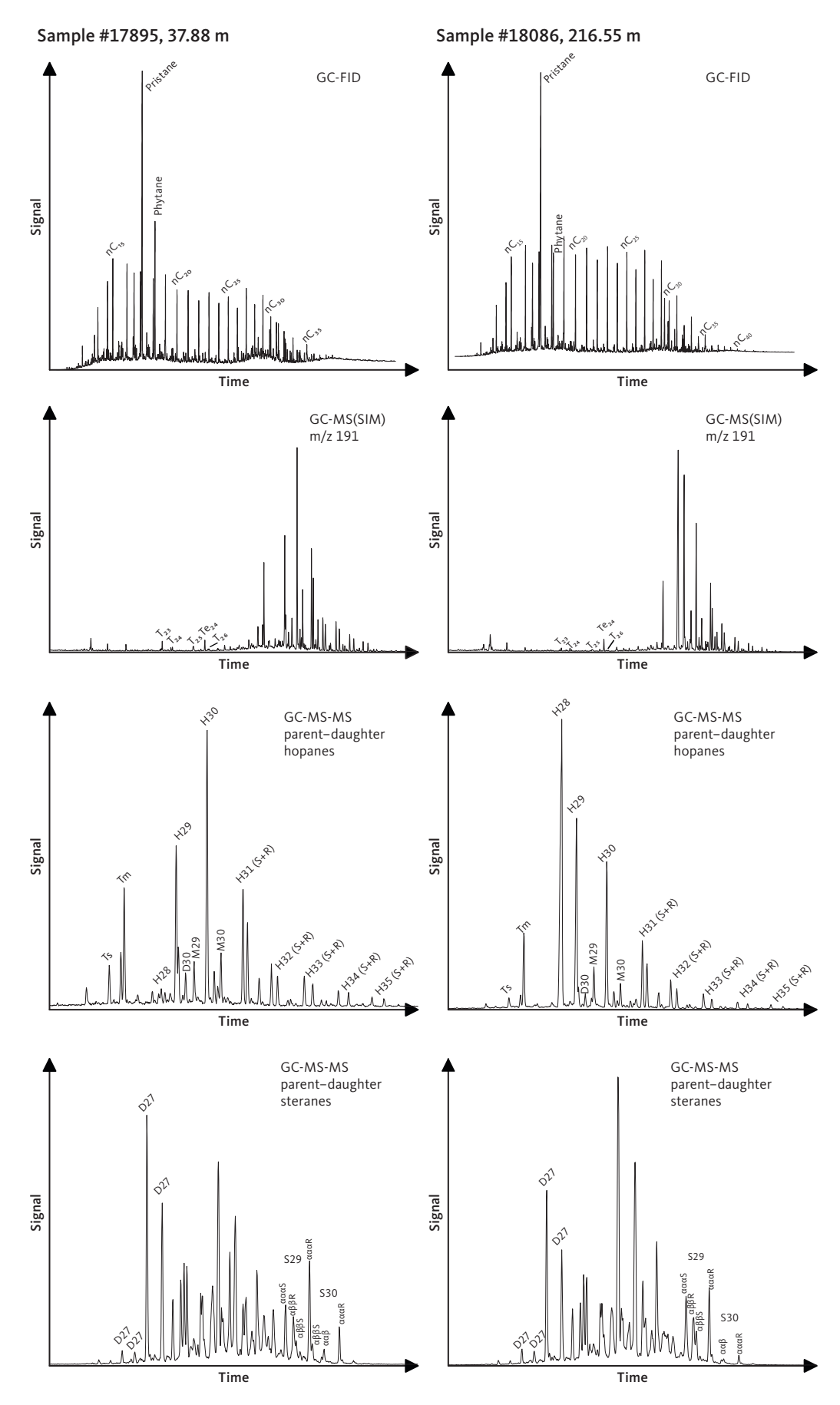
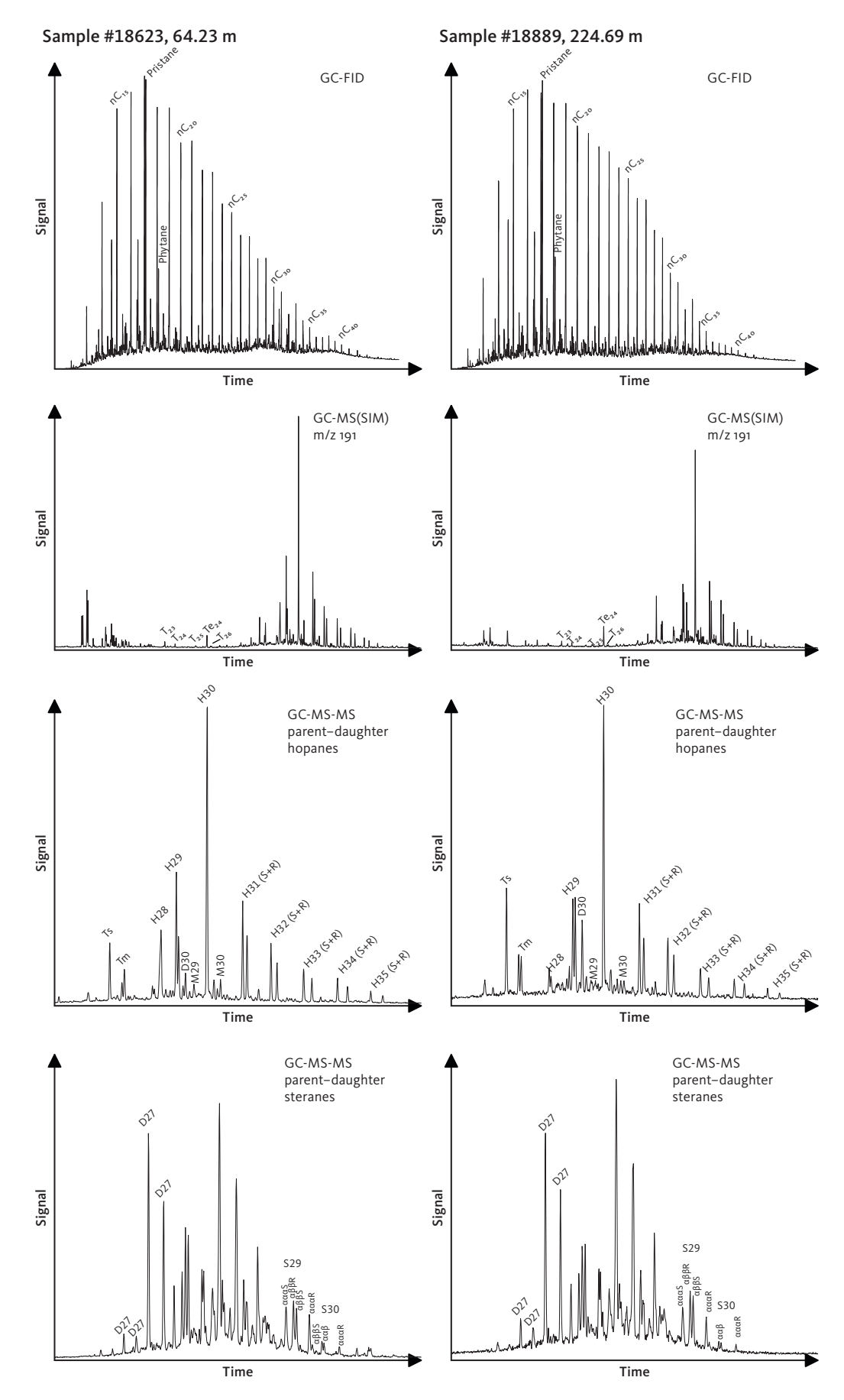


Fig. 9 Biological marker data from the Rødryggen-1 borehole. Characteristic fingerprints of samples representing the upper (sample #17895, 37.88 m, upper Volgian) and lower (sample #18086, 216.55 m, Kimmeridgian) parts of the drilled succession. GC-MS-MS parent-daughter traces for steranes and hopanes represent the sum of five and nine parent-daughter transitions, respectively.



**Fig. 10** Biological marker data from the Brorson Halvø-1 borehole. Characteristic fingerprints of samples representing the upper (sample #18623, 64.23 m, lower Volgian) and lower (sample #18889, 224.69 m, Kimmeridgian) parts of the drilled succession. GC-MS-MS parent-daughter traces for steranes and hopanes represent the sum of five and nine parent-daughter transitions, respectively.

Table 4 Key biological marker data from the Rødryggen-1 borehole

| Sample # | Stratigraphy   | Depth<br>(m) | Pr/Ph | BHN<br>index | D30<br>index | IHR  | нні  | S27 (%) | S28 (%) | S29 (%) | S30 (%) |      |      | Dia/Reg<br>steranes | δ¹³C<br>(total) |
|----------|----------------|--------------|-------|--------------|--------------|------|------|---------|---------|---------|---------|------|------|---------------------|-----------------|
| 17097    | Ryazanian      | 25.00        | 2.52  | 2.89         | 7.81         | 0.12 | 4.89 | 32.1    | 28.3    | 29.0    | 10.6    | 0.30 | 0.29 | 2.41                |                 |
| 17886    | Ryazanian      | 28.89        | 2.15  | 7.57         | 9.35         | 0.11 | 6.39 | 35.9    | 29.2    | 24.2    | 10.6    | 0.30 | 0.33 | 2.16                | -29.1           |
| 17895    | upper Volgian  | 37.88        | 2.55  | 2.13         | 9.22         | 0.11 | 4.69 | 37.1    | 27.9    | 27.1    | 7.9     | 0.29 | 0.33 | 1.96                | -29.0           |
| 17905    | middle Volgian | 47.06        | 2.85  | 1.98         | 9.68         | 0.12 | 4.18 | 35.4    | 27.9    | 26.0    | 10.7    | 0.30 | 0.30 | 1.77                | -29.2           |
| 17916    | middle Volgian | 56.88        | 2.24  | 4.68         | 9.73         | 0.11 | 6.65 | 30.6    | 33.1    | 26.8    | 9.4     | 0.30 | 0.30 | 1.61                | -29.2           |
| 17924    | middle Volgian | 64.47        | 3.34  | 7.79         | 6.01         | 0.11 | 4.24 | 35.1    | 29.7    | 26.8    | 8.3     | 0.30 | 0.30 | 1.72                |                 |
| 17935    | middle Volgian | 74.92        | 3.84  | 29.10        | 7.89         | 0.10 | 5.12 | 35.2    | 31.1    | 25.7    | 8.0     | 0.33 | 0.32 | 1.78                | -29.9           |
| 17944    | middle Volgian | 83.57        | 2.15  | 19.42        | 8.55         | 0.10 | 8.18 | 32.9    | 31.9    | 28.5    | 6.6     | 0.33 | 0.32 | 1.61                | -29.7           |
| 17953    | middle Volgian | 92.23        | 2.04  | 3.12         | 8.26         | 0.10 | 7.16 | 31.9    | 31.6    | 28.6    | 7.8     | 0.33 | 0.29 | 1.28                | -29.9           |
| 17962    | lower Volgian  | 100.73       | 2.21  | 1.40         | 6.23         | 0.10 | 6.42 | 31.5    | 31.7    | 29.0    | 7.9     | 0.35 | 0.30 | 1.52                | -29.4           |
| 17973    | lower Volgian  | 110.15       | 2.38  | 43.26        | 8.57         | 0.11 | 5.54 | 30.7    | 31.3    | 31.5    | 6.5     | 0.37 | 0.33 | 2.37                | -28.4           |
| 17983    | lower Volgian  | 119.77       | 3.19  | 68.03        | 8.71         | 0.12 | 4.23 | 30.6    | 29.6    | 34.7    | 5.0     | 0.38 | 0.36 | 2.58                | -28.1           |
| 17992    | lower Volgian  | 128.22       | 3.82  | 65.55        | 8.70         | 0.12 | 4.20 | 28.2    | 28.7    | 37.1    | 6.0     | 0.41 | 0.23 | 0.77                | -28.2           |
| 18002    | lower Volgian  | 139.26       | 3.13  | 82.51        | 9.27         | 0.11 | 5.53 | 26.7    | 17.8    | 51.0    | 4.4     | 0.42 | 0.24 | 1.54                | -27.3           |
| 18012    | lower Volgian  | 148.46       | 3.13  | 72.91        | 9.62         | 0.11 | 4.51 | 25.8    | 21.1    | 48.7    | 4.4     | 0.44 | 0.23 | 0.77                | -27.2           |
| 18023    | Kimmeridgian   | 158.77       | 2.64  | 70.66        | 9.81         | 0.12 | 4.86 | 28.7    | 27.9    | 37.8    | 5.6     | 0.42 | 0.34 | 2.18                | -27.8           |
| 18032    | Kimmeridgian   | 167.24       | 2.70  | 57.72        | 7.62         | 0.11 | 4.31 | 29.7    | 25.3    | 40.1    | 4.9     | 0.44 | 0.32 | 2.08                | -27.3           |
| 18042    | Kimmeridgian   | 176.33       | 2.51  | 47.73        | 8.73         | 0.10 | 4.63 | 31.8    | 27.3    | 35.4    | 5.6     | 0.43 | 0.32 | 1.81                |                 |
| 18054    | Kimmeridgian   | 187.85       | 4.18  | 28.12        | 7.25         | 0.12 | 2.85 | 31.7    | 27.8    | 33.3    | 7.1     | 0.45 | 0.33 | 2.04                | -27.3           |
| 18064    | Kimmeridgian   | 197.24       | 2.71  | 46.42        | 8.33         | 0.12 | 3.50 | 30.4    | 29.3    | 34.2    | 6.1     | 0.45 | 0.34 | 1.83                | -27.4           |
| 18075    | Kimmeridgian   | 207.21       | 3.07  | 53.48        | 8.45         | 0.11 | 3.84 | 30.3    | 29.2    | 34.6    | 5.8     | 0.49 | 0.41 | 2.08                | -26.7           |
| 18086    | Kimmeridgian   | 216.55       | 3.94  | 76.54        | 7.73         | 0.13 | 3.41 | 28.1    | 27.0    | 40.8    | 4.1     | 0.48 | 0.38 | 2.66                |                 |
| 18094    | Kimmeridgian   | 224.44       | 2.94  | 28.86        | 7.97         | 0.12 | 4.20 | 31.0    | 28.3    | 35.2    | 5.5     | 0.49 | 0.35 | 2.06                | -27.0           |
| 18109    | Kimmeridgian   | 234.66       | 3.54  | 78.08        | 8.37         | 0.12 | 4.36 | 28.2    | 28.1    | 37.9    | 5.8     | 0.49 | 0.37 | 1.59                | -26.6           |

Pr/Ph: pristane/phytane ratio. BNH Index: 100 × (28,30-bisnorhopane/(28,30-bisnorhopane+hopane)). D30 Index: 100×\*( $C_{30}$ -diahopane/( $C_{30}$ -diahopane+hopane)). IHR: isohopane ratio (Nytoft 2011). HHI: Homohopane Index: 100 × (H35 hopanes)/(sum of H31–35 hopanes), S27 (%), S28 (%), S29 (%), S30 (%). normalised distribution of  $C_{27}$ - $C_{30}$  total steranes, S29 (S/(S+R)).  $C_{29}$  sterane 20S/(20S+20R) isomer ratio, S29 (ββ/ββ+αα).  $C_{29}$  sterane αββ/ (αββ+ααα) isomer ratio, Dia/Reg. total diasteranes/total regular steranes,  $C_{29}$ 0 (total). stable carbon isotopic composition, total extract.

 Table 5
 Key biological marker data from the Brorson Halvø-1 borehole

| Sample # | Stratigraphy   | Depth<br>(m) | Pr/Ph | H28<br>index | D30<br>index | IHR  | нні   | S27 (%) | S28 (%) | S29 (%) | S30<br>(%) | S29<br>(S/(S+R)) | S29 $\beta\beta$ / ( $\beta\beta$ + $\alpha\alpha$ ) | Dia/Reg<br>steranes | $\delta^{13}$ C (total) |
|----------|----------------|--------------|-------|--------------|--------------|------|-------|---------|---------|---------|------------|------------------|--|---------------------|-------------------------|
| 18599    | middle Volgian | 41.28        | 2.19  | 0.00         | 8.73         | 0.10 | 12.91 | 34.0    | 28.8    | 25.9    | 11.4       | 0.56             | 0.56   | 3.30                | -30.0                   |
| 18600    | middle Volgian | 42.09        | 2.31  | 0.28         | 7.63         | 0.10 | 12.41 | 33.2    | 27.3    | 26.6    | 12.9       | 0.54             | 0.55   | 3.41                |                         |
| 18611    | lower Volgian  | 52.41        | 2.12  | 0.51         | 7.83         | 0.11 | 12.12 | 27.6    | 29.3    | 34.6    | 8.6        | 0.53             | 0.55   | 3.39                |                         |
| 20158    | lower Volgian  | 52.95        | 2.10  | 0.86         | 7.18         | 0.11 | 12.09 | 28.2    | 29.0    | 34.9    | 7.8        | 0.55             | 0.56   | 3.23                |                         |
| 18623    | lower Volgian  | 64.23        | 3.46  | 22.75        | 7.87         | 0.12 | 9.39  | 27.7    | 25.8    | 39.2    | 7.3        | 0.52             | 0.54   | 3.81                | -28.6                   |
| 18635    | lower Volgian  | 75.28        | 2.52  | 19.46        | 9.87         | 0.12 | 10.22 | 28.0    | 25.3    | 39.5    | 7.2        | 0.54             | 0.55   | 2.73                |                         |
| 18648    | lower Volgian  | 87.78        | 2.67  | 23.49        | 9.60         | 0.12 | 10.01 | 30.9    | 24.4    | 37.2    | 7.6        | 0.53             | 0.56   | 2.32                | -28.8                   |
| 18659    | lower Volgian  | 98.08        | 2.52  | 23.91        | 8.75         | 0.11 | 10.26 | 25.7    | 23.9    | 43.6    | 6.8        | 0.54             | 0.60   | 1.54                | -28.0                   |
| 18672    | lower Volgian  | 111.25       | 2.84  | 24.48        | 7.81         | 0.11 | 10.73 | 24.3    | 19.4    | 50.0    | 6.4        | 0.56             | 0.61   | 1.17                | -27.8                   |
| 18695    | lower Volgian  | 132.43       | 2.35  | 26.22        | 7.76         | 0.12 | 10.12 | 23.8    | 18.7    | 52.2    | 5.2        | 0.54             | 0.60   | 1.45                | -27.4                   |
| 18711    | lower Volgian  | 148.83       | 2.47  | 4.03         | 8.76         | 0.14 | 8.75  | 29.4    | 25.6    | 36.8    | 8.1        | 0.55             | 0.61   | 2.35                |                         |
| 18718    | lower Volgian  | 155.74       | 2.75  | 3.28         | 9.81         | 0.14 | 6.94  | 29.4    | 24.3    | 37.5    | 8.8        | 0.54             | 0.61   | 3.01                | -27.7                   |
| 19820    | Kimmeridgian   | 172.02       | 2.93  | 12.36        | 8.89         | 0.13 | 8.19  | 29.4    | 24.3    | 40.5    | 5.8        | 0.56             | 0.63   | 2.85                |                         |
| 18741    | Kimmeridgian   | 178.19       | 2.99  | 16.32        | 10.04        | 0.15 | 8.49  | 27.0    | 20.1    | 48.2    | 4.8        | 0.53             | 0.62   | 2.19                | -27.8                   |
| 19821    | Kimmeridgian   | 184.35       | 2.87  | 10.19        | 10.86        | 0.13 | 7.75  | 27.9    | 23.3    | 42.7    | 6.1        | 0.54             | 0.65   | 3.13                |                         |
| 18865    | Kimmeridgian   | 201.23       | 2.79  | 9.91         | 14.21        | 0.17 | 8.58  | 28.3    | 21.6    | 44.1    | 6.0        | 0.55             | 0.62   | 3.34                | -26.7                   |
| 18882    | Kimmeridgian   | 217.89       | 2.38  | 4.15         | 20.58        | 0.19 | 10.40 | 30.8    | 23.1    | 39.6    | 6.4        | 0.52             | 0.62   | 1.54                |                         |
| 18889    | Kimmeridgian   | 224.69       | 3.07  | 3.65         | 21.11        | 0.18 | 7.79  | 26.8    | 23.7    | 43.9    | 5.5        | 0.52             | 0.61   | 4.24                | -26.9                   |

Pr/Ph. pristane/phytane ratio, BNH index. 100 × (28,30-bisnorhopane/(28,30-bisnorhopane+hopane)), D30 index. 100 × ( $C_{30}$ -diahopane/( $C_{30}$ -diahopane+hopane)), IHR. isohopane ratio (Nytoft 2011), HHI. Homohopane Index: 100 × (H35 hopanes)/(sum of H31–35 hopanes), S27 (%), S28 (%), S29 (%), S30 (%). normalised distribution of  $C_{27}$ - $C_{30}$  total steranes, S29 (S/(S+R)).  $C_{29}$  sterane 20S/(20S+20R) isomer ratio, S29 (ββ/ββ+αα).  $C_{29}$  sterane αββ/ ( $\alpha$ ββ+ααα) isomer ratio, Dia/Reg. total diasteranes/total regular steranes,  $\delta$ 13C (total). stable carbon isotopic composition, total extract.

Littke *et al.* 1991; Petsch *et al.* 2000; Tang *et al.* 2018; Pan *et al.* 2022). Unravelling the causes for this difference is, however, beyond the scope of the present paper.

# 5.4 Kinex™ modelling

Variations in petroleum generation potential in the shale section of the Rødryggen-1 borehole were

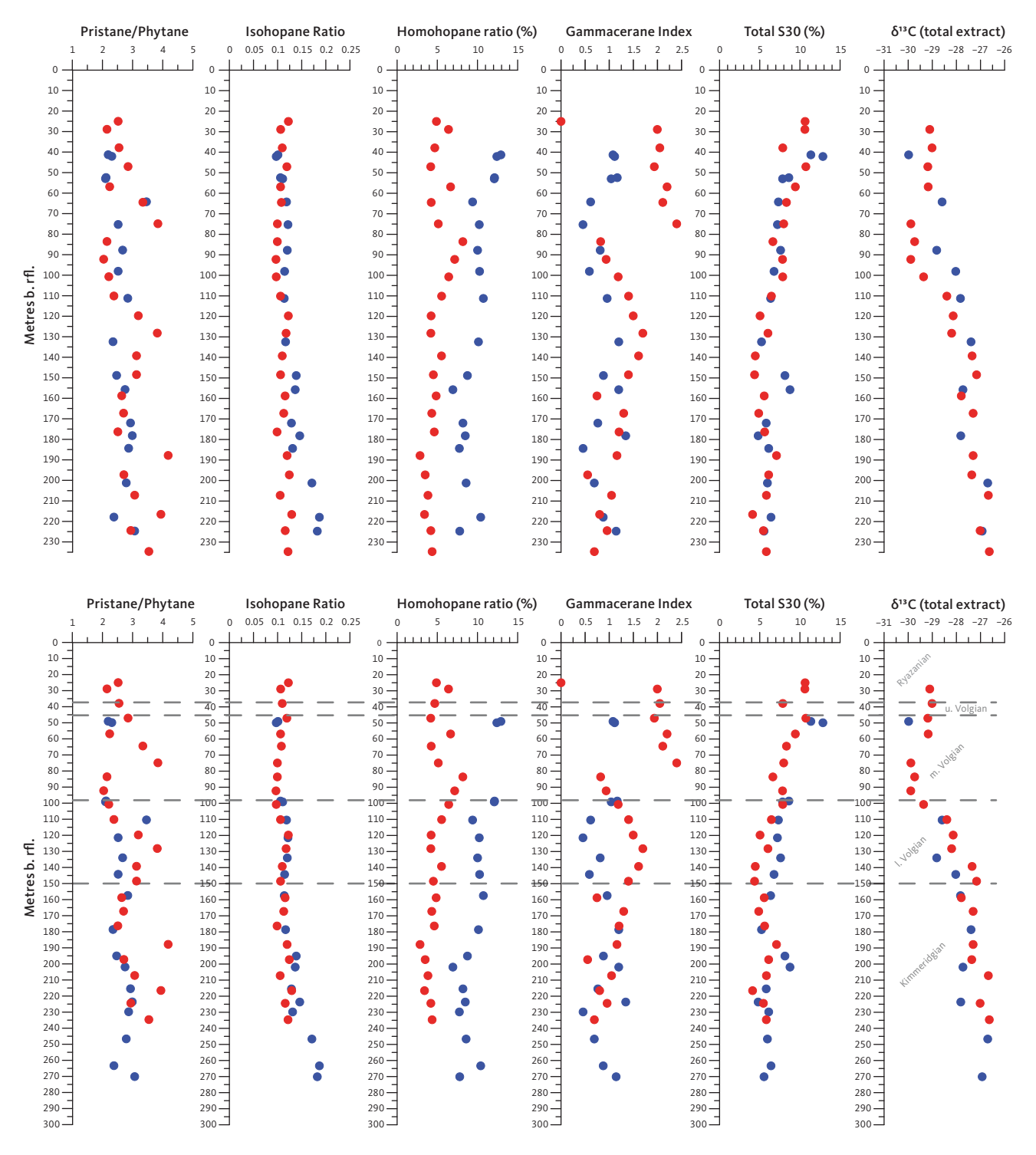


**Fig. 11** Biological marker parameters versus drilled depth below reference level (b.rfl.) for the Rødryggen-1 (**red symbols**) and Brorson Halvø-1 (**blue symbols**) boreholes (**upper panels**) and the Rødryggen-1 (**red symbols**) and Brorson Halvø-1 (**blue symbols**) boreholes taking into account stratigraphic information (**lower panels**; Alsen *et al.* 2023). Two hiatuses in the succession penetrated by the Brorson Halvø-1 borehole have been compensated for by assuming that the thickness of the missing section equals the equivalent section in the Rødryggen-1 borehole, which shows no hiatus. Hence, only samples of the Rødryggen-1 borehole show true drilled depths, while samples below the hiatuses in the Brorson Halvø-1 section have been shifted to greater depths and may even appear deeper than the total depth (TD) of the Brorson Halvø-1 borehole. Stratigraphic ages as defined by the Rødryggen-1 borehole.

quantified by estimating the generated fluid phases (oil and gas) using Kinex™ modelling (ZetaWare Inc.; herein referred to simply as Kinex modelling) to calculate the Ultimate Expulsion Potential (UEP; mmboe/km²). The UEP shows the ultimate expellable volume

of hydrocarbons in million barrels of oil equivalent (mmboe) per km² if the entire shale section cored by Rødryggen-1 passed through the petroleum generation window. Calculation of the UEP applies the kinetics of organofacies B (marine clay-rich shale, largely

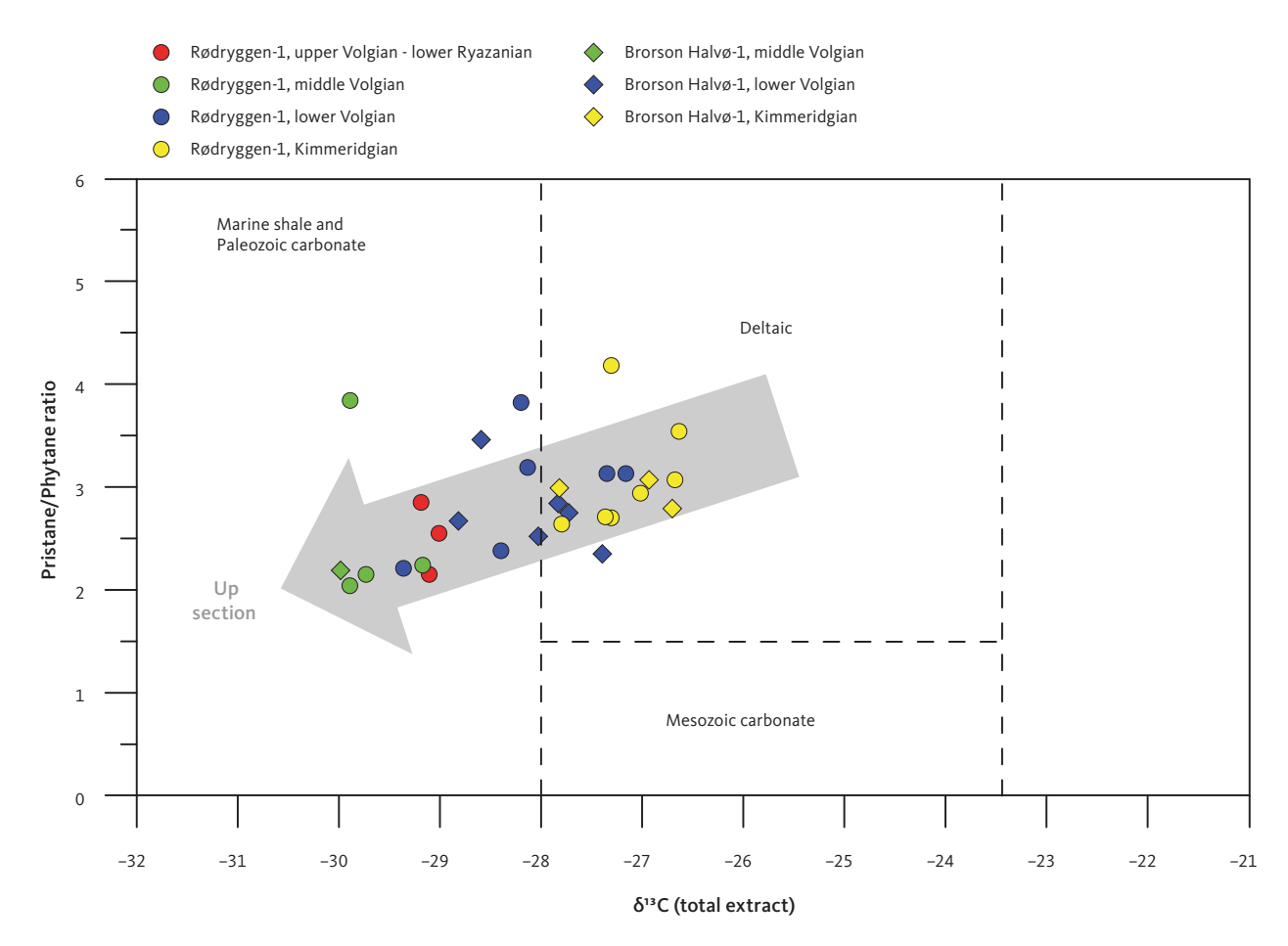


Fig. 12 Stable carbon isotope ratio ( $\delta^{13}$ C) of total extracts versus pristane/phytane ratio. Note gradual isotopic depletion occurs parallel to decreasing average pristane/phytane ratio up-section. Plot modified from Chung *et al.* (1992).

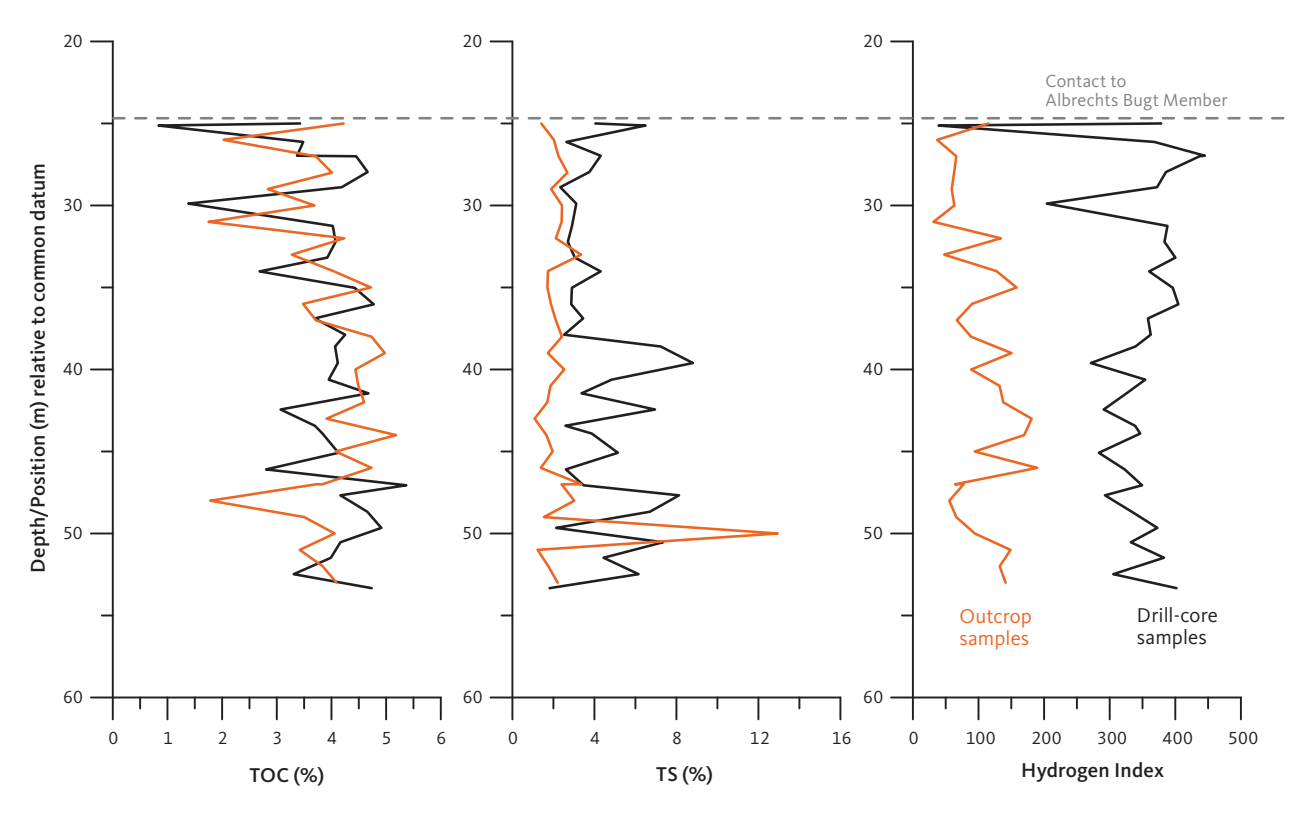
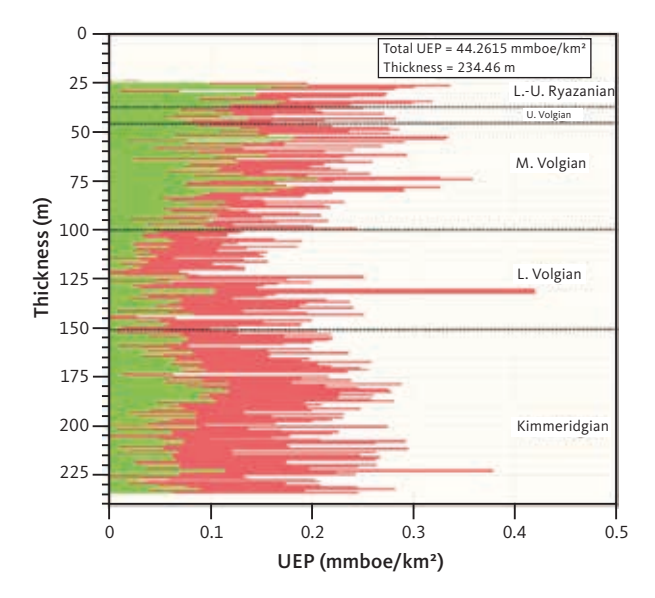
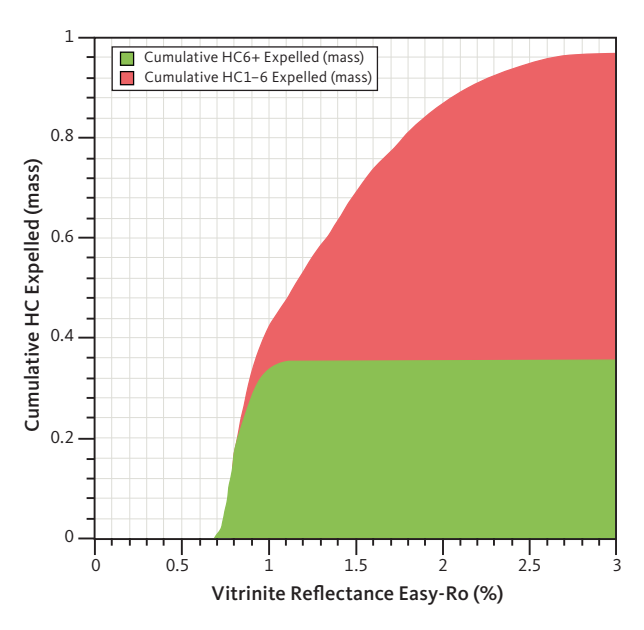


Fig. 13 Comparison of outcrop and borehole data at the Rødryggen-1 drill site. The outcrop profile was sampled using the sharp boundary to the Albrechts Bugt Member as datum. Orange curve: outcrop data. Black curve: Drill-core samples.



**Fig. 14** Ultimate Expulsion Potential (**UEP**) of the cored shale section on Rødryggen-1 borehole. The UEP profile through the shales shows varying source-rock quality and generation potential in terms of generation products. The shales are relatively gas-prone, but the middle Volgian to Ryazanian shales are mostly oil-prone. **L**.: Lower. **M**.: Middle. **U**.: Upper.



**Fig. 15** Cumulative expelled C6+ hydrocarbons (oil, HC6+) and C1-5 hydrocarbons (gas, HC1-6) of the Rødryggen-borehole. Oil generation terminates at about 1.0–1.1% Ro.

equal to Type II kerogen; Pepper & Corvi (1995a)) and the Pepper & Corvi (1995b) expulsion model where the retention of hydrocarbons is only adsorption-controlled (hydrocarbons will expel when the adsorption threshold is exceeded). The shale section was split into 258 subsections based on cuttings sampling density, resulting in an average subsection thickness of 0.91 m. Due to thermal immaturity of the shales (vitrinite reflectance <0.61% Ro), the measured TOC and HI values for each cuttings/subsection were used.

The total UEP of the c. 235 m thick shale section is c. 44 mmboe/km<sup>2</sup>, but the source-rock quality varies significantly through the shales (Fig. 14). The Kimmeridgian and lower Volgian sections show the poorest source-rock quality and are relatively gas-prone. The source-rock quality improves significantly in the middle Volgian to Ryazanian age mudstones that show increased capacity to generate liquid hydrocarbons (Fig. 14). However, overall the mudstone section in Rødryggen-1 is relatively gas-prone and does not possess the outstanding source-rock quality commonly observed in the upper Volgian and Ryazanian shales of the Kimmeridge Clay Formation and equivalents, such as the Spekk, Draupne, Mandal and Farsund Formations in the North Sea and Atlantic Margin (e.g. Von der Dick et al. 1989; Miller 1990; Chakhmakhchev et al. 1994; Klemme 1994; Telnæs et al. 1994; Fowler & McAlpine 1995; Isaksen & Ledje 2001; Ineson et al. 2003; Justwan & Dahl 2005; Justwan et al. 2005, 2006a,b; Petersen et al. 2010). The UEP can be divided into an Ultimate Expulsion Oil (UEO) and an Ultimate Expulsion Gas (UEG), which are c. 15.6 mmboe/km² and c. 28.6 mmboe/km², respectively. This is in line with HI values in the most oil-prone middle Volgian, upper Volgian and Ryazanian shales only reaching maximum values of 431 mg HC/g TOC, 405 mg HC/g TOC and 445 mg HC/g TOC. These moderate maximum HI values may reflect the narrow nature of the rift (approx. 30 km), which allows a background contribution of terrigenous organic matter with low potential for petroleum generation, irrespective of basin stagnation and oxygen deficiency. The relatively gas-prone character of the shales is also illustrated by the modelled cumulative expelled volumes where oil (HC6+) generation and expulsion end at about 1.0-1.1% Ro while significant gas generation continues at higher maturities (Fig. 15).

# 6. Conclusions

The Rødryggen-1 and Brorson Halvø-1 fully cored boreholes were drilled in Wollaston Forland (North-East Greenland, approx. 74°N). They have tested the development in sedimentary environments and petroleum-source potential of Upper Jurassic – Lower Cretaceous organic-rich mudstones at two different positions within an evolving halfgraben, situated at the margin of the main North Atlantic rift system, and thus partially detached from it. The overall halfgraben is, however, segmented in several subblocks, which evolved quasi-independently through the Upper Jurassic – Lower Cretaceous. The two boreholes were thus drilled at different locations within the Permpas–Hühnerbjerg block(s), bounded

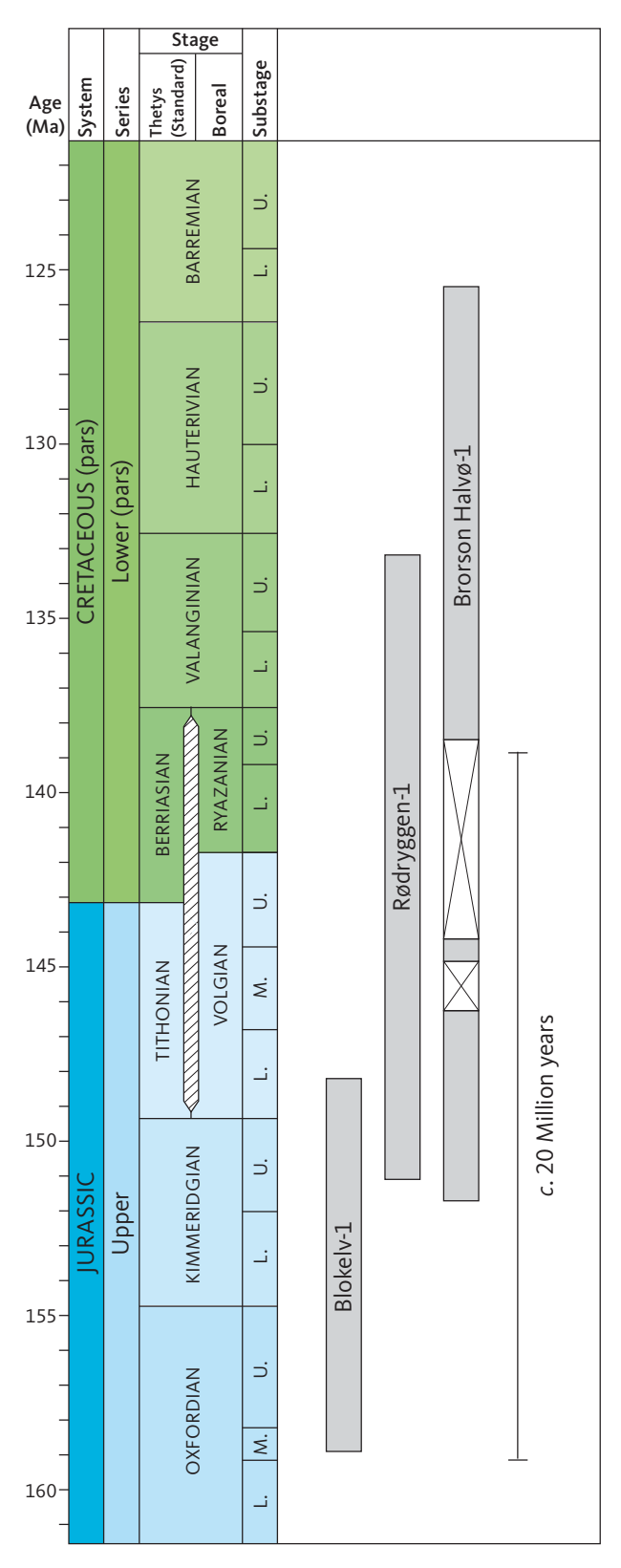


Fig. 16 Summary of the combined stratigraphic coverage of the Blokelv-1 (Jameson Land), Rødryggen-1 and Brorson Halvø-1 boreholes (Wollaston Forland). For details on the Blokelv-1 borehole, see Ineson & Bojesen-Koefoed (2018). Combined information from the three boreholes indicates that deposition of organic-rich mudstones with petroleum-generation potential prevailed for a period of approximately 20 million years in North-East Greenland during the Late Jurassic – Early Cretaceous. U.: Upper. M.: Middle. L.: Lower.

by the Dombjerg Fault to the west and the Hühnerbjerg Fault to the east, which probably were the main controlling faults in the studied block during the Late Jurassic.

The Rødryggen-1 borehole was drilled to a depth of approx. 236 m, in the central part of the basin and includes an uninterrupted mudstone succession ranging in age from the upper Kimmeridgian to the upper Valanginian. The Brorson Halvø-1 borehole was drilled to a depth of approximately 226 m close to the uplifted eastern crest of the same block and includes a succession ranging in age from the upper Kimmeridgian to the lower Barremian, however with two major hiatuses in the middle Volgian and upper Volgian – Ryazanian sections.

Based on the combined indications of several independent parameters such as  $T_{\text{max}'}$  vitrinite reflectance and sterane isomerization ratios, the Rødryggen-1 succession is thermally immature but approaching oil-window maturity, whereas the Brorson Halvø-1 succession is oil-window mature. The causes for the differences in thermal maturity are not clear but may be linked to the presence of abundant Palaeogene intrusions in the vicinity of the Brorson Halvø-1 drill site. Such intrusions are not known near the Rødryggen-1 drill site. Both boreholes show consistent increases in thermal maturity with depth, which is surprising considering the limited depth of the boreholes. The trends may be explained by rapid uplift, which quenched non-linear maturity trends, characteristic of the oil window. A similar trend was reported for the Blokelv-1 borehole in Jameson Land.

Bearing in mind the hiatus and the differences in thermal maturity between the two boreholes, the organic geochemical characteristics of the two successions are remarkably similar, despite the differences in setting within the graben system. Others have demonstrated notable differences in the detailed sedimentology of the two successions, but the impact of sedimentological processes on the organic matter content of the deposits seems to have been trivial in this case. This suggests that the organic matter content of the deposits was governed by higher order processes such as primary productivity and the preservation potential at the sediment-water interface, and that these factors remained rather constant irrespective of the sedimentary processes operating near the seabed.

The Kimmeridgian through Ryazanian succession in general records a transgressive development with gradual decrease in terrigenous organic matter input, increasing bottom-water stagnation oxygen deficiency and marine organic-matter input. Superimposed on the

overall trend are several minor trends related to the detailed development of the rift, discussed in detail by Hovikoski *et al.* (2023a,b).

The petroleum-generation potential of the immature/early mature Kimmeridgian through Ryazanian succession of the Rødryggen-1 borehole may be described as oil-prone or gas-oil-prone, growing increasingly oil-prone upwards. However, Kinex modelling demonstrates that the succession is relatively gasprone throughout due to the relatively high input of terrigenous organic matter due to the rather proximal setting of the basin compared to the outboard basins of the main rift.

A comparison of parallel sets of outcrop and drill-core samples from the Rødryggen outcrop and Rødryggen-1 borehole, respectively, shows that the HI of outcrop samples may be reduced to one third due to weathering. Although the underlying reason for this effect is not documented in full detail, it can be reasonably linked to weathering of abundant, finely disseminated pyrite present in the rocks, the products of which will attack the kerogen and deteriorate its petroleum-generation potential.

In summary, the combined evidence from the drilling of the Blokelv-1 borehole in Jameson Land and the Rødryggen-1 and Brorson Halvø-1 boreholes in Wollaston Forland (Fig. 16) indicates that continuous deposition of mudstones with high petroleum-generation potential prevailed in East and North-East Greenland over a timespan of approximately 20 million years in the Upper Jurassic – Lower Cretaceous.

# **Acknowledgments**

The drilling teams, including John Boserup, Anders Clausen, Peter Turner, Lars (Lasse) Thomsson, Andreas Hjort Frandsen, Anders Pilgaard and Annette Ryge, are thanked for their efforts and for keeping up the good spirits through the very challenging 2009 field season. The pilots Finn Rusanes and Göran Lindmark are thanked for diligent sling-work under very difficult conditions. Ditte Kiel-Dühring and Carsten Guvad are thanked for excellent laboratory work, and Hans Peter Nytoft is thanked for producing biological marker data. Jette Halskov and Annabeth Andersen assisted with the draft work. Helpful and constructive reviews by Drs Erdem Idiz and Iain C. Scotchman are gratefully acknowledged.

# Funding statement

The present work was funded by GEUS and a consortium of different companies of the international petroleum industry, who are all partners in a long-lasting collaborative effort, run by GEUS, concerning the geology of North-East Greenland.

# Competing interests

The authors declare that they have no competing interests

#### **Author contributions**

JABK: Writing – original draft, supervision, project administration, investigation, funding acquisition. PA: Investigation, funding acquisition. MB: Investigation. JH: Investigation, writing – original draft. PJ: Investigation. HNH: Investigation. HIP: Investigation. SP: Investigation. HV: Investigation.

# References

- Alsen, P. & Mutterlose, J. 2009: The early Cretaceous of North-East Greenland: a crossroads of belemnite migration. Palaeogeography, Palaeoclimatology, Palaeoecology 280, 168–182. https://doi.org/10.1016/j.palaeo.2009.06.011
- Alsen, P., Piasecki, S., Nøhr-Hansen, H., Pauly, S., Sheldon, E. & Hovikoski, J. 2023: Stratigraphy of the Upper Jurassic to lowermost Cretaceous in the Rødryggen-1 and Brorson Halvø-1 boreholes, Wollaston Forland, North-East Greenland. GEUS Bulletin 55, 8342 (this volume). https://doi.org/10.34194/geusb.v55.8342
- Bjerager, M., Alsen, P., Bojesen-Koefoed, J., Fyhn, M.B.W., Hovikoski, J., Ineson, J., Nøhr-Hansen, H., Nielsen, L.H., Piasecki, S. & Vosgerau, H. 2020: Cretaceous lithostratigraphy of North-East Greenland. Bulletin of the Geological Society of Denmark **68**, 37–93.
- Birkelund, T. & Perch-Nielsen, K. 1976: Late Palaeozoic Mesozoic evolution of central East Greenland. In: Escher, A. & Watt, W.S. (eds): Geology of Greenland. Geological Survey of Greenland 304–339.
- Bojesen-Koefoed, J.A., et al. 2020: A mid-Cretaceous petroleum sourcerock in the North Atlantic region? Implications of the Nanok-1 fully cored borehole, Hold with Hope, northeast Greenland. Marine and Petroleum Geology 117, 104414. https://doi.org/10.1016/j. marpetgeo.2020.104414
- Bojesen-Koefoed, J.A, Alsen, P., Bjerager, M., Hovikoski, J., Ineson, J.R., Johannessen, P., Olivarius, M., Piasecki, S. & Vosgerau, H. 2023: The Rødryggen-1 and Brorson Halvø-1 fully cored boreholes (Upper Jurassic Lower Cretaceous), Wollaston Forland, North-East Greenland an introduction. GEUS Bulletin **55**, 8350 (this volume). https://doi.org/10.34194/geusb.v55.8350
- Bojesen-Koefoed, J.A., Bjerager, M., Nytoft, H.P., Petersen, H.I., Piasecki, S. & Pilgaard, A. 2018: Petroleum potential of the Upper Jurassic Hareelv Formation, Jameson Land, East Greenland. Geological Survey of Denmark and Greenland Bulletin 42, 85–113. https://doi.org/10.34194/geusb.v42.4314
- Bonow, J.M. & Japsen, P. 2021: Peneplains and tectonics in North-East Greenland after opening of the North-East Atlantic. GEUS Bulletin **45**(1), 5297. https://doi.org/10.34194/geusb.v45.5297
- Chakhmakhchev, A., Sampei, Y. & Suzuki, N. 1994: Geochemical characteristics of oils and source rocks in the Yamal peninsula, West Siberia, Russia. Organic Geochemistry **22**, 311–322. https://doi.org/10.1016/0146-6380(94)90177-5
- Christiansen, F.G., Dam, G., Piasecki, S. & Stemmerik, L. 1992: A review of Upper Palaeozoic and Mesozoic source rocks from onshore East Greenland. In: Spencer, A.M. (ed.): Generation, accumulation and production of Europe's hydrocarbons II. Special Publication of the European Association of Petroleum Geologists 2, 151–161.
- Chung, H.M., Rooney, M.A., Toon, M.B. & Claypool, G.E. 1992: Carbon Isotope composition of marine crude oils (1). AAPG Bulletin 76, 1000– 1007. https://doi.org/10.1306/bdff8952-1718-11d7-8645000102c1865d
- Clayton, J.L. & Swetland, P.J. 1978: Subaerial weathering of sedimentary organic matter. Geochimica et Cosmochimica Acta **42**, 305–312. https://doi.org/10.1016/0016-7037(78)90183-7
- Dahl, B., Bojesen-Koefoed, J.A., Holm, A., Justwan, H., Rasmussen, E. & Thomsen, E. 2004: 05/00955 A new approach to interpreting Rock-Eval S<sub>2</sub> and TOC data for kerogen quality assessment. Organic Geochemistry **35**, 1461–1477. https://doi.org/10.1016/j.orggeochem.2004.07.003
- Fowler, M.G. & McAlpine, K.D. 1995: The Egret member, a prolific Kimmeridgian source rock from offshore eastern Canada. In: Katz, B.J. (ed.): Petroleum source rocks. Springer-Ver- lag 111–130.
- Fyhn, M.B.W. et al. 2021a: Central East and NE Greenland composite tectono-sedimentary element, East Greenland Rifted Margin, Greenland Sea. Geological Society, London, Memoirs 57, M57. https://doi.org/10.1144/M57-2017-15
- Fyhn, M.B.W., Hopper, J.R., Sandrin, A., Lauridsen, B.W., Heincke, B.H., Nøhr-Hansen, H., Andersen, M.S., Alsen, P. & Nielsen, T. 2021b: Three-phased latest Jurassic–Eocene rifting and mild mid-Cenozoic compression offshore NE Greenland. Tectonophysics **815**, 228990. https://doi.org/10.1016/j.tecto.2021.228990
- Henstra, G.A., et al. 2016: Depositional processes and stratigraphic architecture within a coarse-grained rift-margin turbidite system: The

- Wollaston Forland Group, east Greenland. Marine and Petroleum Geology **76**, 187–209. https://doi.org/10.1016/j.marpetgeo.2016.05.018
- Higgins, A.K. 2010: Exploration history and place names of northern East Greenland. Geological Survey of Denmark and Greenland Bulletin **21**, 368 pp. https://doi.org/10.34194/geusb.v21.4735
- Hovikoski, J. et al. 2023a: Late Jurassic Early Cretaceous marine deoxygenation in NE Greenland. Journal of the Geological Society **180** (3), jgs2022–058. https://doi.org/10.1144/jgs2022-058.
- Hovikoski, J., Ineson, J.R, Olivarius, M., Bojesen-Koefoed, J.A, Piasecki, S. & Alsen, P. 2023b: Upper Jurassic Lower Cretaceous of eastern Wollaston Forland, North-East Greenland: a distal marine record of an evolving rift. GEUS Bulletin 55, 8349 (this volume). https://doi.org/10.34194/geusb.v55.8349
- Hovikoski, J., Uchman, A., Alsen, P. & Ineson, J. 2018: Ichnological and sedimentological characteristics of submarine Fan-Delta deposits in a Half-Graben, Lower Cretaceous Palnatokes Bjerg Formation, NE Greenland. Ichnos 26, 28–57. https://doi.org/10.1080/10420940.2017. 1396981
- Ineson, J.R. & Bojesen-Koefoed, J.A. (eds) 2018: Petroleum geology of the Upper Jurassic Lower Cretaceous of East and Northeast Greenland: Blokelv-1 borehole, Jameson Land Basin. Geological Survey of Denmark and Greenland Bulletin **42**, 168 pp. https://doi.org/10.34194/geusb.v42
- Ineson, J.R., Bojesen-Koefoed, J.A., Dybkjær, K. & Nielsen, L.H. 2003: Volgian-Ryazanian 'hot shales' of the Bo Member (Farsund Formation) in the Danish Central Graben, North Sea: stratigraphy, facies and geochemistry. Geological Survey of Denmark and Greenland Bulletin 1, 403–436. https://doi.org/10.34194/geusb.v1.4679
- Isaksen, G.H & Ledje H.I. 2001: Source rock quality and hydrocarbon migration pathways within the greater Utsira High area, Viking Graben, Norwegian North Sea. AAPG Bulletin **85**(5), 861–883. https://doi.org/10.1306/8626ca23-173b-11d7-8645000102c1865d
- Justwan, H. & Dahl, B. 2005: Quantitative hydrocarbon potential mapping and organofacies study in the Greater Balder Area, Norwegian North Sea. Geological Society, London, Petroleum Geology Conference Series 6(1), 1317–1329. https://doi.org/10.1144/0061317
- Justwan, H., Dahl, B., Isaksen, G.H. & Meisingset, I. 2005: Late to middle Jurassic source facies and quality variations, South Viking Graben, North Sea. Journal of Petroleum Geology **28**(3), 241–268. https://doi.org/10.1111/j.1747-5457.2005.tb00082.x
- Justwan, H., Dahl, B. & Isaksen, G.H. 2006a: Geochemical characterisation and genetic origin of oils and condensates in the South Viking Graben, Norway. Marine and Petroleum Geology 23(2), 213–239. https://doi.org/10.1016/j.marpetgeo.2005.07.003
- Justwan, H., Meisingset, I., Dahl, B. & Isaksen, G.H. 2006b: Geothermal history and petroleum generation in the Norwegian South Viking Graben revealed by pseudo-3D basin modelling. Marine and Petroleum Geology 23(8), 791–819. https://doi.org/10.1016/j.marpetgeo.2006.07.001
- Klemme, H.D. 1994: Petroleum systems of the World involving Upper Jurassic source rocks. In: Magoon, L.B & Dow, W.G (eds): The petroleum system from source to trap. AAPG Memoir 60, 51–72. https://doi. org/10.1306/M60585C3
- Leythaeuser, D. 1973: Effects of weathering on organic matter in shales. Geochimica et Cosmochimica Acta **37**(1), 113–120. https://doi.org/10.1016/0016-7037(73)90249-4
- Littke, R., Klussmann, U., Krooss, B. & Leythaeuser, D. 1991: Quantification of loss of calcite, pyrite, and organic matter due to weathering of Toarcian black shales and effects on kerogen and bitumen characteristics. Geochimica et Cosmochimica Acta 55(11), 3369–3378. https://doi.org/10.1016/0016-7037(91)90494-p
- Miller, R.G. 1990: A paleoceanographic approach to the Kimmeridge Clay Formation. In: Huc, A.Y. (ed.): Deposition of organic facies. AAPG Studies in Geology 30, 13–26. https://doi.org/10.1306/st30517c2
- Morgans-Bell, H.S., Coe, A.I., Hesselbo, S.P., Jenkyns, H.C., Weedon, G.P., Marshall, J.E.A., Tyson, R.V. & Williams, C.J. 2001: Integrated stratigraphy of the Kimmeridge clay formation (Upper Jurassic) based on exposures and boreholes in south Dorset, UK. Geological Magazine 138(5), 511–539. https://doi.org/10.1017/s0016756801005738
- Möller, C., Mutterlose, J. & Alsen, P. 2015: Integrated stratigraphy of Lower Cretaceous sediments (Ryazanian–Hauterivian) from

- North-East Greenland. Palaeogeography, Palaeoclimatology, Palaeoecology **437**, 85–97. https://doi.org/10.1016/j.palaeo.2015.07.014
- Nytoft, H.P. 2011: Novel side chain methylated and hexacyclic hopanes: identification by synthesis, distribution in a worldwide set of coals and crude oils and use as markers for oxic depositional environments.

  Organic Geochemistry 42(5), 520–539. https://doi.org/10.1016/j.orggeochem.2011.03.006
- Pan, S., Liao, Y., Jiang, B., Wan, Z. & Wang, F. 2022: Impact of natural weathering on source rocks: organic and inorganic geochemical evidence from the Triassic Chang 7 outcrop profile in Tongchuan of the Southern Ordos Basin (China). International Journal of Coal Geology 263, 104119. https://doi.org/10.1016/j.coal.2022.104119
- Pauly, S., Mutterlose, J. & Alsen, P 2012: Lower Cretaceous (upper Ryazanian–Hauterivian) chronostratigraphy of high latitudes (North-East Greenland). Cretaceous Research 34, 308–326. https://doi. org/10.1016/j.cretres.2011.11.011
- Pepper, A.S. & Corvi, P.J. 1995a: Simple kinetic models of petroleum formation. Part I: oil and gas generation from kerogen. Marine and Petroleum Geology **12**(3), 291–319. https://doi. org/10.1016/0264-8172(95)98381-e
- Pepper, A.S. & Corvi, P.J., 1995b: Simple kinetic models of petroleum formation, Part III: modelling an open system. Marine and Petroleum Geology 12(4), 417–452. https://doi.org/10.1016/0264-8172(95)96904-5
- Petsch, S.T., Berner, R.A. & Eglinton, T.I. 2000: A field study of the chemical weathering of ancient sedimentary organic matter. Organic Geochemistry 31(5), 475–487. https://doi.org/10.1016/s0146-6380(00)00014-0
- Peters, K.E., Walters, C.C. & Moldowan, J.M. 2005: The biomarker guide, volumes 1+2, 1155 pp. Cambridge University Press.
- Petersen, H.I., Nytoft, H.P., Vosgerau, H., Andersen, C., Bojesen-Koefoed, J.A. & Mathiesen, A. 2010: Source rock quality and maturity and oil types in the NW Danish Central Graben: implications for petroleum prospectivity evaluation in an Upper Jurassic sandstone play area. Geological Society, London, Petroleum Geology Conference Series 7(1), 95–111. https://doi.org/10.1144/0070095
- Piasecki, S., Bojesen-Koefoed, J.A. & Alsen, P. 2020: Geology of the Lower Cretaceous in the Falkebjerg area, Wollaston Forland, northern East Greenland. Bulletin of the Geological Society of Denmark 68, 155–170. https://doi.org/10.37570/bgsd-2020-68-07
- Radke, M., Willsch, H. & Welte, D.H. 1980: Preparative hydrocarbon group determination by automated medium pressure liquid chromatography. Analytical Chemistry 52(3), 406–411. https://doi.org/10.1021/ ac50053a009
- Raiswell, R. & Berner, R.A. 1986: Pyrite and organic matter in Phanerozoic normal marine shales. Geochimica et Cosmochimica Acta 50(9), 1967–1976. https://doi.org/10.1016/0016-7037(86)90252-8
- Requejo, A.G., Hollywood, J. & Halpern, H.I. 1989: Recognition and source correlation of migrated hydrocarbons in Upper Jurassic Hareelv Formation, Jameson Land, East Greenland. AAPG Bulletin **73**(9), 1065–1088. https://doi.org/10.1306/44b4a53c-170a-11d7-8645000102c1865d
- Sass, H. & Cypionka, H. 2007: Response of sulphate-reducing bacteria to oxygen. In: Barton, L. & Hamilton, W. (eds): Sulphate-reducing bacteria: Environmental and engineered systems, 167–184. Cambridge University Press. https://doi.org/10.1017/CBO9780511541490.006
- Scotchman, I.C, Doré, A.G. & Spencer, A.M. 2016: Petroleum systems and results of exploration on the Atlantic margins of the UK, Faroes & Ireland: what have we learnt? Geological Society, London, Petroleum Geology Conference series 8(1), 187–197. https://doi.org/10.1144/ PGC8.14
- Searl, A. 1994: Diagenetic destruction of reservoir potential in shallow marine sandstones of the Broadford Beds (Lower Jurassic), northwest Scotland: depositional versus burial and thermal history controls on porosity destruction. Marine and Petroleum Geology 11(2), 131–147. https://doi.org/10.1016/0264-8172(94)90090-6
- Sneider, J.S., DeClarens, P. & Vail, P.R. 1995: Sequence stratigraphy of the Middle to Upper Jurassic, Viking Graben, North Sea. In: Steel, R.J. et al. (eds): Sequence stratigraphy on the Northwest European margin. Norwegian Petroleum Society Special Publications 5, 167–197. https:// doi.org/10.1016/s0928-8937(06)80068-8
- Strogen, D.P., Burwood, R. & Whitham, A.G. 2005: Sedimentology and geochemistry of Late Jurassic organic-rich shelfal mudstones from

- East Greenland: regional and stratigraphic variations in source-rock quality. Geological Society, London, Petroleum Geology Conference Series 6(1), 903–912. https://doi.org/10.1144/0060903
- Surlyk, F. 1978: Submarine fan sedimentation along fault scarps on tilted fault blocks (Jurassic–Cretaceous boundary, East Greenland). Bulletin Grønlands Geologiske Undersøgelse 128, 117. https://doi.org/10.34194/bullggu.v128.6670
- Surlyk, F. 1984: Fan-delta to submarine fan conglomerates of the Volgian-Valanginian Wollaston Forland Group, East Greenland. In: Koster, E.H. & Steel, R.J. (eds): Sedimentology of gravel and conglomerates. Canadian Society of Petroleum Geologists Memoir 10, 359–382
- Surlyk, F. 1990: A Jurassic sea-level curve for East Greenland. Palaeogeography, Palaeoclimatology, Palaeoecology **78**, 71–85. https://doi.org/10.1016/0031-0182(90)90205-I
- Surlyk, F. 2003: The Jurassic of East Greenland: a sedimentary record of thermal subsidence, onset and culmination of rifting. In: Ineson, J.R. & Surlyk, F. (eds): The Jurassic of Denmark and Greenland. Geological Survey of Denmark and Greenland Bulletin 1, 659–722. https://doi. org/10.34194/geusb.v1.4644
- Surlyk, F. et al. 2021: Jurassic stratigraphy of East Greenland. GEUS Bulletin **46**. 6521. https://doi.org/10.34194/geusb.v46.6521
- Surlyk, F. & Clemmensen, L.B. 1983: Rift propagation and eustacy as controlling factors during Jurassic inshore and shelf sedimentation in

- Northern East Greenland. Sedimentary Geology **34**, 119–143. https://doi.org/10.1016/0037-0738(83)90083-0
- Surlyk, F. & Korstgård, J. 2013: Crestal unconformities on an exposed Jurassic tilted fault block, Wollaston Forland, East Greenland as an analogue for buried hydrocarbon traps. Journal of Marine and Petroleum Geology 44, 82–95. https://doi.org/10.1016/j.marpetgeo.2013.03.009
- Tang, X., Zhang, J., Liu, Y., Yang, C., Chen, Q., Dang, W. & Zhao, P. 2018: Geochemistry of organic matter and elements of black shale during weathering in Northern Guizhou, Southwestern China: Their mobilization and interconnection. Geochemistry 78(1), 140–151 http://dx. doi.org/10.1016/j.chemer.2017.08.002
- Taylor, G.H., Teichmüller, M., Davis, A., Diessel, C.F.K., Littke, R. & Robert, P. 1998: Organic Petrology, 704 pp. Gebruder Borntraeger.
- Telnæs, N., Isaksen, G.H. & Douglas, A.G. 1994: A geochemical investigation of samples from the Volgian Bazhenov Formation, Western Siberia, Russia. Organic Geochemistry **21**(5), 545–558. https://doi.org/10.1016/0146-6380(94)90105-8
- Vischer, A. 1943: Die postdevonische Tektonik von Ostgrönland zwischen 74° und 75° N. Br. Kuhn Ø, Wollaston Forland, Clavering Ø und angrenzende Gebiete. Meddelelser om Grønland **133**(1), 195.
- von der Dick, H., Meloche, J.D., Dwyer, J. & Gunther, P. 1989: Source-rock geochemistry and hydrocarbon generation in the Jeanne d'Arc Basin, Grand Banks, offshore eastern Canada. Journal of Petroleum Geology **12**, 51–68. https://doi.org/10.1111/j.1747-5457.1989.tb00220.x